

SYNTHETIC STRATEGIES TO PROBE ENZYMATIC ACTIVITY: INVESTIGATION OF A
NOVEL OXYGEN-DEPENDENT NON-HEME DIIRON MONOOXYGENASE (MIAE)

by

ANDRA LYNN CORDER

Presented to the Faculty of the Graduate School of
The University of Texas at Arlington in Partial Fulfillment
of the Requirements
for the Degree of

DOCTOR OF PHILOSOPHY

THE UNIVERSITY OF TEXAS AT ARLINGTON

August 2014

Copyright © by Andra Lynn Corder 2014

All Rights Reserved

Acknowledgements

Receiving this doctorate was a joint effort. My husband was there to listen, get mad at what I could not, and support me no matter what. Through the hard times, he was there to encourage and inspire. I truly could not have done this without my confidant standing beside me. My darling daughter, Anilin, and all the smiles she gave to encourage me to keep fighting. My parents were my cheerleaders, constantly rooting for my success, and always there to lend a hand when I needed it (even when I claimed I did not). My brother and sister-in-law were my laughter, always finding a way to make me smile and reminding me that every aspect of life does not need to be planned and analyzed.

I thank all the undergraduate teammates I had through the years. Samantha Vogel, Sana Anwar, and Amanda Dark are each amazing women. They were all fantastic mentees, working hard to reach their own individual goals. I am so proud of each one of them, and am blessed to still call each one a close friend.

I also owe a large amount of gratitude and thanks for my professors Dr. Frank Foss and Dr. Brad Pierce. Both were willing to give me a chance after a horrible first year of my graduate career, and their faith in me continued to inspire and push me through the years. The level of patience received from each one of them is awe-inspiring and I cannot begin to express my gratitude. They never stopped pushing me to new limits, and taught me what I was capable of. My peers always said I was crazy for having two professors, but they are both my mentor, and I am lucky for it. Words cannot express my gratitude, and if there is any sad point in my graduating, it is saying farewell. I will truly miss the camaraderie and support they so graciously gave.

Lastly, I would like to thank my committee members, Dr. Carl Lovely and Dr. Johnson-Winters, along with my lab mates. My committee members helped guide me

through the Ph.D. process, and push me forward. Many thanks for all they did for me and my career. As for my lab mates, both the Pierce lab and Foss lab, I will miss all of the friendship, jokes, and chemistry chat. They are all special in their own unique ways, and have taught me many lessons. I appreciate all they have done for me, and they will be missed and thought of often.

July 02, 2014

Abstract

SYNTHETIC STRATEGIES TO PROBE ENZYMATIC ACTIVITY: INVESTIGATION OF A NOVEL OXYGEN-DEPENDENT NON-HEME DIIRON MONOOXYGENASE (MIAE)

Andra Lynn Corder, PhD

The University of Texas at Arlington, 2014

Supervising Professor: Brad S. Pierce and Frank W. Foss, Jr.

Within the anticodon stem loop (ACSL) of tRNA, nucleoside modifications are frequently observed at position 34 (the wobble position) or position 37 (3' adjacent to the anticodon). For instance, nearly all eukaryotic and bacterial tRNAs that read codons starting with uridine are modified by the enzymes MiaA and MiaB. While absent in eukaryotes, some facultative bacteria utilize a non-heme diiron enzyme (MiaE) to catalyze the O₂-dependent hydroxylation of 2-thiomethyl-N⁶-(3-methyl-2-butenylamino) adenosine (ms²i⁶A₃₇) to produce 2-methylthio-N⁶-(4-hydroxyisopentenyl)-adenosine (ms²io⁶A₃₇). In these bacteria, it has been postulated that the extent of the A37-hydroxylation is involved in regulating aromatic amino acid uptake, iron transport, and aerobiosis. The following dissertation details the synthesis of several modified substrate surrogates and their application toward characterizing the active site of MiaE.

Chapter 1 reviews tRNA modifications and the enzymology of MiaE. MiaA and MiaB are briefly discussed, followed by a more detailed review of MiaE activity, catalysis, and spectroscopy.

Chapter 2 details the characterization of the chemo- and stereospecificity of MiaE using three synthetic β-nucleoside substrates [2-thiomethyl-N⁶-(3-methyl-2-butenylamino) adenosine (ms²i⁶A); N⁶-(3-methyl-2-butenylamino) adenosine (i⁶A); and 2-chloro-N⁶-(3-

methyl-2-butenylamino) adenosine (Cl^{2,6}A)]. Remarkably, regardless of the substrate used in peroxide-shunt assays, hydroxylation of the isopentenyl-C4-position was observed with > 97% *E*-stereoselectivity. Moreover, the initial rate of MiaE hydroxylation is highly influenced by the substituent at the C2-position of the nucleoside base [$v_0/[E]$ for ms^{2,6}A > i⁶A > Cl^{2,6}A].

Chapter 3 describes the construction of modified substrate-surrogate spin-probes employed to further interrogate the role of the C2-functionality. Beyond creating a tool to study the enzymes binding pocket, the synthetic strategy targeted the smooth coupling of three subunits (base, ribose, and spin-probe) so that the methodology could be easily used for the investigation of a wide range of biomolecular targets.

Chapter 4 details several proposed experiments to aid in further dissecting the active site of MiaE through the synthesis of new substrates and further biophysical analysis.

Lastly, Chapter 5 is a brief chapter describing the optimization of a Mitsunobu-like process catalytic in phosphine.

Table of Contents

Acknowledgements	iii
Abstract	v
List of Illustrations	ix
List of Tables	xi
Chapter 1 A Transfer-RNA Hypermodification Pathway	1
Chapter 2 Substrate-specificity of Oxygen-dependent MiaE.....	9
2.1 Materials and Methods	10
2.2 Results	21
2.3 Discussion	36
Chapter 3 Synthetic Spin-labeling Strategy for Enzymatic Characterization	41
3.1 Materials and Methods	43
3.1.1 MiaE binding affinity	56
3.2 Discussion	61
Chapter 4 Future Avenues for MiaE	65
4.1 Inductive Effect of C2-Functionality	66
4.2 Oligonucleotide Synthesis of Varying Lengths and Modifications	68
4.3 Electrostatic Interactions of the Substrate-Enzyme Complex	70
4.4 Substrate-Gated Electron Delivery	73
4.5 <i>E-Z</i> Isomerization of MiaE Hydroxylated Substrates	74
Chapter 5 Synthetic Methodology.....	76
5.1 Chapter 2 Experimental.....	77
5.2 Chapter 3 Experimental.....	102
Chapter 6 A Mitsunobu-Like Process Catalytic in Phosphine	117
6.1 Mitsunobu Experimental	120

Appendix A List of Abbreviations	130
Appendix B NMR Spectra	132
Appendix B: Chapter 2 NMR Spectra	133
Appendix B: Chapter 3 NMR Spectra	177
References	203
Biographical Information.....	212

List of Illustrations

Figure 1-1 Biosynthetic pathway for $ms^2io^6A_{37}$	3
Figure 1-2 Catalytic cycle of methane monooxygenase (MMO)	8
Figure 2-1 Synthetic route of MiaE analogs	18
Figure 2-2 Synthetic route of MiaE modified analogs	19
Figure 2-3 Synthesis of (Z/E)-4-hydroxyisopentenylamine hydrochloride	20
Figure 2-4 SDS-PAGE of MiaE purification	22
Figure 2-5 <i>In vivo</i> activity assay of MiaE	23
Figure 2-6 Catalase activity of MiaE	25
Figure 2-7 TLC qualitative substrate screening	26
Figure 2-8 HPLC chromatogram of product formation and stereochemistry	27
Figure 2-9 HILIC chromatogram of <i>E/Z</i> product standards	29
Figure 2-10 Initial rate of Cl^2io^6A formation with increasing H_2O_2 concentration	31
Figure 2-11 Stoichiometric coupling of product formation with substrate consumption	32
Figure 2-12 Electron transport catalysis	33
Figure 2-13 Steady state kinetics by peroxide-shunt (A) and ETC (B)	35
Figure 3-1 Idoxuridine and common nitroxyl labeled nucleosides	41
Figure 3-2 Retrosynthetic analysis of spin-labeled nucleoside	43
Figure 3-3 1,2,3-Tri-O-acetyl-5-azido-5-deoxy-D-ribofuranose (3.3) synthesis	43
Figure 3-4 Nitroxyl ester 3.7 and amide 3.8 synthesis	45
Figure 3-5 Synthesis of functionalized phosphine 3.11	45
Figure 3-6 Staudinger ligation of azido-ribose 3.3 and phosphine 3.11	46
Figure 3-7 Synthesis of alkyne 3.14 and nitrile 3.15	47
Figure 3-8 Alternative “click”-alkyne synthesis	49
Figure 3-9 T7 RNA polymerase expression	51

Figure 3-10 T7 RNA polymerase DEAE column purification.....	53
Figure 3-11 T7 RNA polymerase activity	55
Figure 3-12 Spin-labeled MiaE nucleoside (Cl ²ⁱ⁶ A) synthesis	57
Figure 3-13 Synthesis of spin-labeled ACSL ^{Trp}	58
Figure 3-14 CD spectrum of spin labeled ACSL ^{Trp}	59
Figure 3-15 Spin-labeled Cl ²ⁱ⁶ A (3.22) EPR spectrum.....	60
Figure 3-16 Tandem Staudinger/aza-Wittig ligation	61
Figure 3-17 EPR spectrum of spin-labeled Cl ²ⁱ⁶ A 3.22 binding assay.....	63
Figure 4-1 Proposed mo ²ⁱ⁶ A synthesis.....	68
Figure 4-2 Synthesis of modified nucleoside phosphoramidite monomer	69
Figure 4-3 Crystal structure of MiaE active site.....	70
Figure 4-4 Rate of peroxide shunt product formation with the addition of ACSL ^{Trp}	72
Figure 4-5 UV-vis spectrum of reduced and oxidized ferridoxin (Fd)	74
Figure 6-1 Mitsunobu reaction	117
Figure 6-2 Proposed Mitsunobu catalytic cycle	118
Figure 6-3 Proposed catalytic cycle of Mitsunobu-like reaction.....	118
Figure 6-4 Mitsunobu-like optimization conditions and synthesized substrates.....	119

List of Tables

Table 2-1 α/β substrate hydroxylation.....	30
Table 3-1 Detritylation conditions	44
Table 3-2 Dipolar cycloaddition trials	48
Table 3-3 Benzyle azide dipolar cycloaddition trials	48

Chapter 1

A Transfer-RNA Hypermodification Pathway

Post-transcriptional modifications of transfer RNA (tRNA) have been identified across all phylogenetic domains of life (Archaea, Bacteria, and Eucarya).¹ Ironically, more genes are devoted to enzymes involved in the modification of tRNA nucleosides than to the various tRNA genes themselves.^{1,2} These modifications are made to structurally diversify tRNA from the four canonical nucleoside building blocks [adenosine, (A); guanosine, (G); uridine, (U); and cytosine, (C)].³ At present, nearly 90 structurally unique nucleoside modifications have been identified in tRNA.¹ In many instances, the physiologic role of such modifications is unclear; however, several examples have been identified to suggest that the presence of modified nucleosides in tRNA can impact central metabolism (citric acid cycle), thiamine biosynthesis, and bacterial virulence.⁴ Of these modifications, the best understood are those localized within the anticodon stem loop (ACSL).⁵ Specific modifications within the ACSL region of tRNA have been shown to improve aminoacyl-tRNA selection, regulate gene expression, and decrease translational frame-shifting.¹ One thing that is known for certain is that all organisms put considerable effort into modifying tRNA. *Salmonella typhimurium*, for instance, has close to 50 different tRNA modifying enzymes which aid in the synthesis of the 29 modified nucleosides found.⁴ This indicates that *S. typhimurium* has four times the genetic information devoted to tRNA modifying enzymes than devoted to synthesizing tRNA itself.¹

Within the ACSL, the majority of nucleoside modifications occur at either position 34 (the wobble position) or position 37.⁶ Modifications in proximity to the anticodon aid in recognizing rare codons, and function to restrict or expand codon recognition, causing expression of alternative protein sequences.² The decoding capacity is altered due to the

change in conformational rigidity of the base, or its ability to form hydrogen bonds with the codon (mRNA).⁶ For example, 5-methylaminomethyl-2-thiouridine (mnm⁵s²U₃₄) modification at the wobble position contributes structure and order to the anticodon, causing decoding restriction by reducing conformational dynamics in recognition of specific codons.² In yeast, deletion of enzymes responsible for the mnm⁵s²U₃₄ modification of tRNA^{Lys} restricts cell viability.⁷

In many instances, modification of the nucleoside involves a single chemical step such as the addition of a methyl or thiomethyl group to the base. For example, tRNAs which read codons starting with cystine have the modified nucleoside 1-methylguanosine at position 37 (m¹G₃₇), catalyzed by *TrmD* in bacteria and *Trm5* in eukarya and archaea.⁸ This guanosine modification is important for maintaining the correct reading frame, and avoiding illegitimate base pairing between position 37 of tRNA and mRNA.⁴ Björk and Hagervall both demonstrated that mutant tRNA^{Pro} lacking the TrmD modification promotes a +1 frameshift, proving the modification essential for translational fidelity.^{4,9}

Alternatively, some modifications employ multiple enzymes within a complex biochemical pathway to produce a hypermodified nucleoside. Figure 1-1 illustrates a particularly interesting hypermodification pathway which occurs at adenine-37 (A₃₇) within the ACSL. In facultative anaerobes such as *S. typhimurium*, the extent of A₃₇-modification is believed to regulate aromatic amino acid uptake, enterochelin synthesis, iron transport, and aerobiosis.^{3,4,10}

In the first reaction shown in Figure 1-1, dimethylallyl (Δ^2 -isopentyl) diphosphate-tRNA transferase [E.C. 2.5.1.8], designated MiaA (previously called *trpX*) catalyzes the nucleophilic substitution of the dimethylallyl group from dimethylallyl pyrophosphate (DMAPP) to the exocyclic N⁶-amino nitrogen of A₃₇ to yield N⁶-isopentenyl-adenosine (i⁶A₃₇) with release of inorganic pyrophosphate.¹¹ The enzymology of MiaA, as well as the

role of the isopentenyl modification, has been studied extensively. *N*⁶-isopentenyladenosine (*i*⁶A₃₇) was first identified as a component in yeast tRNA by Hall and coworkers, along with Zachau and Biemann in 1967.¹² The modified nucleoside was isolated from yeast and mammalian tissue, as well as fully characterized and synthesized a year later by Hall's group. They also found that the free nucleoside exhibits cytokinin activity, in which it stimulates cell division and differentiation in plant systems.¹² As with the full tRNA, the modification is not necessary for cell viability; however, prenylation enhances tRNA-ribosomal binding by stabilizing the weak A-U base-pairing between A₃₆ and the uridine of the codon.¹³ MiaA deficiency results in a drastic reduction of tRNA efficiency and an increase in codon context sensitivity, in which the nucleotides neighboring the codon greatly influence translational accuracy.¹⁰ Moore and Poulter demonstrated that the enzyme is a monomer, and the kinetic mechanism is ordered sequential with tRNA binding before DMAPP.¹³ Specificity and recognition of tRNA substrates is predominantly dependent on the A₃₆A₃₇A₃₈ sequence; however, the base pairs located at the collar of the anti-codon stem loop (positions 29-41 and 30-40) and the secondary hair-pin loop configuration of the tRNA may play a role in binding and selectivity.¹⁴ The tRNA substrate can be substituted with a 17-base pair oligonucleotide corresponding to the stem-loop of tRNA (ACSL); however, this substitution results in a *K_m* two orders of magnitude higher than the full length tRNA, suggesting the presence of binding interactions distal to the ACSL.¹⁵

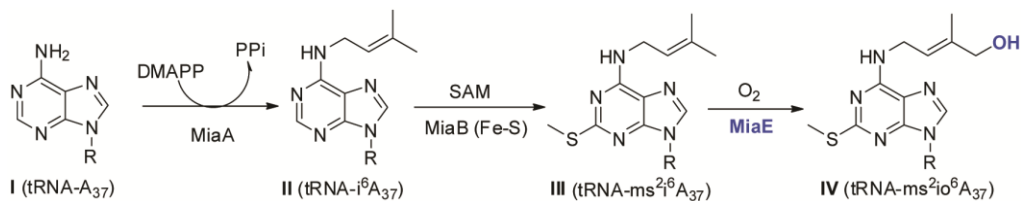


Figure 1-1 Biosynthetic pathway for *ms*²*io*⁶A₃₇

The second enzymatic transformation involves the C-H insertion of a sulfur atom and subsequent methylation of i^6A_{37} at the C2-position to produce 2-methylthio- N^6 -isopentyl-adenosine ($ms^{2,6}i^6A_{37}$). With the notable exception of $tRNA_{i.V.}^{Ser(GGA)}$, nearly all eukaryotic and bacterial tRNAs that read codons starting with U contain the $ms^{2,6}i^6A$ -modification.^{1,3} The enzyme that catalyzes this remarkable transformation is Δ^2 -isopentenylpyrophosphate tRNA-adenosine transferase, designated MiaB. MiaB is a member of the ancient radical S-adenosylmethionine (SAM) methylthiotransferases (MTTase), which perform both radical SAM dependent sulfur insertion and methylation to modify tRNA and ribosomal proteins.¹⁶ As with other members of the radical SAM family, MiaB contains a catalytic $[4Fe-4S]^{2+/1+}$ -cluster coordinated within a conserved CXXXCXXC sequence.^{17,18} However, unique among MTTase is the inclusion of a second $[4Fe-4S]$ -cluster, the role of this cluster has recently become a matter of some debate.¹⁹ The radical SAM cluster catalyzes the reductive cleavage of SAM to produce a 5'-deoxyadenosyl radical (Ado●) ultimately responsible for H-atom abstraction at the C2-position of i^6A_{37} . SAM serves as the source of the methyl group within $ms^{2,6}i^6A_{37}$ -tRNA.²⁰ Until recently, the source of the S-atom was believed to come from the second 'sacrificial' $[4Fe-4S]$ -cluster.²¹ Experiments in which apo-MiaB is reconstituted with iron and selenium under turnover conditions, incorporation of selenium was observed within the product nucleotide ($ms^{2,6}i^6A_{37}$), thus implying that MiaB was itself the source of the product S (or Se)-atom.²⁰ However, it was recently demonstrated that multiple turnovers of methylthiolation could be observed for MiaB if supplied with an exogenous sulfur co-substrate.¹⁹ On this basis, it was proposed that the second $[4Fe-4S]$ -clusters serves not as a sacrificial source of S-atoms, but instead as a true enzymatic cluster which activates sulfide or methylsulfide for insertion on the substrate.²²

The final enzyme in this pathway (MiaE, 2-methylthio- N^6 -isopentenyl-adenosine(37)-tRNA monooxygenase) catalyzes the O_2 -dependent hydroxylation of $ms^{2,6}A_{37}$ to produce 2-methylthio- N^6 -(4-hydroxyisopentenyl)-adenosine ($ms^{2,6}io^6A_{37}$).²³ While MiaE can utilize io^6A_{37} as a substrate, whole cell assays suggest a preference for $ms^{2,6}A_{37}$.²⁴⁻²⁶ This highly selective oxygen incorporation was first identified in the late 1960's; however, the gene encoding the hydroxylase responsible (*miaE*) was not identified until the 1990's. A few years later, Persson and coworkers were able to demonstrate the importance of the hydroxylation in metabolic regulation. *MiaE* mutants were tested for aerobic growth on various carbon sources lacking specific citric acid cycle intermediates. Interestingly, mutants defect in the *miaE* gene were unable to grow on malate, fumarate, and succinate.²⁷ These *miaE* mutants did not exhibit decreased catalytic activity or expression of citric acid cycle enzymes. Furthermore, their uptake of dicarboxylic acids was also unaffected.²⁷ Based on these observations, it has been suggested that *Salmonella typhimurium* utilizes the hypermodified $ms^{2,6}io^6A_{37}$ as a signal for the availability of molecular oxygen. Thus, $ms^{2,6}io^6A_{37}$ may serve as a means to help regulate aerobiosis.^{1,6,25}

MiaA and MiaB are common in both eukaryotes and prokaryotes;²⁸ however, MiaE is found only within a small subset of facultative anaerobic enterobacteria and plant-associated bacteria such as *S. typhimurium*, *Rhizobium leguminosarum*, *Corynebacterium fascians*, and *Agrobacterium tumefaciens*.^{28,29} The presence of the fully modified $ms^{2,6}io^6A_{37}$ across phylogenetic domains was accompanied with discrepancies within the literature regarding the stereochemistry of isolated $ms^{2,6}io^6A_{37}$. For example, it was reported that $ms^{2,6}io^6A_{37}$ isolated from plants exhibited (Z)-stereochemistry. Interestingly, in this same report it was observed that the (E)-isomer of io^6A_{37} could be isolated as a free-base.³⁰ Thus, suggesting the possibility of an independent pathway for

cytokinin synthesis independent of MiaE. This hypothesis was never explored further. Among bacterial enzymes, it was reported that $Z\text{-ms}^2\text{io}^6\text{A}_{37}$ was the MiaE-product observed from various plant-associated bacteria (*Rhizobium leguminosarum*, *Agrobacterium tumefaciens*, and *Corynebacterium fascians*).³¹ The first instance of $E\text{-ms}^2\text{io}^6\text{A}_{37}$ was reported by Ajitkumar and Cherayil for the non-plant associated γ -*proteobacteria*, *Azotobacter vinelandii*.²⁸ Based on this observation it was proposed that other non-plant associated bacteria (such as *S. typhimurium*) may also produce the (E)- instead of the (Z)-isomer. This is perhaps a tenuous hypothesis given only 58% identity between *S. typhimurium* and *A. vinelandii*.

Characterization of the protein itself was not investigated until 2007 by Mathevon and coworkers.²³ Through size exclusion chromatography, they indicated that MiaE exhibits a monomeric (α) protein conformation. They also utilized UV-visible spectroscopy, electron paramagnetic resonance (EPR) spectroscopy, Mössbauer and hyperfine sublevel correlation (HYSCORE) spectroscopies to demonstrate that the MiaE protein is a carboxylate-bridged non-heme diiron hydroxylase;²³ however, separate MiaE preparations resulted in incongruent EPR spectrums. The authors hypothesize that the as-isolated diiron center exists as three separate forms: (I) a mixed-valent hydroxo-bridged $[\text{Fe}^{\text{II}}\text{-OH-Fe}^{\text{III}}]$ center; (II) an EPR-silent oxo-bridged $[\text{Fe}^{\text{III}}\text{-O-Fe}^{\text{III}}]$; (III) an EPR-silent hydroxo-bridged $[\text{Fe}^{\text{III}}\text{-OH-Fe}^{\text{III}}]$. Due to the mixture of diiron sites, it was unclear whether the active form was hydroxo or oxo-bridged. The Pierce group is currently investigating and characterizing the separate diiron forms.³² Hydroxylase activity was also investigated *in vitro* utilizing cell-free extracts, along with either NADPH or H_2O_2 addition. HPLC analysis was used as a qualitative assessment for the production of $\text{ms}^2\text{io}^6\text{A}$. The activity assays performed were lacking; however, positive results with the

addition of an electron source or oxidant brought forth the postulation that MiaE operates in a similar fashion to MMO.²³

Sequence alignment and spectroscopic characterization (EPR/Mössbauer) of MiaE performed by Mathevon (2007) and Kaminska (2008) confirmed that it is a member of the non-heme diiron family of enzymes.^{23,29} Other members of this family include the well-studied bacterial multicomponent methane monooxygenase (MMO), toluene-monooxygenases (T₂MOH and T₄MOH), phenol hydroxylase (PH), the small subunit of ribonucleotide reductase (R2), and stearyl-acyl carrier protein Δ^9 -desaturase ($\Delta 9D$).³³⁻³⁵ Due to sequence homology and the overall electronic similarity between the aforementioned non-heme diiron enzymes, the reaction cycle for this class of enzymes is postulated from the extensive characterization of MMO, represented in Figure 1-2. Diverse techniques, including stop flow and rapid quench kinetics, along with various spectroscopic studies, have been used to investigate the intermediates of the mechanism by which MMO isolated from *Methylococcus capsulatus* (Bath) reductively activates dioxygen to produce methanol.³⁶⁻³⁸ The catalytic cycle begins with the two electron reduction, derived from NADPH or NADH, of the resting diferric center to produce a diferrous cluster (intermediate A, Figure 1-2). The diferrous center then reductively activates molecular oxygen to produce a high-valent peroxy species (Fe^{III}-O-O-Fe^{III}, intermediate B), which rearranges to form the strongly oxidizing bis- μ -oxo species, deemed “compound Q”, responsible for substrate oxidation (intermediate C).^{39,40} Hydrogen atom abstraction from the substrate by compound Q, followed by radical rebound and product release regenerates the resting state enzyme, completing the cycle (intermediate D).^{23,39-41} This natural cycle, involving specific interactions with electron transfer proteins, can be bypassed by a ‘peroxide-shunt’ pathway, exhibited by many heme oxidase and non-heme diiron enzymes.⁴¹ Addition of hydrogen peroxide, two

reducing equivalents and dioxygen, are delivered to the resting diferic center. Heterolytic cleavage of the peroxide generates the high valent substrate-oxidizing intermediate (intermediate B, Figure 1-2). This pathway removes the need for an external electron source, but frequently at the cost of product yield and specificity.^{33,34,42}

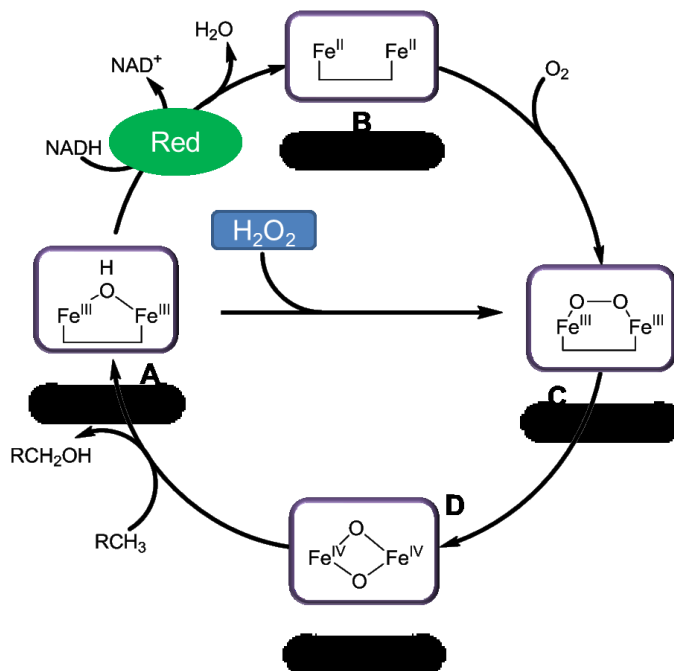


Figure 1-2 Catalytic cycle of methane monooxygenase (MMO)

Historically, the enzymes involved in these nucleoside biotransformations have provided a rich area of enzymatic mechanistic study. The biological significance of these transformations has inspired biomimetic investigation proving useful for anticancer, antibiotic, and antiviral studies.^{43,44} Providing molecular tools to understanding these mechanisms may aid in relating tRNA modifications to human health, as well as the incorporation of bio-inspired catalysts into the synthetic repertoire.^{45,46} The following chapters describe a bioorganic approach to the investigation of MiaE through the development of synthetic tools.

Chapter 2

Substrate-specificity of Oxygen-dependent MiaE

Non-heme enzymes and model complexes have historically attracted considerable interest in bioinorganic chemistry. Extraordinary chemical transformations occur in diiron-metalloenzymes identified throughout the biological kingdom.⁴⁷ The biological significance of these transformations has inspired biomimetic investigation in an attempt to understand the vast number of functionally and structurally diverse enzymes responsible for the incredible ambidexterity exhibited in the chemical oxidations they initiate.⁴² Diiron sites accomplish a multitude of reactions ranging from molecular oxygen transport, aliphatic desaturation, one-electron oxidation, and hydrocarbon hydroxylation.⁴⁸ The vast majority of these alluring non-heme diiron enzymes are multimeric.⁴⁹ The active site is customarily positioned within a four-helix bundle in the α subunits of a non-covalent heterotrimeric dimer $(\alpha\beta\gamma)_2$ conformation, as seen in bacterial multicomponent monooxygenase (BMM) enzymes.^{48,50} In contrast to the multimeric protein configuration exhibited by the non-heme diiron monooxygenases characterized thus far, MiaE exhibits a monomeric (α) protein configuration, containing a single active site as indicated by size exclusion chromatography²³ and analytical ultracentrifugation.⁴⁵ This is the first example found within literature of a monomeric non-heme diiron oxygenase. Therefore, this enzyme provides a unique opportunity to study a minimal non-heme diiron enzyme in the absence of any potential for cooperatively.

This chapter outlines the synthesis of three nucleoside substrate surrogates [N^6 -isopentenyl-adenosine (i^6A); 2-methylthiol- N^6 -isopentenyl-adenosine, (ms^2i^6A); and 2-chloro- N^6 -isopentenyl-adenosine, (Cl^2i^6A)] such that the chemo and stereospecificity of recombinant MiaE cloned from *Salmonella typhimurium* could be examined. In these assays, the non-heme diiron peroxide-shunt was used along with the native electron-

transport chain to perform steady-state kinetic assays.⁵¹ Both the (*Z*)- and (*E*)-isomers of the hydroxylated products [*N*⁶-(4-hydroxyisopentenyl)-adenoside (*io*⁶A); 2-methylthiol-*N*⁶-(4-hydroxyisopentenyl)-adenoside (*ms*²*io*⁶A), 2-chloro-*N*⁶-(4-hydroxyisopentenyl)-adenoside (*Cl*²*io*⁶A)] were synthesized for use as standards in HPLC enzymatic assays and confirmation of MiaE product stereochemistry. Remarkably, for all synthetic nucleosides, MiaE was capable of chemo- and stereoselective *E*-hydroxylation at the terminal C4-position of the isopentenyl-group. Moreover, the results obtained from steady-state experiments suggest that even in the absence of macromolecular tRNA:MiaE interactions, the substrate-affinity of MiaE is largely dominated by inductive effects at the C2-position of the nucleoside base. This observation is consistent with the observation that MiaE preferentially hydroxylates *ms*²*i*⁶A- over *i*⁶A-tRNA *in vivo*.²⁵

2.1 Materials and Methods

Cloning. The *miaE* gene was isolated from *Salmonella enterica* strain LT2 genomic DNA [ATCC 700720] using primers purchased from Integrated DNA Technologies (<https://www.idtdna.com>). A two-step PCR amplification was used to isolate the ORF from genomic DNA and incorporate restriction sites (Sgf I/Pme I) for Flexi-vector cloning (Promega, Madison, WI), followed by insertion of a recognition site for tobacco etch virus protease (TEV). First, (*miaE* specific) PCR reaction primers: forward 5- (AAC CTG TAC TTC CAG TCC AAT TAC CCG CAA ATA CTC TCT CCG G)-3; reverse 5-(GCT CGA ATT CGT TTA AAC TAT CCG GCG GCT GGC ACG CCG CTA TG)-3. Second (TEV site insertion) primers: forward: 5-(GGT TGC GAT CGC CGA AAA CCT GTA CTT CCA GTC C)-3'; reverse: 5'-(GTG TGA GCT CGA ATT CGT TTA AAC)-3. The DNA produced by this two-step PCR amplification was cloned into an isopropyl β-D-1-thiogalactopyranoside (IPTG) inducible T7 vector (designated pVP80K) obtained from the University of Wisconsin, Center for Eukaryotic Structural Genomics (UW CESG).

Sequence verification of *miaE* was performed in the life sciences department at UTA by the Genomics Core Facility (http://gcf.uta.edu/Core_Facility/Core_Facility.html). The resulting plasmid (pMIAE80K) expresses an N-terminal fusion of maltose binding protein (MBP) and MiaE. The two proteins are separated by a recognition sequence for tobacco etch virus (TEV) protease such that cleavage of the two proteins can be performed following purification. *NOTE: Within the ORF for the miaE gene, two possible start codons are present.*²³ *However, only constructs generated from the second start codon resulted in a soluble (29 kDa) protein product.*

For *in vivo* MiaE activity assays, a second 'untagged' MiaE construct (pMIAEK) was cloned into the commercially available pF1K flexi-vector (Promega). PCR primers: *Sfg I*-forward; 5-(TTT AAC AGC GAT CGC ATG AAT TAC CCG CAA ATA)-3'; *Pme I*-reverse; 5'-(GTG GTG TTT AAA CTT ATC CGG CGG CTG GCA CGC CGC)-3'. Forward and reverse restriction sites are underlined for clarity. Sequence verification was performed as described above. Expression of soluble protein (29 kDa) was confirmed by SDS PAGE. *NOTE: BL21(DE3) E. coli cells transformed with the 'untagged' MiaE vector (pMIAEK) have a significantly lower growth rate (~2-fold) in LB-media as compared to cells transformed with the MBP-tagged vector (pMIAE80K). Moreover, cells transformed with pMIAEK showed a significant decrease in cell growth upon induction. This was partly remedied by decreasing the induction temperature from 25 to 17 °C and increasing the time before harvesting cells. We speculate that the N-terminal MBP-tag attenuates promiscuous activity of MiaE within E. coli during basal expression. For this reason, the pMIAEK vector was used only for in vivo activity confirmation whereas the pMIAE80K vector was used for over expression, purification, and in vitro enzymatic assays.*

Media and growth conditions. The pMIAE80K vector was transformed into chemically competent BL21(DE3) *E. coli* (Novagen) by heat-shock and grown overnight at 37 °C on a lysogeny broth (LB)⁵⁰ agar plate in the presence of 25 µg/mL Kanamycin (Kan). The following day, a single colony was selected for growth in liquid LB (Kan) media for training on antibiotic prior to inoculation of 10-L BF-110 fermentor (New Brunswick Scientific) at 37 °C. Cell growth was followed by optical density at 600 nm (OD₆₀₀). Induction was initiated by addition of 0.5 mM IPTG, 1 mM ferrous ammonium sulfate, and 20 g casamino acids at an OD₆₀₀ ~4. Additionally, upon induction the temperature of the bioreactor was decreased from 37 °C to 25 °C and agitation was set to maintain an O₂ concentration of 20% relative to air-saturated media. After 4 hours of induction, the cells were pelleted by centrifugation (Beckman-Coulter Avanti J-E, JA 10.5 rotor) at 18,600 × g for 15 min, and the paste was stored at -80 °C. Confirmation of MiaE expression was performed by SDS-PAGE of lysed cells before and after IPTG induction.

Protein purification. Approximately 25 g of cell paste was suspended in a 50 mL of lysis buffer (20 mM HEPES, 40mM NaCl, pH 8.0), and thawed in an ice bath with 10 µg/mL each of lysozyme, deoxyribonuclease I, and ribonuclease with gentle stirring for 30 min. The cell suspension was sonicated in a 30 second on/off pulse cycle for a total of 10 min. The resulting cell free extract was centrifuged (JA 20 rotor) at 48,000 × g for 60 min at 4 °C. The supernatant was loaded onto a fast flow DEAE column pre-equilibrated in lysis buffer, and the protein was eluted by NaCl gradient (40 mM to 350 mM NaCl in 20 mM HEPES, 0.3 mM Tris[2-carboxyethyl] phosphine (TCEP), pH 8.0). The fractions containing the MBP-MiaE protein, determined by SDS-PAGE, were concentrated via Amicon N₂ stir cell equipped with an YM 30 ultrafiltration membrane. TEV protease was used to cleave the fusion protein by overnight storage at 4 °C. The cleaved fusion protein was desalted by dialysis (Spectra/por, Spectrum Laboratories Inc.)

in lysis buffer. To separate MBP from MiaE enzyme, the desalted protein was re-loaded through the DEAE Sepharose column equilibrated in lysis buffer. The protein was eluted on a linear NaCl gradient (0 mM to 350 mM NaCl in 20 mM HEPES, pH 8.0) and fractions containing only MiaE were identified by SDS PAGE and UV-visible spectroscopy. Stoichiometric iron incorporation in purified MiaE was verified by UV-visible spectroscopy on the basis of the Fe-associated bands typically observed between 320 and 380 nm. Only fractions with $A_{280}/A_{370} \sim 7.8 \pm 0.3$ were pooled and concentrated (YM 10 ultra-membrane) for use in experiments. For the purified MiaE enzyme, the published extinction coefficient at 280 nm ($60,000 \text{ M}^{-1} \text{ cm}^{-1}$) was used to quantify protein samples.²³ Within experimental error (5-10%), determination of protein concentration by UV-visible spectroscopy and standard Bio-Rad protein assay (Bio-Rad Laboratories Inc.) were equivalent.

TEV purification and cleavage conditions. The TEV expression vector (pMHTΔ238) was a generous gift from Dr. Russell Wrobel and Professor Brian G. Fox (UW CESG). Expression and cell growth was performed as described for pMIAE80K. Approximately 10 g of TEV cell paste was thawed in 20 mL of IMAC buffer A (20 mM NaH_2PO_4 , 500 mM NaCl, 1 mM β -mercaptoethanol, pH 7.5) in an ice bath for 30 min. The suspension containing 10 $\mu\text{g}/\text{mL}$ each of lysozyme, deoxyribonuclease I, and ribonuclease was pulse sonicated for 10 min, and centrifuged in a $48,000 \times g$ (JA 20 rotor) for 60 min. The supernatant was collected and loaded onto a 5-mL Hi-Trap immobilized metal affinity chromatography (IMAC) column (GE Healthcare) pre-equilibrated in IMAC buffer A. The column was washed with 5 column volumes (25 mL) of IMAC buffer A prior to elution of TEV enzyme with 2 column volumes of IMAC buffer B (350 mM imidazole in IMAC A, pH 7.5). Excess imidazole was removed by dialysis (Spectra/por, Spectrum Laboratories Inc.) in IMAC buffer A. An Amicon N_2 stir cell

equipped with YM-10 ultrafiltration membrane was used to concentrate the TEV protease. Aliquots (1 mL) of TEV were stored at 1 mg/mL in 50% glycerol at -20 °C. For a typical cleavage reaction, 1 OD₂₈₀ of TEV protease was used per 5 OD₂₈₀ of MBP-MiaE fusion protein.

Analytical ultracentrifugation. The native molecular weight, oligomeric state, and sedimentation coefficient of purified MiaE was determined by Virgil Schirf (schirfv@biochem.uthscsa.edu) and Borries Demeler (demeler@biochem.uthscsa.edu) at the UT Health Science Center (San Antonio, TX), Center for Analytical Ultracentrifugation of Macromolecular Assemblies (CAUMA, <http://www.cauma.uthscsa.edu/>). Three samples (500 µL) of purified MiaE were prepared at 4.7, 9.3, and 15.5 µM within 20 mM HEPES, 100 mM NaCl, pH 8.0 for sedimentation analysis. The monomeric state of MiaE was confirmed by both genetic algorithm and Monte Carlo analysis.^{52,53}

Catalase activity. An oxygen electrode was used to measure the rate of oxygen produced upon H₂O₂ addition to enzyme solutions to measure the low-level catalase activity of MiaE.^{23,54} Dioxygen concentration was determined polarographically using a standard Clark electrode (Hansatech Instruments, Norfolk, England) within a jacketed 2.5-mL cell at 25 ± 2 °C. The electrode was bathed in a saturated solution of KCl and separated from the buffer using a gas-permeable membrane. The electrode was calibrated by measuring the deflection in the voltage upon adding ~500 units of catalase (Sigma-Aldrich, St. Louis) to a buffer with a known concentration of H₂O₂ [$\epsilon_{(250)} = 16.7 \text{ M}^{-1} \text{ cm}^{-1}$]. Confirmation of initial hydrogen peroxide concentration in buffered solutions was performed using the amplex red hydrogen peroxide/peroxidase kit for spectrophotometric determination ($\lambda = 560 \text{ nm}$) of H₂O₂ (Invitrogen, cat. No. A22188). Once the reaction reached completion, the amplitude for the change in voltage was used to determine a

response factor for the electrode. The reaction was initiated by injection of MiaE resulting in final enzyme concentration of 5 μM .

Spectroscopy. All UV-visible measurements were performed on an Agilent 8453 photo diode array spectrometer (Santa Clara, CA). Sample temperature was held constant by a 13 L circulating water bath and a thermostatable cell holder (89054A) with magnetic stirrer. All measurements were made in ES Quartz cuvettes (NSG Precision Cells, Farmingdale, NY).

Ferredoxin (Fd), and Ferredoxin NADP⁺-reductase (FdR). Ferredoxin purification and characterization method was followed as previously described and its concentration was determined by $\epsilon_{420 \text{ nm}} = 9,700 \text{ M}^{-1}\text{cm}^{-1}$.⁵⁵ Spinach FdR was purchased from Sigma Aldrich (CAS No. 9029-33-8) and reconstituted to desired concentration in 20 mM Tris buffer (pH 8.0) before use.

Qualitative TLC activity assays. For initial substrate screening, TLC was utilized to analyze product formation. At selected time points, 10 μL of sample aliquots were removed, heat denatured, and cooled to 0 °C. The reaction mixture (1 μL) was spotted onto a silica gel 60 F₂₅₄ TLC plate (VWR) alongside 5.8 mM of the appropriate standard. After spotting the sample on the TLC plate, a heat-gun was used to completely dry the plate prior to elution. The TLC plate was eluted in 15% methanol in dichloromethane, dried with a heat gun, and stained in potassium permanganate for assay analysis.

*In vivo activity assay.*⁵⁶ In a typical experiment, duplicate cultures (1 L each) of *E. coli* BL21(DE3) transformed with the untagged MiaE expression vector (pMIAEK) were grown in LB (25 $\mu\text{g}/\text{mL}$ kanamycin) at 37 °C as described above. As a control, a separate culture of BL21(DE3) *E. coli* transformed with the TEV expression vector (pMHT Δ 238) was prepared for comparison. Upon reaching OD₆₀₀ ~0.8, one culture was harvested and the cells collected by centrifugation; this 'pre-induction' control sample was

prepared for comparison cultures following IPTG induction. The remaining two cultures transformed with pMIAEK and pMHTΔ238 were induced by addition of 0.5 mM IPTG, 2 g/L casamino acids, 1x Fe-solution (50 μM), and allowed to express for an additional 4 hours at 25 °C prior to harvesting by centrifugation.⁵⁶

Total RNA was recovered by phenol extraction and ethanol precipitation as described previously.^{23,57} Briefly, RNA was extracted from the cell free extract solution by addition of an equal volume of phenol:chloroform (5:1). Following vortex-mixing, the aqueous phase containing RNA was recovered. This process was repeated 3 times. The pooled aqueous extracts were then mixed with 2.5-volumes of ethanol and stored on ice to precipitate RNA. After 2 hours on ice, the RNA pellet was recovered by decantation of supernatant, dried, and reconstituted in autoclaved MQ H₂O. Since both ms²i⁶A and ms²io⁶A are relatively hydrophobic, LiCl washes were not utilized to fractionate tRNA from rRNA.⁵⁸ From each culture (pre-induced, IPTG induced MiaE, and IPTG induced TEV), samples of total RNA were hydrolyzed by nuclease P1 (Sigma Aldrich, Cat. No. N8630) and then dephosphorylated using bacterial alkaline phosphatase, (Invitrogen, Cat. No. 18011-015) according to published methods.²³ The resulting samples were analyzed by reverse phase HPLC using the method developed by Gehrke *et al.*⁵⁵ HPLC instrumentation: Shimadzu quaternary pump LC (LC-20AD XR/LC 30AD) equipped with a diode array photodiode array detector (SPD-M20A); Column, Phenomenex, Gemini-NH 3 μm C18 110 Å; 150 cm × 4.6 mm; Mobile phase, (A) 2.5% methanol in 0.01 M NH₄H₂PO₄; pH 5.1, (B) 20% methanol in 0.01 M NH₄H₂PO₄; pH 5.3, (C) 35% acetonitrile in 0.01 M NH₄H₂PO₄; pH 4.9; injection volume, 50 μL; flow rate, 1 mL/min; column temperature, 25 °C; UV-visible detection wavelength (254 nm).⁵⁶

In vitro HPLC activity assays. Given the decreased number of nucleoside analytes present in peroxide-shunt enzymatic assays, the reverse-phase HPLC method

and column was modified from that used in whole cell *in vivo* assays to decrease the retention times.^{11,23,55} Therefore, attention was turned towards the use of a hydrophilic interaction liquid chromatography (HILIC) column (AZYP Frulic-N). It was found that with an isocratic elution of 98% acetonitrile and 2% aqueous buffer comprised of 2% triethylamine, 3% acetic acid at a rate of 2 mL/min, the HILIC column gave much shorter retention times, while maintaining baseline separation. Numerous samples were injected without any sign of column degradation or clogging. Substrate retention times ranged from 4 to 6 minutes, while product retention times ranged from 10 to 16 minutes. The reliability of the HILIC column was tested for *in vitro* assays, giving results within 5% of those obtained by C18 column. Therefore, this method provided equivalent resolution of peaks with a significantly shorter run time.

LC-MS/MS and data analysis. Verification of enzymatic product was performed by multiple reaction monitoring (MRM) using a triple quadrupole LC-MS/MS [Shimadzu Scientific Instruments, LCMS 8040]⁵⁹. MRM involves two stages of analyte mass analysis. During the first stage, the ion of interest is preselected in quadrupole 1, and fragmented by collisional excitation in the pressurized collision cell (quadrupole two). During the second stage, only a small number of specific fragments are analyzed in quadrupole three. This enhances the lower detection limit, allowing for analysis of low concentration artifacts with decreased background interference. The molecular ions (M^+) of the enzyme substrate (370 m/z) and product (386 m/z) were selected for secondary fragmentation. MRM optimization was then employed to maximize transition intensity and sensitivity for each fragment allowing for quantitation of product ions. The optimized MRM method was used to verify both substrate and product by direct injection of enzymatic assays. These results were compared to direct injection of synthetic standards.

Synthesis of nucleoside analogues. Three ribonucleosides were prepared as shown in Figure 2-1. (See *Chapter 5 Synthetic Methodology* for detailed experimental procedures.) 2-methylthio-*N*⁶-isopentenyl-adenosine (**2.5a**), *ms*²*i*⁶A₃₇, was prepared from commercially available thioxanthine. Selective S-methylation of thioxanthine was achieved by adding dimethyl sulfate while maintaining a temperature below 30 °C.⁶⁰ It should be noted that several methylating agents and conditions were tested, however many resulted in O-methylation, N-methylation, or methylation of any mixture thereof.⁶¹ One notable attempt was the methylthiolation of 2-chloro-6-protected purine using sodium methanethiolate and dimethyl disulfide.⁶² Diazotization followed by nucleophilic addition was also attempted using guanine and dimethyl disulfide.⁶³ The latter trial finally led to the idea of selective S-methylation of thioxanthine. The corresponding product was then chlorinated by addition of phosphorus oxychloride and N,N-dimethylaniline, producing 2-methylthio-*N*⁶-chloropurine (**2.1a**).⁶⁰ 2-Isopentenylamine hydrochloride (**2.2**),

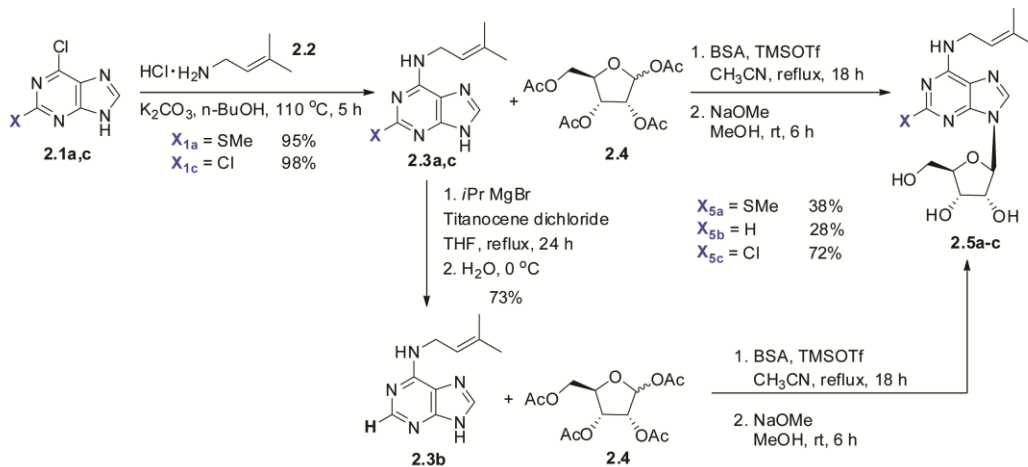


Figure 2-1 Synthetic route of MiaE analogs

was synthesized via Gabriel synthesis,^{64,65} and due to the compounds hygroscopic nature, was conveniently isolated as the HCl salt.⁶⁶ 2-Isopentenylamine hydrochloride

(**2.2**) was added by chemoselective nucleophilic aromatic substitution at the C6-position.^{67,68} Freshly prepared 1,2,3,5-tetra-*O*-acetyl-*D*-ribofuranose (**2.4**)⁶⁹ was then coupled to the purine via modified Vorbrüggen coupling^{70,71} and subsequently deprotected by saponification to provide the desired product, **2.5a**. Analogues **2.5b-c** were synthesized in a similar manner from commercially available xanthine, which was converted to 2,6-dichloropurine.⁷² 2-chloro-*N*⁶-isopentenyl-purine was accessed by chemoselective nucleophilic aromatic substitution at the C6-position.⁷³ *N*⁶-isopentenyl-adenosine (**2.5b**) was prepared by utilizing Grignard conditions for hydrodehalogenation at the C2-position (**2.3c** to **2.3b**).⁷⁴

Hydroxylated **2.8a-c**, expected MiaE oxidation products, were constructed as illustrated in Figure 2-2, using (*E*)-4-hydroxyisopentenylamine hydrochloride (**2.6**) in place of amine **2.2**. *N*-Boc glycine methyl ester (**2.9**) could be converted to aldehyde (**2.10**) directly by reduction with diisobutylaluminumhydride (DIBAL) or by conversion to

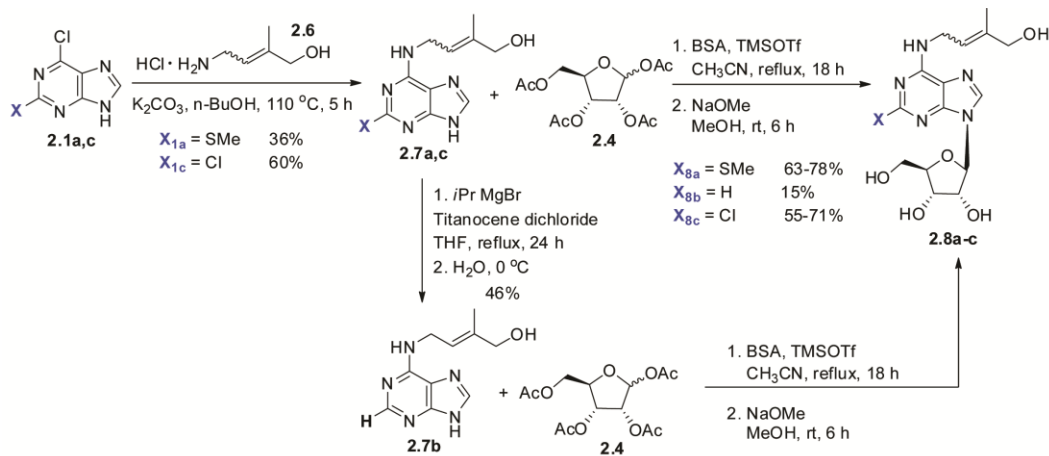


Figure 2-2 Synthetic route of MiaE modified analogs

N-Boc ethanolamine then selective oxidation (not shown).⁷⁵ It proved easier to monitor the temperature and progression of the direct aldehyde formation versus the full reduction to the alcohol followed by oxidation back to the aldehyde. Aldehyde **2.10** was

converted to either (*Z*)- (**2.11**) or (*E*)-4-amino-2-methylbut-2-enoic acid ethyl ester-4-carboxylic acid-*tert*-butyl ester (**2.12**) by Horner-Wadsworth-Emmons olefination. For clarity, *Z*-stereoisomers in synthetic schemes are designated by a prime ('). *E*-selectivity was obtained by utilizing the milder Masamune and Roush HWE conditions using DBU and lithium chloride. Altering the base from DBU to *n*-butyl lithium and decreasing the temperature of the reaction allowed for the production of the kinetic *Z*-diastereomer in a 4:1 ratio.⁷⁶ DIBAL (for (*Z*)-isomer) or lithium aluminum hydride (for (*E*)-isomer) treatment reduced the ester to the alcohol. Interestingly, lithium aluminum hydride also saturated the alkene of the (*Z*)-isomer, and DIBAL treatment of the (*E*)-isomer resulted in poor yield. The alcohol was then deprotection with hydrochloric acid, to afford (*Z*)-(**2.6'**) or (*E*)-4-hydroxyisopentenylamine hydrochloride (**2.6**) respectively (Figure 2-3). For further synthetic details, refer to Chapter 5.

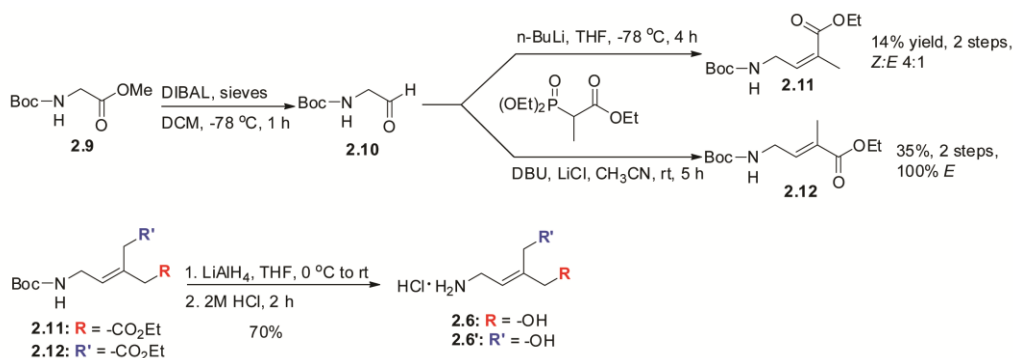


Figure 2-3 Synthesis of (*Z*/*E*)-4-hydroxyisopentenylamine hydrochloride

Steady-state kinetic assays. Hydroxylation of substrate surrogates **2.5a-c** by MiaE were assayed utilizing the peroxide-shunt pathway,^{41,42} frequently observed with heme and non-heme iron oxygenase enzymes, and by native electron transport pathway. The standard assay conditions for peroxide-shunt catalysis included the addition of 25 μL of 400 μM purified MiaE, 25 μL of 23 mM substrate [3:2 DMSO:HEPES buffer (20 mM

HEPES, 50 mM sodium chloride buffer, pH 8)], 25 μ L of 120 mM hydrogen peroxide in HEPES buffer, and 25 μ L HEPES buffer to bring the final volume to 100 μ L. Assay conditions for electron-transport catalysis included the addition of 25 μ L of 1.1 mM purified MiaE, 23 μ L of 10 mM substrate (3:2 DMSO: HEPES buffer), 0.4 mg NADPH, 160 μ L of 230 μ M ferridoxin, 10 μ L of 0.01 U ferridoxin reductase, and 280 μ L HEPES buffer to bring the final volume to 500 μ L. MiaE was added last, and the reaction was separated into 100 μ L aliquots. The reactions were carried out at 27 $^{\circ}$ C, and followed for up to one hour. At selected time points, the sample was heat inactivated at 95 $^{\circ}$ C for 1 minute, and then cooled to 0 $^{\circ}$ C in an ice bath. The sample was centrifuged at 14,000 rpm for 15 minutes, transferred into a Costar[®] Spin-X[®] centrifuge tube filter, and filtered at 11,500 rpm for 3 minutes. For samples analyzed via HILIC (Fruvic-N) HPLC method, 100 μ L of eluent was added prior to initial centrifugation. Since peak distortion can be caused by variable aqueous content in HILIC separations,⁷⁷ an additional 1300 μ L of eluent was added to each sample, resulting in an overall 15-fold dilution in the mobile phase. The results were then analyzed by thin layer chromatography (TLC), HPLC (273 nm), and LC-MS/MS in MRM mode as described previously.

2.2 Results

Purification. Recombinant MiaE from *Salmonella typhimurium* was purified and assayed for Fe-content as described in *Materials and Methods*. As indicated by Figure 2-4, the IPTG-inducible MBP-MiaE fusion protein exhibits an apparent molecular weight of ~70 kDa as observed by SDS PAGE. Overnight cleavage with TEV protease resulted in two protein bands ~40 kDa and ~25 kDa, for MBP and MiaE, respectively (Figure 2-4, lane 6). Following buffer exchange by dialysis, MiaE and MBP were easily resolved by a secondary DEAE anion exchange column as shown in (Figure 2-4, lane 7). The molecular weight of MiaE observed by SDS PAGE (~25 kDa) is slightly lower than the

value expected based on its amino acid sequence (29 kDa).²³ Therefore, both size exclusion chromatography and analytical ultracentrifugation were utilized to confirm that purified MiaE has a monomeric (α) protein conformation in solution. Indeed, in all samples analyzed, no detectable mass action effect were observed and the predicted molecular weight (29,360 Da) was consistent with the monomeric molecular weight of MiaE. These findings were within 1% of the molecular weight calculated from the amino acid sequence (29,013.5 Da) and are consistent with those previously published for this enzyme.²³

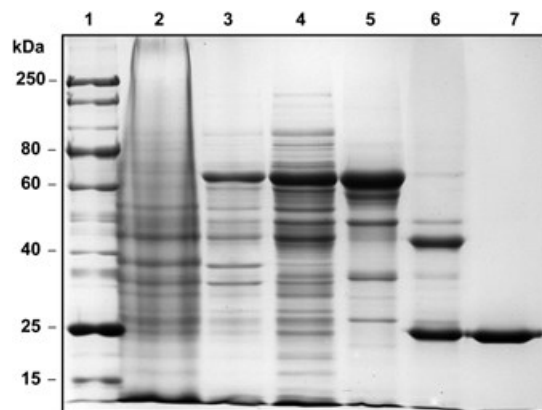


Figure 2-4 SDS-PAGE of MiaE purification

SDS PAGE (12 %) of sequential MiaE purification steps. Lane: **1**, protein markers; **2**, pre-IPTG induced; **3**, post-IPTG induced; **4**, cell free extract; **5**, MBP-MiaE fusion isolated from DEAE AX column A, **6**, TEV cleaved fusion protein; **7**, isolated MiaE following anion exchange DEAE column B.

In vivo MiaE activity. The activity of recombinant MiaE was confirmed in whole cell assays following a similar protocol as described previously.^{23,27} In these experiments, *E. coli* BL21(DE3) was transformed with either the '*untagged MiaE*' or TEV vector (pMIAEK and pMHT Δ 238, respectively) for comparison of total nucleoside

extracts. Samples were prepared as described in *Materials and Methods*. Both pMIAEK (*untagged MiaE*) and pMHT Δ 238 (TEV) vectors have the same Promega flexi-vector backbone and antibiotic resistance, therefore RNA extracts isolated from cells transformed with pMHT Δ 238 offer a reasonable baseline for nucleoside distribution in the absence of MiaE. The chromatograms shown in Figure 2-5 represents the nucleosides obtained from *E. coli* post-IPTG induction (4-hours) of TEV (A) and untagged MiaE (B). Of particular note are the peaks observed at 67 and 81 minutes designated by (○ and ●, respectively). The peak at 81 minutes (●) is observed in all nucleoside samples collected

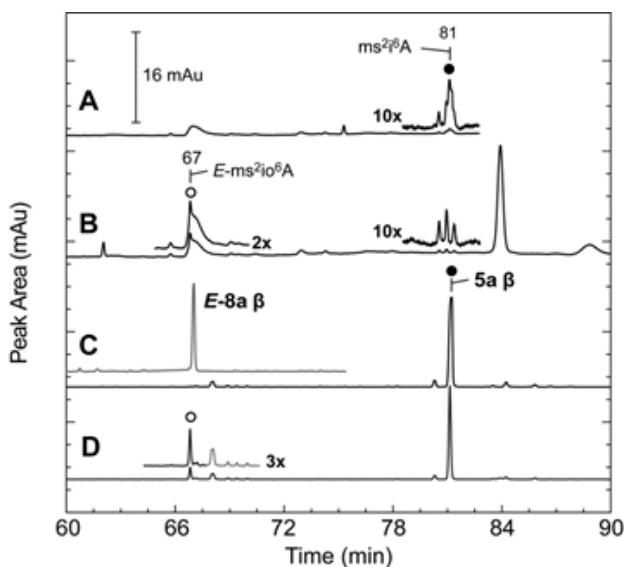


Figure 2-5 *In vivo* activity assay of MiaE

Reverse phase C18 HPLC chromatogram of hydrolyzed tRNA nucleosides extracted from IPTG-induced *E. coli* BL21(DE3) transformed with (A) pMHT Δ 238 and (B) pMIAEK. Assignment of (*E*)-ms²io⁶A (67 min) and ms²i⁶A (81 min) β -epimers were confirmed by comparison of retention times and UV-visible spectra to synthetic standards (C). For clarity, a selected time point (30 min) is shown in trace D for the MiaE peroxide-shunt catalyzed hydroxylation of **2.5a**.

for pre- and post-IPTG induction of pMIAEK, as well as cells transformed with pMHT Δ 238. On the basis of its retention time, UV-visible spectra, and coelution with synthetic standards (trace C; **2.5a**, β -epimer), this peak is assigned to ms^2i^6A . Alternatively, the 67 min. peak (\circ) is only observed following IPTG induction of pMIAEK, and coelutes with *E*-**2.8a**, β -epimer. On the basis of these experiments, it is clear that recombinant MiaE is catalytically active in whole cells.⁵⁶ Moreover, as illustrated in Figure 2-5 (trace D), the **2.5a**-hydroxylated product generated by MiaE peroxide-shunt nicely overlaps with the *E*- ms^2i^6A -product observed in whole cell assays. Thus, the native stereoselectivity of MiaE appears unperturbed in peroxide-shunt assays.

Catalase activity. Many non-heme diiron oxygenase enzymes exhibit limited catalase activity as a result of the peroxide-shunt pathway.⁵⁴ While this activity is several orders of magnitude less than that of a 'true' catalase enzyme, this assay can be diagnostic of the specific activity of purified MiaE in the absence of the native ($ms^2i^6A_{37}$) substrate. In these experiments, a standard Clarke-type oxygen electrode was used to monitor the amount and initial rate of O₂-evolved upon addition of as-isolated MiaE to a buffered solution (20 mM HEPES, 100 mM NaCl, and pH 8) containing hydrogen peroxide (Figure 2-6). The volume of each reaction was fixed at 1.5 mL with a final MiaE Fe₂-site concentration of 5 μ M. For analysis, initial rates were normalized for enzyme concentration ($v_0/[E]$) and H₂O₂ concentrations were varied between 15 and 80 μ M at 25 °C. As shown in Figure 2-6, full enzymatic saturation kinetics was not observed within the range of H₂O₂ utilized (0-80 μ M). However, from the linear portion of the curve, the pseudo-second order rate constant was determined ($k_{obs} \sim 1,480 \text{ M}^{-1} \cdot \text{s}^{-1}$). The stoichiometry of H₂O₂ consumed per O₂ generated was determined by addition of (120 μ M) H₂O₂ to a buffered solution containing 10 μ M MiaE. Upon completion of the reaction

(2 min), the O₂ concentration within the solution increased by 62 μM. In multiple replicates, formation of 1.1 ± 0.2 (n = 5) mol of O₂ is observed upon addition of 2 mol H₂O₂.⁴⁵

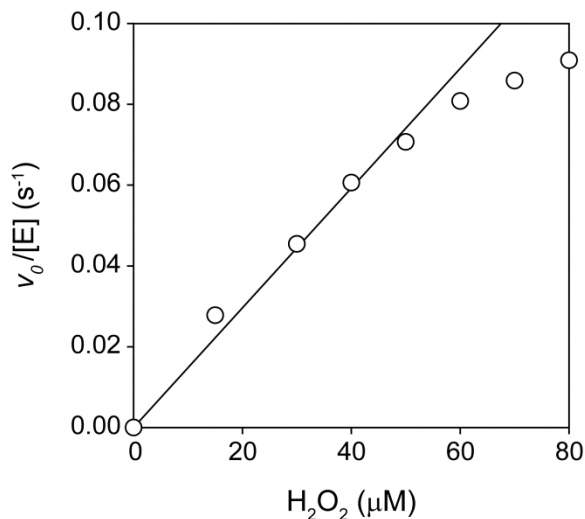


Figure 2-6 Catalase activity of MiaE

Steady-state kinetics of MiaE catalase activity as measured by O₂-selective Clarke electrode. The pseudo-second order rate constant was determined by linear regression (*solid line*; $k_{obs} = 1480 \text{ M}^{-1} \cdot \text{s}^{-1}$). Assay conditions: 100 μM MiaE (Fe₂-sites), 20 mM HEPES, 50 mM NaCl, pH 8, H₂O₂ (0.5 - 80 μM).

Hydroxylation of substrate-surrogates by peroxide shunt. Non-heme diiron monooxygenases often exhibit a peroxide shunt pathway, which can be exploited to bypass the native electron transport chain necessary for *in vivo* catalysis. For initial screening of synthetic substrate-surrogates, TLC was used to qualitatively observe the formation of hydroxylated products and decay of the starting material. Using this method, preliminary assays were performed to determine if the ms²i⁶A₃₇ substrate-analogues [2-isopentylamine hydrochloride (**2.2**), 2-chloro-N⁶-isopentyl-purine (**2.3c**), 2-chloro-N⁶-

isopentenyl-adenosine (**2.5c**) were hydroxylated by MiaE in the presence of hydrogen peroxide (20 mM). As a control, duplicate samples were prepared in the absence of MiaE to verify that the observed products were not the result of direct oxidation by H₂O₂. An additional control sample was prepared using heat-denatured MiaE. In these preliminary assays, complex **2.2** showed no obvious sign of decay with MiaE over the course of the experiment (1 hour), and the limited solubility of complex **2.3c** made analysis impossible. However, complex **2.5c** showed an obvious decay with time and concomitant formation of a new spot (Figure 2-7). Moreover, the R_F-value (0.18) for this new spot correlates with that of the synthesized 2-chloro-N⁶-((*E*)-4-hydroxyisopentenyl)-adenosine (**2.8c**). Preparatory TLC and high resolution mass spectral analysis indicated a mass equivalent to expected product [HRMS (EI) found 386.1231 *m/z*; calculated 386.1153 Da]. No products were observed in control samples within the time scale of these reactions.

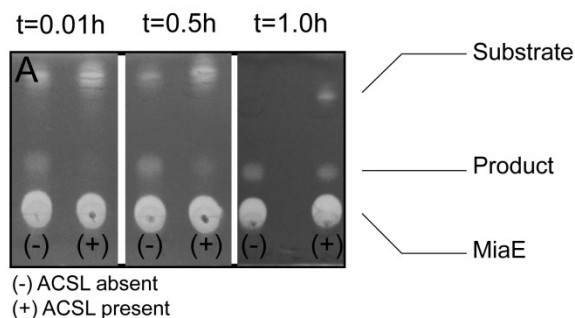


Figure 2-7 TLC qualitative substrate screening

Qualitative substrate screening was performed by thin layer chromatography (TLC) to analyze product formation. TLC indicates loss of substrate **2.5c** and appearance of MiaE hydroxylated product with time. Product formation was also investigated with and without the addition of the ACSL^{Trp}, indicated by (+) and (-) respectively. TLC stained in KMnO₄ to aid in qualitative analysis.

To confirm that the MiaE hydroxylated product corresponds to the synthetic (**2.8c**) product, spike assays were performed in which the synthetic product was added into samples taken from the *in vitro* MiaE assay. As with the experiments described above, control experiments performed in the absence of MiaE or utilizing heat-denatured MiaE

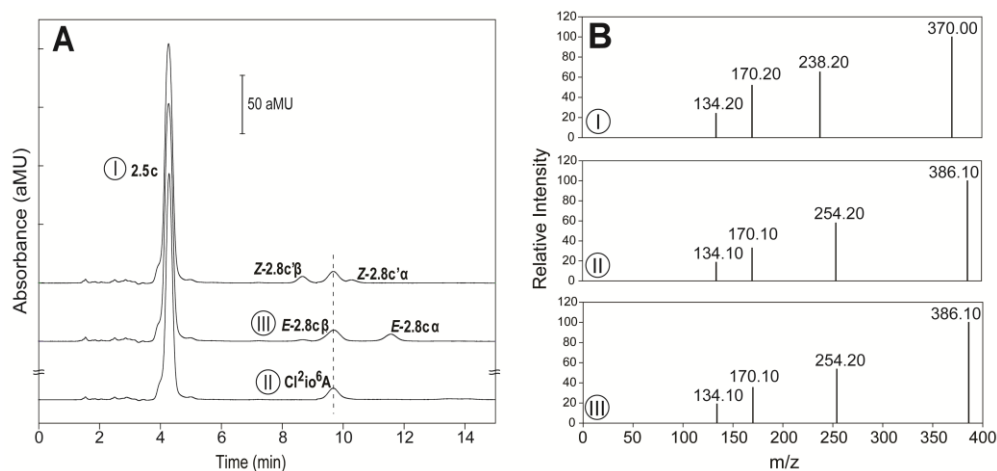


Figure 2-8 HPLC chromatogram of product formation and stereochemistry (A) HILIC chromatogram of product formation, along with spike analysis to verify structure and stereochemistry. Bottom chromatogram represents *in vitro* enzymatic assay. Middle chromatogram represents the spike addition of **E-2.8c** diastereomeric mixture. Top chromatogram represents the spike addition of **Z-2.8c** diastereomeric mixture. The product of the MiaE transformation correlates with the β -epimer of the **E-2.8c** stereoisomer as indicated by overlapping retention time (*dashed line*) and an increase in the **E-2.8c** β peak area upon spike addition. (B) LC-MS/MS spectra of MRM transitions of designated product ions. The top panel (I) represents the substrate **2.5c**, while the middle panel (II) represents the enzymatic product (both obtained by direct injection of *in vitro* assay). The bottom panel (III) represents the synthetic product standard **E-2.8c**.

showed no detectable peaks corresponding to **2.8c** formation. Figure 2-8A (*bottom*) shows a representative chromatogram obtained from the MiaE assay. The larger peak observed at a retention time of 4.32 min corresponds to the enantiomerically pure β -substrate (**2.5c**) whereas the MiaE hydroxylated product is observed at 9.70 minutes. For clarity, these peaks are designated I and II, respectively.

The two remaining chromatograms in Figure 2-8A represent the same MiaE assay sample in which a diastereomeric mixture of α/β *E*-**2.8c** (*middle*) and *Z*-**2.8c** (*top*) was added to the sample. In addition to the peak corresponding to substrate (**2.5c**), two additional peaks are observed in the middle chromatogram at 9.70 and 11.69 min corresponding to the β - and α -diastereomers of *E*-**2.8c**, respectively. The peak corresponding to the β -epimer of the synthetic *E*-**2.8c** is designated by III. For comparison, addition of the diastereomeric mixture of *Z*-**2.8c** (α -epimer, 10.16; and β -epimer, 8.64 minutes) is shown in the top chromatogram of Figure 2-8A. Given that an enantiomerically pure substrate was utilized in enzymatic reactions, the observed increase in peak area of the *E*-**2.8c** β -enantiomer with spike addition, along with the overlapping retention time (*dashed line*), strongly supports assignment of the MiaE product (β -**2.8c**) and *E*-stereochemistry. Representative chromatograms of product standards *E*-**2.8c** and *Z*-**2.8c**, along with selected enzymatic assays utilizing substrate **2.5c**, are provided in Figure 2-9. For all substrates assayed (**2.5a-c**), no more than 2% of the hydroxylated *Z*-product was ever observed within the time scale of peroxide-shunt assays.

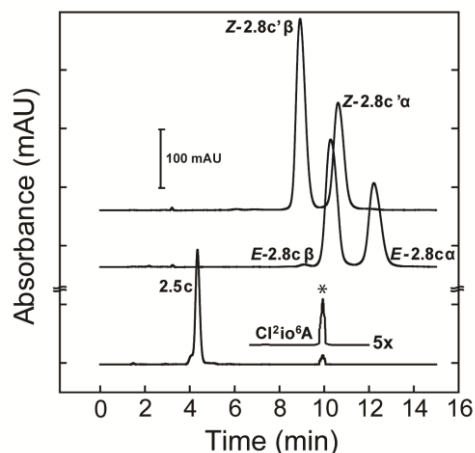


Figure 2-9 HILIC chromatogram of *E/Z* product standards

Diastereomeric mixtures of both *E-2.8c* and *Z-2.8'c* standards were analyzed by HILIC chromatography alongside enzymatic assay of **2.5c** in order to evaluate stereoselectivity. Top line represents *Z-2.8'c*, middle line represents *E-2.8c*, and bottom chromatograph represents an enzymatic assay. Chromatogram indicates similar retention times of enzymatic product and the *E-2.8c* standard.

In all aforementioned assays, enantiomerically pure substrate (β) was utilized, which left the question of configurational specificity. To investigate MiaE selectivity regarding β -epimer versus α -epimer confirmation, enantiomerically pure α -substrate was submitted to assay conditions. Product formation of the α -hydroxylated epimer was detected by reverse phase C18 HPLC. As indicated in Table 2-1, MiaE also hydroxylated the α -confirmer. A diastereomeric mixture of α/β -**2.5a** was also evaluated, and, within error, both α - and β -epimers (**2.5a-c**) were hydroxylated at comparable rates (Table 2-1).

Table 2-1 α/β substrate hydroxylation

α -epimer	retention time (min)	peak area
α -5a	62.013	110.2889
α -ms ² io ⁶ A	54.947	16.2215

α/β mixture	retention time (min)	peak area
α -5a	62.007	103.505
β -5a	61.667	168.6368
α -ms ² io ⁶ A	54.941	17.9272
β -ms ² io ⁶ A	54.013	22.8308

As final verification of *MiaE* hydroxylated product, LC-MS/MS was performed on the peaks designated I, II, and III using MRM transitions of respective product ions as described in *Materials and Methods*. The top panel (I) Figure 2-8B represents the substrate **2.5c** mass spectrum (370 m/z molecular ion), whereas the middle and bottom panels represents the mass spectrum obtained from the enzymatic product (II) and synthetic β -epimer *E*-**2.8c** standard (III), respectively. The molecular ion (M^+) is observed in each, with an increase of 16 (hydroxyl ion) in both the enzymatic product (II) and product standard (III) [$M^+ = 386.1$ m/z]. The m/z 238 of **2.5c**, along with the m/z 254 of enzymatic product and *E*-**2.8c** is the result of the ribose cleavage and thus also exhibit an increase in mass by 16 m/z consistent with hydroxylation. The m/z 170 fragment is a result of isopentenyl cleavage, followed by m/z 134 representing a loss of HCl. In light of the matching fragmentation patterns and relative intensities obtained for *MiaE* product (II) and the synthetic product standard *E*-**2.8c** (III), the increase in molecular ion by 16 m/z, and overlapping retention times obtained in spike assays described above, it appears that the *MiaE* hydroxylated product generated by peroxide shunt assays can be attributed to *E*-Cl²io⁶A.

Optimal concentration of H₂O₂ for MiaE peroxide-shunt assays was determined by the method of isolation. In these experiments, the concentration of substrate **2.5c** was fixed (5.8 mM) while H₂O₂ concentrations were varied from 5 to 50 mM. The reaction was initiated by addition of 100 μM MiaE (Fe₂-sites) at 27 °C. At selected time points (1-9 min), sample aliquots were removed for heat inactivation (95 °C for 1 minute) and spin-filtered to remove denatured protein as described in *Materials and Methods*. Figure 2-10 shows the initial rate ($v_0/[E]$) of product (Cl²io⁶A) produced as a function of initial hydrogen peroxide concentration. As with the catalase assays full saturation of MiaE is never observed within the concentration range utilized for these experiments (1-50 mM). Since visible signs of protein denaturation were observed at H₂O₂ concentrations ~40 mM, the decrease in $v_0/[E]$ observed is likely due to enzymatic degradation and not substrate saturation. Therefore, 30 mM H₂O₂ was used for subsequent assays.

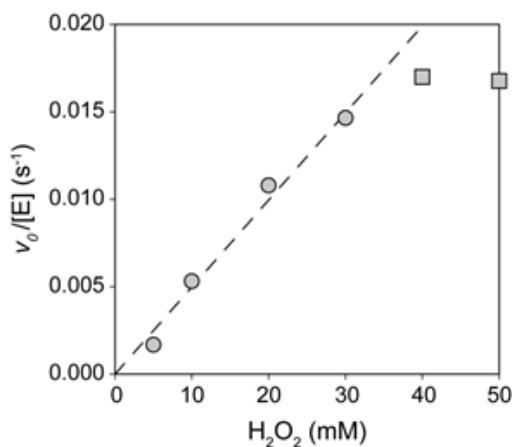


Figure 2-10 Initial rate of Cl²io⁶A formation with increasing H₂O₂ concentration
 Enzyme normalized initial rate ($v_0/[E]$) of Cl²io⁶A formation with increasing H₂O₂ concentration. The pseudo-second order rate constant was determined by linear regression (*dashed line*; $k_{obs} = 5.0 \text{ M}^{-1}\cdot\text{s}^{-1}$). Assay conditions: 100 μM MiaE, 5.8 mM **2.5c**, 25 mM HEPES, 50 mM NaCl, pH 8, H₂O₂ (5-50 mM).

As illustrated in Figure 2-11, the rate of substrate (**2.5c**) degradation (●) at 30 mM H₂O₂ is kinetically matched to the rate of product (Cl²io⁶A) formation (■). Moreover, in the absence of MiaE (Figure 2-11, Δ), no decay of **2.5c** (or formation of Cl²io⁶A) can be observed within the time scale of these experiments. This observation indicates that H₂O₂ cannot (by itself) specifically oxidize the substrate and that product decay and substrate formation are coupled (1:1 stoichiometry) within the MiaE peroxide-shunt assay. By contrast, given the low-level catalase activity of MiaE it is unlikely that the stoichiometry of H₂O₂ consumed per mol of product is closely matched.

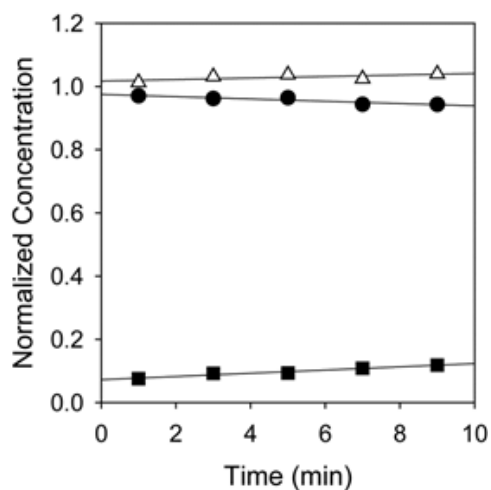


Figure 2-11 Stoichiometric coupling of product formation with substrate consumption. Stoichiometric coupling of **2.5c** decay (●) and Cl²io⁶A formation (■) in Mia peroxide shunt pathway. Within error, the rate of substrate decay and product formation is kinetically matched (0.01 min⁻¹). The control of **2.5c** in the absence of MiaE (Δ, H₂O₂ only) is overlaid for comparison. Assay conditions: 100 μM MiaE, 5.8 mM **2.5c**, 30 mM H₂O₂, 25 mM HEPES, 50 mM NaCl, 15-20 % DMSO (v/v), pH 8.

Hydroxylation of substrate-surrogates by electron transport catalysis. While the peroxide-shunt pathway removes the need for an external electron source, such

reactions are frequently slower and exhibit decreased chemo- and stereoselectivity as compared to reactions utilizing a functional electron transport chain. Therefore, in order to better understand the physiologically relevant MiaE catalytic system, a functional electron transport chain was constructed on the basis of what has worked previously with the soluble stearyl-ACP Δ^9 -desaturase (Figure 2-12).^{78,79} In these reactions, NADPH is utilized as the terminal electron source and then ferredoxin reductase (FdR) and ferredoxin (Fd) are utilized to provide an electron transport chain (ETC) to shuttle electrons from NADPH to the diiron active site of MiaE. The catalyzed hydroxylation of

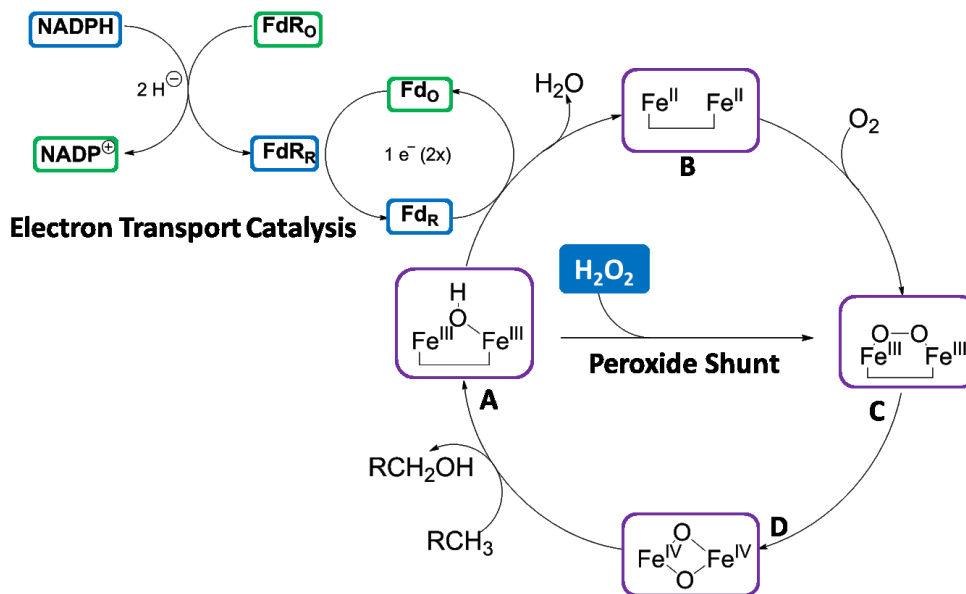


Figure 2-12 Electron transport catalysis

In order to accomplish catalytic turnover under native catalysis, an electron source, along with a oxidoreductase, is necessary. NADPH is utilized as the terminal electron source and ferredoxin reductase (FdR) and ferredoxin (Fd) are utilized to provide an electron transport chain (ETC) to shuttle electrons from NADPH to the diiron active site of MiaE.

free i^6A nucleoside is vastly slower when compared to the larger MiaA modified i^6A -ASCL^{Trp} construct.³² As shown in the inset of Figure 2-13B, like the peroxide-shunt assays, full substrate saturation of MiaE is never observed within the solubility limit of the nucleoside (~5 mM). However, from the slope of the line, the pseudo-second order rate constant (approximately k_{cat}/K_m) can be determined ($1.9 \pm 0.1 \text{ M}^{-1}\text{s}^{-1}$). By comparison to the V/K determined for i^6A -ACSL substrate, $\sim 11,000 \text{ M}^{-1}\text{s}^{-1}$ (Figure 2-13B), a nearly 6,000-fold increase in enzymatic efficiency is imparted by reactions containing the 17 nucleotide i^6A -ASCL^{Trp} as compared to the free i^6A nucleoside (**2.5b**).³² As with peroxide-shunt assays reported, the product of (Fd/FdR-ETC) steady-state assays retains nearly stoichiometric (>98%) *E*-stereoselectivity. To our knowledge, this represents the first instance of steady-state kinetic values reported for any MiaE enzyme.

Substrate-Analogue Study. MiaE specificity for synthetic substrate-analogues (**2.5a-c**) was determined using the method of isolation as described above. However, in these experiments the hydrogen peroxide concentration was fixed at 30 mM while varying the concentration of nucleosides (**2.5a-c**). Given the low solubility of synthetic nucleosides (**2.5b** in particular), dimethyl sulfoxide (DMSO) was added to the enzymatic reactions to increase the upper limit of substrate concentration. Control reactions containing up to 20% (v/v) DMSO showed no effect on the rate of Cl^2i^6A formation by MiaE peroxide shunt. Only at DMSO concentrations exceeding 25% (v/v) was a noticeable decrease observed in the rate of peroxide-shunt product hydrolysis. Therefore, all of the enzymatic assays described below were carried out in the standard HEPES buffer with 20% DMSO (v/v).

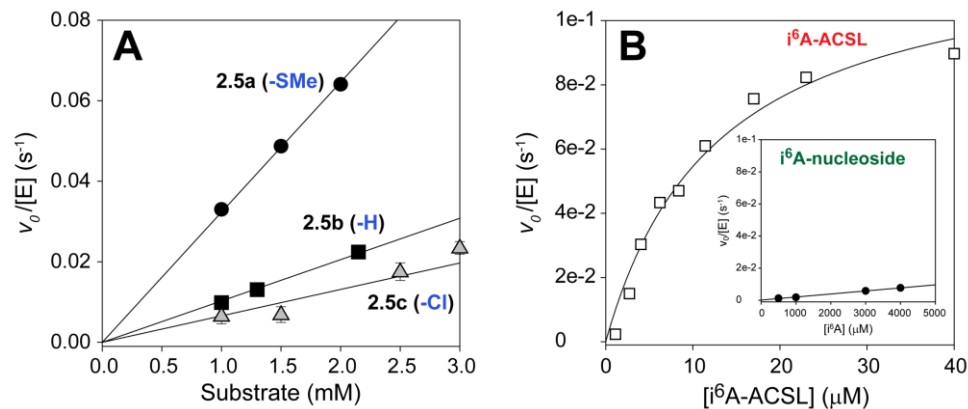


Figure 2-13 Steady state kinetics by peroxide-shunt (A) and ETC (B)

(A) Enzyme normalized initial rate ($v_0/[E]$) of product (ms^2i^6A , io^6A , and Cl^2i^6A) formation with increasing substrate concentration. The pseudo-second order rate constant for **2.5a** (\bullet , -SMe), **2.5b** (\blacksquare , -H), and **2.5c** (Δ , -Cl) was determined by linear regression to be 32.3, 10.3, and 6.6 $M^{-1}\cdot s^{-1}$, respectively. Assay conditions: 100 μM MiaE, 30 mM H_2O_2 , 25 mM HEPES, 50 mM NaCl, 15-20 % DMSO (v/v), pH 8, **2.5a-c** (1-3 mM). (B) Hydroxylation of i^6A -ACSL (MiaA modified ACSL^{Trp}) utilizing electron transfer catalysis (ETC) was $\sim 6,000$ -fold more efficient than ETC of synthetic nucleoside i^6A (**2.5b**).

For each assay, the concentration of substrate analogue was varied from 0.5-4 mM (depending on solubility) at fixed H_2O_2 concentration (30 mM). As previously stated, reactions were initiated by addition of 100 μM MiaE (Fe_2 -sites) at 27 $^{\circ}C$ and sample aliquots were taken at times ranging from 1 - 9 minutes. HPLC sample preparation was carried out as described previously. Figure 2-13A shows the initial rate of product formation (ms^2i^6A , io^6A , and Cl^2i^6A) plotted against the starting concentration of each substrate (**2.5a-c**) analogue. Each substrate saturation kinetic experiments were

performed in duplicate. For clarity, only the error observed in the initial rate of **2.8c** formation is indicated in Figure 2-13A.

As expected, the initial rate of product formation increases to a maximal value with increasing substrate concentration. However, at elevated concentrations, the rate of product formation decreases significantly for each nucleoside suggesting something analogous to substrate-inhibition or decreased enzyme activity near the solubility limit of the synthetic nucleosides (**2.5a-c**). Given the complexity of this system, development of a full kinetic model is complicated and prone to over-interpretation. However, as with H₂O₂ saturation experiments, comparison of initial rates within the linear range (1-3 mM) can be made. A plot of the initial rate of product formation (**2.8a-c**) versus substrate concentration is shown in Figure 2-13A. As in H₂O₂-saturation experiments, all initial rates are normalized for enzyme concentration ($v_0/[E]$). At fixed H₂O₂ concentration (30 mM), the slope of the line can be interpreted as the pseudo-second order rate constant (approximately k_{cat}/K_m). On the basis of this interpretation, the rate MiaE catalyzed H₂O₂-shunt hydroxylation for **2.5a** (SMe), **2.5b** (H), and **2.5c** (Cl) can be estimated as 32.3, 10.3, and 6.6 M⁻¹·s⁻¹, respectively.

2.3 Discussion

Nucleoside substrate synthesis. A divergent synthetic strategy led to the preparation of three nucleoside mimics with varied functionalization at the C2-position, 2-SMe (ms²i⁶A), 2-H (i⁶A), and 2-Cl (Cl²i⁶A). Additionally, two diastereomers of each expected oxidized product were prepared, giving rise to six additional nucleosides (*E/Z*-ms²io⁶A, (*E/Z*)-io⁶A, and (*E/Z*)-Cl²io⁶A). The Vorrbrüggen coupling of the purine derivatives to tetraacetylribose provided a metal-free preparation, and resulted in comparable yields.⁸⁰⁻⁸² The nucleosides were synthesized in eleven or fewer steps from commercially available materials and with 10-15% overall yield. As discussed below, the

synthesis of these nucleosides allowed for the stereochemical determination of the MiaE modified product (*E*-ms²io⁶A), along with the overall effect of the C2-functionalization on rate of product formation.

Characteristics of S. typhimurium MiaE. The monomeric (α) configuration of MiaE reported here is in agreement with previous reports.²³ This trait is quite unusual for non-heme diiron enzymes and, to our knowledge, has only been reported for the non-enzymatic member of this family, hemerythrin (Hr).⁸³⁻⁸⁵ Typically, the quaternary structures of non-heme diiron enzymes are multimeric in their native form.⁴⁹ In fact, the most common quaternary structure observed for this family of enzymes is homodimeric (α_2). Whereas, the most common structural motif observed among the hydroxylase components within the BMM class of non-heme diiron monooxygenases is a heterotrimeric dimer ($\alpha\beta\gamma$)₂ configuration.⁵⁰ Interestingly, both R2 and Δ 9D have been reported to exhibit 'half-sites' reactivity, implying that the two protomers of these (α_2)-enzymes do not act independently during catalysis.^{79,86-88} Historically, both the structural complexity and the potential for 'half-sites' reactivity within this class of enzymes have significantly complicated the spectroscopic and mechanistic characterization of non-heme diiron enzymes. Therefore the monomeric (α) protein configuration of MiaE represents a minimalist enzymatic structure which could potentially provide a unique point of comparison to other enzymes within this class.

Hydroxylation of substrate-surrogates. It has been demonstrated in previous literature that peroxide-shunt catalysis is frequently slower and exhibits decreased chemo- and stereoselectivity as compared to reactions utilizing a functional electron transport chain.^{33,41,42} In order to compare the two catalytic cycles, and to better understand the physiologically relevant MiaE catalytic system, a functional electron transport chain was constructed.³² Both the peroxide-shunt and electron transport

hydroxylation of the free i^6A nucleoside progressed at comparable rates and resulted in identical selectivity. However, the catalyzed hydroxylation of free i^6A nucleoside is vastly slower when compared to the larger i^6A -ACSL construct.³² By comparison to the V/K determined for i^6A -ACSL substrates, a nearly 6,000-fold increase in enzymatic efficiency is imparted by reactions containing the 17 nucleotide ACSL^{Trp} as compared to the free i^6A nucleoside. When considering the energy associated, it is apparent that this vast increase in efficiency is due to more than binding interactions alone. Several spectroscopic evaluations of MiaE in the presence of substrate have sense been performed.³² CD, EPR, and Mössbauer spectroscopic analysis demonstrates a conformational change upon ACSL addition; however, synthetic nucleosides were unable to elicit the same response.³² This then suggests that the binding of the ACSL may act as an effector protein, which alters the conformation of the enzyme, aiding in electron delivery to the diiron center. Further investigation of substrate-gated electron delivery to the active site is underway.

MiaE substrate specificity influenced by C2-position substitution of nucleoside.

Initial attempts to demonstrate MiaE hydroxylation of the free purine (substrates **2.3a-c**) were not successful given the insolubility of the base in the absence of ribose. Interestingly, within error both α - and β -epimers (**2.5a-c**) were hydroxylated at comparable rates. This observation suggests that the ribose ring does not represent a significant enzyme-substrate point of interaction. Furthermore, since the C2-position of the nucleoside is quite distant from the point of enzymatic hydroxylation, given the observed difference in second order reaction rate [**2.5a** (SMe) > **2.5b** (H) > **2.5c** (Cl)], it is reasonable to speculate that the nucleosides C2-substituent significantly influences the MiaE binding affinity. For example, at a fixed substrate concentration (2.0 mM), the rate of **2.5a**-hydroxylation is over three-fold that of **2.5b**-hydroxylation. Interestingly, a similar

substrate preference has also been observed for ms^2i^6A - and i^6A -bearing tRNA substrates.²⁷ Therefore, it is possible that the enzymatic substrate specificity is largely a function of the nucleoside base and not due to the conformational difference within the global tRNA tertiary structure.

(E/Z)-stereochemistry of MiaE hydroxylated products (io^6A , Cl^2io^6A , and ms^2io^6A). The peroxide-shunt pathway is a common feature among non-heme diiron (and heme) oxygenase enzymes.^{41,42,57,89} The use of a peroxide-shunt simplifies the enzymatic catalysis by removing the need for an enzymatic electron-transfer pathway. However, peroxide-shunt enzymatic activities are significantly lower than native catalysis due to the competing catalase-activity, and the potential for promiscuous Fenton-type reactions leading to enzymatic degradation. Therefore, peroxide-shunt experiments should be considered diagnostic of native MiaE catalysis, but are less useful for the development of a kinetic mechanism. Additionally, relative to reactions catalyzed in the presence of their electron-transfer chain, many non-heme oxygenases exhibit decreased stereo- and chemoselectivity by peroxide-shunt.^{33,41,42} For instance, it was found that, in the presence of protein B, MMOH demonstrates a 3-fold greater selectivity in the presence of dioxygen relative to peroxide-shunt induction.³³ By contrast, MiaE peroxide-shunt demonstrates a clear stereospecificity in that only the (*E*)-isomer of the hydroxylated nucleosides (**2.8a-c**) are observed. Indeed, for all substrate analyses, < 2% of the (*Z*)-isomer was ever identified in peroxide-shunt reactions. As with peroxide-shunt assays reported, the product of (Fd/FdR-ETC) steady-state assays retains nearly stoichiometric (>98%) *E*-stereoselectivity. Moreover, as illustrated in Figure 2-5, *in vivo* product formation during MiaE IPTG-induction is also consistent with the (*E*)-isomer of ms^2io^6A . Thus the peroxide-shunt MiaE product is consistent with native catalysis. This result was not readily anticipated given discrepancies within the literature regarding the

stereochemistry of $ms^2io^6A_{37}$ isolated across phylogenetic domains. For example, early on it was reported that $ms^2io^6A_{37}$ isolated from plants exhibited (Z)-stereochemistry. Interestingly, in this same report it was observed that the (E)-isomer of io^6A_{37} could be isolated as a free-base³⁰. Thus, suggesting the possibility of an independent pathway for cytokinin synthesis independent of MiaE. Alternatively, this observation may simply be the result of E/Z-isomerization. Regardless, this hypothesis was never explored further. Among bacterial enzymes, it was reported that Z- $ms^2io^6A_{37}$ was the MiaE-product observed from various plant-associated bacteria (*Rhizobium leguminosarum*, *Agrobacterium tumefaciens*, and *Corynebacterium fascians*).³¹ The first instance of E- $ms^2io^6A_{37}$ was reported by Ajitkumar and Cherayil for the non-plant associated γ -proteobacteria, *Azotobacter vinelandii*.²⁸ Based on this observation it was proposed that other non-plant associated bacteria (such as *Salmonella typhimurium*) may also produce the (E)- instead of the (Z)-isomer. This is perhaps a tenuous hypothesis given only 58% identity between *S. typhimurium* and *A. vinelandii* MiaE. To our knowledge, this work represents the first direct confirmation of the *S. typhimurium* MiaE stereospecificity.

Chapter 3

Synthetic Spin-labeling Strategy for Enzymatic Characterization

Since the discovery of idoxuridine, the first anti-viral nucleoside drug (Figure 3-1, first compound),⁴³ nucleosides and their derivatives have gained considerable attention. Nucleoside analogs are now used in pharmaceuticals as anti-cancer, antiviral and immunosuppressant drugs,⁴⁴ agrochemistry as herbicides and insecticides,⁹⁰ and biotechnology in DNA sequencing and enzymology.⁴⁵ The intricate structures of many nucleoside natural products have also made them interesting targets for total synthesis.^{91,92} As the employment of nucleoside derivatives increases, providing biomolecular and small molecule tools will be important for investigating and understanding the molecular targets and mechanisms of physiological action.

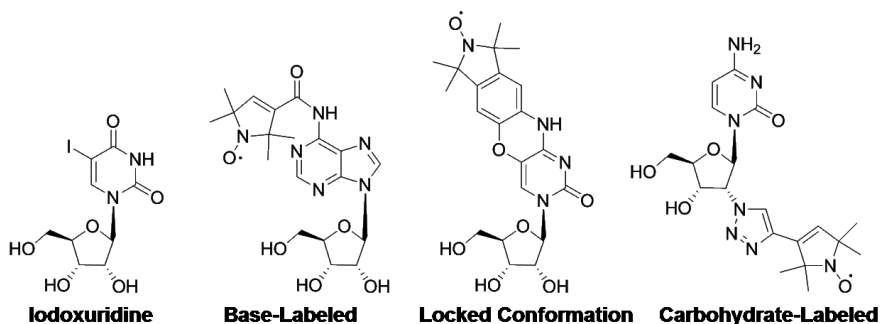


Figure 3-1 Idoxuridine and common nitroxyl labeled nucleosides

The application of spin-labels to interrogate a variety of structures, exemplified by the nitroxyl radical, has gained popularity within the last two decades, especially biological sciences, to gain insight into structure, function, and biomolecular interactions. The nitroxyl radical is generally covalently bound to the biologically active molecule to generate a functional spin probe (Figure 3-1), and changes in the electronic environment, such as the binding of an effector protein or substrate, are monitored by electron paramagnetic resonance (EPR) spectroscopy. Beyond gaining information on

macromolecular characteristics proximal to site of spin-labeled attachment, EPR techniques (such as double electron-electron resonance (DEER) or pulsed electron-electron double resonance (PELDOR)) can be used to measure long range interactions of two paramagnetic species up to 25 Å apart.⁹³ Changes in distance can also be followed by EPR on the submillisecond time scale, which can provide insight into conformational alterations.⁹⁴ While the incorporation of spin-labels onto proteins and lipids has vastly evolved over the decades (site-directed spin labeling, SDSL), the synthesis of spin-labeled nucleosides still lacks efficiency and diversity. The majority of nitroxyl labels are attached to the purine or pyrimidine base of the nucleoside,^{95,96} or at the 2'-position of the carbohydrate moiety (represented in Figure 3-1).⁹⁷ While these designs have their uses, they are restricted when investigating biomolecular interactions involving binding of the nucleoside base, and limit the variety of enzymes which may be investigated. Due to these limitations, it would be advantageous to develop alternative labeling positions to minimize undesired interactions.

Here, we demonstrate the total synthesis of 5'-carbohydrate spin-labeled nucleosides, retrosynthetically demonstrated in Figure 3-2. The synthetic strategy targets the smooth coupling of three subunits (base, ribose, and spin-label) so that the methodology may be easily used for the investigation of a wide range of biomolecular targets. By incorporating the 5'-azido modified ribofuranose, post-synthetic spin-labeling is possible, allowing for oligonucleotide synthesis followed by site-directed labeling. The tetrazole produced through click-ligation increases rigidity in the spin system, diminishing EPR spectral broadening, allowing for increased sensitivity towards minute changes. To demonstrate utility, the tertiary interactions of T7 RNA polymerase will be analyzed upon binding to 5'- carbohydrate spin labeled guanosine.

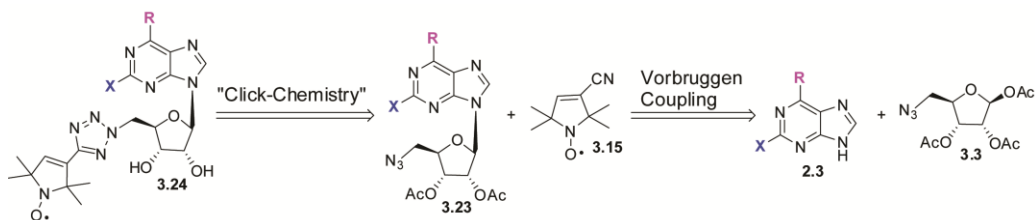


Figure 3-2 Retrosynthetic analysis of spin-labeled nucleoside

3.1 Materials and Methods

Synthesis of carbohydrate moiety. 1,2,3-Tri-O-acetyl-5-azido-5-deoxy-D-ribofuranose **3.3** was synthesized through regioselective protecting group methodology (Figure 3-3).⁹⁸ The 5'-hydroxyl was selectively tritylated by maintaining a temperature below 30 °C, followed by acetylation of the remaining hydroxyl groups, giving compound **3.1**. The 5'-position was then selectively deprotected, which was unexpectedly difficult due to intramolecular acyl migration from the 2'-position to the 5'-position. A number of conditions were evaluated in an attempt to decrease percentage of acyl-migration (Table 3-1). Moderate yield with little migration was achieved in formic acid and ether (3:2 ratio, 0.5 M), while monitoring temperature.⁹⁹ Lastly, the primary alcohol was mesylated,

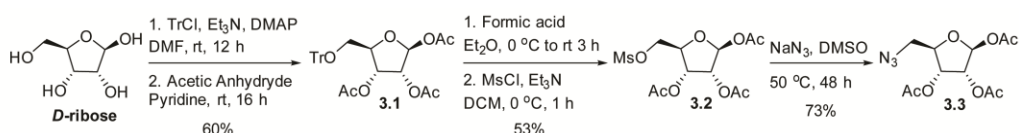


Figure 3-3 1,2,3-Tri-O-acetyl-5-azido-5-deoxy-D-ribofuranose (**3.3**) synthesis

priming the hydroxyl group for nucleophilic displacement by sodium azide, giving azido-ribose **3.3** in five steps. Reduction of the azide to the amine was attempted in order to achieve nucleophilic coupling between the carbohydrate and spin-label; however upon reduction, the tetrahydrofuran rearranged to the piperidine. This rearrangement could be

due to the nucleophilicity of nitrogen, along with the equilibrium that exists between furanose and pyranose, with pyranose formation favored in polar solvents.¹⁰⁰

Table 3-1 Detritylation conditions

Conditions	Time (hr)	Temperature	Yield (%)
1.5 eq TsOH, 1 M MeOH	3	0 °C to rt	<5
2 eq FeCl ₃ *6H ₂ O, 0.05 M DCM	24	rt	<5
Formic Acid:EtOAc (2:3, 0.2 M)	12	rt	<5
Formic Acid:Ether (1:1, 0.2 M)	9	rt	68 ^a
Formic Acid:Ether (3:2, 0.5 M)	3	rt	70 ^a
Formic Acid:Ether (3:2, 0.5 M)	3	0 °C to rt	80
Formic Acid:Ether (3:2, 0.75 M)	3	0 °C to rt	70
Formic Acid:Ether (3:2, 0.85 M)	3	0 °C to rt	75 ^a
Formic Acid:Ether (3:2, 1.0 M)	3	0 °C to rt	56 ^a

a: Acyl migration observed

Synthesis of nitroxyl spin-label. In order to ensure the coupling partners react selectively without interference of biological functionality, we focused on two main ligation reactions: Staudinger ligation, and Huisgen 1,3-dipolar cycloaddition (“click”-ligation). A divergent synthetic strategy was used to synthesize numerous nitroxyl spin-labels in order to evaluate the ligation step (Figure 3-4). First, commercially available 2,2,6,6-tetramethyl-4-piperidone was di-brominated, giving 3,5-dibromo-2,2,6,6-tetramethyl-4-piperidone hydrobromide (**3.4**). Favorskii rearrangement with sodium methoxide in methanol afforded the corresponding α,β -unsaturated ester **3.5**. The rearrangement can be applied to other alkoxides, yielding numerous esters in good yield.¹⁰¹ Ammonium hydroxide was also employed in the rearrangement to achieve the corresponding amide **3.6**.¹⁰² The pyrroline oxidation was then conducted using sodium tungstate in the presence of hydrogen peroxide.¹⁰¹ The oxidation required two aliquot additions of

hydrogen peroxide to aid in full substrate conversion. The second aliquot was generally added after 24 hours. With the ester-radical **3.7** and amide-radical **3.8** in hand, several oxidation states can be easily achieved, leading to a number of diverse coupling partners.

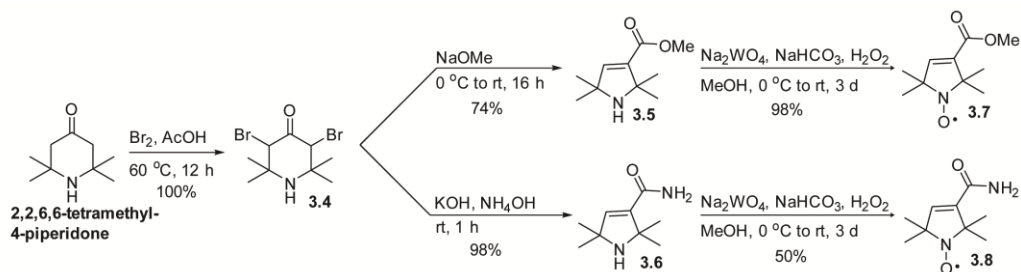


Figure 3-4 Nitroxyl ester **3.7** and amide **3.8** synthesis

Staudinger ligation trials. In an attempt to bypass the intramolecular rearrangement of the carbohydrate moiety upon azide reduction, we hoped to accomplish chemoselective condensation by utilizing traceless Staudinger ligation (Figure 3-5).¹⁰³ First, reduction of the ester with sodium hydroxide afforded the carboxylic acid **3.10**. To synthesize the functionalized phosphine, the pyrroline carboxylic acid was coupled to *o*-diphenylphosphinophenol **3.9**¹⁰⁴ through EDCI (*N*-(3-dimethylaminopropyl)-*N*-ethylcarbodiimide hydrochloride) coupling, affording phosphine **3.11** (Figure 3-5) (see

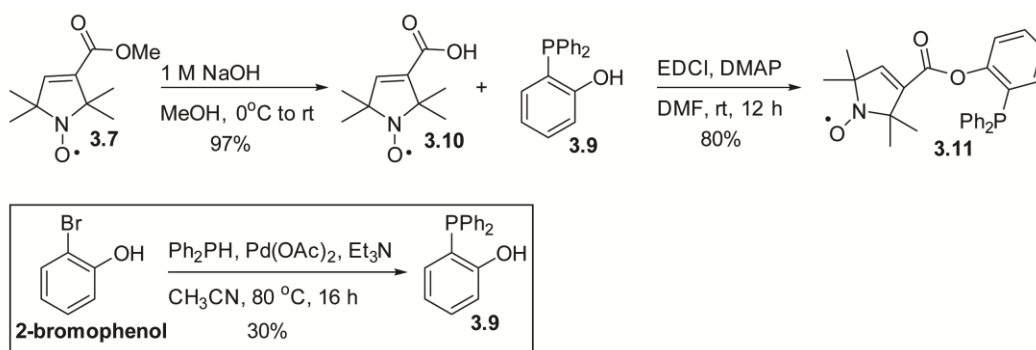


Figure 3-5 Synthesis of functionalized phosphine **3.11**

Chapter 5 for additional methodology). Unfortunately, synthesis of the starting *o*-diphenylphosphinophenol **3.9** (Figure 3-5 inset), along with the functionalized phosphine **3.11**, was not as straightforward as anticipated. Several trials with varying conditions resulted in low yielding product formation for both reactions. Large amounts of by-product formation due to reactant instability, speculatively due to hydrolysis, made purification and analysis impractical.

Nevertheless, coupling of 5'-azido ribose **3.3** with phosphine **3.11** was attempted using Bernardi's methodology in an effort to derivatize phosphine **3.11**¹⁰⁴; however, no product was observed (Figure 3-6), perhaps a result of aza-ylide rearrangement. Structural elucidation of the spin-labeled phosphine **3.11** was never obtained due to poor product yield and degradation. Owing to procedural shortcomings, Staudinger ligation attempts were terminated.

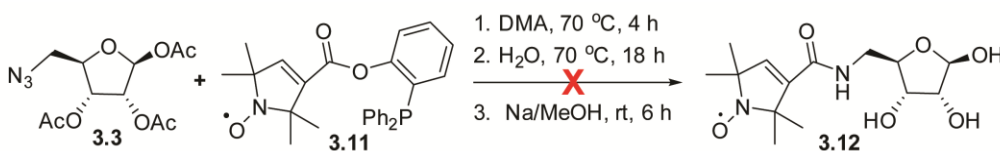


Figure 3-6 Staudinger ligation of azido-ribose **3.3** and phosphine **3.11**

Huisgen 1,3-dipolar cycloaddition trials. Attention was then redirected toward dipolar cycloaddition, or “click”-ligation. The carboxylic acid **3.10** was transformed to the acid chloride, followed by Lewis acid mediated acylation using bis(trimethylsilyl)acetylene. The corresponding alkyne **3.13** was then deprotected to afford alkyne **3.14** (Figure 3-7).¹⁰⁵ However, after reviewing the spectroscopic data, it appears that the alkyne IR stretching frequency $\sim 2100\text{-}2200\text{ cm}^{-1}$ is absent, along with the NMR chemical shift of alkyne ^1H ; therefore, the synthesis of alkyne **3.14**, and possible rearrangement/cyclization, needs to be investigated more thoroughly. Nitrile **3.15** was

synthesized through the dehydration of amide **3.8** using trifluoroacetic anhydride and pyridine (Figure 3-7).¹⁰⁶

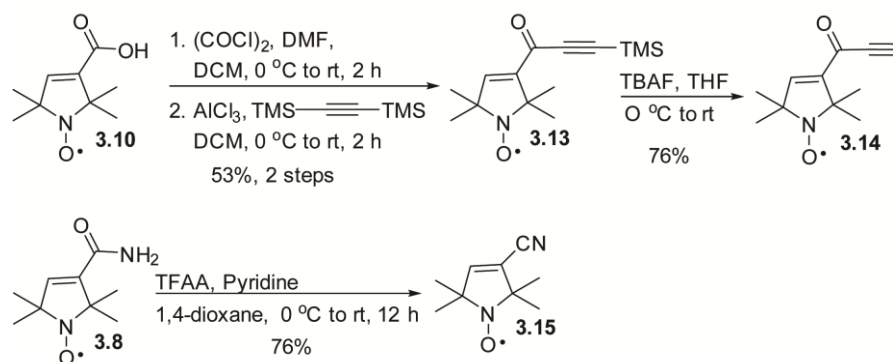
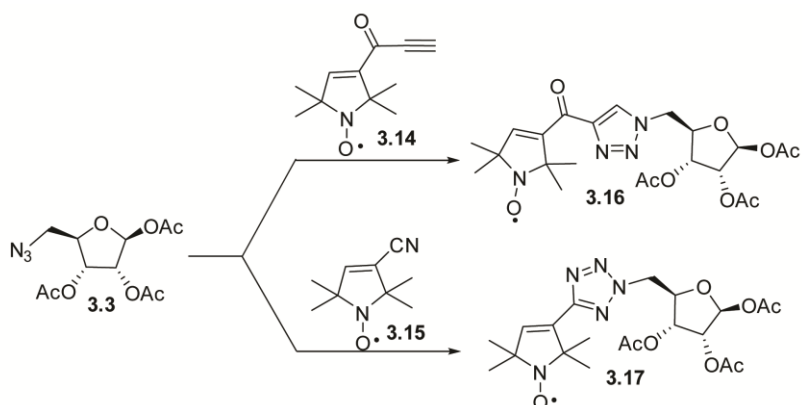


Figure 3-7 Synthesis of alkyne **3.14** and nitrile **3.15**

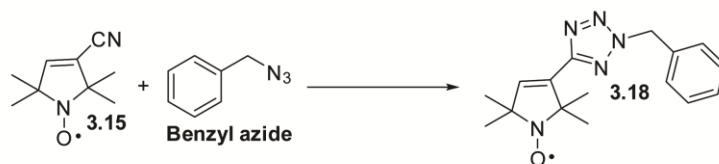
Both the nitrile and alkyne were evaluated under varying ligation conditions (Table 3-2).¹⁰⁷ Due to issues with structural conformation of **3.14**, the alkyne ligation was only attempted under general alkyne ligation conditions. Unfortunately, neither functional group resulted in product formation during acetate protected azido-ribose **3.3** coupling, with the exception of the first entry of Table 3-2, performed at high temperature and resulting in poor yield. To investigate the nitroxyl spin-label's coupling ability, we exchanged the azido ribose for benzyl azide, a very efficient substrate in "click-chemistry". Though nitroxyl spin-labels have previously been shown to undergo cycloaddition,¹⁰⁸ within a few trials (Table 3-3), it became evident that our nitroxyl spin-label was not suitable for [1,3]-cycloaddition. This may be due to a mismatch of functionality located on the 1,3-dipole, azide **3.3**, and the dipolarophile, alkyne **3.14** or nitrile **3.15**.

Table 3-2 Dipolar cycloaddition trials



Reactant	Solvent	Catalyst	Temperature (°C)	Time (hr)	Yield (%)
3.15	Neat	-	120	48	24
3.15	THF	2.5 eq. CuI, DIPEA	25	48	<5
3.14	THF	2.5 eq. CuI, DIPEA	25	48	<5
3.14	Toluene	2.5 eq. CuI, DIPEA	25	48	<5
3.15	DMSO	1.2 eq. CuSO ₄ , NaAsc	80	48	<5
3.15	t-BuOH:H ₂ O (1:2)	1.2 eq. CuSO ₄ , NaAsc	80	48	<5
3.15	DMSO	1.2 eq. Cu(OAc) ₂ , NaAsc	80	48	<5
3.15	t-BuOH:H ₂ O (1:2)	1.2 eq. Cu(OAc) ₂ , NaAsc	80	48	<5
3.15	DMSO	1.2 eq. CuSO ₄ , NaAsc, Na ₂ CO ₃	80	24	<5
3.15	t-BuOH:H ₂ O (1:2)	1.2 eq. CuSO ₄ , NaAsc, Na ₂ CO ₃	80	24	<5
3.15	DCM	10 mol% Cu ₂ (OTf) ₂ * Benzene	60	24	<5

Table 3-3 Benzyle azide dipolar cycloaddition trials



Solvent	Catalyst	Temperature (°C)	Time	Yield (%)
Neat	-	70	1 week	<5
tBuOH:H ₂ O (2:1)	CuSO ₄	60	1 week	<5 ^a
tBuOH:H ₂ O (2:1)	CuSO ₄ , NaAsc	60	48 hrs	<5
Toluene	2.5 eq. CuI, DIPEA	70	4 days	<5

^a: No observed change in starting material

Attention was then directed towards synthesizing a more suitable alkyne (Figure 3-8). Carboxylic acid **3.10** was easily reduced to the corresponding alcohol **3.19** using lithium aluminum hydride in ether. The alcohol was then mesylated, which was immediately displaced through nucleophilic substitution by trimethylsilylacetylene. The resulting alkyne **3.21** was deprotected, giving compound **3.22**. Further cycloaddition trials are currently being pursued.

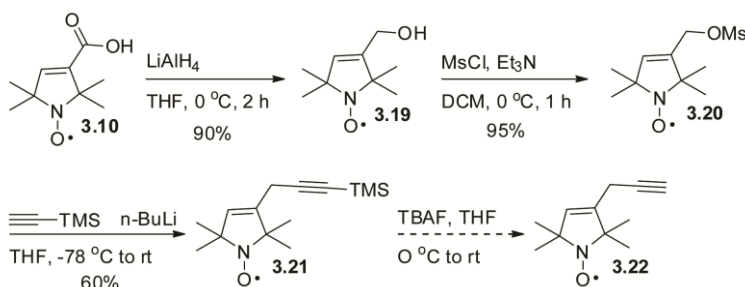


Figure 3-8 Alternative “click”-alkyne synthesis

Free radical NMR spectroscopy. ^1H NMR spectra were recorded on JEOL 300 or 500 MHz spectrometers. In order to obtain ^1H spectrum of radical containing compounds, a reducing agent, phenylhydrazine, was added to a small aliquot of pure sample. Generally, phenylhydrazine (0.1 mmol) was first added to CDCl_3 (0.6 mL). The solution was then added to approximately 10 mg of free radical compound. ^1H NMR was taken immediately. If the solution was allowed to sit for any length of time, a solid white precipitate formed and an increase in byproducts was observed. Thiophenol (0.1 mmol) proved more suitable than phenylhydrazine, however byproducts were still observed within an hour after addition.

EPR spectroscopy. X-band (9 GHz) EPR spectra were recorded on a Bruker (Billerica, MA) EMX Plus spectrometer equipped with a bimodal resonator (Bruker model 4116DM). A modulation frequency of 1 kHz and attenuation of 20 dB at room

temperature was used for all EPR spectra. All experimental data used for spin-quantitation were collected under non-saturating conditions. EPR spectra were simulated and quantified using Spin Count (ver. 3.1.2), written by Professor M. P. Hendrich at Carnegie Mellon University. The simulations were generated with consideration of all intensity factors, both theoretical and experimental, to allow for determination of species concentration. The only unknown factor relating the spin concentration to signal intensity was an instrumental factor that is specific to the microwave detection system. However, this was determined by the spin standard, Cu(EDTA), prepared from a copper atomic absorption standard solution purchased from Sigma-Aldrich. It should also be noted that the calculated concentration based on the EPR spectrum is solvent dependent. When DMSO, dichloromethane, or methanol was used, calculated concentration appeared higher than in aqueous buffer. Due to the observed solvent effect, an organic soluble $[\text{Cu}(\text{Bipy})_3]^{2+}$ standard was made. Briefly, $\text{Cu}(\text{OAc})_2$ (1.0 mmol) was added to 2,2-bipyridine (Bipy, 1.5 mmol) in methanol (7 mL) and stirred overnight. Sample was then diluted to varying molarities for electron calibration. For sample analysis, compounds were dissolved in appropriate solvent to obtain a $\sim 0.5\text{-}1.0\ \mu\text{M}$ solution.

T7 RNA polymerase media and growth conditions. The pAR1219 vector, which carries the gene for T7 RNA polymerase on an ampicillin resistant plasmid, was transformed into chemically competent BL21(DE3) *E. coli* (Novagen) by heat-shock and grown overnight at 37 °C on a Luria Bertani agar plate in the presence of 100 $\mu\text{g}/\text{mL}$ Ampicillin (Amp).¹⁰⁹ The following day, a single colony per flask was selected for growth in liquid LB (Amp) media for training on antibiotic prior to inoculation of two 500 mL cultures, supplemented with 20 mL of 20% glucose and 1 mL of 1 M magnesium sulfate and grown at 37 °C. It should be noted that cell growth was also monitored in M9TB buffer as suggested by literature.^{110,111} M9TB, supplemented with 100 $\mu\text{g}/\text{mL}$ Amp, was

made by mixing 1 L TB (10 g tryptone and 5 g NaCl), 50 mL of 20x M9 (1.5 g KH_2PO_4 , 3 g Na_2HPO_4 , 0.5 g NH_4Cl), 20 ml 20% glucose, and 1 mL 1M MgSO_4 , all autoclaved separately prior to mixing. No difference in cell growth was observed between the LB media verses M9TB media. Cell growth was followed for approximately 4 hours by optical density at 600 nm (OD_{600}). Induction was initiated by addition of 0.5 mM IPTG, 1 mM magnesium sulfate, and 2 g/L casamino acids at an $\text{OD}_{600} \sim 0.6$. Additionally, upon induction the temperature was decreased from 37 °C to 25 °C. After 4 hours, the cells

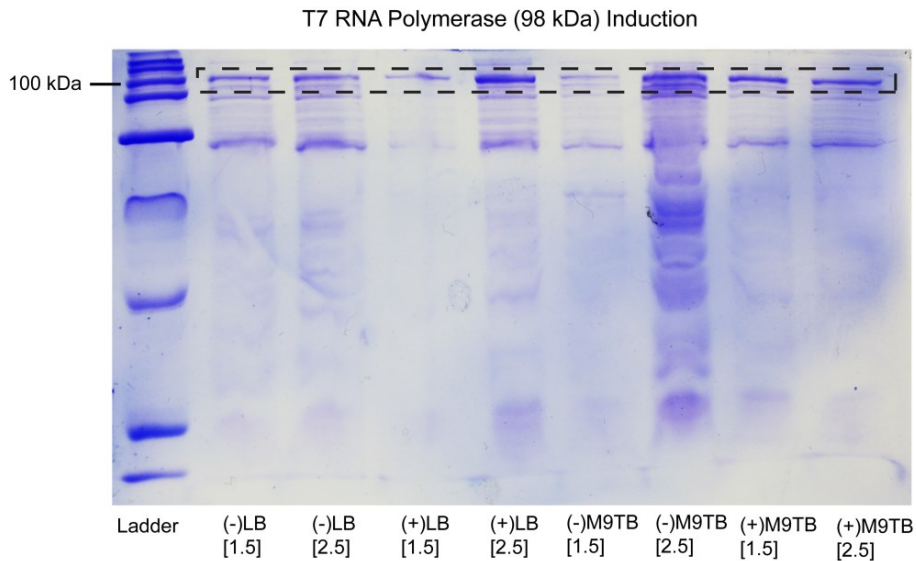


Figure 3-9T7 RNA polymerase expression

T7 RNA induction visualized using SDS-PAGE electrophoresis. The top band, represented by a dashed box, is the expressed RNA polymerase (98 kDa). Lanes labeled (-) are pre-IPTG-induction, while lanes labeled (+) are post-induction. The samples labeled LB were expressed in LB broth, and those labeled M9TB were expressed in M9TB broth. The bracketed numbers represent the concentration of the sample created for the SDS-PAGE gel. In comparing (+)LB [2.5] to (+)M9TB[2.5], there appears to be no difference in amount of T7 RNA polymerase expressed.

were pelleted by centrifugation (Beckman-Coulter Avanti J-E, JA 10.5 rotor) at $18,600 \times g$ for 15 minutes, and the cell paste was stored at $-80\text{ }^{\circ}\text{C}$. Generally 6-7 g of cell paste was obtained. Confirmation of T7 RNA polymerase expression was performed by SDS-PAGE of lysed cells before and after IPTG induction (Figure 3-9).

T7 RNA polymerase protein purification. Approximately 6 g of cell paste was suspended in 24 mL of Tris-HCl buffer (50 mM Tris-HCl, 20mM NaCl, 2 mM EDTA, 1 mM dithiothreitol, pH 8.0). Cell lysis was initiated with the addition of 6 mL fresh egg white lysozyme (1.5 mg/mL in Tris-HCl buffer). Due to T7 RNA polymerase sensitivity to possible proteolysis, phenylmethylsulfonyl fluoride (PMSF, 50 μL of a 20 mg/mL solution in isopropanol) and 50 μL of a protease inhibitor cocktail (supplied by the Mandal laboratory, University of Texas at Arlington) was added as extra precaution. The cell paste was allowed to stand on ice for 20 minutes. 2.5 mL of 0.8% sodium deoxycholate was then added, and suspension was allowed to stand for additional 20 minutes. To complete lysis and decrease viscosity, cell suspension was sonicated in a 30 second on/off pulse cycle for a total of 5 minutes. Ammonium sulfate (5 mL of 2 M solution) and additional Tris-HCl buffer (12 mL) was added, bringing the final volume of lysate to 50 mL. To aid in nucleic acid precipitation, Polymin P (polyethyleneimine, 5 mL of 10% solution, adjusted to pH = 8.0 with concentrated HCl) was slowly added to lysate while stirring on ice. After standing on ice for 20 minutes, precipitate was removed by centrifugation (JA 20 rotor) at $40,000 \times g$ for 20 min at $4\text{ }^{\circ}\text{C}$.

The supernatant was concentrated to $\sim 5\text{ mL}$ via Amicon N_2 stir cell equipped with an YM 30 ultrafiltration membrane, then loaded onto a DEAE Sepharose fast flow column (2 x 15 cm, GE Healthcare 17-0709-01) pre-equilibrated in low salt buffer I (50 mM NaCl, 1 mM EDTA, 10 mM potassium phosphate-monobasic, 5 % glycerol, 10 mM β -mercaptoethanol, pH = 8.0), and set to a flow rate of 1.2 mL/min.¹¹² The protein was

washed with 600 mL low salt buffer I, then eluted by linear NaCl gradient (100 mM to 500 mM NaCl in salt buffer I). The fractions containing the polymerase (97 kDa), determined by SDS-PAGE, were concentrated via Amicon N₂ stir cell equipped with an YM 30 ultrafiltration membrane (Figure 3-10). The concentrated fractions were then loaded onto

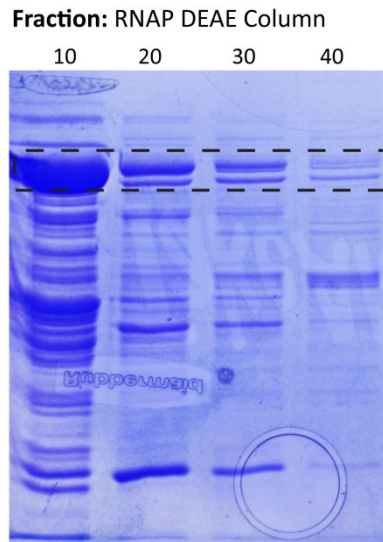


Figure 3-10 T7 RNA polymerase DEAE column purification

Every tenth fraction collected from the DEAE column was analyzed via SDS-PAGE electrophoresis. The dashed box highlights the fractions containing T7 RNA polymerase (97 kDa).

a Cibacron Blue 3GA Agarose, Type 3000 column (Sigma-Aldrich C1285, 2 x 15 cm) pre-equilibrated with buffer II (250 mM NaCl, 1 mM EDTS, 10 mM KH₂PO₄, 1 mM dithiothreitol, 5% glycerol, pH = 8.0) set to a flow rate of 0.8 mL/min. T7 RNA polymerase was washed with 250 mL buffer II, followed by 50 mL of buffer II containing 1 mM ATP and 1 mM GTP, and eluted with 500 mL high salt buffer II (buffer II with 1.5 M NaCl). The polymerase fractions were then pooled and dialyzed against buffer III (100 mM NaCl, 0.1 mM EDTA, 10 mM KHPO₄, 5% glycerol, 1 mM dithiothreitol, pH = 8.0). The purified

enzyme was concentrated, separated into aliquots, and stored in liquid nitrogen dewer. For purified T7 RNA polymerase, an extinction coefficient at 280 nm ($1.40 \times 10^5 \text{ M}^{-1} \text{ cm}^{-1}$) was used to quantify protein samples.

A size exclusion column was also attempted immediately after DEAE column, but to no avail. Briefly, 1000 μL of concentrated fractions from DEAE column were loaded onto a pre-equilibrated (40 mM Tris-HCl, 50 mM NaCl, pH = 8.0) Sephacryl S-100 column (2 x 15 cm). The protein was then eluted with the same buffer at a flow rate of 1 mL/min. No additional separation as compared to the DEAE column was observed.

T7 RNA polymerase activity. To test activity of polymerase, RNA synthesis of DNA template containing region from -20 to -1 of class III T7 RNA polymerase promoter, followed by the complement RNA sequence desired was analyzed. In order to create a transcription template, a complementary strand must be annealed to the promoter portion of the template. The promoter sequence may vary in length; however the 17-20 nucleotide fragments generally insures proper annealing and product formation. Template DNA strand (tRNA^{Phe} template): 5'-TGC CCG GAC TCG GAA TCG AAC CAA GGA CAC GGG GAT TTT CAA TCC CCT GCT CTA CCG ACT GAG CTA TCC GGG CTA TAG TGA GTC GTA TTA-3'. RNA promoter: 5'-TAA TAC GAC TCA CTA TAG GG-3'. DNA template (3 μL of 100 μM) and RNA polymerase promoter (2 μL of 100 μM) were added to 15 μL transcription buffer (autoclaved 40 mM Tris-HCl, pH = 8.0, 10 mM MgCl_2 , 5 mM dithiothreitol, 2 mM Triton-X). To ensure proper annealing, the mixture was heated to 90 °C for 3 minutes, and then allowed to cool in ice bath. Nucleoside 5'-triphosphate mixture (NTP mix, 5 μL of 10 mM solution), Murine RNase inhibitor (BioLabs M0314G, 2 μL of 40,000 U/mL solution), and RNA polymerase (23 μL of 107 μM) were added. Purchased RNA polymerase (BioLabs M0251S) was used as a control (2 μL of 50,000 U/mL, 21 μL buffer for final volume of 50 μL). Reaction was then allowed to proceed at 37

°C for 3 hours. RNA synthesis was analyzed by Agarose gel electrophoresis, or 12% PAGE/7 M Urea electrophoresis.

12% PAGE/ 7 M Urea electrophoresis. 12% PAGE/7 M Urea was prepared by first making 500 mL 20x TBE buffer (121.6 g Tris-base, 9.3 g EDTA, 55 g boric acid). 100 mL stock solution of 12% PAGE/7 M Urea (10 g acrylamine: bisacrylamide (29:1), 35 g Urea, 4.16 mL 20x TBE buffer) was then prepared. After assembling the electrophoresis apparatus used for SDS-PAGE, 100 μ L 10% ammonium persulfate (APS) and 4 μ L *N,N,N',N'*-tetramethyl-ethane-1,2-diamine (TEMED) was added to 10 mL of 12% PAGE/7

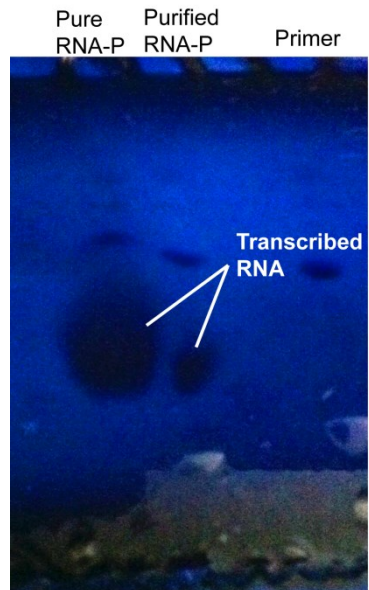


Figure 3-11 T7 RNA polymerase activity

T7 RNA polymerase activity was observed using 12% PAGE/7 M Urea electrophoresis. The first designated lane represents RNA transcription using purchased RNA polymerase. The second designated lane represents RNA transcription using purified RNA polymerase. The fourth designated lane is the RNA primer template. The shadows correspond to the transcribed RNA.

M Urea and poured into glass plate assembly. Gels solidified within 15-20 minutes. Electrophoresis was then completed according to SDS-PAGE protocols, running the gels at 200 V for 30-45 minutes in 1x TBE buffer. After completion, glass plates were removed from apparatus, and gels transferred onto Saran Wrap. A handheld UV lamp was then used to locate a UV shadow, indicating site of migration of RNA product (Figure 3-11).

3.1.1 *MiaE* binding affinity

MiaE binding affinity. Steady state kinetic analysis of *MiaE*, cloned from *S. typhimurium*, revealed the enzyme's preference for the ms^2i^6A substrate over nucleosides with varying functionality at the C2-position ($ms^2i^6A > i^6A > Ci^2i^6A$) (see previous chapters). This observed selectivity suggests that the inductive strength of the nucleosides C2-substituent may play a major role in the *MiaE* binding. The observed initial rate for each substrate-surrogate could be an issue of either kinetic regulation (rate-limiting product release), or thermodynamics (low binding-affinity). In order to further investigate the binding affinity of *MiaE*, incorporation of the aforementioned nitroxyl spin-label was performed on both a synthetic nucleoside surrogate and the anticodon stem-loop (ACSL) of tRNA. Electron paramagnetic spectroscopy (EPR) was employed to monitor the increase in spin-anisotropy upon binding of the spin-labeled substrates within the active site of *MiaE*.

Synthesis of *MiaE* spin-labeled nucleoside. Even though the click-ligation of the nitroxyl spin-label and carbohydrate moiety was low yielding, we were able to complete the synthesis of a spin-labeled modified nucleoside for the investigation of *MiaE* (Figure 3-12). First, 2-chloro- N^6 -isopentenyl-purine **2.3c** was coupled to 1,2,3-Tri-O-acetyl-5-azido-5-deoxy-D-ribofuranose **3.3** via modified Vorbrüggen coupling. In comparison to previous Vorbrüggen coupling reactions, the yield was quiet low. It appears that the 5'-azide is interfering with the nucleophilic addition, but for reasons unknown. Stannic

chloride is often added as a Lewis acid, intended to increase the reactivity of the carbohydrate moiety, and may be beneficial in this case.^{81,113} The click-ligation of the resulting nucleoside **3.23** with the cyano-nitroxide **3.15**, followed by saponification, yielded the Cl²¹⁶A spin-labeled nucleoside **3.24** (see *Chapter 5 Synthetic Methodology* for additional experimentation).

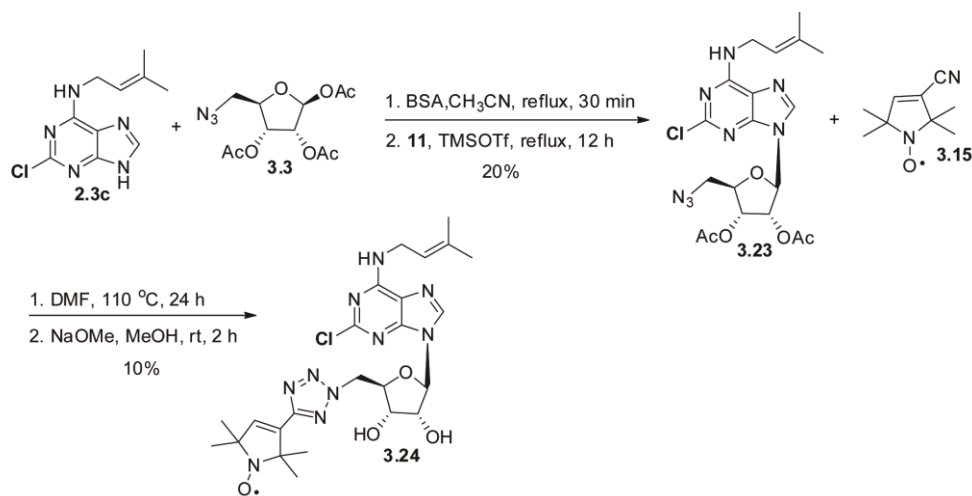


Figure 3-12 Spin-labeled MiaE nucleoside (Cl²¹⁶A) synthesis

Synthesis of MiaE spin-labeled anticodon stem-loop (ACSL). To gain further insight into the topology and binding characteristics of MiaE, a nitroxyl radical was also attached to the ACSL^{Trp} analog Figure 3-13. The small 17 nucleoside RNA oligomer corresponding to the anticodon stem-loop of *Salmonella typhimurium* was purchased from Integrated DNA Technology (idtdna.com). Disulfied-modified ACSL^{Trp} (sequence: 5'-CCG GUC UCC AAA ACC GG/3ThioMC3-D/-3') was first reconstituted in an annealing buffer (5 mM HEPES, 50 mM potassium chloride, and 2 mM magnesium chloride, pH = 7.00) to a final concentration of 500 μM. To ensure homogeneous RNA folding into a stable hair-pin loop, solutions of RNA oligomers were temperature annealed as described previously.¹¹⁴ Briefly, using a PCR thermocycler (MJ mini gradient thermal cycler/Bio-Rad)

the temperature of RNA solutions was raised to 95 °C over the course of 2 min. After 1 minute at 95 °C, solutions were cooled to 4 °C over the course of 35 min. Appropriate secondary structure was confirmed by Circular Dichroism, Jasco J-715

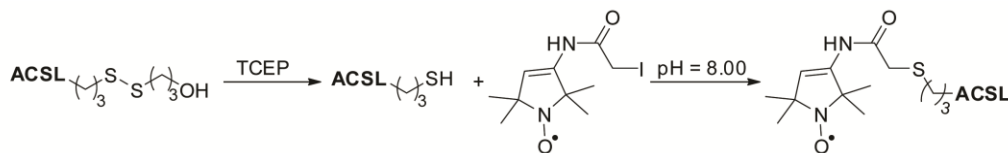


Figure 3-13 Synthesis of spin-labeled ACSL^{Trp}

spectropolarimeter (Jasco Inc., Easton, MD, USA) (Figure 3-14). To reduce the disulfide tag, one equivalent of Tris-(2-carboxyethyl)phosphine hydrochloride (TCEP-HCl) solution (500 μM, 60 μL) was added to the ACSL^{Trp} (500 μM, 60 μL), and kept at 4 °C overnight. Two equivalence of disodium phosphate buffer (240 μL, 50 mM, pH = 8.00) was added to the ACSL^{Trp} reaction, and placed on ice for 5 minutes to allow thiol deprotonation. 3-(2-iodoacetamido)-PROXYL (Sigma Aldrich 253421) was then added in ten times molar excess (20 μL; 800 μM), and the reaction was kept at 4 °C overnight. QIAquick Nucleotide Removal Kit (QIAGEN, 28706) was used to purify the spin-labeled ACSL^{Trp}. Autoclaved water was used to elute the product in the final step of the purification. The spin-labeled ACSL^{Trp} was then concentrated by ethanol precipitation¹¹⁵, and reconstituted in autoclaved ACSL buffer (250 μL; 30 mM HEPES, 100 mM potassium chloride, 2 mM magnesium chloride, pH = 7.00). A second CD spectrum was performed in order to ensure hair-pin-loop configuration (represented by red square, Figure 3-14).

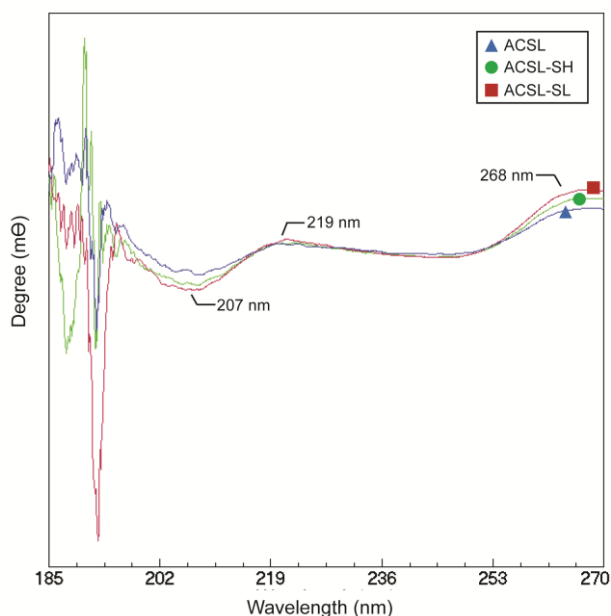


Figure 3-14 CD spectrum of spin labeled ACSL^{Trp}

The blue triangle spectrum represents the reconstituted annealed disulfied-modified ACSL^{Trp} (sequence: 5'-CCG GUC UCC AAA ACC GG/3ThioMC3-D/-3'). The green circle spectrum represents the reduced ACSL^{Trp}-SH. The red square spectrum represents the final spin-labeled ACSL^{Trp}. CD spectrum was compared to unlabeled ACSL^{Trp} standard. All spectrum were analyzed in annealing buffer (5 mM HEPES, 50 mM potassium chloride, and 2 mM magnesium chloride, pH = 7.00).

MiaE expression and purification. MiaE expression and purification method was described previously in Chapter 2.⁴⁵ The purity and concentration of MiaE protein was determined by UV-vis spectroscopy ($A_{280}/A_{370} \sim 7.8$ and $\epsilon_{370 \text{ nm}} = 5,100 \text{ M}^{-1}\text{cm}^{-1}$). All UV-visible measurements were performed on an Agilent 8453 photo diode array spectrometer (Santa Clara, CA). Measurements were made in ES Quartz cuvettes (NSG Precision Cells, Farmingdale, NY).

EPR binding assays. Samples for room temperature analysis were loaded into capillary tubes, and then placed into EPR tubes, necessary for solvents of high dielectric constants. To ensure full binding of MiaE substrates, a 3 fold excess of enzyme was added to either spin-labeled Cl^{2,6}A **3.22** or spin-labeled ACSL^{Trp}. EPR parameters for room temperature samples: attenuation, 20 dB; microwave frequency, 9.64 GHz; modulation amplitude, 9.0 mT; $S = \frac{1}{2}$, $g_x = g_y = g_z = 2.008$ (Figure 3-15). In an attempt to gain sensitivity, 175 μ L of concentrated samples were loaded into EPR tubes (height of roughly 25 mm), and frozen in liquid nitrogen. The EPR probe was then equipped with a liquid nitrogen dewer, and samples were analyzed at 77 K. To reduce vibrational noise

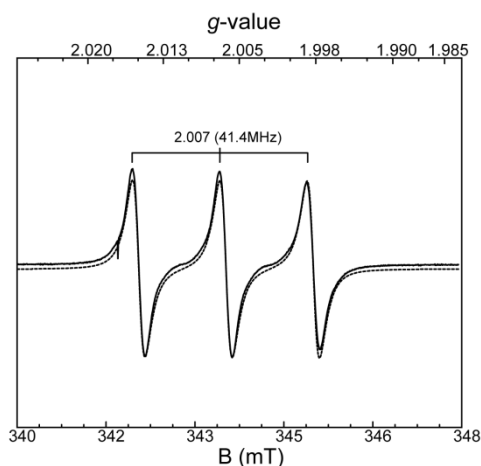


Figure 3-15 Spin-labeled Cl^{2,6}A (3.22) EPR spectrum

Spectroscopic simulation (dashed line) overlaid on spin-labeled Cl^{2,6}A (**3.22**) EPR spectrum (solid line). The simulations were generated with consideration of all intensity factors, both theoretical and experimental, to allow for determination of species concentration. EPR instrumental parameters: microwave frequency (\perp), 9.64 GHz; microwave attenuation, 30 dB; modulation amplitude, 9.0 mT; temperature, 298 K. $S = \frac{1}{2}$, $g_x = g_y = g_z = g_e$.

due to the boiling of liquid nitrogen, a collar was placed around the EPR tubes. The collar had a small gap to relieve pressure build up, and was adjusted to optimum height to ensure sensitivity. Due to large amount of sample necessary, 3 fold molar excess of enzyme was problematic, therefore liquid nitrogen samples were prepared in either 1:1 ratio substrate: enzyme, or slight molar excess of MiaE (1 equivalent spin-labeled Cl^{2,6}A **3.22** to 1.2 equivalence MiaE). EPR parameters for samples ran at 77 K: attenuation, 35 dB; microwave frequency, 9.64 GHz; modulation amplitude, 9.0 mT.

3.2 Discussion

5'-carbohydrate spin-labeled nucleoside synthesis. Many of the aforementioned reactions involving nitroxide functionalization proceeded in relatively acceptable yields; however, several resulted in numerous by-products due to the presence of the nitroxyl radical. The click-ligation trials shown in Table 3-1 and Table 3-2 also proved problematic when reagents and high temperatures resulted in reduction or degradation due to radical reactivity. It was then proposed to oxidize the pyrroline amine to the nitroxide after “click”-ligation to the carbohydrate moiety.¹⁰⁸ The functionalization of the pyrroline is currently underway.

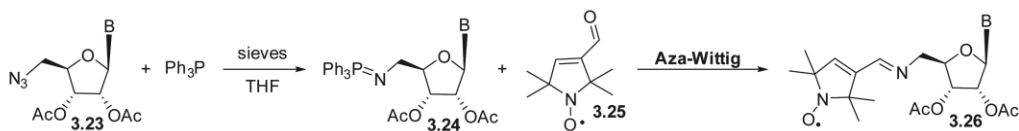


Figure 3-16 Tandem Staudinger/aza-Wittig ligation

Beyond the cumbersome radical, click-ligation may not be the best coupling parameters. An alternative approach involves a tandem Staudinger/aza-Wittig reaction (Figure 3-16).¹¹⁶ First, the Staudinger reaction of 5'-azido-ribose nucleoside **3.23** with triphenylphosphine, using sieves to ensure dry conditions, would afford Wittig reagent **3.24**. After oxidizing the nitroxyl alcohol **3.17** to aldehyde **3.25** using manganese dioxide,

the nitroxyl radical would be primed to undergo aza-Wittig reaction with compound **3.24**. The corresponding imine **3.26** could then be reduced, if desired, using sodium borohydride. This tandem reaction sequence has some limitations, requiring stringent exclusion of water and the possibility of **3.24** rearrangement, but implores little functionalization of already synthesized coupling partners.

EPR binding assays. EPR analysis of enzymatic binding to both spin-labeled Cl²ⁱ⁶A **3.22** and spin-labeled ACSL^{Trp} performed at room temperature demonstrated no anisotropy difference when compared to substrate standards. Upon cooling samples to 77 K, slight deviations in hyperfine coupling (*A*), a result of the interaction between the magnetic moment of the electron spin with that of a nucleus with a non-zero nuclear spin, and *g*-strain, due to slight variations in paramagnetic center orientation, indicating anisotropy upon enzymatic binding. These subtle differences are represented in Figure 3-17. Each spectrum was scaled for concentration. The dashed spectra represent each sample simulation. The bottom chromatogram (designated by a triangle) represents the substrate standard Cl²ⁱ⁶A spin labeled nucleoside **3.22** (Cl²ⁱ⁶A*, 14 μM), with $g_{x,y,z} = [2.006, 2.003, 1.998]$; $A_{x,y,z} = [-, 101, - \text{ MHz}]$; $\sigma g_{x,y,z} = [0.005, 0.002, 0.001]$. The middle chromatogram (circle) represents a 1:1 ratio of Cl²ⁱ⁶A* **3.22** (6 μM) and MiaE, with $g_{x,y,z} = [2.008, 2.002, 1.997]$; $A_{x,y,z} = [-, 102, - \text{ MHz}]$; $\sigma g_{x,y,z} = [0.004, 0.002, 0.005]$. The top chromatogram (square) represents Cl²ⁱ⁶A* **3.22** (7 μM) in the presence of a slight excess of MiaE (1.2 equivalence), with $g_{x,y,z} = [2.007, 2.003, 1.998]$; $A_{x,y,z} = [-, 102, - \text{ MHz}]$; $\sigma g_{x,y,z} = [0.003, 0.002, 0.004]$. The slight variation in hyperfine coupling between Cl²ⁱ⁶A* **3.22** standard and that with MiaE exists predominantly in *A_y* orientation (with *A_x* pertaining to lowest field shift, and *A_z* being highest field shift). An additional inequality resulting in MiaE addition is in *g*-strain (σg_z) of the *z* orientation, a difference of 0.001 to 0.005. The increased *g*-anisotropy observed suggests enzymatic binding to Cl²ⁱ⁶A* **3.22**.

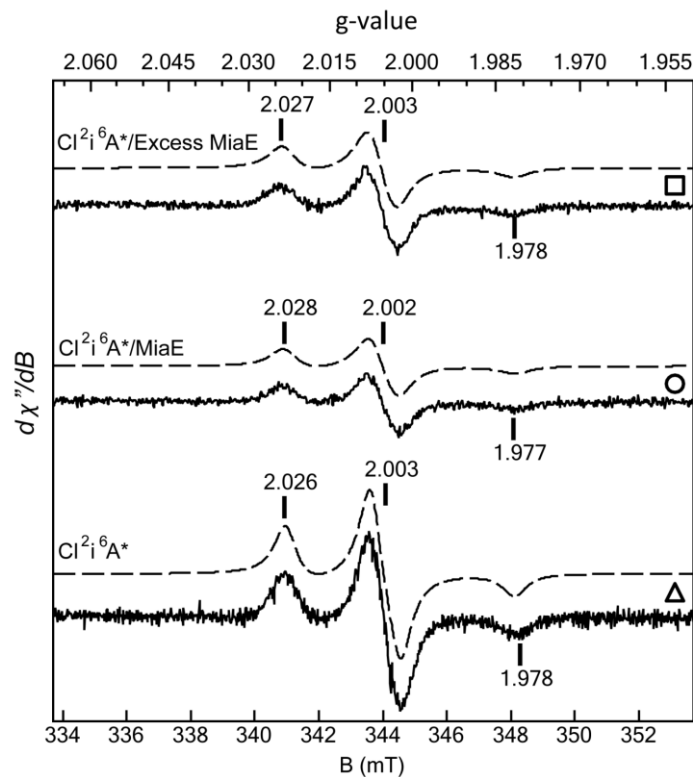


Figure 3-17 EPR spectrum of spin-labeled $Cl^{2i6}A$ **3.22** binding assay

EPR spectrum of spin-labeled $Cl^{2i6}A$ **3.22** binding assay. The dashed spectra are simulations of respective assays. The bottom spectrum (designated by a triangle) represents the spin-labeled $Cl^{2i6}A$ **3.22** ($Cl^{2i6}A^*$, 14 μM). The middle spectrum (circle) represents a one-to-one ratio of $Cl^{2i6}A^*$ (6 μM) to MiaE. The top spectrum (square) represents **3.22** (7 μM) in the presence of excess MiaE. Each spectrum is scaled for concentration, and is a scan average of three total scans. Attenuation, 35 dB; microwave frequency, 9.64 GHz; modulation amplitude, 9.0 mT; $S = 1/2$.

The binding of the ACSL^{Trp} spin-label (binding assays for MiaE: ASL^{Trp} spin-label are not shown) was hypothesized to have larger anisotropy effects due to increased Van Der Waals interactions (tighter binding). Unfortunately, issues regarding spin-labeling of the

ACSL^{Trp} in high concentrations limited definitive proof of this hypothesis. Due to cost of RNA, attention was redirected toward synthesizing ACSL^{Trp} in-house using the newly purified T7 RNA polymerase. Once the ACSL spin-label is synthesized in higher concentrations, anisotropy assays should be achievable.

T7 RNA polymerase purification and activity. Activity of the polymerase was only observed after purifying the enzyme using both the DEAE and Cibacron Blue 3GA Agarose (Sigma Aldrich) column chromatography. After Polymin P precipitation and DEAE chromatography, the T7 RNA polymerase is nearly 50% pure, however contaminating DNA fragments and nucleases may be present. The Blue 3GA column is efficient at further purification, and subsequent activation, by interacting with nucleoside binding enzymes. Cibacron Blue 3GA has the ability to bind to several enzymes with affinities to nucleotide cofactors, for example kinases, restriction endonucleases, albumin, and dehydrogenases.¹¹⁷ For polymerase elution, low concentrations of ATP and GTP were added to eluent for elution due to T7 RNA polymerases higher affinity for the nucleotides versus the Blue dye. Due to the high cost of GTP, removing it from the eluent may be a possibility, but conditions need to be further optimized. T7 RNA polymerase also has a marked preference for the presence of GTP at positions +1 or +2 due to large stabilizing forces. For this reason, many include the addition of GTP to help initiate DNA transcription.¹¹⁸ For this reason, it is believed that attaching the nitroxyl radical to guanosine will result in enzymatic binding and observed anisotropy, providing proof of concept for the construction of the 5'-carbohydrate spin-labeled nucleoside.

Chapter 4

Future Avenues for MiaE

Dioxygen serves in a multitude of roles which greatly affect aerobic life. The most commonly known is its role as a terminal electron acceptor in processes such as respiration and oxidative phosphorylation. Secondly, it serves as the source of oxygen which is incorporated into molecules essential in biological systems. In addition to the synthesis of hormones, neurotransmitters, amino acids, and signaling molecules, oxygen incorporation aids in carbon sequestering, biodegradation, and metabolism.¹¹⁹ Beyond energy conversion and oxygen incorporation, dioxygen can be converted into alternative forms for the development of highly specialized reagents for processes such as catalysis. One instance of this is the role of dioxygen in the biosynthesis of penicillin antibiotics.¹²⁰

Life is dependent upon dioxygen molecules predominantly due to the high potential reactivity held in check by its molecular structure. The triplet ground state of molecular dioxygen forms a kinetic barrier from reacting with the singlet ground state of most organic and biological molecules. The two unpaired electrons in the degenerate molecular orbitals of dioxygen are spin forbidden from reacting with singlet molecules.¹²⁰ The only way to overcome this energetically unfavorable reaction is to excite dioxygen to one of its singlet states by a free-radical pathway or complexation with a paramagnetic metal.³³ Both pathways are generally unfavorable and/or inaccessible at ambient temperatures. However, nature accomplishes this process at ambient temperature with high specificity and selectivity.

Understanding nature's oxygen activation strategies could give rise to new pharmaceutical applications, alternative green biodegradation systems, fuel and industrial approaches, along with catalytic design for a myriad of synthetic processes. For this reason, non-heme enzymes and model complexes have attracted considerable interest.

Diiron sites accomplish a multitude of reactions ranging from molecular oxygen transport, aliphatic desaturation, one-electron oxidation, and hydrocarbon hydroxylation.⁴⁸ The vast majority of these alluring non-heme diiron enzymes are multimeric.⁴⁹ The active site is customarily positioned within a four-helix bundle in the α subunits of a non-covalent heterotrimeric dimer $(\alpha\beta\gamma)_2$ configuration, as seen in bacterial multicomponent monooxygenase (BMM) enzymes.^{48,50} In contrast to the multimeric protein configuration exhibited by the non-heme diiron monooxygenases characterized thus far, MiaE exhibits a monomeric (α) protein configuration, containing a single active site as indicated by size exclusion chromatography²³ and analytical ultracentrifugation.⁴⁵ This is the first example found within literature of a monomeric non-heme diiron oxygenase. Therefore, this enzyme provides a unique opportunity to study a minimal non-heme diiron enzyme in the absence of any potential for cooperativity. A multitude of spectroscopy, structure analysis, biophysical chemistry, and synthetic chemistry has contributed to understanding MiaE's oxygen activation mechanism, yet there is still much to learn. The following chapter outlines several proposed experiments in order to aid in the further dissection of MiaE.

4.1 Inductive Effect of C2-Functionality

Chapter 2 described the synthesis of three nucleoside substrate surrogates [N^6 -isopentenyl-adenosine (i^6A); 2-methylthiol- N^6 -isopentenyl-adenosine, (ms^2i^6A); and 2-chloro- N^6 -isopentenyl-adenosine, (Cl^2i^6A)] such that the chemo and stereospecificity of recombinant MiaE cloned from *Salmonella typhimurium* could be examined. Remarkably, for all synthetic nucleosides, MiaE was capable of chemo- and stereoselective *E*-hydroxylation at the terminal C4-position of the isopentenyl-group. Moreover, the results obtained from steady-state experiments suggest that even in the absence of

macromolecular tRNA: MiaE interactions, the substrate-affinity of MiaE is largely dominated by inductive effects at the C2-position of the nucleoside base.

Furthermore, since the C2-position of the nucleoside is quite distant from the point of enzymatic hydroxylation, given the observed difference in second order reaction rate [**2.5a** (SMe) > **2.5b** (H) > **2.5c** (Cl)], it is reasonable to speculate that the nucleosides C2-substituent significantly influences the MiaE binding affinity. For example, at a fixed substrate concentration (2.0 mM), the rate of **2.5a**-hydroxylation is over three-fold that of **2.5b**-hydroxylation. Interestingly, a similar substrate preference has also been observed for ms²i⁶A- and i⁶A-bearing tRNA substrates²⁷. Therefore, it is possible that the enzymatic substrate specificity is largely a function of the nucleoside base and not due to the conformational difference within the global tRNA tertiary structure. However, to fully support this hypothesis, the effect of alternative C2-functionality of comparable steric interaction needs to be evaluated. The methoxy functional group, for instance, is moderately more electronically activating in comparison to methylthiol, yet still comparable in size. If MiaE selectivity is truly affected by the electron donating versus withdrawing capabilities of the C2-functionality, then the kinetic analysis of the methoxy group should result with an increase in reaction rate. In addition, the methoxy functional group is not a “native substrate” of MiaE, and should therefore further prove this postulation.

Synthetically achieving 2,6-disubstituted purines tends to hold some difficulties, mainly due to the relatively electron-rich C2-position.¹²¹ However, by taking advantage of the difference in reactivity of the C2 versus C6-position, selective nucleophilic addition at the C6-position followed by cross-coupling at the C2-position, is generally quite successful.¹²² A plausible synthetic route to the C2-methoxy substrate begins with 2,6-dichloropurine (Figure 4-1). 2-Isopentenylamine hydrochloride (**2.2**) could then be added

by chemoselective nucleophilic aromatic substitution at the C6-position (synthesis described in chapter 2). Ullman-type coupling between the aryl halide and acetic acid, followed by reduction of the ester, would generate 2-methoxy-*N*⁶-isopenentenyl-purine. Alternative approach involves either the addition of 1 M sodium methoxide to 2-chloro-*N*⁶-isopenentenyl-purine (**2.3c**)¹²¹, or potentially Buchwald-Hartwig cross-coupling. Vorbrüggen coupling of the purine **4.1** with 1,2,3,5-tetra-*O*-acetyl-*D*-ribofuranose, followed by saponification, would give substrate surrogate 2-methoxy-*N*⁶-isopenentenyl-adenosine **4.2** (mo²ⁱ⁶A). The same approach can be taken using hydroxyisopenentenylamine hydrochloride **2.6** at the C6-position to generate the expected MiaE modified adenosine, allowing for kinetic investigation.

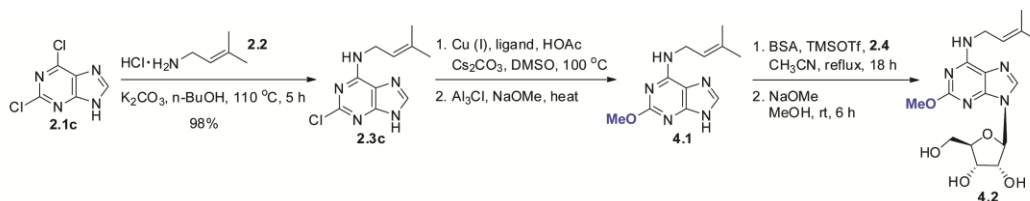


Figure 4-1 Proposed mo²ⁱ⁶A synthesis

4.2 Oligonucleotide Synthesis of Varying Lengths and Modifications

Thus far, the single nucleoside substrate surrogate and the 17-basepair anticodon stem loop of the tRNA substrate have been analyzed; however, we have yet to investigate oligonucleotides varying in length to determine optimum binding interactions. It is possible that the full ACSL of tRNA is not necessary for sufficient binding. Determining optimum binding interactions could, therefore, give an alternative approach to disentangling the binding pocket. High-yielding sequential DNA oligonucleotides have been synthesized for years using phosphoramidite chemistry; however, this process is seemingly more difficult when attempting with RNA due to protective group migration/selectivity between the 2'- versus 3'- hydroxyls. To overcome this lack of

regioselectivity, the 3'- and 5'- hydroxyls can be simultaneously protected using di-tert-butylsilyl bis(trifluoromethanesulfonate).¹²³ This protection scheme then leaves the 2'-hydroxyl free to be regioselectively protected (Figure 4-2). The 2'-hydroxyl protecting group must therefore be amine stable and fluoride-labile to accomplish subsequent selective deprotection. Dellinger and coworkers were able to accomplish this feat in high yield by using 2'-O-(1,1-dioxo-1 λ 6-thiomorpholine-4-carbothioate) (TC) protection.¹²⁴ The 2'-hydroxyl is first converted to a reactive thiocarbonylimidazole intermediate **4.4**, which can then be displaced by 2'-O-(1,1-dioxo-1 λ 6-thiomorpholine-4-carbothioate), producing the 2'-O-TC protected nucleoside **4.5**. The 3',5'-cyclic silane can then be deprotected using hydrogen fluoride/pyridine solution. Nucleoside **4.6** is then set up for general phosphoramidite chemistry. The primary 5'-hydroxyl is selectively protected with 4,4'-dimethoxytriphenylmethyl chloride (DMT-Cl), leaving the secondary alcohol (3'-OH) available to be phosphitylated with (2-cyanoethyl)-N,N-diisopropylchlorophosphoramidite.

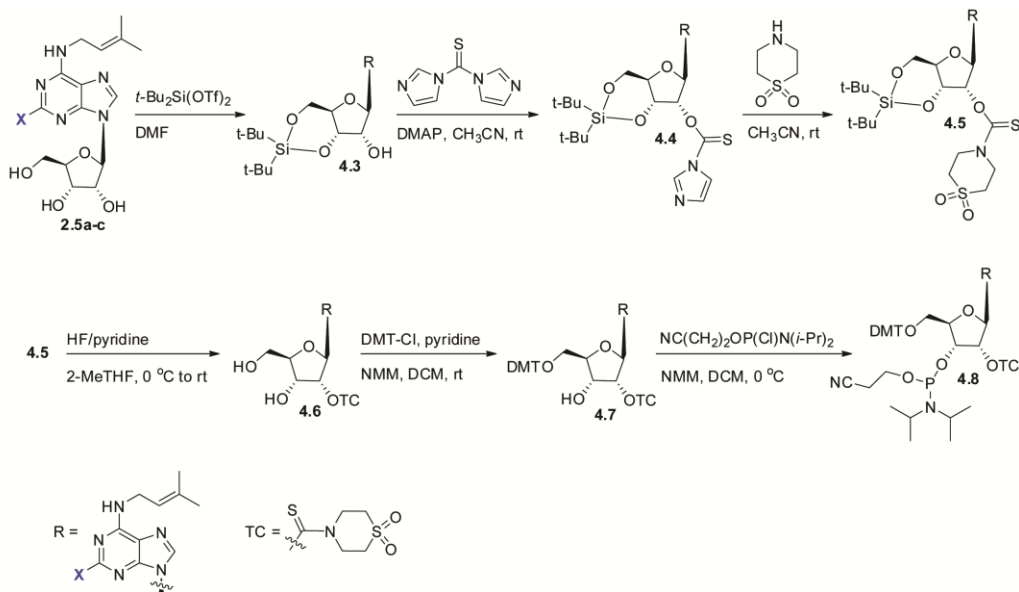


Figure 4-2 Synthesis of modified nucleoside phosphoramidite monomer

The oligonucleotide sequence can then be stepwise assembled in the direction of 3'- to 5'-terminus through a routine synthetic cycle of: 1. detritylation, 2. coupling, 3. DMT-protection (capping), and 4. oxidation.¹²⁵

4.3 Electrostatic Interactions of the Substrate-Enzyme Complex

Beyond serving as an intermediate for oligonucleotide synthesis, the phosphoramidite monomer could also be an attractive substrate for MiaE. Analysis of the enzymatic crystal structure revealed lysine residues (indicated in yellow) flanking the diiron active site (indicated in red) (Figure 4-3). These positively charged residues could easily bind to the negative phosphine backbone of the tRNA construct, increasing binding efficiency and possibly even altering enzyme configuration. Negatively charged prosthetic

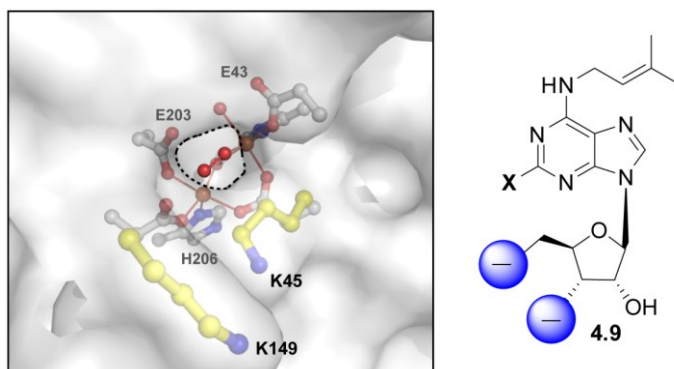


Figure 4-3 Crystal structure of MiaE active site

The crystal structure of the active site of MiaE (left) highlights two lysine residues located within close proximity to the diiron center (red), indicated in yellow, with the terminal positive amine indicated in blue. A small opening to the hydrophobic active site is indicated by black dashed lines. The right nucleoside **4.9** is a cartoon representation of the possible functionality that could be added to increase binding efficiency to MiaE. Negatively charged functionality placed at the 3' and 5' positions of the carbohydrate moiety may interact with the positive lysine residues.

groups positioned at the 3' and 5' positions of the ribose, highlighted in blue of compound **4.9**, could allude to the role of electrostatics for the substrate-enzyme interaction.

Electrostatic interactions absent in nucleoside binding may also explain why enzyme configuration is altered upon ACSL binding, yet absent with nucleoside binding as shown by EPR, CD, and Mössbauer spectroscopy.³²

Interestingly, EPR spectra of bacterial multicomponent diiron monooxygenases upon binding of respective oxidoreductases closely resemble that of MiaE upon ACSL addition.^{41,126-128} However, due to difficulties caused by the the multimeric structure of these enzymes, little is understood regarding the specific mode of action of oxygenase effector proteins.¹²⁹ This suggests that MiaE may also be an excellent model system to study protein-effector interactions and their impact on diiron site conformation. To investigate the possibility of the ACSL acting as an effector protein, chemical rescue experiments involving the addition of an unmodified ACSL^{Trp} to the MiaE hydroxylation of nucleoside i⁶A (**2.5b**) under peroxide-shunt catalysis was undertaken.

Chemical rescue experimentation. The standard assay conditions for peroxide-shunt catalysis included the addition of 25 μ L of 400 μ M purified MiaE, 6 μ L of 1 mM ACSL (1.2 equivalence compared to MiaE concentration), 25 μ L of 23 mM substrate [3:2 DMSO:HEPES buffer (20 mM HEPES, 50 mM sodium chloride buffer, pH 8)], 25 μ L of 120 mM hydrogen peroxide in HEPES buffer, and additional HEPES buffer to bring the final volume to 100 μ L. MiaE was added last to initiate the reaction. The reactions were carried out at 27 °C, and followed for designated time. At selected time points, the sample was heat inactivated at 95 °C for 1 minute, and then cooled to 0 °C in an ice bath. The sample was centrifuged at 14,000 rpm for 15 minutes, transferred into a Costar[®] Spin-X[®] centrifuge tube filter, and filtered at 11,500 rpm for 3 minutes. For samples analyzed via HILIC (Frulic-N) HPLC method, 100 μ L of eluent was added prior to initial

centrifugation. Since peak distortion can be caused by variable aqueous content in HILIC separations⁷⁷, an additional 1300 μL of eluent was added to each sample, resulting in an overall 15-fold dilution in the mobile phase. The results were then analyzed by HPLC (273 nm) as described previously.

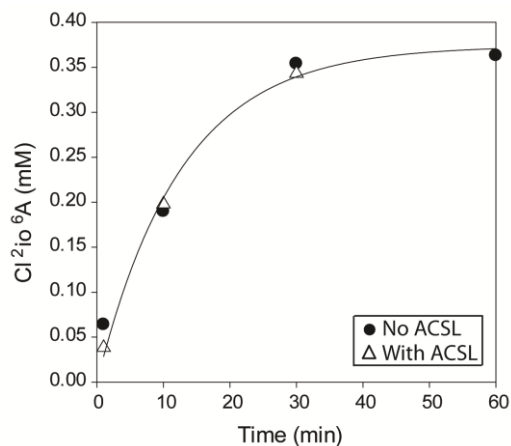


Figure 4-4 Rate of peroxide shunt product formation with the addition of ACSL^{Trp}. Rate of peroxide shunt product formation was observed with and without the addition of ACSL^{Trp}. The trial represented by the black circle is in the absence of ACSL^{Trp}, while that represented by the outlined triangle is in the presence of ACSL^{Trp}. The addition of a possible effector-protein does not alter rate of Cl²i⁶A (**2.5c**) hydroxylation under peroxide shunt conditions.

Unfortunately, no change in rate of product formation was observed (Figure 4-4), which was unanticipated. Two scenarios were deemed possible: (I) the ACSL would bind, altering conformation, and allow an increased rate in nucleoside hydroxylation, (II) the ACSL would bind so tightly that the nucleoside would be unable to enter the active site, resulting in a decreased rate of nucleoside hydroxylation. As stated previously, peroxide-shunt catalysis has many drawbacks, mainly decreased selectivity and increased

promiscuity. Assays utilizing native electron-transport catalysis should be evaluated in order to fully conclude that there is no change in rate observed with and without the presence of the ACSL^{Trp}.

4.4 Substrate-Gated Electron Delivery

The active site conformational change observed by EPR may alter the redox potential of the MiaE active site or potentially the electron-transfer pathway. Similar behavior has been observed for enzyme-substrate complex of the non-heme iron enzyme $\Delta 9D$.¹³⁰ UV-vis spectroscopy could be used to evaluate this possibility. In these experiments, the rate of diiron site reduction of MiaE by reduced ferredoxin (Fd) can be measured in the presence and absence of ACSL to evaluate the role of tRNA binding in gating electron delivery to the MiaE active site. Reactions would be initiated by mixing anaerobic oxidized MiaE and chemically reduced Fd. The number of electrons delivered can be determined from the change in absorbance at 420 nm using the difference in molar absorptivity of the oxidized ($9.7 \text{ mM}^{-1} \text{ cm}^{-1}$) and reduced ($4.7 \text{ mM}^{-1} \text{ cm}^{-1}$) Fd.

Fundamental experiments using chemically reduced ferredoxin and oxidized MiaE were performed under anaerobic conditions and monitored by UV-vis spectroscopy (Figure 4-5). Upon ferredoxin oxidation, a result of MiaE reduction, the charge-transfer-bands of ferredoxin's two Fe-S bonds increases in absorptivity, as seen by the top, dashed line, UV-vis spectrum of Figure 4-5. The grey arrows indicate the two Fe-S bonds at wavelengths of $\sim 420 \text{ nm}$ and $\sim 480 \text{ nm}$. After several attempts, we were able to achieve anaerobic conditions, however this is not trivial, and there were still issues with assay methodology. However, preliminary results did indicate that the addition of ACSL^{Trp} increases the rate of MiaE reduction. Due to issues with the anaerobic procedure, methodology needs to be optimized, and additional evaluations performed in order to fully support initial findings.

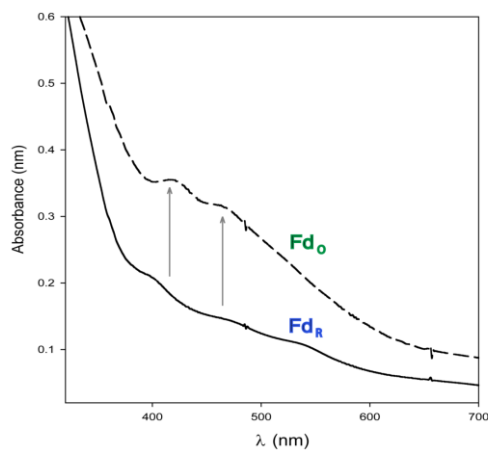


Figure 4-5 UV-vis spectrum of reduced and oxidized ferridoxin (Fd)

The bottom, solid line, UV-vis spectrum represents that of fully reduced ferredoxin.

Upon oxidation, a result of MiaE reduction, the charge-transfer-bands of ferredoxin's two Fe-S bonds increases in absorptivity, as seen by the top, dashed line, UV-vis spectrum. The grey arrows indicate the two Fe-S bonds at wavelengths of ~420 nm and 480 nm.

4.5 *E-Z* Isomerization of MiaE Hydroxylated Substrates

Both the (*Z*)- and (*E*)-isomers of the hydroxylated products [N^6 -(4-hydroxyisopentenyl)-adenoside (io^6A); 2-methylthiol- N^6 -(4-hydroxyisopentenyl)-adenoside (ms^2io^6A), 2-chloro- N^6 -(4-hydroxyisopentenyl)-adenoside (Cl^2io^6A)] were synthesized for standards in HPLC enzymatic assays and confirmation of MiaE product stereochemistry. During standard analysis, it was noted that the io^6A and ms^2io^6A appeared to isomerize from the (*E*) to the (*Z*)-isomer with prolonged use. Interestingly, this isomerization was never detected for the (*E*)- Cl^2io^6A , and the *E*- ms^2io^6A seemed to isomerize at a slower rate in comparison to (*E*)- io^6A . It also appears that the (*Z*)-isomer does not isomerize, indicating that it is the thermodynamically stable conformer. Playtis and coworkers commented on the N^6 -side chain isomerization observed for ribosylzeatin

(io^6A) and ms-ribosylzeatin (ms^2io^6A); however they only evaluated the isomerization of (Z)- to (E)-isomer, with no conversion observed.¹³¹ This observation is especially interesting due to the lack of comment in literature claiming that the only observed product of MiaE hydroxylation is the (Z)- ms^2io^6A .

Kinetic investigation of the rate of isomerization, along with determining if this is light, temperature, and/or solvent dependent, would be of interest. This would be further insightful if there truly is an observed difference in rate of conversion for io^6A , ms^2io^6A , and Cl^2io^6A . Preliminary data suggests that the relative order of isomerization is $io^6A > ms^2io^6A > Cl^2io^6A$. This indicates that there may be a possibility of H-bonding between the C2-functionality and the hydroxyl moiety of the isopentenyl group, increasing stability of the (Z)-isomer. Further experimentation needs to be performed in order to verify this hypothesis.

Chapter 5

Synthetic Methodology

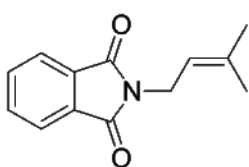
General Materials and Methods. All reactions were performed under high purity argon gas, which was passed through a drying tube containing calcium sulfate (Drierite), using flame-dried glassware. Reaction solvents *N,N*-dimethylformamide (DMF), methanol, dichloromethane (DCM), *n*-butanol (*n*-BuOH), and acetonitrile (MeCN) were all purchased in DriSolv[®] containers (EMD). *n*-BuOH was dried further over activated sieves. All commercially available reagents were purchased from Sigma Aldrich, Acros, or EMD, and were used as obtained unless otherwise stated.

All reactions were stirred magnetically and monitored by analytical thin layer chromatography using Merck silica gel F-254 pre coated aluminum-backed plates. Plates were visualized by UV light (254 nm) and appropriate developing stains when applicable: ninhydrin (Nin, amines), potassium permanganate (KMnO₄, functional groups sensitive to oxidation). 230-400 mesh silica gel (SiliCycle Inc.) was used for all normal phase chromatography. Solvent conditions and R_f values indicated refer to column conditions used for compound purification. All yields refer to chromatographically and spectroscopically pure compounds, along with diastereomer specified, unless otherwise noted. ¹H and ¹³C NMR spectra were recorded on JEOL 300 or 500 MHz spectrometers. Chemical shifts are reported in δ (ppm) units using residual protio solvent as the internal standard (¹H NMR: CDCl₃ = 7.26, CD₃OD = 3.31, DMSO-*d*₆ = 2.50 and ¹³C NMR: CDCl₃ = 77.0, CD₃OD = 49.0, DMSO-*d*₆ = 39.5). Data is reported as follows: chemical shift multiplicity (s = singlet, d = doublet, t = triplet, q = quartet, m = multiplet, dd = doublet of doublets, td = triplet of doublets, tq = triplet of quartets, bs = broad singlet), and *J*-couplings are listed when multiplicity is significantly resolved. Infrared spectra were

recorded using solid compounds (neat) on a Jasco FT-IR 460Plus. Frequencies are given in reciprocal centimeters (cm^{-1}) and only selected characteristic absorbances are reported. Low-resolution mass spectra (MS) and high-resolution mass spectra (HRMS) were performed at the University of Illinois at Urbana-Champaign Mass Spectrometry Laboratory. Melting points are uncorrected and were run on a Mel-Temp II (Laboratory Devices, USA) apparatus. Notebook pages are indicated in brackets following compound name and number (for example [ALC0101] indicates notebook 1, experiment number 1).

Footnote: (†) Indicates reactions modified from referenced literature.

5.1 Chapter 2 Experimental

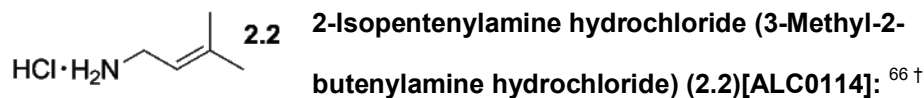


***N*⁶-(3,3-dimethylallyl)phthalimide (*N*-(3-methyl-2-butenyl)phthalimide) (S1-1)[ALC0101]:⁶⁴**

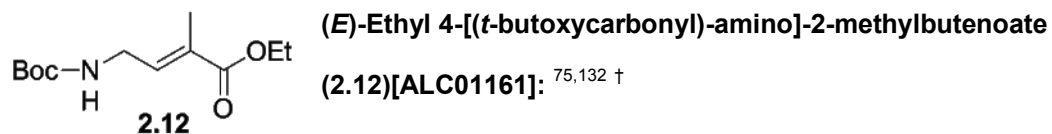
In a flame-dried round bottom flask equipped with reflux condenser, 3, 3-dimethylallyl bromide (3.7 mL, 0.03 mol) was added to a solution of potassium phthalimide (7.0 g, 0.04 mol) in DMF (50 mL), and stirred at 120 °C for 1 hour. The solution was then heated to 160 °C and stirred for an additional 18 hours. The resulting mixture was poured over ice (100 mL) and washed with DCM (5 x 50 mL). The organic extracts were washed with 0.1 M sodium hydroxide (2 x 100 mL), and then water (2 x 50 mL). The organic extracts were then dried over magnesium sulfate, decanted, and the filtrate was concentrated *in vacuo*. The resulting crude yellow solid was recrystallized in ethanol (50 mL) to give 5.5 g (0.02 mol, 66%) of cream-colored crystals ($R_f = 0.2$; 1% ethyl acetate: hexane). ¹H NMR (300 MHz, CDCl₃) δ 7.80 (2 H, m), 7.68 (2 H, m), 5.26 (1 H, t, $J = 7.2$ Hz), 4.26 (2 H, d, $J = 7.2$ Hz), 1.82 (3 H, s), 1.69 (3 H, s). ¹³C

NMR (125 MHz, CDCl₃) δ 168.2, 137.2, 133.8, 132.3, 123.2, 118.4, 35.8, 25.7, 17.9.

Melting point was not obtained for compound.



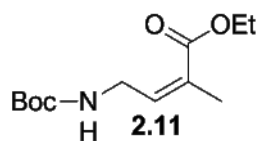
In a sealed tube, aqueous hydrazine monohydrate (220 μ L, 7.0 mmol) was added to a stirred solution of phthalimide **S1-1** (1.0 g, 4.7 mmol) in methanol (5 mL), and heated to reflux for 30 minutes. The resulting white precipitate was dissolved in water (10 mL), and concentrated *in vacuo*. The resulting crude white solid was dissolved in water (13 mL), and concentrated hydrochloric acid (2 mL) was added drop-wise. The resulting white precipitate was filtered through a bed of Celite, and washed with water. The filtrate was concentrated, and impurities were precipitated in methanol (7-10 mL). The impurities were removed by filtering through a bed of Celite, and the filtrate was once again concentrated *in vacuo* to afford 0.51 g (4.0 mmol, 85%) pale-yellow solid (R_f = 0.2; 20% methanol: DCM). ¹H NMR (500 MHz, DMSO-*d*₆) δ 8.06 (2 H, bs), 5.19 (1 H, t, J = 7.0 Hz), 3.34 (2 H, d, J = 7.0 Hz), 1.68 (3 H, s), 1.62 (3 H, s). ¹³C NMR (125 MHz, DMSO-*d*₆) δ 138.7, 117.6, 70.4, 42.5, 36.9, 32.7. Melting point was not obtained for compound.



N-Boc-glycine methyl ester **2.9** (1.8 g, 10 mmol) was placed in a flame-dried round bottom flask. **2.9** was dissolved in DCM (30 mL), and cooled to -78 °C. DIBAL (1 M in hexane, 15 mL) was added via syringe dropwise over a period of 30 minutes. The reaction was then stirred at -78 °C for an additional hour. The reaction was quenched with saturated aqueous sodium potassium tartrate (6 mL), and then allowed to

warm to room temperature. The resulting gel was filtered through a pad of Celite, and washed with copious amounts of DCM. The filtrate was concentrated *in vacuo*, giving the crude aldehyde (1.2 g, 7.5 mmol) as a clear oil, which was used immediately.

Triethyl 2-phosphonopropionate (4.8 mL, 22.5 mmol), DBU (1.3 mL, 9.0 mmol), lithium chloride (795 mg, 18.8 mmol) and acetonitrile (40 mL) were cooled to 0 °C. The crude aldehyde (**2.10**) (1.2 g, 7.5 mmol) was dissolved in acetonitrile (11 mL), and slowly added to the reaction via syringe. The mixture was allowed to warm slowly to room temperature, and monitored by TLC. The reaction was then concentrated, and partitioned between a 2:1 mixture of DCM (10 mL): water (5 mL), and extracted with DCM (5 mL x 3). The organic layer was separated and washed with brine (5 mL). The organic extract was dried with magnesium sulfate, decanted, and concentrated *in vacuo*. Column chromatography of the resulting viscous liquid afforded 778 mg *E*-isomer (3.2 mmol, 32% over two steps, 100% *E*-isomer) ($R_f = 0.6$; 20% ethyl acetate: hexane). $^1\text{H NMR}$ (500 MHz, CDCl_3) δ 6.60 (1 H, m), 4.83 (1 H, s), 4.14 (2 H, q, $J = 7.2$ Hz), 3.85 (2 H, m), 1.81 (3 H, s), 1.39 (9 H, s), 1.22 (3 H, t, $J = 7.2$ Hz). $^{13}\text{C NMR}$ (125 MHz, CDCl_3) δ 167.6, 155.8, 138.2, 129.3, 79.5, 60.7, 38.9, 28.4, 14.2, 12.5.



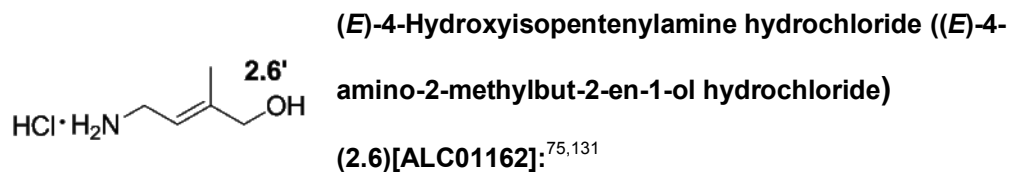
(Z)-Ethyl 4-[(*t*-butoxycarbonyl)-amino]-2-methylbutenoate

(2.11)[ALC01292]:^{132,133}

N-Boc-glycine methyl ester (**2.9**) was converted to the crude

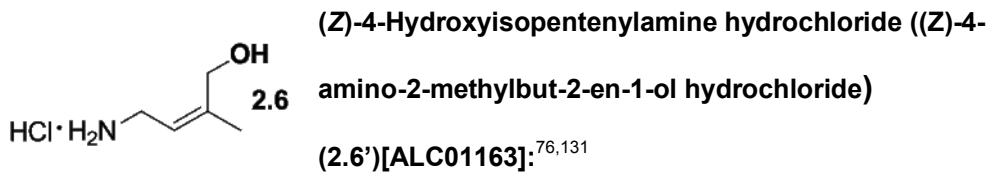
aldehyde as previously described. Triethyl 2-phosphonopropionate (2.5 mL, 12 mmol) and THF (20 mL) were cooled to -78 °C. *n*-BuLi (1.6 M in hexane, 7.5 mL) was added to the mixture, and stirred for 30 minutes. The crude aldehyde was dissolved in THF (30 mL), and slowly added to the phosphonate via syringe. The reaction was stirred at -78 °C for 2.5 h. After completion, the reaction was quenched by the slow addition of saturated

aqueous ammonium chloride (9 mL). The reaction was then allowed to warm to room temperature. The mixture was then concentrated *in vacuo*, dissolved in DCM (10 mL): H₂O (5 mL) (2:1), and extracted with DCM (5 mL x 3). The organic layer was separated and washed with brine (5 mL). The organic extracts were then dried with magnesium sulfate, decanted, and then concentrated *in vacuo*. Column chromatography of resulting viscous liquid afforded 297 mg of the desired *Z*-isomer (1.2 mmol, 11% over two steps), and 72 mg of the *E*-isomer (0.3 mmol) (*R_f* (*Z*) = 0.6; 20% ethyl acetate: hexane). ¹H NMR (500 MHz, CDCl₃) δ 5.88 (1 H, t, *J* = 5.4 Hz), 5.14 (1H, bs), 4.06 (2 H, q, *J* = 7.1 Hz), 3.95 (2 H, d, *J* = 5.3 Hz), 1.76 (3 H, s), 1.31 (9 H, s), 1.17 (3 H, t, *J* = 7.1 Hz). ¹³C NMR (125 MHz, CDCl₃) δ 167.3, 156.0, 140.6, 128.7, 79.1, 60.4, 39.6, 28.3, 20.0, 14.2.



2 M Lithium aluminium hydride in THF (910 µL, 1.8 mmol) was placed in a flame-dried round bottom flask, and cooled to -10 °C in an ice/acetone bath. The ester (**2.12**) (111 mg, 0.5 mmol) was dissolved in THF (5.6 mL) and added to the reaction dropwise via syringe. The reaction was allowed to warm slowly to room temperature, and monitored by TLC (40% ethyl acetate: hexane). The reaction was then cooled to 0 °C, and water (2-3 mL) was slowly added. The desired compound was extracted using DCM (5 mL), and then washed with brine (5 mL). The organic extract was dried with sodium sulfate, decanted, and the filtrate was concentrated *in vacuo* to afford 87 mg (0.4 mmol, 80%) of colorless oil (*R_f* = 0.45; 1:1 ethyl acetate: hexane). ¹H NMR (500 MHz, CDCl₃) δ 5.38 (1 H, t, *J* = 5.5 Hz), 4.78 (1 H, bs), 3.89 (2 H, s), 3.67 (2 H, d, *J* = 5.3 Hz), 3.12 (1 H, s), 1.59 (3 H, s), 1.32 (9 H, s).

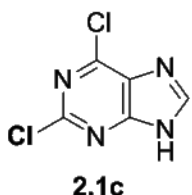
1 M hydrochloric acid (4.0 mL) was then added to the alcohol (87.5 mg, 0.43 mmol), and allowed to stir for 2 hours. A white solid was obtained by concentrating the reaction *in vacuo*, giving 59 mg of a white solid (0.4 mmol, 80%). ¹H NMR (500 MHz, CD₃OD) δ 5.56 (1 H, t, *J* = 7.0 Hz), 3.97 (2 H, s), 3.61 (2 H, d, 6.9 Hz), 1.71 (3 H, s). ¹³C NMR (125 MHz, CD₃OD) δ 143.5, 114.5, 65.8, 36.6, 12.6. Melting point was not obtained for compound.



In a flame-dried round bottom flask, the ester (**2.11**) (257 mg, 1.1 mmol) was dissolved in DCM (5 mL). The solution was then cooled to -78 °C, and DIBAL (3 mL, 1 M in hexane) was slowly added via syringe. The reaction was followed by TLC (1:1 ethyl acetate: hexane). Upon completion, the reaction was quenched at -78 °C with fresh saturated aqueous sodium potassium tartrate (6-9 mL). The reaction was allowed to warm to room temperature. Once at room temperature, the mixture was filtered through a pad of Celite, and washed with DCM (20 mL). The reaction was concentrated *in vacuo* to afford 213 mg (1.1 mmol, 99% yield) colorless oil (*R_f* = 0.47; 1:1 ethyl acetate: hexane). ¹H NMR (500 MHz, CDCl₃) δ 5.26 (1 H, t, *J* = 6.9 Hz), 4.78 (1 H, bs), 4.10 (2 H, s), 3.71 (2 H, d, *J* = 6.9 Hz), 1.81 (3 H, s), 1.38 (9 H, s).

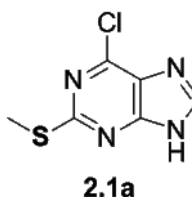
1 M hydrochloric acid (8.0 mL) was then added to the alcohol (213 mg, 1.1 mmol), and allowed to stir for 2 hours. A white solid was obtained by concentrating the reaction *in vacuo*, giving 145 mg of a white solid (1.1 mmol, 100%). ¹H NMR (500 MHz, CD₃OD) δ 5.42 (1 H, t, *J* = 6.0 Hz), 3.80 (2 H, d, *J* = 5.8 Hz), 3.41 (2 H, d, *J* = 6.0 Hz),

1.56 (3 H, s). ^{13}C NMR (125 MHz, CD_3OD) δ 156.0, 123.7, 65.8, 36.6, 14.2. Melting point was not obtained for compound.



2, 6-Dichloropurine (2.1c)[ALC0117]: ⁷²

In a sealed tube, pyridine (2.7 mL, 0.03 mol) was added to xanthine (5.0 g, 0.03 mol) and stirred. Phosphorous oxychloride (6.0 mL, 0.07 mol) was added dropwise via syringe, and the solution was heated to 180 °C for 5 hours. The resulting black solution was poured over ice-water (100 mL) slowly, and allowed to stir for 20 minutes. The organic material was then extracted with a 1:1 solution of diethyl ether: ethyl acetate (5 x 20 mL), and washed with brine (20 mL). The organic extracts were dried over sodium sulfate, decanted, and the filtrate was concentrated *in vacuo* to give 2.05 g (0.01 mol, 33%) of a yellow solid (R_f = 0.15; 3% methanol: DCM). ^1H NMR (500 MHz, $\text{DMSO}-d_6$) δ 8.70 (1 H, s), 3.29 (1 H, s). ^{13}C NMR (125 MHz, $\text{DMSO}-d_6$) δ 156.6, 151.3, 148.5, 148.0, 129.1. Melting point was not obtained for compound.



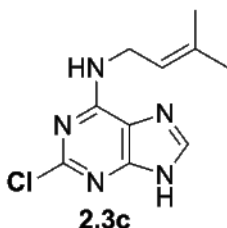
2-Methylthio-6-chloropurine (2.1a)[ALC01133]: ⁶⁰

2-Thioxanthine (200 mg, 1.2 mmol) was placed in a flame-dried round bottom flask, and DMF (5 mL) was added. The solution was cooled to 0 °C. Dimethyl sulfate (280 μL , 3.0 mmol) was added dropwise over a 30 minute time frame to insure that the reaction temperature did not significantly increase. After addition of dimethyl sulfate, the reaction was allowed to warm to room temperature, and monitored by TLC. The orange-yellow mixture was concentrated *in vacuo* and recrystallized in water (20 mL). The solid was filtered, washed with cold water (5 mL) and dried *in vacuo* to give 140 mg (0.8 mmol, 65%) of a light yellow solid (R_f =

0.17; 10% methanol: DCM). ^1H NMR (500 MHz, $\text{DMSO-}d_6$) δ 8.08 (1 H, s), 2.53 (3 H, s).

^{13}C NMR (125 MHz, $\text{DMSO-}d_6$) δ 156.4, 153.9, 142.1, 139.7, 110.8, 13.6.

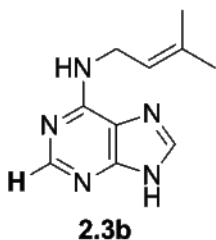
Phosphorous oxychloride (16 mL, 1.7 mol) and *N,N*-dimethylaniline (1.6 mL, 12.6 mmol) were added to 2-methylthioxanthine (1.00 g, 6.0 mmol). The round bottom flask was equipped with a reflux condenser, and the reaction was refluxed for 4 hours. The resulting black solution was concentrated to a viscous black gum, which was purified via column chromatography (R_f = 0.56; 10% methanol: DCM) to give 1.07 g (5 mmol, 89%) of a cream-yellow solid. ^1H NMR (500 MHz, $\text{DMSO-}d_6$) δ 8.48 (1 H, s), 2.53 (3 H, s). ^{13}C NMR (125 MHz, $\text{DMSO-}d_6$) δ 164.8, 155.3, 148.4, 145.7, 127.2, 14.7. Melting point was not obtained for compound.



2-Chloro-*N*⁶-isopentenyl-purine (2-chloro-6-(3-methyl-2-butenylamino)purine) (2.3c)[ALC0157]: ⁷³†

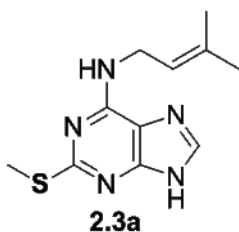
Potassium carbonate (2.15 g, 15.0 mmol), 2,6-dichloropurine (**2.1c**) (1.20 g, 6.0 mmol), 2-isopentenylamine hydrochloride (**2.2**) (876 mg, 7.0 mmol), and *n*-Butanol (15 mL) were added into a sealed tube under inert atmosphere. The reaction was stirred at 110 °C overnight. The reaction was then cooled to room temperature and concentrated *in vacuo* to a yellow-brown solid. Impurities were then precipitated in methanol (30 mL), and removed by filtering through a pad of Celite. The filtrate was concentrated *in vacuo*, and then crystallized in water (30 mL). The resulting solid was filtered and washed with cold water. The solid was then dried under vacuum to give 907 mg (4.0 mmol, 66%) of a slight brown solid (R_f = 0.17; 3% methanol: DCM) with a melting point of 178-181 °C. The wide melting point range observed is thought to be due to the hygroscopic nature of the purine. ^1H NMR (500 MHz, $\text{DMSO-}d_6$) δ 8.07 (1 H, s), 5.24 (1 H, t, J = 5.5 Hz), 3.96 (2 H, d, J = 5.3 Hz), 1.68 (3 H, s), 1.64 (3 H,

s). ^{13}C NMR (125 MHz, $\text{DMSO-}d_6$) δ 154.4, 153.1, 151.3, 139.9, 135.6, 120.8, 113.2, 39.9, 25.9, 18.4.



***N*⁶-Isopentenyl-purine (6-(3-methyl-2-butenylamino)purine) (2.3b)[ALC01144]:** ⁷⁴

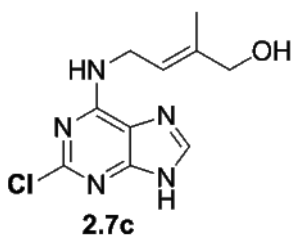
2-Chloro-*N*⁶-isopentenyl-purine (**2.3c**) (300 mg, 1.3 mmol), THF (4 mL), and titanocene dichloride (31.5 mg, 0.1 mmol) were added into a round bottom flask equipped for reflux. 3 M isopropylmagnesium bromide in 2-methyltetrahydrofuran (4.0 mL) was added slowly, and refluxed for 24 hours. The reaction was then cooled to 0 °C, and water (5 mL) was added slowly. The product was extracted with ethyl acetate (5 mL x 3), and washed with brine (5 mL). The organic extracts were then dried with magnesium sulfate, decanted, and concentrated *in vacuo* to afford 185 mg (0.9 mmol, 69% yield) light-mustard colored solid (R_f = 0.37; 10% methanol: DCM). ^1H NMR (500 MHz, $\text{DMSO-}d_6$) δ 8.15 (1 H, s), 8.05 (1 H, s), 7.58 (1 H, bs), 5.28 (1 H, t, J = 5.7 Hz), 4.02 (2 H, d, J = 5.5 Hz), 1.65 (3 H, s), 1.62 (3 H, s). ^{13}C NMR (125 MHz, $\text{DMSO-}d_6$) δ 152.9, 151.8, 139.4, 133.7, 122.8, 66.5, 31.0, 25.9, 18.3, 14.2. Melting point was not obtained for compound.



2-Methylthio-*N*⁶-isopentenyl-purine (2-thiomethyl-6-(3-methyl-2-butenylamino)purine) (2.3a)[ALC01136]: ^{68,134 †}

[Following the procedure for 2-chloro-*N*⁶-isopentenyl-purine (**2.3c**)]. 2-Methylthio-6-chloropurine (**2.1a**) (142 mg, 0.7 mmol), 2-isopentenylamine hydrochloride (**2.2**) (104 mg, 0.9 mmol), and potassium carbonate (256 mg, 1.9 mmol) were added into a flame-dried sealed tube and purged with argon. *n*-Butanol (3.5 mL) was added via syringe, and the reaction was stirred at 110 °C overnight.

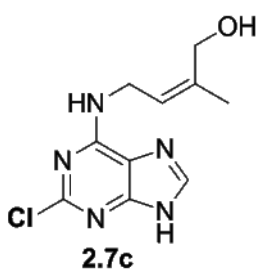
The reaction was cooled to room temperature the next day, and filtered through a pad of Celite, washing with methanol. The filtrate was concentrated *in vacuo* to give a tan yellow solid. Impurities were precipitated in methanol, which were filtered off through a bad of Celite. The impurities were washed with cold methanol, and the resulting filtrate was concentrated *in vacuo* to give 159 mg of a tan-yellow solid (0.6 mmol, 85% yield) ($R_f = 0.52$; 10% methanol:DCM). $^1\text{H NMR}$ (500 MHz, $\text{DMSO-}d_6$) δ 7.93 (1 H, s), 7.76 (1 H, bs), 5.25 (1 H, t, $J = 6.5$ Hz), 3.98 (2 H, m, $J = 5.2$ Hz), 2.41 (3 H, s), 1.62 (3 H, s), 1.60 (3 H, s). $^{13}\text{C NMR}$ (125 MHz, $\text{DMSO-}d_6$) δ 164.1, 153.9, 150.8, 138.1, 133.6, 122.6, 117.0, 39.0, 26.0, 18.4. Melting point was not obtained for compound.



2-Chloro- N^6 -((*E*)-4-hydroxyisopentenyl)-purine (2-chloro-6-((*E*)-4-amino-2-methylbut-2-en-1-ol)purine)

(2.7c)[ALC01118]:

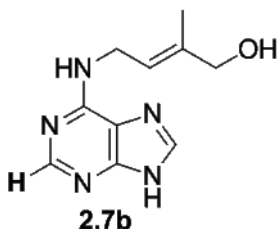
2,6-Dichloropurine (**2.1c**) (266 mg, 1.4 mmol), (*E*)-4-hydroxyisopentenylamine hydrochloride (**2.6**) (233 mg, 1.7 mmol), and potassium carbonate (506 mg, 3.7 mmol) were added into a flame-dried round bottom flask and purged with argon. *n*-Butanol (5 mL) was added via syringe, and the reaction mixture was stirred at 110 °C overnight. The reaction was allowed to cool to room temperature, and then concentrated *in vacuo* to a slight brown solid. The solid was purified via column chromatography ($R_f = 0.40$; 10% methanol:DCM) affording 215 mg of an off white solid (0.8 mmol, 57%). $^1\text{H NMR}$ (500 MHz, $\text{DMSO-}d_6$) δ 8.19 (1H, bs), 8.07 (1 H, s), 5.46 (1 H, t, $J = 5.8$ Hz), 4.74 (1 H, bs), 4.01 (2 H, d, $J = 5.7$ Hz), 3.75 (2 H, s), 1.64 (3 H, s). $^{13}\text{C NMR}$ (125 MHz, $\text{DMSO-}d_6$) δ 155.1, 153.5, 150.9, 139.8, 138.5, 120.2, 118.4, 65.3, 39.9, 14.2. HRMS (ES) m/z (M^+) calculated for $\text{C}_{10}\text{H}_{13}\text{ClN}_5\text{O}$ 354.0879, found 354.0871. Melting point was not obtained for compound.



2-Chloro-*N*⁶-((*Z*)-4-hydroxyisopentenyl)-purine (2-chloro-6-((*Z*)-4-amino-2-methylbut-2-en-1-ol)purine)

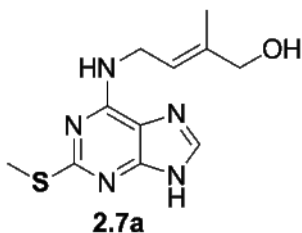
(2.7c')[ALC01300]:

[Following procedure for 2-chloro-*N*⁶-((*E*)-hydroxyisopentenyl)-purine (**2.7c**).] Potassium carbonate (510 mg, 3.7 mmol), 2,6-dichloropurine (**2.1c**) (257 mg, 1.5 mmol), and (*Z*)-4-hydroxyisopentenylamine hydrochloride (**2.6'**) (170 mg, 1.2 mmol) were added into a flame-dried round bottom flask and purged with argon. *n*-Butanol (5 mL) was added, and the reaction was stirred at 115 °C overnight. The reaction was cooled to room temperature, and then concentrated to give a brown viscous liquid. The viscous liquid was then fully dissolved in water (5 mL) and extracted with a 3:1 mixture of ethyl acetate: ether (5 mL x 3). The organic extract was washed with brine (3 mL). The resulting organic extract was then dried with sodium sulfate, decanted, and concentrated *in vacuo*. The concentrated organic extract was then crystallized from ethyl acetate and hexane (3:1 mixture of approximately 10 mL). 232 mg (0.9 mmol, 75% yield) of a cream colored solid was afforded ($R_f = 0.34$; 10% methanol:DCM). ¹H NMR (500 MHz, CD₃OD) δ 7.99 (1 H, s), 5.44 (1 H, t, $J = 7.0$ Hz), 4.25 (2 H, s), 3.29 (2 H, s), 1.81 (3 H, s). ¹³C NMR (125 MHz, DMSO-*d*₆) δ 159.8, 151.5, 144.3, 122.7, 67.8, 60.2, 30.8, 21.7, 19.1, 14.1. HRMS (ESI) m/z (M+H)⁺ calculated for C₁₀H₁₃ClN₅O 354.0809, found 354.0897. Melting point was not obtained for compound.



***N*⁶-((*E*)-4-Hydroxyisopentenyl)-purine (6-((*E*)-4-amino-2-methylbut-2-en-1-ol)purine) (2.7b)[ALC01145].¹³⁵**

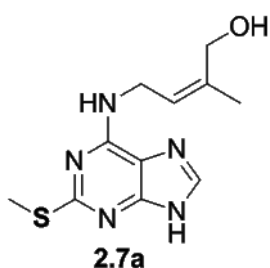
2-Chloro-*N*⁶-((*E*)-4-hydroxyisopentenyl)-purine (**2.7c**) (107 mg, 0.4 mmol), THF (2 mL), and titanocene dichloride (10.5 mg, 0.04 mmol) were added into a round bottom flask equipped for reflux. 3 M isopropylmagnesium bromide in 2-methyltetrahydrofuran (2 mL) was added dropwise via syringe. The reaction was refluxed for 24 hours. The reaction was then cooled to 0 °C, and water (5 mL) was added slowly. The product was extracted with ethyl acetate (5 mL x 3), and washed with brine (5 mL). The organic extracts were dried with magnesium sulfate, decanted, and concentrated *in vacuo* to afford 41.8 mg (0.2 mmol, 50% yield) light-brown colored solid (*R*_f = 0.21; 10% methanol: DCM). ¹H NMR (500 MHz, DMSO-*d*₆) δ 8.14 (1 H, s), 8.04 (1 H, s), 7.63 (1 H, bs), 5.49 (1 H, t, *J* = 5.6 Hz), 4.71 (1 H, bs), 4.07 (2 H, d, *J* = 5.4 Hz), 3.75 (2 H, s), 1.62 (3 H, s). ¹³C NMR (125 MHz, DMSO-*d*₆) δ 154.8, 152.9, 139.2, 137.6, 121.3, 66.4, 37.8, 29.6, 14.2. Melting point was not obtained for compound.



2-Methylthio-*N*⁶-((*E*)-4-hydroxyisopentenyl)-purine (2-thiomethyl-6-((*E*)-4-amino-2-methylbut-2-en-1-ol)purine) (2.7a)[ALC01164].¹³⁴

[Following procedure for 2-chloro-*N*⁶-((*E*)-4-hydroxyisopentenyl)-purine (**2.7c**).] Potassium carbonate (102 mg, 0.7 mmol), 2-methylthio-6-dichloropurine (**2.1a**) (63 mg, 0.3 mmol), and (*E*)-4-hydroxyisopentenylamine hydrochloride (**2.6**) (40 mg, 0.3 mmol) were added into a flame-dried round bottom flask and purged with argon. *n*-Butanol (1.6 mL) was added via syringe, and the reaction was stirred at 115 °C overnight. The reaction was cooled to

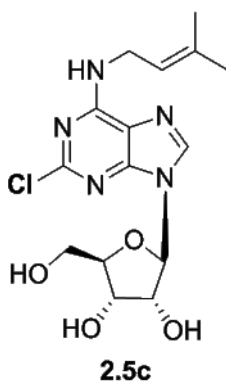
room temperature the following morning. The mixture was then filtered through a pad of Celite, and washed with methanol and DCM (10 mL each). The filtrate was concentrated to a slight brown solid, which was purified via column chromatography ($R_f = 0.30$; 10% methanol:DCM) to afford a light yellow solid (0.03 mmol, 10%). ^1H NMR (500 MHz, DMSO- d_6) δ 7.90 (1 H, s), 7.80 (1 H, bs), 5.46 (1 H, t, $J = 5.5$ Hz), 4.70 (1 H, bs), 4.03 (2 H, d, $J = 5.3$ Hz), 3.75 (2 H, s), 2.41 (3 H, s), 1.63 (3 H, s). ^{13}C NMR (125 MHz, DMSO- d_6) δ 164.1, 161.2, 153.9, 138.1, 137.7, 121.2, 120.0, 115.9, 66.4, 14.2. Melting point was not obtained for compound.



2-Methylthio- N^6 -((Z)-4-hydroxyisopentenyl)-purine (2-thiomethyl-6-((Z)-4-amino-2-methylbut-2-en-1-ol)purine (2.7a')) [ALC0205].¹³⁴

[Following procedure for 2-chloro- N^6 -((Z)-4-hydroxyisopentenyl)-purine (2.7c').] Potassium carbonate (283 mg, 2.1 mmol), 2-methylthio-6-dichloropurine (**2.1a**) (128 mg, 0.6 mmol), and (Z)-4-hydroxyisopentenylamine hydrochloride (**2.6'**) (106 mg, 0.8 mmol) were added into a flame-dried round bottom flask and purged with argon. *n*-Butanol (2 mL) was added, and the reaction was stirred at 115 °C overnight. The reaction was cooled to room temperature the following morning. The mixture was then concentrated to a brown viscous liquid. The viscous liquid was then dissolved in water (5 mL) and extracted with a 3:1 mixture of ethyl acetate: ether (5 mL x 3). The organic extracts were washed with brine (5 mL). The organic extract was then dried with sodium sulfate, decanted, and concentrated *in vacuo*. The concentrated organic extract was then crystallized in ethyl acetate and hexane (3:1 mixture of approximately 7 mL). The resulting solid was filtered, washing with cold ethyl acetate (3 mL). The solid was then dried under vacuum to afford

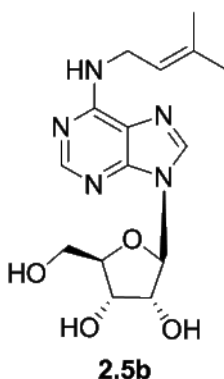
112 mg (0.4 mmol, 66% yield) of a cream colored solid ($R_f = 0.26$; 8% methanol: DCM). ^1H NMR (500 MHz, CD_3OD) δ 7.87 (1 H, s), 5.46 (1 H, t, $J = 7.09$ Hz), 4.19 (2 H, s), 3.29 (2 H, d, $J = 7.08$ Hz), 2.51 (3 H, s), 1.80 (3 H, s). ^{13}C NMR (125 MHz, CD_3OD) δ 165.8, 138.4, 137.9, 123.4, 60.2, 57.0, 37.2, 20.1, 17.0, 13.1. Melting point was not obtained for compound.



2-Chloro- N^6 -isopentenyl-adenosine (2-chloro-6-(3-methyl-2-butenylamino) adenosine) (2.5c)[ALC0175]:⁸²

2-Chloro- N^6 -isopentenyl-purine (**2.3c**) (500 mg, 2.1 mmol) was dissolved in acetonitrile (8.7 mL). *N,O*-bis(trimethylsilyl)acetamide, BSA, (856 μL , 3.5 mmol) was added. The reaction flask was adapted with a condenser, and heated to reflux for 15 minutes. In another round bottom flask, 1,2,3,5-tetra-*O*-acetyl-*D*-ribofuranose (**2.4**) (557 mg, 1.8 mmol) was dissolved in acetonitrile (8.7 mL). The ribose solution was then syringed into the reaction, and trimethylsilyl trifluoromethanesulfonate, TMSOTf, (475 μL , 2.6 mmol) was added. The reaction was then heated to reflux for 12 hours. The reaction was cooled to room temperature, and a 2:1 mixture of chloroform (50 mL): water (25 mL) was added. The organic extract was washed with water until a pH \sim 6 was obtained. The organic extracts were dried over sodium sulfate, decanted, and concentrated *in vacuo*. The resulting viscous liquid was purified via column chromatography ($R_f = 0.38$; 3% methanol:DCM) to afford 616 mg of a white solid (1.2 mmol, 71% isolated α/β nucleoside). Data for major epimer (β), in agreement with referenced literature: ^1H NMR (500 MHz, $\text{DMSO-}d_6$) δ 7.83 (1 H, s), 6.12 (1 H, s), 5.73 (1 H, t, $J = 5.0$ Hz), 5.55 (1 H, t, $J = 5.0$ Hz), 4.64 (1 H, t, $J = 5.0$ Hz), 4.35 (2 H, d, $J = 5.1$ Hz), 4.10 (2 H, m), 2.07 (9 H, m), 2.02 (2 H, s), 1.68 (6 H, s).

Sodium methoxide (201 mg, 3.7 mmol) was dissolved in methanol (18 mL), and the solution was added to the white solid (616 mg, 1.2 mmol). The reaction was stirred at room temperature for 6 hours. Glacial acetic acid was added dropwise to the mixture to achieve a pH of ~6. The reaction was then concentrated *in vacuo* to a slight yellow viscous oil, which was purified via column chromatography ($R_f = 0.38$; 5% methanol:DCM) to afford 437 mg of an off white solid (1.18 mmol, 95% pure β -epimer). The reaction resulted in a ratio of 1:3 α : β of isolated nucleoside. Diastereomeric ratio was determined by both HPLC and ^1H NMR (based on anomeric peak, chemical shift = 5.77 ppm). Separation of α/β mixture was possible by column conditions mentioned, and yield noted is based on pure β -epimer. Data for major epimer (β): ^1H NMR (500 MHz, $\text{DMSO-}d_6$) δ 7.87 (1 H, s), 7.18 (1 H, bs), 5.77 (1 H, d, $J = 6.8$ Hz), 5.28 (1 H, d, $J = 6.7$ Hz), 4.90 (1 H, m), 4.37 (1 H, s), 4.24 (1 H, s), 4.14 (1 H, m), 4.02 (1 H, m), 3.87 (1 H, d, $J = 12.5$ Hz), 3.70 (1 H, d, $J = 12.5$ Hz), 1.70 (6 H, s). ^{13}C NMR (125 MHz, $\text{DMSO-}d_6$) δ 155.2, 153.7, 150.0, 134.6, 121.6, 119.1, 87.9, 85.2, 74.2, 70.9, 61.9, 49.1, 25.9, 18.4. MS (ESI) m/z 372.2 (33%, $\text{M}+2$, isotope), 370.2 (100%, $\text{M}+\text{H}^+$). HRMS (ESI) m/z ($\text{M}+\text{H}^+$)⁺ calculated for $\text{C}_{15}\text{H}_{21}\text{ClN}_5\text{O}_4$ 370.1204, found 370.1282. HPLC: (Kinetex) $\beta = 60.66$ minutes; (Fruic-N) $\beta = 4.32$ minutes. Within three attempts, a reproducible melting point was not obtained. The wavering wide range observed is believed to be due to the hygroscopic nature of the nucleoside.



***N*⁶-isopentenyl-adenosine (6-(3-methyl-2-butenylamino)adenosine) (2.5b)[ALC01223]:⁸²**

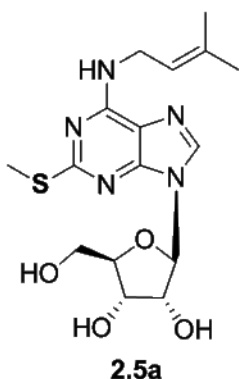
[Following procedure for 2-chloro-*N*⁶-isopentenyl-adenosine (2.5c).]

*N*⁶-Isopentenyl-purine (2.3b) (85 mg, 0.42 mmol), acetonitrile (1.7 mL), and BSA (205 μ L, 0.8 mmol) were heated to reflux for 15 minutes. 1,2,3,5-tetra-*O*-acetyl-*D*-ribofuranose (2.4) (111 mg, 0.35 mmol), and acetonitrile (1.7 mL) were combined in a separate round

bottom flask. After the purine mixture was allowed to reflux for 15 minutes, the ribose mixture was added via syringe. TMSOTf (95 μ L, 0.5 mmol) was then added slowly via syringe, and the reaction was heated to reflux for 12 hours. The reaction was then cooled to room temperature. The resulting mixture was washed with water to obtain a pH of ~6. The organic extracts were concentrated *in vacuo*, and purified via column chromatography (8% methanol: DCM) to afford 90 mg of a viscous clear liquid (0.2 mmol, 55% mixture of α/β nucleoside). Data for major epimer (β), in agreement with referenced literature: ¹H NMR (500 MHz, DMSO-*d*₆) δ 8.84 (1 H, s), 8.82 (1 H, s), 6.43 (1 H, d, *J* = 3.8 Hz), 6.33 (1 H, d, *J* = 5.1 Hz), 6.01 (1 H, m), 5.60 (1 H, m), 4.39 (2 H, d, *J* = 3.7 Hz), 4.22 (1 H, m), 2.09 (2 H, s), 2.02 (9 H, m).

Sodium methoxide (31 mg, 0.6 mmol) and methanol (3 mL) were added to the nucleoside (90 mg, 0.2 mmol) in a round bottom flask, and stirred at room temperature for 6 hours. Glacial acetic acid was added to obtain a pH of ~6. The reaction was then concentrated *in vacuo*, and purified via column chromatography (*R*_f = 0.05; 5% methanol: DCM) to give 30 mg a white solid (0.092 mmol, 50% pure β -epimer). Reaction resulted in a ratio of 2:3 α/β of isolated nucleoside. Diastereomeric ratio was determined by both HPLC and ¹H NMR (based on anomeric peak, chemical shift = 5.95 ppm). Separation of α/β mixture was possible by column conditions mentioned, and the yield noted is based

on pure β -epimer. Data for major epimer (β): ^1H NMR (300 MHz, CD_3OD) δ 8.23 (1 H, s), 8.20 (1 H, s), 5.94 (1 H, d, $J = 5.8$ Hz), 5.36 (1 H, m), 4.72 (1 H, t, $J = 5.7$ Hz), 4.31 (1 H, m), 4.16 (2 H, m), 3.85 (1 H, d, $J = 12.6$ Hz), 3.75 (1 H, d, $J = 12.6$ Hz), 1.75 (6 H, s). ^{13}C NMR (125 MHz, $\text{DMSO}-d_6$) δ 153.0, 152.0, 151.8, 142.4, 140.1, 139.8, 120.0, 89.7, 86.9, 80.5, 75.2, 71.4, 62.2, 24.5, 16.7. MS (ESI) m/z 335.1 (20%, $\text{M}+\text{H}^+$), 221.1 (78%), 136.0 (100%). HRMS (ESI) m/z ($\text{M}+\text{H}^+$)⁺ calculated for $\text{C}_{15}\text{H}_{21}\text{N}_5\text{O}_4$ 335.1594, found 335.1593. HPLC: (Kinetex) $\alpha = 53.52$ minutes, $\beta = 55.15$ minutes; (Fruic-N) $\beta = 6.09$ minutes. Melting point was not obtained for compound.



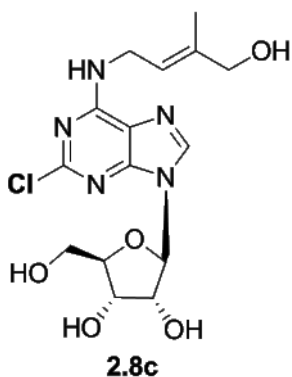
2-Methylthio- N^6 -isopentenyl-adenosine (2-thiomethyl-6-(3-methyl-2-butenylamino) adenosine) (2.5a)[ALC01142]:¹³⁴

[Following procedure for 2-chloro- N^6 -isopentenyl-adenosine (2.5c).] 2-Methylthio- N^6 -isopentenyl-purine (2.3a) (86 mg, 0.4 mmol), acetonitrile (1.4 mL), and BSA (186 μL , 0.8 mmol) were heated to reflux for 15 minutes. 1,2,3,5-tetra-O-acetyl-*D*-ribofuranose (2.4) (92 mg, 0.3 mmol), and acetonitrile (1.4 mL),

were combined in a separate round bottom flask. Once the purine mixture was allowed to reflux for 15 minutes, the ribose mixture was added via syringe. TMSOTf (78 μL , 0.4 mmol) was then added slowly, and the reaction was heated to reflux for 12 hours. The reaction was then cooled to room temperature, and washed with water to obtain a pH of ~ 6 . The organic extracts were concentrated *in vacuo*, and purified via column chromatography (5% methanol: DCM) to afford a 42 mg viscous clear liquid (0.08 mmol, 29% isolated α/β nucleoside). Data for major epimer (β), in agreement with referenced literature: ^1H NMR (500 MHz, $\text{DMSO}-d_6$) δ 8.14 (1 H, s), 8.03 (1 H, bs), 6.12 (1 H, d, $J = 5.0$ Hz), 5.64 (1 H, t, $J = 5.7$ Hz), 5.37 (1 H, t, $J = 5.7$ Hz), 5.23 (1 H, m), 4.79 (1 H, m) (1

H, d, $J = 3.7$ Hz), 4.36 (1 H, d, $J = 3.7$ Hz), 4.17 (1 H, m), 3.98 (2 H, m), 2.49 (3 H, s), 2.03 (9 H, m), 1.94 (2 H, s), 1.62 (6 H, s).

Sodium (42 mg, 0.3 mmol) and methanol (1 mL) were added together. The nucleoside (42 mg, 0.08 mmol) was then added, and stirred at room temperature for 6 hours. Glacial acetic acid was added to obtain a pH of ~ 6 . The reaction was concentrated *in vacuo*, and purified via column chromatography ($R_f = 0.08$; 5% methanol: DCM) to give 17 mg a white solid (0.08 mmol, 57% pure β -epimer). The reaction resulted in a ratio of 2:3 α : β of isolated nucleoside, determined by HPLC and ^1H NMR (based on anomeric peak, chemical shift = 5.89 ppm). Separation of α / β mixture was possible by column conditions mentioned, and the yield noted is based on pure β -epimer. Data for major epimer (β): ^1H NMR (500 MHz, $\text{DMSO-}d_6$) δ 7.77 (1 H, s), 5.89 (1 H, d, $J = 6.0$ Hz), 5.24 (1 H, t, $J = 7.1$ Hz), 4.97 (1 H, t, $J = 6.0$ Hz), 4.73 (1 H, m), 4.35 (2 H, s), 4.05 (1 H, m), 3.85 (2 H, m), 2.43 (3 H, s), 1.66 (6 H, s). ^{13}C NMR (125 MHz, $\text{DMSO-}d_6$) δ 139.4, 139.0, 133.8, 122.5, 117.6, 88.7, 86.0, 85.5, 79.6, 75.6, 73.8, 71.0, 62.1, 61.6, 25.9, 18.4. MS (ESI) m/z 381.1 (27%, $\text{M}+\text{H}^+$), 249.1 (55%), 234.1 (100%), 206.0 (80%), 181.0 (47%). HRMS (ESI) m/z ($\text{M}+\text{H}^+$) calculated for $\text{C}_{16}\text{H}_{23}\text{N}_5\text{O}_4\text{S}$ 381.1471, found 381.1470. HPLC: (Kinetex) $\alpha = 61.93$ minutes, $\beta = 62.30$ minutes; (Frulic-N) $\beta = 4.76$ minutes. Melting point was not obtained for compound.

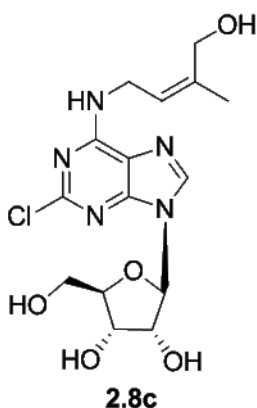


2-Chloro-*N*⁶-((*E*)-4-hydroxyisopentenyl)-adenosine (2-chloro-6-((*E*)-4-amino-2-methylbut-2-en-1-ol) adenosine) (2.8c)[ALC01121]:

[Following procedure for 2-chloro-*N*⁶-isopentenyl-adenosine (2.5c).] 2-Chloro-*N*⁶-((*E*)-4-hydroxyisopentenyl)-purine (2.7c) (212 mg, 0.8 mmol), acetonitrile (3.5 mL), and BSA (407 μL, 1.7 mmol) were heated to reflux for 15 minutes. 1,2,3,5-tetra-*O*-acetyl-*D*-ribofuranose (2.4) (221 mg, 0.7 mmol), and acetonitrile (3.5 mL) were combined in a separate round bottom flask. Once the purine mixture had refluxed for 15 minutes, the ribose mixture was added via syringe. TMSOTf (190 μL, 1.0 mmol) was then added slowly via syringe, and the reaction was heated to reflux for 12 hours. The reaction was cooled to room temperature, then washed with water to obtain a pH of ~6. The organic extracts were concentrated *in vacuo*, and purified via column chromatography (R_f = 0.11; 5% methanol: DCM) to afford 328 mg a viscous clear liquid (0.6 mmol, 92% isolated α/β nucleoside). Data for major epimer (β): ¹H NMR (500 MHz, DMSO-*d*₆) δ 8.14 (1 H, s), 6.13 (1 H, d, J = 2.9 Hz), 5.47 (1 H, m), 4.97 (1 H, m), 4.90 (2 H, t, J = 1.5 Hz), 4.75 (1 H, d, J = 2.7 Hz), 4.32 (1 H, s), 4.18 (1 H, m), 3.74 (2 H, d, J = 5.9 Hz), 3.63 (1 H, m), 2.07 (2 H, s), 2.02 (9 H, m), 1.63 (3 H, s).

Sodium methoxide (104 mg, 1.9 mmol) and methanol (10 mL) were added to the nucleoside (328 mg, 0.6 mmol), and stirred at room temperature for 6 hours. Glacial acetic acid was added to obtain a pH of ~6. The reaction was concentrated *in vacuo*, and purified via column chromatography (R_f = 0.10; 10% methanol: DCM) to give 150 mg of a white solid (0.4 mmol, 60% pure α/β nucleoside). The reaction resulted in a ratio of 1:3 $\alpha:\beta$ of isolated nucleoside, determined by HPLC and ¹H NMR (based on anomeric peak, chemical shift = 5.74 ppm). Data for major epimer (β): ¹H NMR (500 MHz, DMSO-*d*₆)

δ 8.35 (1 H, s), 7.82 (1 H, bs), 5.74 (1 H, d, $J = 5.5$ Hz), 5.47 (1 H, t, $J = 5.5$ Hz), 5.04 (1 H, bs), 4.73 (1 H, s), 4.48 (1 H, t, $J = 5.3$ Hz), 4.09 (1 H, t, $J = 5.3$ Hz), 4.01 (1 H, t, $J = 5.5$ Hz), 3.91 (1 H, m), 3.75 (2 H, s), 3.61 (1 H, m), 3.51 (1 H, m), 1.64 (3 H, s). ^{13}C NMR (125 MHz, DMSO- d_6) δ 170.6, 155.6, 155.0, 153.4, 149.9, 140.0, 138.6, 120.0, 87.9, 85.2, 74.2, 70.9, 65.2, 61.9, 14.2. MS (ESI) m/z 388.1 (7%, M+2, isotope), 386.1 (20%, M+H $^+$), 304.0 (8%), 302.0 (25%), 238.1 (20%), 236.1 (60%), 172.0 (33%), 170.0 (100%). HRMS (ESI) m/z (M+H) $^+$ calculated for C $_{15}$ H $_{21}$ ClN $_5$ O $_5$ 386.1231, found 386.1231. HPLC: (Kinetex) $\beta = 52.44$ minutes; (Frulic-N) $\beta = 10.06$ minutes. Melting point was not obtained for compound.

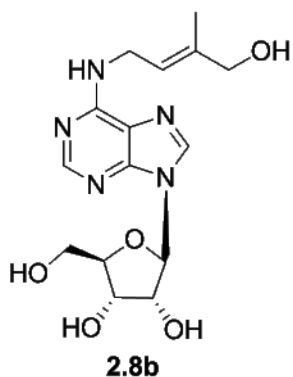


2-Chloro- N^6 -((Z)-4-hydroxyisopentenyl)-adenosine (2-chloro-6-((Z)-4-amino-2-methylbut-2-en-1-yl) adenosine) (2.8c')[ALC0202]:

[Following procedure for 2-chloro-6-((E)-4-hydroxyisopentenyl)-adenosine (2.8c)] 2-Chloro- N^6 -((Z)-4-hydroxyisopentenyl)-purine (2.7c') (200 mg, 0.8 mmol), acetonitrile (3.3 mL), and BSA (580 μL , 2.4 mmol) were heated to reflux for 15 minutes. 1,2,3,5-tetra- O -acetyl- D -ribofuranose (2.4) (210 mg, 0.7 mmol), and acetonitrile (3.3 mL) were added together in a separate round bottom flask. After the purine mixture had refluxed for 15 minutes, the ribose mixture was added via syringe. TMSOTf (179 μL , 1.0 mmol) was then added slowly via syringe, and the reaction was heated to reflux for 12 hours. The reaction was concentrated *in vacuo*, then dissolved in a 2:1 mixture of chloroform (4 mL): H $_2$ O (2 mL). The organic extract was washed with water to obtain a pH of ~ 6 . The organic extracts were then dried with sodium sulfate, decanted, and concentrated *in vacuo*. The viscous liquid was purified via column chromatography ($R_f = 0.11$; 5% methanol: DCM) to

afford 287 mg (0.6 mmol, 71% isolated α/β nucleoside) of a viscous clear liquid. Data for major epimer (β): ^1H NMR (500 MHz, CD_3OD) δ 7.87 (1 H, s), 5.27 (1 H, bs), 6.14 (1 H, d, $J = 5.7$ Hz), 5.74 (1 H, m), 5.32 (1 H, m), 4.39 (2 H, m), 4.26 (3 H, m), 3.39 (1 H, bs), 2.12 (9 H, m), 2.07 (2 H, s), 1.80 (3 H, s).

Sodium methoxide (91 mg, 1.7 mmol) and methanol (3 mL) were added to the nucleoside (287 mg), and stirred at room temperature for 6 hours. Glacial acetic acid was added to obtain a pH of ~ 6 . The reaction was concentrated *in vacuo*, and purified via column chromatography ($R_f = 0.10$; 8% methanol: DCM) to give 121 mg of a white solid (0.3 mmol, 56% α/β nucleoside) with a melting point of 190-215 $^\circ\text{C}$ (the wide melting point range is believed to be due to the hygroscopic nature of the nucleoside). The reaction resulted in a ratio of 1:2 $\alpha:\beta$ of isolated nucleoside, determined by HPLC and ^1H NMR (based on anomeric peak, chemical shift = 5.88 ppm). Data for major epimer (β): ^1H NMR (500 MHz, $d\text{-CD}_3\text{OD}$) δ 8.16 (1 H, m), 5.88 (1 H, d, $J = 6.9$ Hz), 5.41 (1 H, t, $J = 7.1$ Hz), 4.63 (1 H, m), 4.30 (1 H, m), 4.17 (3 H, m), 4.12 (1 H, dd, $J = 9.9, 2.8$ Hz), 3.86 (1 H, dd, $J = 9.8, 2.7$), 3.71 (2 H, m), 1.79 (3 H, s). ^{13}C NMR (125 MHz, CD_3OD) δ 154.8, 148.9, 140.3, 138.9, 122.5, 119.0, 89.7, 86.5, 80.3, 74.2, 71.1, 62.0, 60.3, 37.5, 20.3. MS (ESI) m/z 388.1 (33%, $\text{M}+2$, isotope), 386.1 (100%, $\text{M}+\text{H}^+$), 256.1 (17%), 254.1 (50%). HRMS (ESI) m/z ($\text{M}+\text{H}^+$) $^+$ calculated for $\text{C}_{15}\text{H}_{21}\text{ClN}_5\text{O}_5$ 386.1231, found 386.1226. HPLC: (Fruhic-N) $\beta = 8.71$ minutes.

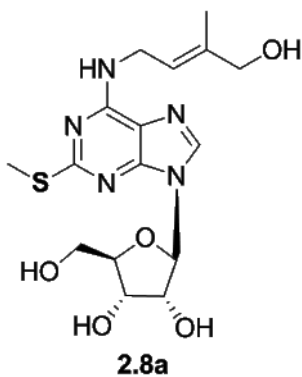


***N*⁶-((*E*)-4-Hydroxyisopentenyl)-adenosine (6-((*E*)-4-amino-2-methylbut-2-en-1-ol) adenosine) (2.8b)[ALC01253]:** ^{131,134}

[Following procedure for 2-chloro-*N*⁶-((*E*)-4-hydroxyisopentenyl)-adenosine (2.8c).] *N*⁶-((*E*)-Hydroxyisopentenyl)-purine (2.7b) (20 mg, 0.09 mmol), acetonitrile (0.4 mL), and BSA (50 μ L, 0.2 mmol) were heated to reflux for 30 minutes. 1,2,3,5-tetra-*O*-acetyl-*D*-ribofuranose (2.4) (25 mg, 0.08 mmol), and acetonitrile (0.4 mL) were combined in a separate round bottom flask. After the purine mixture had refluxed for 30 minutes, the ribose mixture was added slowly via syringe. TMSOTf (23 μ L, 0.1 mmol) was then added slowly via syringe, and the reaction was heated to reflux for 12 hours. The reaction was then cooled to room temperature and washed with water to obtain a pH of \sim 6. The organic extracts were concentrated *in vacuo*, and purified via column chromatography (R_f = 0.21; 10% methanol: DCM) to afford 20 mg of a viscous clear liquid (0.04 mmol, 50% isolated α/β nucleoside). Data for major epimer (β), in agreement with referenced literature: ¹H NMR (300 MHz, CD₃OD) δ 8.19 (1 H, s), 8.18 (1 H, s), 6.19 (1 H, d, J = 5.3 Hz), 6.01 (1 H, m), 5.68 (1 H, t, J = 4.6 Hz), 4.41 (2 H, m), 3.95 (2 H, s), 3.43 (1 H, m), 3.29 (2 H, s), 2.12 (2 H, s), 2.09 (9 H, m), 1.76 (3 H, s).

Sodium methoxide (6.5 mg, 0.1 mmol) and methanol (0.5 mL) were added to the nucleoside (20 mg, 0.04 mmol), and stirred at room temperature for 6 hours. Glacial acetic acid was added to acidify to pH of \sim 6. The reaction was concentrated *in vacuo*, and purified via column chromatography (R_f = 0.10; 10% methanol: DCM) to give 13 mg of a clear viscous liquid (0.04 mmol, 92% isolated α/β nucleoside). The reaction resulted in a ratio of 2:3 α/β of isolated nucleoside, determined by HPLC and ¹H NMR (based on anomeric peak, chemical shift = 5.80 ppm). Data for major epimer (β): ¹H NMR (500

MHz, DMSO- d_6) δ 8.31 (1 H, s), 8.30 (1 H, s), 8.18 (1 H, bs), 5.80 (1 H, d, J = 5.2 Hz), 5.48 (1 H, t, J = 6.0 Hz), 4.65 (1 H, m), 4.52 (1 H, m), 4.11 (2 H, s), 3.91 (1 H, m), 3.74 (2 H, s), 3.62 (1 H, dd, J = 11.2, 3.4 Hz), 3.52 (1 H, dd, J = 11.2, 3.4 Hz), 1.62 (3 H, s). ^{13}C NMR (125 MHz, DMSO- d_6) δ 172.1, 165.8, 155.2, 52.6, 140.1, 137.8, 88.6, 86.4, 79.8, 75.9, 70.3, 66.7, 61.7, 33.9, 17.4, 14.2. MS (ESI) m/z 354.2 (100%, $\text{M}+\text{H}^+$), 352.2 (50%). HRMS (ESI) m/z ($\text{M}+\text{H}^+$)⁺ calculated for $\text{C}_{15}\text{H}_{22}\text{N}_5\text{O}_5$ 352.1611, found 352.1621. HPLC: (Kinetex) β = 53.27 minutes; (Fruic-N) β = 15.52 minutes.

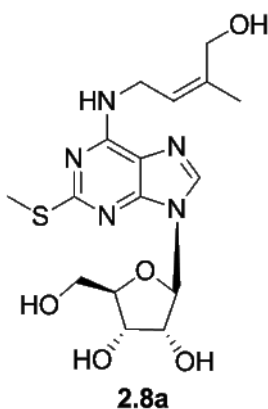


2-Methylthio- N^6 -((E)-4-hydroxyisopentenyl)-adenosine (2-thiomethyl-6-((E)-4-amino-2-methylbut-2-en-1-ol) adenosine) (2.8a)[ALC01257]:^{131,134}

[Following procedure for 2-chloro- N^6 -((E)-4-hydroxyisopentenyl)-adenosine (2.8c).] 2-Methylthio- N^6 -((E)-4-hydroxyisopentenyl)-purine (2.7a) (70 mg, 0.3 mmol), acetonitrile (1 mL), and BSA (194 μL , 0.8 mmol) were heated to reflux for 30 minutes. 1,2,3,5-tetra- O -acetyl- D -ribofuranose (2.4) (70 mg, 0.2 mmol), and acetonitrile (1 mL) were combined in a separate round bottom flask. Once the purine mixture had refluxed for 30 minutes, the ribose mixture was added via syringe. TMSOTf (60 μL , 0.3 mmol) was then added slowly via syringe, and the reaction was heated to reflux for 12 hours. The reaction was then cooled to room temperature and washed with water to obtain a pH \sim 6. The organic extracts were concentrated *in vacuo*, and purified via column chromatography (R_f = 0.15; 5 % methanol: DCM) to afford 73 mg a viscous, slightly yellow, liquid (0.2 mmol, 63% isolated α/β nucleoside). Data for major epimer (β), in agreement with referenced literature: ^1H NMR (500 MHz, DMSO- d_6) δ 7.98 (1 H, s), 6.11 (1 H, d, J = 4.7 Hz), 5.75 (1 H, t, J = 5.0 Hz), 5.40 (1 H, m), 4.38 (1 H, m), 4.26 (1 H,

m), 3.93 (2 H, s), 3.42 (1 H, m), 3.29 (2 H, s), 2.53 (3 H, s), 2.10 (2 H, s), 2.06 (9 H, m), 1.76 (3 H, s).

Sodium methoxide (23 mg, 0.4 mmol) and methanol (2 mL) were added to the nucleoside (73 mg, 0.2 mmol), and stirred at room temperature for 6 hours. Glacial acetic acid was added to acidify to a pH ~6. The reaction was concentrated *in vacuo*, and purified via column chromatography (5% methanol: DCM) to give 40 mg of a light yellow solid (0.1 mmol, 72% α/β nucleoside). The reaction resulted in a ratio of 2:3 $\alpha:\beta$ of isolated nucleoside, determined by HPLC and ^1H NMR (based on anomeric peak, chemical shift = 5.78 ppm). Data for major epimer (β): ^1H NMR (500 MHz, CD_3OD) δ 8.15 (1 H, s), 7.88 (1 H, bs), 5.78 (1 H, d, $J = 3.6$ Hz), 5.46 (1 H, d, $J = 6.4$ Hz), 4.55 (1 H, t, $J = 5.6$), 4.11 (2 H, m), 3.89 (1 H, m), 3.74 (2 H, s), 3.59 (1 H, dd, $J = 12.5, 4.9$ Hz), 3.47 (1 H, dd, $J = 12.09, 5.00$ Hz), 2.45 (3 H, s), 1.67 (3 H, s). ^{13}C NMR (125 MHz, $\text{DMSO}-d_6$) δ 173.1, 164.6, 154.3, 139.0, 137.9, 120.9, 117.7, 87.8, 85.5, 73.8, 66.7, 62.1, 49.1, 33.2, 17.3, 14.2. MS (ESI) m/z 400.2 (100%, $\text{M}+\text{H}^+$), 398.1 (45%). HRMS (ESI) m/z ($\text{M}+\text{H}^+$) calculated for $\text{C}_{16}\text{H}_{24}\text{N}_5\text{O}_5\text{S}$ 398.1498, found 398.1486. HPLC: (Kinetex) $\beta = 54.24$ minutes; (Fruvic-N) $\beta = 10.38$ minutes. Melting point was not obtained for compound.



2-Methylthio- N^6 -((*Z*)-4-hydroxyisopentenyl)-adenosine (2-thiomethyl-6-((*Z*)-4-amino-2-methylbut-2-en-1-ol) adenosine) (2.8a'**)[ALC0208]:^{131,134}**

[Following procedure for 2-chloro- N^6 -((*E*)-4-hydroxyisopentenyl)-adenosine (**2.8c**).] 2-Methylthio- N^6 -((*Z*)-4-hydroxyisopentenyl)-purine (**2.7a'**) (112 mg, 0.4 mmol), acetonitrile (1.8 mL), and BSA (308 μL , 1.3 mmol) were heated to reflux for 30 minutes.

1,2,3,5-tetra-O-acetyl-*D*-ribofuranose (**2.4**) (111 mg, 0.4 mmol), and acetonitrile (1.8 mL)

were combined in a separate round bottom flask. Once the purine mixture had refluxed for 30 minutes, the ribose mixture was added via syringe. TMSOTf (95 μ L, 0.5 mmol) was then added slowly via syringe, and the reaction was heated to reflux for 12 hours. The reaction was concentrated *in vacuo*, then dissolved in a 2:1 ratio of chloroform (4 mL): H₂O (2 mL). The organic extract was washed with water to obtain a pH of ~6. The organic extracts were dried with sodium sulfate, decanted, and concentrated *in vacuo*. The resulting viscous brown liquid was purified via column chromatography (R_f = 0.30; 5% methanol: DCM) to afford 144 mg (0.3 mmol, 78% isolated α/β nucleoside) of a viscous clear liquid. Data for major epimer (β), in agreement with referenced literature: ¹H NMR (500 MHz, CD₃OD) δ 7.97 (1 H, s), 5.28 (1 H, m), 6.09 (1 H, d, J = 3.6 Hz), 5.43 (1 H, t, J = 7.1 Hz), 4.40 (1 H, m), 4.35 (2 H, m), 4.18 (2 H, m), 3.29 (2 H, s), 2.52 (3 H, s), 2.07 (9 H, m), 1.97 (2 H, s), 1.77 (3 H, s).

Sodium methoxide (44 mg, 0.8 mmol) and methanol (3 mL) were added to the nucleoside (144 mg), and stirred at room temperature for 6 hours. Glacial acetic acid was added to obtain a pH of ~6. The reaction was concentrated *in vacuo*, and purified via column chromatography (R_f = 0.10; 10% methanol: DCM) to give 83 mg of a cream-yellow solid (0.2 mmol, 78% isolated α/β nucleoside) with a melting point of 170-195 °C (the wide melting point range is believed to be due to the hygroscopic nature of the nucleoside). The reaction resulted in a ratio of 2:3 α : β of isolated nucleoside, determined by HPLC and ¹H NMR (based on anomeric peak of purified nucleoside, chemical shift = 5.89 ppm). Data for major epimer (β): ¹H NMR (500 MHz, d- CD₃OD) δ 8.05 (1 H, s), 5.89 (1 H, d, J = 5.9 Hz), 5.45 (1 H, t, J = 6.0 Hz), 4.72 (1 H, t, J = 5.9 Hz), 4.32 (1 H, m), 4.21 (1 H, bs), 3.83 (1 H, d, J = 2.9 Hz), 3.72 (2 H, m), 3.29 (2 H, s), 2.52 (3 H, s), 1.79 (3 H, s). ¹³C NMR (125 MHz, CD₃OD) δ 165.9, 153.5, 138.9, 138.4, 123.3, 117.1, 89.4, 86.2, 80.0, 73.9, 71.0, 62.0, 60.3, 37.2, 20.3, 13.3. MS (ESI) m/z 398.1(100%, M+H⁺), 266.1

(15%). HRMS (ESI) m/z (M+H)⁺ calculated for C₁₆H₂₄N₅O₅S 398.1498, found 398.1498.

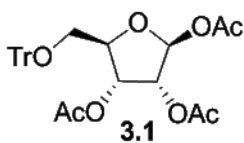
HPLC: (Fruhic-N) β = 9.91 minutes.

5.2 Chapter 3 Experimental

See section 5.1 for general information.

Free radical NMR spectroscopy. ^1H NMR spectra were recorded on JEOL 300 or 500 MHz spectrometers. In order to obtain ^1H spectrum of radical containing compounds, a reducing agent, such as phenylhydrazine or thiophenol, was added to a small aliquot of pure sample. Generally, phenylhydrazine (0.1 mmol) was first added to CDCl_3 (0.6 mL). The solution was then added to approximately 10 mg of free radical compound. ^1H NMR was taken immediately. If the solution was allowed to sit for any length of time, a solid white precipitate formed and an increase in byproducts was observed. Thiophenol (0.1 mmol) proved more suitable than phenylhydrazine, however byproducts were still observed within an hour after addition. ^1H NMR of phenylhydrazine (500 MHz, CDCl_3) δ 7.25 (2 H, m), 6.83 (3 H, m), 5.18 (1 H, bs), 3.57 (2 H, bs).

EPR spectroscopy. X-band (9 GHz) EPR spectra were recorded on a Bruker (Billerica, MA) EMX Plus spectrometer equipped with a bimodal resonator (Bruker model 4116DM). A modulation frequency of 1 kHz and attenuation of 20 dB at room temperature was used for all EPR spectra. For further information regarding EPR spectroscopy, see Chapter 3, section 3.1 Materials and Methods.

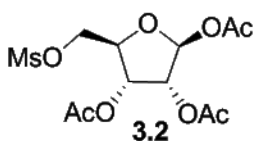


1,2,3-Tri-O-acetyl-5-O-trityl-D-ribofuranose (3.1)[ALC01270]:⁹⁸

^1D -ribose (3.0 g, 20 mmol), trityl chloride (6.7 g, 24 mmol), 4-dimethylaminopyridine (DMAP, 245 mg, 0.2 mmol), and triethylamine (5.6 mL, 0.04 mol) were suspended in dimethylformamide (40 mL). The reaction was then allowed to stir at room temperature overnight. The next morning, mixture was slowly quenched by the addition of water (25 mL). The desired compound was extracted using DCM (10 mL x 3) and ethyl acetate (10 mL x 2). The organic extracts

were washed with aqueous ammonium chloride (15 mL), and brine (10 mL). The organic extracts were then dried with sodium sulfate, decanted, and concentrated *in vacuo*. The crude mixture was then purified by flash chromatography (80% ethyl acetate: hexane) to afford 5.4 g of clear viscous liquid (14 mmol, 70%).

5-O-trityl-D-ribofuranose (5.4 g, 14 mmol) was then dissolved in pyridine (14 mL) and cooled to 0 °C. Acetic anhydride (10 mL) was slowly added via syringe, and the solution was allowed to slowly warm to room temperature and stir for a total of 16 hours. The reaction was concentrated *in vacuo* via azeotrope with toluene: ethanol (1:1). The crude product was dissolved in DCM, and washed with saturated aqueous sodium bicarbonate (10 mL), 1 M HCl (10 mL), and brine (10 mL). The organic extracts were then concentrated *in vacuo* and purified by flash chromatography (40% ethyl acetate: hexane) to afford 4.9 g (9.5 mmol, 67%) of predominantly β -1,2,3-Tri-O-acetyl-5-O-trityl-D-ribofuranose, a viscous clear liquid. ¹H NMR (500 MHz, CDCl₃) δ 7.44 (6 H, d, *J* = 8.1 Hz), 7.28 (9 H, m), 6.19 (1 H, s), 5.48 (1 H, m), 5.44 (1 H, d, *J* = 4.8 Hz), 4.31 (1 H, m), 3.34 (1 H, dd, *J* = 4.0, 6.3 Hz), 3.16 (1 H, dd, *J* = 4.1, 5.2 Hz), 2.04 (3 H, s), 2.00 (3 H, s), 1.98 (3 H, s). ¹³C NMR (125 MHz, CDCl₃) δ 169.7, 169.6, 169.5, 143.8, 98.4, 86.8, 81.0, 77.6, 77.2, 76.8, 74.4, 70.9, 63.3, 60.5, 21.2, 20.6, 20.6, 14.3.



1,2,3-Tri-O-acetyl-5-O-mesylyl-D-ribofuranose

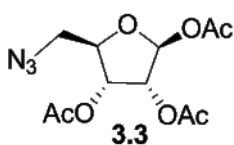
(3.2)[ALC0236]^{98,99†}

1,2,3-Tri-O-acetyl-5-O-trityl-D-ribofuranose **3.1** (4.9 g, 9.5 mmol)

was dissolved in ether (8 mL), then cooled to 0 °C. Ethereal formic acid (12 mL; 3:2 formic acid: ether ratio) was slowly added via syringe. The reaction was allowed to warm to room temperature over a 3 hour period. The reaction was then diluted with additional ether (5 mL), washed with saturated aqueous sodium bicarbonate (10 mL x 3). The

compound was then extracted using ethyl acetate (10 mL x 3), and washed with brine (5 mL). The organic extracts were then dried with sodium sulfate, decanted, and concentrated *in vacuo* to affording a clear viscous liquid (8.0 mmol, 85%, $\alpha:\beta = 1:3$ based on anomeric peak, chemical shift = 6.07 ppm). (60 % ethyl acetate: hexane). Major product (β -epimer) $^1\text{H NMR}$ (500 MHz, CD_3OD) δ 6.07 (1 H, s), 5.34 (1 H, dd, $J = 1.7, 4.1$ Hz), 5.30 (1 H, dd, $J = 1.6, 4.0$ Hz), 4.16 (1 H, m), 3.72 (1 H, dd, $J = 4.4, 7.8$ Hz), 3.59 (1 H, dd, $J = 4.4, 7.8$ Hz), 2.09 (3 H, s), 2.06 (3 H, s), 2.03 (3 H, s).

1,2,3-Tri-*O*-acetyl-D-ribofuranose (1.2 g, 4.3 mmol) was dissolved in DCM (10 mL) and triethylamine (780 μL), then cooled to 0 °C. Mesyl chloride (366 μL , 4.7 mmol) was then added dropwise. The reaction was monitored closely via TLC until complete. A saturated aqueous solution of sodium bicarbonate (5 mL) was then added at 0 °C, and the mixture was allowed to warm to room temperature. The reaction mixture was then washed with an additional sodium bicarbonate aliquot (5 mL), and brine (5 mL). The organic extracts were then dried with sodium sulfate, decanted, and concentrated *in vacuo* to afford 1,2,3-Tri-*O*-acetyl-5-*O*-mesyl-D-ribofuranose **3.2**, a viscous clear liquid (4.3 mmol, 100%, 1:3 $\alpha:\beta$). β -epimer $^1\text{H NMR}$ (500 MHz, CDCl_3) δ 6.13 (1 H, s), 5.35 (2 H, m), 4.43-4.37 (2 H, m), 3.05 (3 H, s), 2.13 (3 H, s), 2.11 (3 H, s), 2.08 (3 H, s).



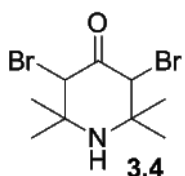
1,2,3-Tri-*O*-acetyl-5-azido-D-ribofuranose (3.3)[ALC01265]:^{98 †}

1,2,3-Tri-*O*-acetyl-5-*O*-mesyl-D-ribofuranose **3.2** (1.5 g, 4.3 mmol)

was dissolved in DMSO (4 mL). Sodium azide (820 mg, 12.6 mmol)

was added, and the reaction was heated to 50 °C for 48 hours. Upon cooling, the reaction was diluted with ethyl acetate: water (3:2, 10 mL). The product was then extracted with ethyl acetate: ether (4:1, 5 mL x 3), and washed with brine (5 mL). The organic extracts were then dried with sodium sulfate, decanted, and concentrated *in*

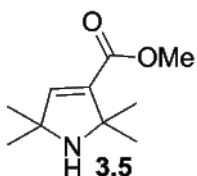
vacuo to afford 1.0 g (3.4 mmol, 80 %, 1:5 α : β based on anomeric peak of chemical shift 6.15 ppm) of the viscous liquid. ^1H NMR (500 MHz, d - CDCl_3) δ 6.15 (1 H, s), 5.41-5.34 (2 H, m), 4.30 (1 H, m), 3.64 (1 H, dd, J = 4.0, 9.5 Hz), 3.28 (1 H, dd, J = 4.1, 9.5 Hz), 2.12 (3 H, s), 2.11 (3 H, s), 2.05 (3 H, s). ^{13}C NMR (125 MHz, CDCl_3) δ 169.8, 169.5, 169.2, 98.1, 80.5, 74.4, 70.4, 51.5, 21.1, 20.6, 20.6.



3,5-Dibromo-2,2,6,6-tetramethyl-4-piperidone hydrobromide

(3.4)[ALC01254]:¹⁰¹

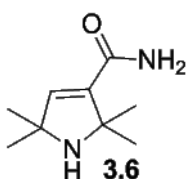
Bromine (1.5 mL, 29 mmol) was added dropwise to a 0 °C solution of 2,2,6,6-tetramethyl-4-piperidone (1.5 g, 9.7 mmol) in acetic acid (9 mL). The reaction was allowed to warm to room temperature, and then stirred vigorously at 60 °C overnight. The reaction was then cooled in an ice-bath, and then the resulting precipitate was isolated by suction filtration. The collected solid was washed with acetic acid (5 mL x 3), water (2.5 mL), and ether (5 mL x 2). The resulting solid was then dried by suction, affording 3.0 g (9.0 mmol, 100%) white solid. ^1H NMR (500 MHz, $\text{DMSO}-d_6$) δ 5.38 (2 H, s), 4.40 (1 H, bs), 1.62 (6 H, s), 1.29 (6 H, s). ^{13}C NMR (125 MHz, $\text{DMSO}-d_6$) δ 188.54, 64.84, 60.70, 28.22, 22.55. Melting point was not obtained for compound.



2,2,5,5-Tetramethyl-3-carbomethoxyproline (3.5)[ALC01230]:¹³⁶

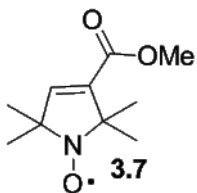
A fresh solution of sodium methoxide was prepared by slowly adding sodium (875 mg, 38 mmol) to anhydrous methanol (20 mL). The sodium methoxide solution was then cooled to 0 °C after all of the sodium had dissolved. Dibromo-piperidone **3.4** (3.0 g, 9.6 mmol) was added in 5 portions. The rearrangement was warmed to room temperature and stirred overnight. The resulting mixture was concentrated *in vacuo*. Impurities were then precipitated with ether (30 mL), and the

resulting solid was removed by suction filtration. 10% aqueous potassium carbonate solution (15 mL) was added to the filtrate, and the compound of interest was extracted using ether (10 mL x 3). The organic extracts were then dried with potassium carbonate, decanted, and concentrated *in vacuo* to afford 1.42 g yellow solid (7.8 mmol, 81%). (5% methanol: DCM). ^1H NMR (500 MHz, CDCl_3) δ 6.63 (1 H, s), 3.74 (3 H, s), 1.40 (6 H, s), 1.28 (6 H, s). ^{13}C NMR (125 MHz, $\text{DMSO}-d_6$) δ 164.4, 149.0, 138.9, 65.8, 63.4, 51.2, 29.9, 29.8. IR ν 2977, 2929, 2860, 1653, 1300 cm^{-1} . Melting point was not obtained for compound.



2,2,5,5-Tetramethyl-3-carbamidopyrroline (3.6)[ALC0261]:^{136,137}

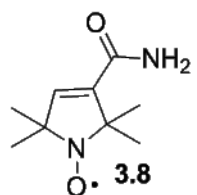
Dibromo-piperidone **3.4** (0.5 g, 1.6 mmol) was added in 5 portions to a solution of potassium hydroxide (224 mg, 4 mmol) and 30% aqueous ammonium hydroxide (13 mL). The mixture was then stirred at room temperature for one hour. The compound of interest was then extracted using chloroform (15 mL x 2), ethyl acetate (15 mL x 3). The organic extracts were then washed with brine (5 mL). The organic extracts were then dried with magnesium sulfate, decanted, and concentrated *in vacuo*. Impurities were then precipitated with a 3:1 ratio of methanol: hexane (10 mL). The resulting solid was filtered through a pad of Celite. The filtrate was concentrated *in vacuo*, affording quantitative yield of a cream-yellow solid. (5% methanol: DCM). ^1H NMR (500 MHz, CD_3OD) δ 6.33 (1 H, s), 1.41 (6 H, s), 1.29 (6 H, s). ^{13}C NMR (125 MHz, $\text{DMSO}-d_6$) δ 168.2, 141.9, 141.5, 66.9, 63.6, 28.4, 28.3. IR ν 3424, 3184, 2515, 1671, 1403, 1366 cm^{-1} . Melting point was not obtained for compound.



2,2,5,5-Tetramethyl-3-carbomethoxypyrroline-1-oxyl

(3.7)[AD0204]:^{102,136 †}

2,2,5,5-Tetramethyl-3-carbomethoxypyrroline **3.5** (1.3 g, 6.8 mol), sodium bicarbonate (1.2 g, 13.6 mol), and sodium tungstate (400 mg, 1.4 mol) were dissolved in methanol (13 mL) and cooled to 0 °C. 30% aqueous hydrogen peroxide (3.6 mL) was added dropwise over thirty minutes. The yellow suspension was warmed to room temperature, and allowed to stir for 24 hours. An additional aliquot of hydrogen peroxide (1 mL) and sodium tungstate (400 mg, 1.4 mol) was then added, and the reaction was allowed to stir for an additional 24 hours. The solution was then concentrated *in vacuo*. Water (30 mL) was added and the product was extracted with DCM (15 mL x 4). The organic extract was then dried with sodium sulfate, decanted, and concentrated *in vacuo* to give 1.3 g of the yellow solid (6.5 mol, 96%). (50% ethyl acetate:hexane). ¹H NMR (300 MHz, CDCl₃) δ 4.14 (1 H, s), 3.82 (3 H, s), 1.47 (6 H, s), 1.36 (6 H, s). IR ν 2977, 2929, 2860, 1739, 1462, 1363, 1306 cm⁻¹. EPR: S = ½; g_x=g_y=g_z= 2.006. Melting point was not obtained for compound.

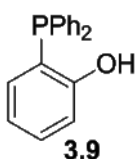


2,2,5,5-Tetramethyl-3-carbamidopyrroline-1-oxyl

(3.8)[ALC0264]:^{136,137}

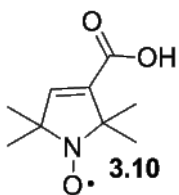
2,2,5,5-Tetramethyl-3-carbamidopyrroline **3.6** (725 mg, 4.3 mmol), sodium bicarbonate (722 mg, 8.6 mmol), and sodium tungstate (632 mg, 2.2 mmol) were dissolved in methanol (9 mL) and cooled to 0 °C. 30% aqueous hydrogen peroxide (3 mL) was added dropwise over thirty minutes. The yellow suspension was warmed to room temperature, and allowed to stir for 24 hours. An additional aliquot of hydrogen peroxide (1 mL) and sodium tungstate (400 mg, 1.4 mol) was then added, and the reaction was allowed to stir for an additional 24 hours. The

solution was then concentrated *in vacuo*. Water (20 mL) was added and the product was extracted with DCM (10 mL x 4). The organic extract was then dried with sodium sulfate, decanted, and concentrated *in vacuo* to give 420 mg of the yellow solid (2.3 mmol, 53%). (5% methanol: DCM). $^1\text{H NMR}$ (500 MHz, CDCl_3) δ 4.45 (1 H, s), 1.53 (6 H, s), 1.41 (6 H, s). IR ν 3416, 3213, 2857, 1660, 1639, 1400, 1367 cm^{-1} . EPR: $S = \frac{1}{2}$; $g_x = g_y = g_z = 2.007$. Melting point was not obtained for compound.



O-Diphenylphosphinophenol (3.9)[ALC0249]:^{104,138 †}

O-Bromophenol (500 μL , 4.7 mmol), palladium acetate (106 mg, 0.5 mmol), and triethylamine (4 mL, 28 mmol) were dissolved in acetonitrile (10 mL) under inert and dry conditions. Diphenylphosphine (985 μL , 5.7 mmol) was added slowly, and the reaction was refluxed for 24 hours. The reaction was then concentrated *in vacuo*, and purified via flash chromatography (10% ethyl acetate: hexane) to give 598 mg of a viscous brown liquid (2.2 mmol, 30%). ($R_f = 0.4$, 5% methanol: DCM) $^1\text{H NMR}$ (500 MHz, CDCl_3) δ 7.73-7.48 (14 H, m). $^{31}\text{P NMR}$ (121 MHz, CDCl_3) 22.2. $^{13}\text{C NMR}$ (125 MHz, CDCl_3) δ 132.7, 132.7, 130.9, 130.7, 129.1, 128.9.

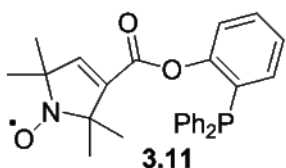


2,2,5,5-Tetramethyl-3-carboxypyrroline-1-oxyl

(3.10)[ALC0291]:^{102,139 †}

2,2,5,5-Tetramethyl-3-carboxypyrroline-1-oxyl **3.7** (1.30 g, 6.5 mmol) was added to 1 M sodium hydroxide (10 mL) and methanol (10 mL) solution at 0 $^{\circ}\text{C}$. The reaction was stirred for six hours while it was allowed to warm to room temperature. The solution was then concentrated *in vacuo* by half, and acidified to pH = 3 with 3 M HCl. The reaction was then concentrated *in vacuo* to dryness. The product was dissolved in hot ethyl acetate, cooled, and the resulting precipitate was

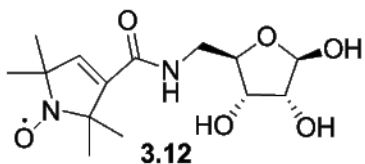
filtered through Celite, washing with ethyl acetate. The resulting filtrate was then concentrated *in vacuo* to give 1.2 g yellow solid (6.5 mmol, 100%). ¹H NMR (500 MHz, CDCl₃) δ 6.49 (1 H, s), 1.51 (6 H, s), 1.46 (6 H, s). IR ν 3415, 2979, 2936, 1699, 1466, 1355, 1287 cm⁻¹. EPR: S = ½; g_x=g_y=g_z= 2.006. Melting point was not obtained for compound.



3-(Diphenylphosphinocarbonyl)-2,2,5,5-

tetramethylpyrroline-1-oxyl (3.11)[ALC0242]:¹⁰⁴

O-Diphenylphosphinophenol **3.9** (50 mg, 0.2 mmol), 2,2,5,5-tetramethyl-3-carboxypyrroline-1-oxyl **3.10** (40 mg, 0.2 mmol), 1-ethyl-3-(3-dimethylaminopropyl)carbodiimide (EDCI, 207 mg, 1.1 mmol), potassium carbonate (50 mg, 0.4 mmol) and DMAP (11 mg, 0.1 mmol) were dissolved in DMF (0.7 mL) and stirred at room temperature for 12 hours. The orange reaction was then quenched with saturated aqueous ammonium chloride (5 mL x 3). The product was then extracted using ethyl acetate (5 mL x 2) and DCM (5 mL x 2), and washed with brine (5 mL). The organic extracts were then dried with sodium sulfate, decanted, and concentrated *in vacuo* to afford 44 mg viscous liquid, which could not be confirmed as product. (R_f = 0.6, 5% methanol: DCM). IR ν 3054, 2981, 2927, 1710, 1433, 1174 cm⁻¹. EPR: S = ½; g_x=g_y=g_z= 2.006.



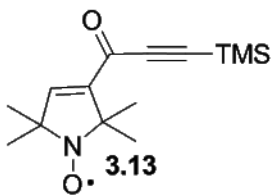
3-[[N-(1,2,3-Tri-O-acetyl-D-

ribofuranose)amino]carbonyl]-2,2,5,5-

tetramethylpyrroline-1-oxyl (3.12)[ALC0247]:¹⁰⁴

3-(Diphenylphosphinocarbonyl)- 2,2,5,5-tetramethylpyrroline-1-oxyl **3.11** (37 mg, 0.08 mmol) and 1,2,3-Tri-O-acetyl-5-azido-D-ribofuranose **3.3** (20 mg, 0.06 mmol) were

dissolved in *N,N*-dimethylacetamide (DMA, 0.5 mL) under inert atmosphere, and heated to 70 °C. The disappearance of starting material was monitored by TLC (5% methanol: DCM). After four hours, the majority of compound **3.3** had been consumed, however the majority of the nitroxyl appeared to be present by TLC. Water (0.3 mL) was added and the reaction was allowed to stir overnight. The solution was then concentrated *in vacuo* and compounds formed were separated by column chromatography. Spectral analysis of each compound produced revealed that the expected product was not formed. The major product did not contain a radical by EPR spectroscopy. While the obtained NMR spectra could not be conclusively assigned, the major product resembled a carbohydrate moiety. It appears that compound **3.3** rearranged to form a pyranose ring, proposed due to the absence of the 5' proton peaks by ¹H NMR. It is also apparent that the nitroxyl radical reacted, indicated by its absence as observed by EPR analysis.

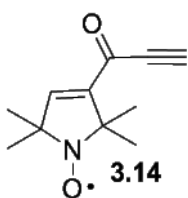


3-(2-Propyn-3-(trimethylsilyl)-1-yn-1-yl)-2,2,5,5-tetramethylpyrrolidine-1-oxyl (3.13)[ALC0278]:¹⁰⁵

2,2,5,5-Tetramethyl-3-carboxypyrrolidine-1-oxyl **3.10** (200 mg, 1.1 mmol) was dissolved in DCM and cooled to 0 °C. Oxalyl chloride (373 μ L, 4.3 mmol) was added slowly. After gas evolution decreased, the reaction was allowed to warm to room temperature, and stirred for two additional hours. The unreacted oxalyl chloride and DCM were then removed under a stream of argon at 55 °C to give crude acid chloride.

The crude pyrrolidine acid chloride was then dissolved in DCM (2 mL), cooled to 0 °C, and bis(trimethylsilyl)acetylene (252 μ L, 1.2 mmol) was added. Anhydrous aluminum chloride (150 mg, 1.1 mmol) was added slowly in three portions. The reaction was then warmed to room temperature, and allowed to stir for two additional hours. The reaction

mixture was concentrated *in vacuo*, and the product was purified via column chromatography to afford 150 mg of yellow solid. ($R_f = 0.2$, 5% methanol: DCM). The NMR spectrum, ^1H NMR (500 MHz, CDCl_3) δ 4.68 (1 H, s), 1.85 (12 H, s), 1.36 (9 H, s), revealed an unexpected shift for the trimethylsilyl group. We attempted to derivatize the compound in the following step as a method of further characterization.

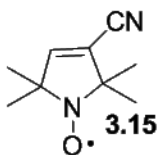


3-(Prop-2-yn-1-one)-2,2,5,5-tetramethylpyrroline-1-oxyl

(3.14)[ALC0280]:^{105,140}

3-(Prop-3-(trimethyl)silyl-2-yn-1-one)-2,2,5,5-tetramethylpyrroline-1-oxyl

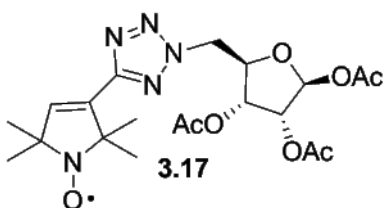
3.13 (150 mg, 0.6 mmol) was dissolved in anhydrous THF (3 mL), and cooled to 0 °C. 1 M Tetra-*N*-butylammonium fluoride (TBAF) solution in THF (0.5 mL) was added slowly. The ice bath was then removed, and the reaction was monitored by TLC. After one hour the reaction was cooled to 0 °C, and quenched with saturated aqueous ammonium chloride (8 mL) and water (5 mL). The product was extracted using DCM (5 mL x 3), and washed with brine (5 mL). The organic extract was then dried with sodium sulfate, decanted, and concentrated *in vacuo* to give 78 mg (major product) cream solid. ($R_f = 0.3$, 5% methanol: DCM). ^1H NMR was similar to compound **3.13**, and alkyne proton is absent. Alkyne IR stretching frequency $\sim 2100\text{ cm}^{-1}$ is also absent (IR ν 2963, 2933, 2875, 1685, 1460, 1364 cm^{-1}), indicating that major compound of reaction is not anticipated product.



2,2,5,5-Tetramethyl-3-cyanopyrroline-1-oxyl (3.15)[ALC0265]:^{106,141}

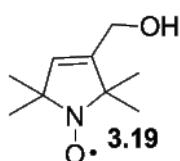
2,2,5,5-Tetramethyl-3-carbonylaminopyrroline-1-oxyl **3.8** (140 mg, 0.8 mmol), pyridine (183 μL , 2.3 mmol) and 1,4-dioxane (2 mL) were cooled to 0 °C. Trifluoroacetic anhydride (322 μL , 2.3 mmol) was added slowly. The reaction was

allowed to warm to room temperature and stirred overnight. The reaction was then diluted with chloroform (3 mL), washed with water (5 mL x 2). The organic extracts were then dried with magnesium sulfate, decanted, and concentrated *in vacuo*. The product was crystallized in hexane, and resulting precipitate was separated using suction filtration. The solid was then dried under vacuum to afford 96 mg of a cream solid (0.6 mmol, 75%). (Rf = 0.7, 70% ethyl acetate: hexane). $^1\text{H NMR}$ (300 MHz, CDCl_3) δ 6.42 (1 H, s), 1.35 (6 H, s), 1.28 (6 H, s). IR ν 3043, 2984, 2861, 2220, 1654, 1278, 1165 cm^{-1} . EPR: $S = \frac{1}{2}$; $g_x = g_y = g_z = 2.007$. Melting point was not obtained for compound.



1-(1,2,3-Tri-O-acetyl-D-ribofuranosylmethyl)-5-(2,2,5,5-tetramethylpyrroline-1-oxyl)-1H-tetrazole (3.17)[AD01154]:

2,2,5,5-Tetramethyl-3-cyanopyrroline-1-oxyl **3.15** (45 mg, 0.3 mmol) and 1,2,3-Tri-O-acetyl-5-azido-D-ribofuranose **3.3** (55 mg, 0.2 mmol) were added together in a small sealed vial and heated to 100 °C for 24 hours. The reaction was purified by column chromatography to afford 18 mg of viscous brown liquid (0.04 mmol, 20%). (Rf = 0.18, 70% ethyl acetate: hexane). $^1\text{H NMR}$ (300 MHz, CDCl_3) δ 6.17 (1 H, s), 5.92 (2 H, m), 4.58 (1 H, m), 4.34 (1 H, t, $J = 4.9$ Hz), 4.15 (1 H, m), 2.13 (2 H, s), 2.09 (9 H, m), 1.35 (6 H, s), 1.28 (6 H, s). IR ν 3086, 3069, 3056, 2977, 2931, 2851, 2227, 1621, 1460, 1279, 1157, 1088 cm^{-1} . EPR: $S = \frac{1}{2}$; $g_x = g_y = g_z = 2.007$. Melting point was not obtained for compound.

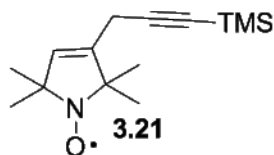


2,2,5,5-Tetramethyl-3-hydroxymethylpyrroline-1-oxyl

(3.19)[ALC0294]:^{102,139}

2,2,5,5-Tetramethyl-3-carboxypyrroline-1-oxyl **3.10** (200 mg, 1.1 mmol)

was dissolved in THF (5 mL) and cooled to 0 °C. 2 M Lithium aluminum hydride solution in THF (1.6 mL) was added slowly. The reaction was then allowed to warm to room temperature and stirred for two hours. The solution was then cooled back down to 0 °C and quenched with the slow addition of water (5 mL). The product was then extracted with ethyl acetate (3 mL x 4), and washed with brine (5 mL). The organic extracts were then dried with sodium sulfate, decanted, and concentrated *in vacuo* to afford 125 mg of yellow solid (1.1 mmol, 100%). (R_f = 0.4, 5% methanol: DCM). ¹H NMR (500 MHz, CDCl₃) δ 5.66 (1 H, s), 4.27 (2 H, s), 1.44 (6 H, s), 1.43 (6 H, s). IR ν 3374, 2973, 2929, 2867, 1463, 1359, 1028 cm⁻¹. EPR: S = ½; g_x=g_y=g_z= 2.006. Melting point was not obtained for compound.

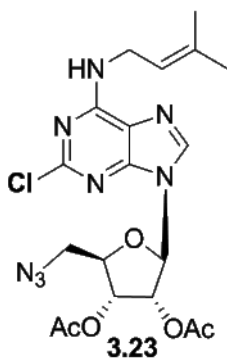


3-(Prop-3-(trimethyl)silyl-2-yne)-2,2,5,5-tetramethylpyrroline-1-oxyl (3.21)[ALC02107]:

2,2,5,5-Tetramethyl-3-hydroxymethylpyrroline-1-oxyl **3.19** (200

mg, 1.8 mmol) and triethylamine (367 μL, 2.6 mmol) were dissolved in DCM (8 mL) and cooled to 0 °C. Mesyl chloride (203 μL, 2.6 mmol) was added dropwise, and the reaction was allowed to warm to room temperature and stirred one hour. The reaction was then washed with brine (5 mL). The organic extract was dried with magnesium sulfate, decanted, and concentrated *in vacuo* to give 330 mg (1.7 mmol, 95%) of a yellow solid (2,2,5,5-Tetramethyl-3-methyl-O-mesylpyrroline-1-oxyl (**3.20**)[ALC0298]), which was used immediately. IR ν 2973, 2929, 2967, 1445, 1441, 1355, 1177, 972 cm⁻¹.

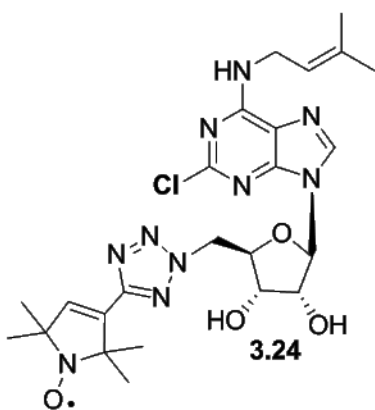
Trimethylsilyl acetylene (77 μL , 0.5 mmol) was dissolved in THF (2 mL), cooled to 0 $^{\circ}\text{C}$, and *n*-butyl lithium (2.5 M in hexane, 200 μL , 0.5 mmol) was added slowly. The mixture was then warmed to room temperature. In a second round bottom flask, 2,2,5,5-tetramethyl-3-methyl-*O*-mesylpyrroline-1-oxyl **3.20** (80 mg, 0.4 mmol) was dissolved in THF (2 mL) and cooled to 0 $^{\circ}\text{C}$. The acetylene mixture was then added slowly, and warmed to room temperature slowly. After warming, the reaction was cooled back down to 0 $^{\circ}\text{C}$ in order to quench with saturated aqueous ammonium chloride (3 mL). The product was extracted using DCM (3 mL x 3), and washed with brine (3 mL). The organic extract was dried with sodium sulfate, decanted, and concentrated *in vacuo* to afford 63 mg of a viscous yellow liquid (0.3 mmol, 75%). ^1H NMR (500 MHz, CDCl_3) δ 5.30 (1 H, s), 4.06 (2 H, s), 1.39 (6 H, s), 1.34 (6 H, s), 0.08 (9 H, s). IR ν 2974, 2929, 2865, 2178, 1465, 1357, 1158 cm^{-1} . EPR: $S = \frac{1}{2}$; $g_x = g_y = g_z = 2.006$.



2-Chloro- N^6 -isopentenyl-7-(2,3-tri-*O*-acetyl-5-azido-*D*-ribofurano)-adenosine (3.23)[ALC0279]:

2-Chloro- N^6 -isopentenyl-purine (**2.3c**) (500 mg, 2.1 mmol) was dissolved in acetonitrile (8.8 mL). *N,O*-bis(trimethylsilyl)acetamide, BSA, (1 mL, 4.2 mmol) was added, the reaction flask was adapted with a condenser, and heated to reflux for 15 minutes. In a separate round bottom flask, 1,2,3,-tetra-*O*-acetyl-5-azido-*D*-ribofuranose (**3.3**) (527 mg, 1.8 mmol) and acetonitrile (8.8 mL) were combined. Once the purine mixture had refluxed for 15 minutes, the ribose mixture was added to the reaction via syringe. TMSOTf, (475 μL , 2.6 mmol) was then added slowly via syringe. The reaction was then heated to reflux for 12 hours. The reaction was cooled back to room temperature, and chloroform (50 mL): water (25 mL) was added. The organic extract was washed with water until a pH of ~ 6 was

obtained. The organic extracts were dried over sodium sulfate, decanted, and concentrated *in vacuo*. The desired compound was purified via column chromatography ($R_f = 0.4$; 10% methanol:DCM) to afford 162 mg of a white solid (0.4 mmol, 22%). Data for major epimer (β): ^1H NMR (500 MHz, CD_3OD) δ 8.81 (1 H, s), 6.38 (1 H, d, $J = 5.3$ Hz), 5.97 (1 H, t, $J = 5.3$ Hz), 5.67 (1 H, t, $J = 5.3$ Hz), 4.44 (1 H, m), 4.25 (2 H, m), 3.75 (2 H, m), 2.14 (3 H, s), 2.07 (3 H, s), 1.52 (6 H, s). ^{13}C NMR (125 MHz, $\text{DMSO-}d_6$) δ 170.1, 170.0, 162.1, 155.4, 152.9, 150.6, 146.9, 127.0, 87.4, 81.7, 73.0, 70.8, 52.1, 51.2, 48.6, 45.7, 31.8, 27.0, 19.5, 19.2, 19.1. Melting point was not obtained for compound.



3-(2-Chloro- N^6 -isopentenyl-adenosine)-5-(2,2,5,5-tetramethylpyrroline-1-oxyl)-1H-tetrazole

(3.24)[ALC0288]:

2,2,5,5-Tetramethyl-3-cyanopyrroline-1-oxyl **3.15** (84 mg, 0.5 mmol) and 2-chloro- N^6 -isopentenyl-7-(2,3-tri-O-acetyl-5-azido-D-ribofuran-1-yl)-purine **3.23** (162 mg, 0.3 mmol) were added together in a small sealed vial

and heated to 100 °C for 24 hours. The reaction was purified by column chromatography to give 20 mg of white solid (0.03 mmol, 24%). ($R_f = 0.26$, 5% methanol: DCM).

Sodium (2 mg, 0.09 mmol) was dissolved in anhydrous methanol (1 mL), and the solution was added to the white solid (20 mg, 0.03 mmol). The reaction was stirred at room temperature for 3 hours. Glacial acetic acid was added dropwise to achieve a pH of ~6. The reaction was then concentrated *in vacuo* to afford a slight yellow viscous oil. The oil was purified via column chromatography ($R_f = 0.38$; 5% methanol:DCM) to afford 8 mg of an off white solid (0.01 mmol, 42% isolated α : β nucleoside) with an α : β ratio of 1:3, determined by NMR (based on anomeric peak of chemical shift 6.16 ppm). Data for major

epimer (β): $^1\text{H NMR}$ (500 MHz, CD_3OD) δ 6.41 (1 H, s), 6.16 (1 H, s), 5.36 (2 H, m), 5.19 (1 H, m), 4.33 (1 H, m), 3.63 (1 H, dd, $J = 4.0, 10.0$ Hz), 3.28 (1 H, dd, $J = 4.0, 9.9$ Hz), 2.12 (3 H, s), 2.11 (3 H, s), 1.34 (6 H, s), 1.27 (6 H, s). IR ν 3119, 2976, 2931, 2851, 2227, 1360, 1164, 1105 cm^{-1} . EPR: $S = \frac{1}{2}$; $g_x = g_y = g_z = 2.007$. HRMS (ESI) m/z (M+H) $^+$ calculated for $\text{C}_{24}\text{H}_{33}\text{ClN}_{10}\text{O}_4$ 560.2375, found 560.2345. Melting point was not obtained for compound.

Chapter 6

A Mitsunobu-Like Process Catalytic in Phosphine

**The following work was completed as a graduate member of the CJOB Laboratory.

In 1967, Prof. Oyo Mitsunobu discovered the dehydrative coupling of an alcohol with acidic components to form amides, esters, ethers, and so on, using the combination of a reducing (phosphine) and oxidizing (azo) reagent (Figure 6-1).^{142,143} One of the major attractions of the Mitsunobu reaction is the inversion of the alcohol starting material's stereochemistry; however, there are several noteworthy drawbacks. One drawback is the addition of four reagents (an alcohol, an acid/pro-nucleophile, a phosphine, and a hydrazine derivative), leading to significant issues with product isolation and purification, particularly related to the phosphine oxide and urea byproducts.¹⁴⁴ Therefore, much research has been directed toward developing catalytic alternatives to facilitate product purification.

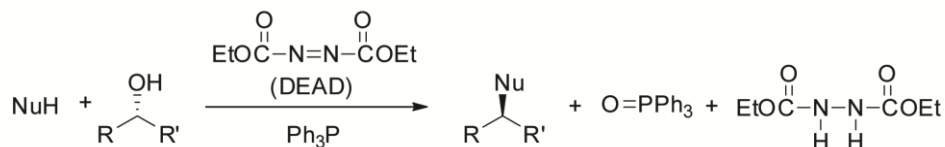


Figure 6-1 Mitsunobu reaction

Several methodologies have been employed towards facilitating the Mitsunobu reaction. Toy and coworkers discovered that the hydrazine derivative could be added catalytically, with the use of iodosobenzene diacetate, reducing the hydrazine byproduct, and therefore increasing ease of isolation (Figure 6-2).¹⁴⁴ Influenced by their discovery, and O'Brien's development of the Wittig reaction catalytic in phosphine,¹⁴⁵ we hoped to develop a dual catalytic Mitsunobu reaction, catalytic in both hydrazine and phosphine.

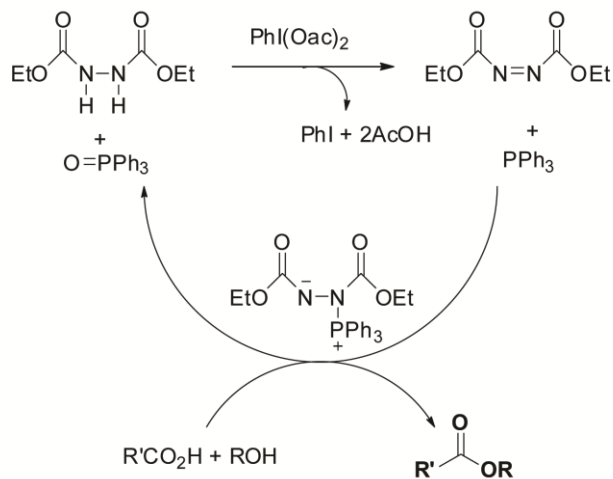


Figure 6-2 Proposed Mitsunobu catalytic cycle

During optimization studies of the Mitsunobu catalytic in phosphine, we discovered that the yield increased from roughly 30% to 80% by eliminating the addition of the azo compound. The proposed mechanistic cycle is demonstrated in Figure 6-3.

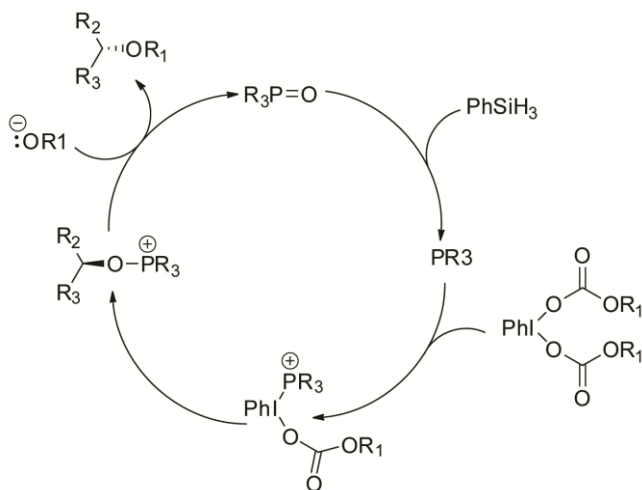


Figure 6-3 Proposed catalytic cycle of Mitsunobu-like reaction

It was also determined that by exchanging the acetate groups on the iodosobenzene diacetate complex with the desired acid, yield increased yet again. With further

optimization of reaction conditions, the Mitsunobu-like reaction catalytic in phosphine was developed (Figure 6-4). Further efforts will be continued by the O'Brien lab to verify mechanistic details, such as proving inversion of stereochemistry and determining diastereomeric ratios.

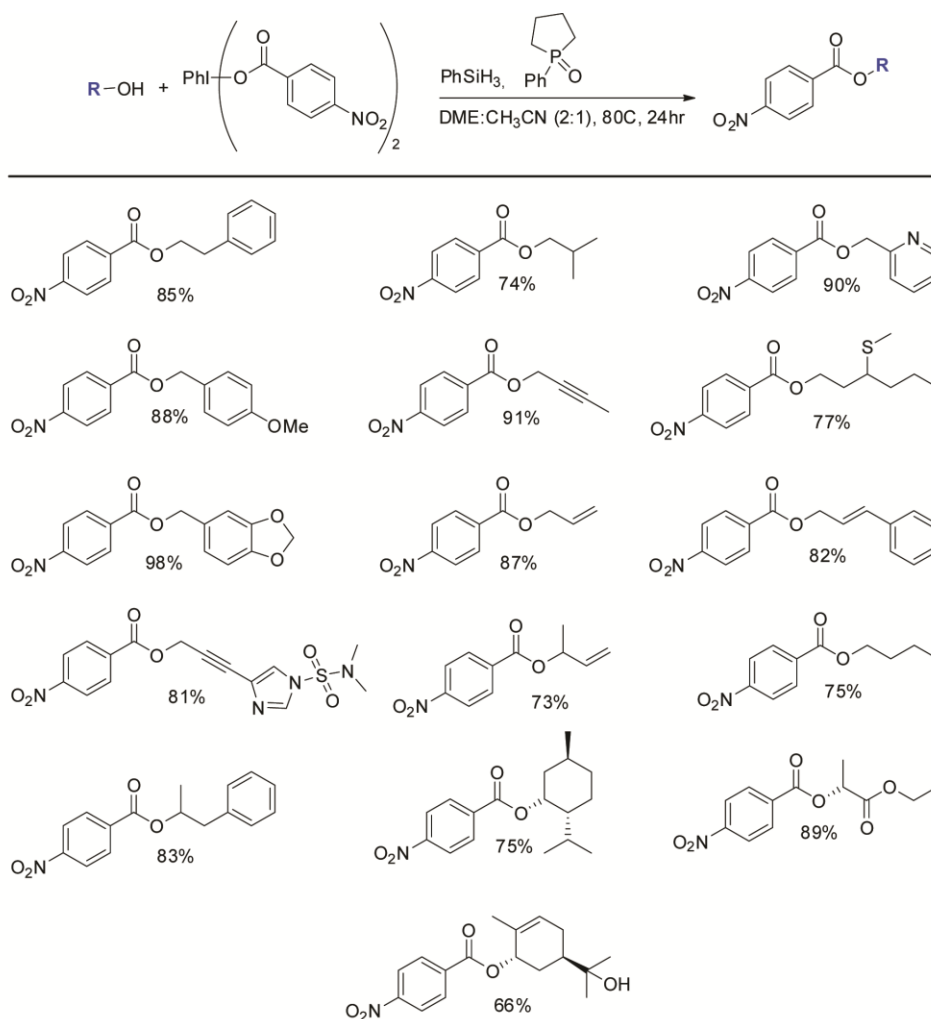


Figure 6-4 Mitsunobu-like optimization conditions and synthesized substrates

6.1 Mitsunobu Experimental

General Experimental. All reagents were purchased from commercial sources and were used without further purification, unless otherwise stated. Dry DME and ACN (stored over 4Å molecular sieves) were purchased from Sigma Aldrich and handled under argon. Deuterated solvents were purchased from Cambridge Isotope Laboratories, Inc. Thin Layer Chromatography (TLC) was performed on Sorbent Technologies Silica G w/UV 254 aluminum-backed plates, and spots were visualized using UV light (254 nm), potassium permanganate, or phosphomolybdic acid stains. Column chromatography purifications were carried out using the flash technique on Sorbent Technologies 60 (230 x 400 mesh). NMR spectra were recorded on JEOL ECX-300 and JEOL Eclipse+ 500 spectrometers. The chemical shifts (δ) for ^1H are given in parts per million (ppm) referenced to the residual proton signal of the deuterated solvent (CDCl_3 at δ 7.26 ppm); coupling constants, when multiplicity is significantly resolved, are expressed in hertz (Hz). The following abbreviations are used: s = singlet, d = doublet, t = triplet, m = multiplet, dd = doublet of doublets, dt = doublet of triplets, dq = doublet of quartets, q = quartet, and qn = quintet. Hydrogenations were performed on an H-Cube Midi™, manufactured by ThalesNano, Hungary. All experiments were conducted under an atmosphere of dry argon unless otherwise noted, using Schlenk technique.

3-Methyl-1-phenylphospholane-1-oxide (6.1):

Rapidly, in air, commercially available 3-methyl-1-phenyl-2-phospholene-1-oxide (3.0 g, 16 mmol, CAS 707-61-9) is weighed into a 500 mL round-bottom flask. Methanol (300 mL) was added to prepare a 0.05 M solution. The phospholene oxide was hydrogenated via the H-Cube Midi™ with a catalyst cartridge containing 10% Pd/C. The reduction occurred at ambient temperature, under 20 bar H_2 , at 1 mL/min flow rate.

Methanol was removed *in vacuo* to yield **5.1** as a viscous, 2:1 mixture of diastereomers in 100% yield. An alternative reduction, using borane, has been published; however, in our hands this was found to be significantly lower yielding than the H-Cube™ method. ¹H and ³¹P spectra match previously reported data.

Iodobenzene-bis(4-nitrobenoate) (**6.2**):

Rapidly, in air, 4-nitrobenzoic acid (3.3 g, 20 mmol, CAS 62-23-7) and iodobenzene diacetate (3.2 g, 10 mmol, CAS 3240-34-4) were added to a 500 mL round bottom flask. 70 mL of Chlorobenzene was then added. The reaction was placed on the rotary evaporator at 50 °C and 200 rpm. The reaction was allowed to commence until all solvent had evaporated leaving the product as a white powder. The flask was then placed on a hi-vac system to remove any remaining solvent. The compound was filtered through a frit, concentrated *in vacuo*, and washed with pentane. The compound was removed, placed back into a round bottom flask and returned to the hi-vac to obtain 100% yield. ¹H NMR (300 MHz, DMSO-*d*₆) δ: 7.51-8.26 (m, Ar H, 13H). ¹³C NMR (300 MHz, DMSO-*d*₆) δ: 70.83, 95.44, 124.30, 128.25, 131.25, 136.91, 137.65, 150.58, 166.36.

Catalytic Mitsunubo: General procedure

In air, to a tarred 1-dram vial was added phosphine oxide **6.1** (19 mg, 0.10 mmol) and iodobenzene material **6.2** (402 mg, 0.75 mmol, 1.5 equiv.) and equipped with a stir-bar. The vial was then sealed with a septum and purged with argon. For primary alcohol substrates a solvent system of anhydrous DME (1.5 mL) was added. For secondary alcohol substrates, a solvent system composed of anhydrous DME and acetonitrile (ratio of 2:1, 1 mL: 0.5 mL respectively) was added. Phenylsilane (80 μL, 0.63 mmol, 1.3

equiv.) was then added at this point. Alcohol (0.5 mmol, 1 equiv.) was added slowly by syringe needle, with consecutive equal additions every hour for the first 5 hours. If the alcohol was a solid, it was weighed out into a separate 1-dram vial. A mixed solution of 0.5 mL DME and acetonitrile (ratio of 2:1, 0.3 mL: 0.2 mL respectively) was added to the vial allowing it to be pulled into a syringe for the hourly addition. The remaining 1.0 mL of solvent was added to the reaction vial in a ratio of 2:1 DME to Acetonitrile (0.6 mL and 0.3 mL respectively). The reaction was heated at 80 °C for 24 h. The crude reaction was filtered through a plug of celite with ethyl acetate, concentrated in vacuo, and purified via flash column chromatography.

Phenethyl-4-nitrobenzoate was obtained from the reaction of 2-phenylethyl alcohol (60 μ L, 0.5 mmol, 1.0 equiv.), phosphine oxide **6.1** (19 mg, 0.10 mmol), iodobenzene material **6.2** (402 mg, 0.75 mmol, 1.5 equiv.), and phenylsilane (80 μ L, 0.63 mmol, 1.3 equiv.) in DME (1.5 mL) at 80°C for 24 h. The crude product was purified via flash column chromatography (3% ethyl acetate in pentane, R_f = 0.22) to afford 5.3 as a pale yellow solid (115 mg, 85%); ^1H NMR (500 MHz, CDCl_3) δ : 3.10 (t, 2H), 4.58 (t, 2H), 7.25-7.33 (m, Ar H, 5H), 8.16 (d, Ar H, 2H), 8.27 (d, Ar H, 2H). ^{13}C NMR spectroscopic data is in accordance with literature.

4-Methoxybenzyl-4-nitrobenzoate was obtained from the reaction of 4-Methoxybenzyl alcohol (62.07 μ L, 0.5 mmol, 1.0 equiv.), phosphine oxide **6.1** (19.4 mg, 0.10 mmol), iodobenzene material **6.2** (402 mg, 0.75 mmol, 1.5 equiv.), and phenylsilane (80 μ L, 0.63 mmol, 1.3 equiv.) in DME (1.5 mL) at 80 °C for 24 h. The crude product was purified via flash column chromatography (5.0% ethyl acetate in pentane, R_f = 0.29) to afford 5.4 as an off white solid (126.4 mg, 88%); ^1H NMR (500 MHz, CDCl_3) δ : 3.81 (s,

3H), 5.33 (s, 2H), 6.93 (d, 2H), 7.39 (d, 2H), 8.20 (d, Ar H, 2H), 8.25 (d, Ar H, 2H). ^{13}C NMR spectroscopic data is in accordance with literature.

2-Butyn-4-nitrobenzoate was obtained from the reaction of 2-butyn-1-ol (37 μL , 0.5 mmol, 1.0 equiv.), phosphine oxide **6.1** (19 mg, 0.10 mmol), iodobenzene material **6.2** (402 mg, 0.75 mmol, 1.5 equiv.), and phenylsilane (80 μL , 0.6 mmol, 1.3 equiv.) in DME (1.5 mL) at 80 $^{\circ}\text{C}$ for 24 h. The crude product was purified via flash column chromatography (5% ethyl acetate in pentane, $R_f = 0.29$) to afford **5.5** as a light yellow solid (99 mg, 91%); ^1H NMR (500 MHz, CDCl_3) δ : 1.89 (t, 3H), 4.93 (q, 2H), 8.24 (d, Ar H, 2H), 8.28 (d, Ar H, 2H). ^{13}C NMR (500 MHz, CDCl_3) δ : 3.78, 54.28, 72.66, 84.19, 123.65, 131.01, 135.62, 148.05, 150.65, 164.61.

Piperonyl-4-nitrobenzoate was obtained from the reaction of piperonyl alcohol (76.0 mg, 0.5 mmol, 1.0 equiv.), phosphine oxide **6.1** (19 mg, 0.10 mmol), iodobenzene material **6.2** (402 mg, 0.75 mmol, 1.5 equiv.), and phenylsilane (80 μL , 0.63 mmol, 1.3 equiv.) in DME (1.5 mL) at 80 $^{\circ}\text{C}$ for 24 h. The crude product was purified via flash column chromatography (7% ethyl acetate in pentane, $R_f = 0.23$) to afford **5.6** as a pale yellow solid (147 mg, 98%); ^1H NMR (500 MHz, CDCl_3) δ : 5.28 (s, 2H), 5.97 (s, 2H), 6.81 (d, 1H), 6.92 (d, 2H), 8.21 (d, Ar H, 2H), 8.26 (d, Ar H, 2H). ^{13}C NMR (500 MHz, CDCl_3) δ : 67.75, 101.39, 108.46, 109.28, 122.74, 123.62, 129.02, 130.88, 135.62, 148.05, 150.65, 164.61.

Allyl-4-nitrobenzoate was obtained from the reaction of allyl alcohol (34 μL , 0.5 mmol, 1.0 equiv.), phosphine oxide **6.1** (19 mg, 0.10 mmol), iodobenzene material **6.2** (402 mg, 0.75 mmol, 1.5 equiv.), and phenylsilane (80 μL , 0.63 mmol, 1.3 equiv.) in DME

(1.5 mL) at 80°C for 24 h. The crude product was purified via flash column chromatography (2% ethyl acetate in pentane, Rf = 0.19) to afford 5.7 as a yellow viscous oil (90 mg, 87%); ¹H NMR (500 MHz, CDCl₃) δ: 4.87 (dt, 2H), 5.32 (dd, 1H), 5.43 (dd, 1H), 6.04 (m, 1H), 8.23 (d, Ar H, 2H), 8.27 (d, Ar H 2H). ¹³C NMR spectroscopic data is in accordance with literature.

Cinnamyl-4-nitrobenzoate was obtained from the reaction of cinnamyl alcohol (67 mg, 0.5 mmol, 1.0 equiv.), phosphine oxide **6.1** (19 mg, 0.10 mmol), iodobenzene material **6.2** (402 mg, 0.75 mmol, 1.5 equiv.), and phenylsilane (80 μL, 0.6 mmol, 1.3 equiv.) in DME (1.5 mL) at 80°C for 24 h. The crude product was purified via flash column chromatography (3% ethyl acetate in pentane, Rf = 0.22) to afford 5.8 as a dark yellow oil (116 mg, 82%); ¹H NMR (500 MHz, CDCl₃) δ: 5.03 (d, 2H), 6.41 (dt, 1H), 6.76 (d, 1H), 7.33-7.43 (m, Ar H, 5H), 8.24 (d, Ar H, 2H), 8.27 (d, Ar H, 2H). ¹³C NMR (500 MHz, CDCl₃) δ: 66.60, 122.41, 123.65, 126.80, 128.47, 128.78, 130.88, 133.40, 133.44, 133.48, 150.66, 164.60.

n-Butyl-4-nitrobenzoate was obtained from the reaction of 1-Butanol (45.7 μL, 0.5 mmol, 1.0 equiv.), phosphine oxide **6.1** (19 mg, 0.10 mmol), iodobenzene material **6.2** (402 mg, 0.75 mmol, 1.5 equiv.), and phenylsilane (80 μL, 0.6 mmol, 1.3 equiv.) in DME (1.5 mL) at 80°C for 24 h. The crude product was purified via flash column chromatography (2% ethyl acetate in pentane, Rf = 0.25) to afford 5.9 as a yellow viscous oil (83 mg, 75%); ¹H NMR (300 MHz, CDCl₃) δ: 0.99 (t, 3H), 1.49 (q, 2H), 1.78 (q, 2H), 4.37 (t, 2H), 8.20 (d, Ar H, 2H), 8.27 (d, Ar H, 2H). ¹³C NMR (300 MHz, CDCl₃) δ: 13.99, 19.48, 30.90, 66.09, 69.78, 123.79, 130.92, 136.15, 165.34.

Isobutyl-4-nitrobenzoate was obtained from the reaction of 2-Methyl-1-propanol (46 μ L, 0.5 mmol, 1.0 equiv phosphine oxide **6.1** (19 mg, 0.10 mmol), iodobenzene material **6.2** (402 mg, 0.75 mmol, 1.5 equiv.), and phenylsilane (80 μ L, 0.6 mmol, 1.3 equiv.) in DME (1.5 mL) at 80°C for 24 h. The crude product was purified via flash column chromatography (2% ethyl acetate in pentane, Rf = 0.25) to afford 5.10 as a pale yellow solid (82 mg, 74%); ^1H NMR (500 MHz, CDCl_3) δ : 1.03 (d, 6H), 2.11 (m, 1H), 4.15 (d, 2H), 8.22 (d, Ar H, 2H), 8.27 (d, Ar H, 2H). ^{13}C NMR (500 MHz, CDCl_3) δ : 19.22, 27.92, 71.99, 123.63, 130.73, 135.96, 150.58, 164.79.

Isoamyl-4-nitrobenzoate was obtained from the reaction of 3-Methyl-1-butanol (55.09 μ L, 0.5 mmol, 1.0 equiv.), phosphine oxide **6.1** (19 mg, 0.10 mmol), iodobenzene material **6.2** (402 mg, 0.75 mmol, 1.5 equiv.), and phenylsilane (80 μ L, 0.63 mmol, 1.3 equiv.) in DME (1.5 mL) at 80°C for 24 h. The crude product was purified via flash column chromatography (2% ethyl acetate in pentane, Rf = 0.25) to afford 5.11 as a yellow viscous oil (93 mg, 79%); ^1H NMR (300 MHz, CDCl_3) δ : 0.98 (d, 6H), 1.69 (q, 2H), 1.77 (m, 1H), 4.40 (t, 2H), 8.19 (d, Ar H, 2H), 8.27 (d, Ar H, 2H). ^{13}C NMR (300 MHz, CDCl_3) δ : 22.57, 25.29, 37.35, 64.73, 123.62, 130.74, 135.96, 150.56, 164.84.

2-Pyridinemethanol-4-nitrobenzoate was obtained from the reaction of 2-Pyridinemethanol (48 μ L, 0.5 mmol, 1.0 equiv.), phosphine oxide **6.1** (19 mg, 0.10 mmol), iodobenzene material **6.2** (402 mg, 0.75 mmol, 1.5 equiv.), and phenylsilane (80 μ L, 0.6 mmol, 1.3 equiv.) in DME (1.5 mL) at 80°C for 24 h. The crude product was purified via flash column chromatography (30% ethyl acetate in pentane with 0.2% triethylamine, Rf = 0.25) to afford 5.12 as a light brown solid (116 mg, 90%); ^1H NMR (500 MHz, CDCl_3) δ : 5.49 (s, 2H), 7.25 (t, 1H), 7.42 (d, 1H), 7.72 (m, 1H), 8.26 (d, Ar H, 2H), 8.27 (d, Ar H,

2H), 8.60 (d, 1H). ^{13}C NMR (500 MHz, CDCl_3) δ : 68.13, 122.18, 123.68, 124.03, 131.02, 135.31, 137.03, 149.79, 150.54, 155.13, 164.47.

3-(methylthio)-1-hexyl-4-nitrobenzoate was obtained from the reaction of 3-(Methylthio)-1-hexanol (76 μL , 0.5 mmol, 1.0 equiv.), phosphine oxide **6.1** (19 mg, 0.10 mmol), iodobenzene material **6.2** (402 mg, 0.75 mmol, 1.5 equiv.), and phenylsilane (80 μL , 0.6 mmol, 1.3 equiv.) in DME (1.5 mL) at 80°C for 24 h. The crude product was purified via flash column chromatography (3% ethyl acetate in pentane, R_f = 0.22) to afford **5.13** as a yellow viscous oil (114 mg, 77%); ^1H NMR (500 MHz, CDCl_3) δ : 0.91 (t, 3H), 1.43-1.52 (m, 2H), 1.53-1.61 (m, 2H), 1.91-1.99 (m 2H), 2.03 (s, 3H), 2.66 (m, 1H), 4.52 (t, 2H), 8.17 (d, Ar H, 2H), 8.26 (d, Ar H, 2H). ^{13}C NMR (500 MHz, CDCl_3) δ : 12.50, 13.99, 20.14, 32.88, 36.65, 43.17, 64.02, 123.63, 130.74, 135.75, 150.59, 164.70.

4-Nitrobenzoic acid 3-(1-dimethylsulfamoyl-1-H-imidazol-4-yl)prop-2-ynyl ester was obtained from the reaction of alcohol (114 mg, 0.5 mmol, 1.0 equiv.) a kind donation from The Lovely Group, phosphine oxide **6.1** (19 mg, 0.10 mmol), iodobenzene material **6.2** (402 mg, 0.75 mmol, 1.5 equiv.), and phenylsilane (80 μL , 0.6 mmol, 1.3 equiv.) in DME (1.5 mL) at 80°C for 24 h. The crude product was purified via flash column chromatography (35% ethyl acetate in pentane with 2% triethylamine, R_f = 0.18) to afford **5.14** as a yellow viscous oil (153 mg, 81%); ^1H NMR (500 MHz, CDCl_3) δ : 2.86 (s, 6H), 5.17 (s, 2H), 7.42 (d, 1H), 7.82 (d, 1H), 8.24 (d, Ar H, 2H), 8.27 (d, Ar H, 2H). ^{13}C NMR (500 MHz, CDCl_3) δ : 38.28, 53.92, 79.35, 84.38, 121.69, 123.70, 125.01, 131.07, 134.87, 136.70, 150.82, 164.06.

1-Phenyl-2-(4-nitrobenzoate) was obtained from the reaction of 1-Phenyl-2-propanol (68 μ L, 0.5 mmol, 1.0 equiv.), phosphine oxide **6.1** (19 mg, 0.10 mmol), iodobenzene material **6.2** (402 mg, 0.75 mmol, 1.5 equiv.), and phenylsilane (80 μ L, 0.6 mmol, 1.3 equiv.) in a mixed solvent system of DME and acetonitrile (ratio of 2:1, 1 mL: 0.5 mL respectively) at 80°C for 24 h. The crude product was purified via flash column chromatography (3% ethyl acetate in pentane, R_f = 0.27) to afford 5.15 as a light yellow solid (118 mg, 83%); ¹H NMR (500 MHz, CDCl₃) δ : 1.38 (d, 3H), 2.94 (q, 1H), 3.07 (q, 1H), 5.39 (m, 1H), 7.24-7.27 (m, Ar H, 5H), 8.15 (d, Ar H, 2H), 8.26 (d, Ar H, 2H). ¹³C NMR (500 MHz, CDCl₃) δ : 19.61, 42.34, 73.50, 123.57, 126.81, 128.56, 129.51, 130.68, 136.18, 137.21, 150.75, 164.07.

3-Buten-2-(4-nitrobenzoate) was obtained from the reaction of 3-Buten-2-ol (43 μ L, 0.5 mmol, 1.0 equiv.), phosphine oxide **6.1** (19 mg, 0.10 mmol), iodobenzene material **6.2** (402 mg, 0.75 mmol, 1.5 equiv.), and phenylsilane (80 μ L, 0.6 mmol, 1.3 equiv.) in a mixed solvent system of DME and acetonitrile (ratio of 2:1, 1 mL: 0.5 mL respectively) at 80 °C for 24 h. The crude product was purified via flash column chromatography (2% ethyl acetate in pentane, R_f = 0.22) to afford 5.16 as an orange liquid (80 mg, 73%); ¹H NMR (500 MHz, CDCl₃) δ : 1.43 (d, 3H), 5.16 (d, 1H), 5.30 (d, 1H), 5.57 (m, 1H), 5.91 (m, 1H), 8.16 (d, Ar H, 2H), 8.23 (d, Ar H, 2H). ¹³C NMR (500 MHz, CDCl₃) δ : 20.07, 72.96, 116.76, 123.59, 130.79, 136.06, 137.11, 150.57, 163.97.

L-menthol-4-nitrobenzoate was obtained from the reaction of L-menthol (78.13 mg, 0.5 mmol, 1.0 equiv.), phosphine oxide **6.1** (19 mg, 0.10 mmol), iodobenzene material **6.2** (402 mg, 0.75 mmol, 1.5 equiv.), and phenylsilane (80 μ L, 0.6 mmol, 1.3 equiv.) in a mixed solvent system of DME and acetonitrile (ratio of 2:1, 1 mL: 0.5 mL

respectively) at 80 °C for 24 h. The crude product was purified via flash column chromatography (1% ethyl acetate in pentane, R_f = 0.22) to afford 5.17 as a yellow solid (114 mg, 75%); ¹H NMR (500 MHz, CDCl₃) δ: 0.79 (d, 3H), 0.93 (t, 7H), 1.14 (m, 2H), 1.56 (m, 2H), 1.73 (m, 2H), 1.90 (m, 1H), 2.12 (d, 1H), 4.96 (m, 1H), 8.20 (d, Ar H, 2H), 8.27 (d, Ar H, 2H). ¹³C NMR (500 MHz, CDCl₃) δ: 16.56, 20.82, 22.09, 23.66, 26.66, 31.54, 34.27, 40.93, 47.27, 76.61, 123.57, 130.74, 136.30, 150.50, 164.28.

Soberol-4-nitrobenzoate was obtained from the reaction of soberol (85 mg, 0.5 mmol, 1.0 equiv.), phosphine oxide **6.1** (19 mg, 0.10 mmol), iodobenzene material **6.2** (402 mg, 0.75 mmol, 1.5 equiv.), and phenylsilane (80 μL, 0.6 mmol, 1.3 equiv.) in a mixed solvent system of DME and acetonitrile (ratio of 2:1, 1 mL: 0.5 mL respectively) at 80 °C for 24 h. The crude product was purified via flash column chromatography (20% ethyl acetate in pentane, R_f = 0.21) to afford 5.18 as a pale yellow solid (105 mg, 66%); ¹H NMR (500 MHz, CDCl₃) δ: 1.18 (d, 6H), 1.59 (m, 2H), 1.73 (s, 3H), 1.84 (m, 2H), 2.21 (m, 2H), 5.54 (s, 1H), 5.81 (d, 1H), 8.19 (d, Ar H, 2H), 8.26 (d, Ar H, 2H). ¹³C NMR (500 MHz, CDCl₃) δ: 20.79, 26.71, 27.01, 27.61, 30.07, 39.71, 72.10, 72.83, 123.61, 128.84, 130.49, 130.82, 136.16, 150.57, 164.41.

Ethyl-L-lactate-4-nitrobenzoate was obtained from the reaction of ethyl-L-lactate (57.0 μL, 0.5 mmol, 1.0 equiv.), phosphine oxide **6.1** (19 mg, 0.10 mmol), iodobenzene material **6.2** (402 mg, 0.75 mmol, 1.5 equiv.), and phenylsilane (80 μL, 0.6 mmol, 1.3 equiv.) in a mixed solvent system of DME and acetonitrile (ratio of 2:1, 1 mL: 0.5 mL respectively) at 80 °C for 24 h. The crude product was purified via flash column chromatography (5% ethyl acetate in pentane, R_f = 0.16) to afford 5.19 as a yellow viscous oil (118 mg, 89%); ¹H NMR (500 MHz, CDCl₃) δ: 1.27 (t, 3H), 1.64 (d, 3H), 4.22

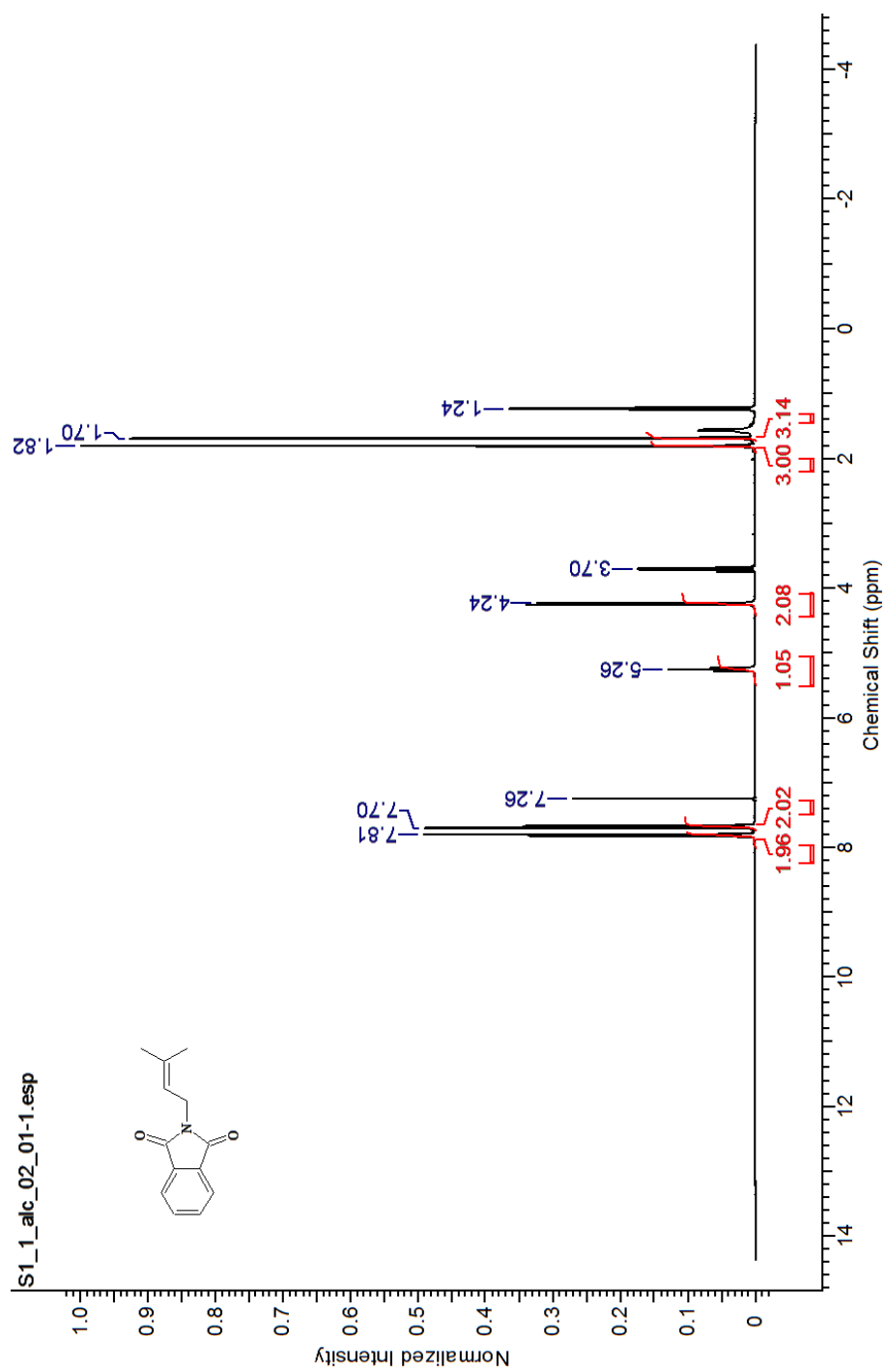
(q, 2H), 5.32 (q, 1H), 8.23 (d, Ar H, 2H), 8.28 (d, Ar H, 2H). ^{13}C NMR (500 MHz, CDCl_3) δ :
14.18, 17.06, 61.75, 70.04, 123.64, 131.05, 134.97, 150.80, 164.16, 170.29.

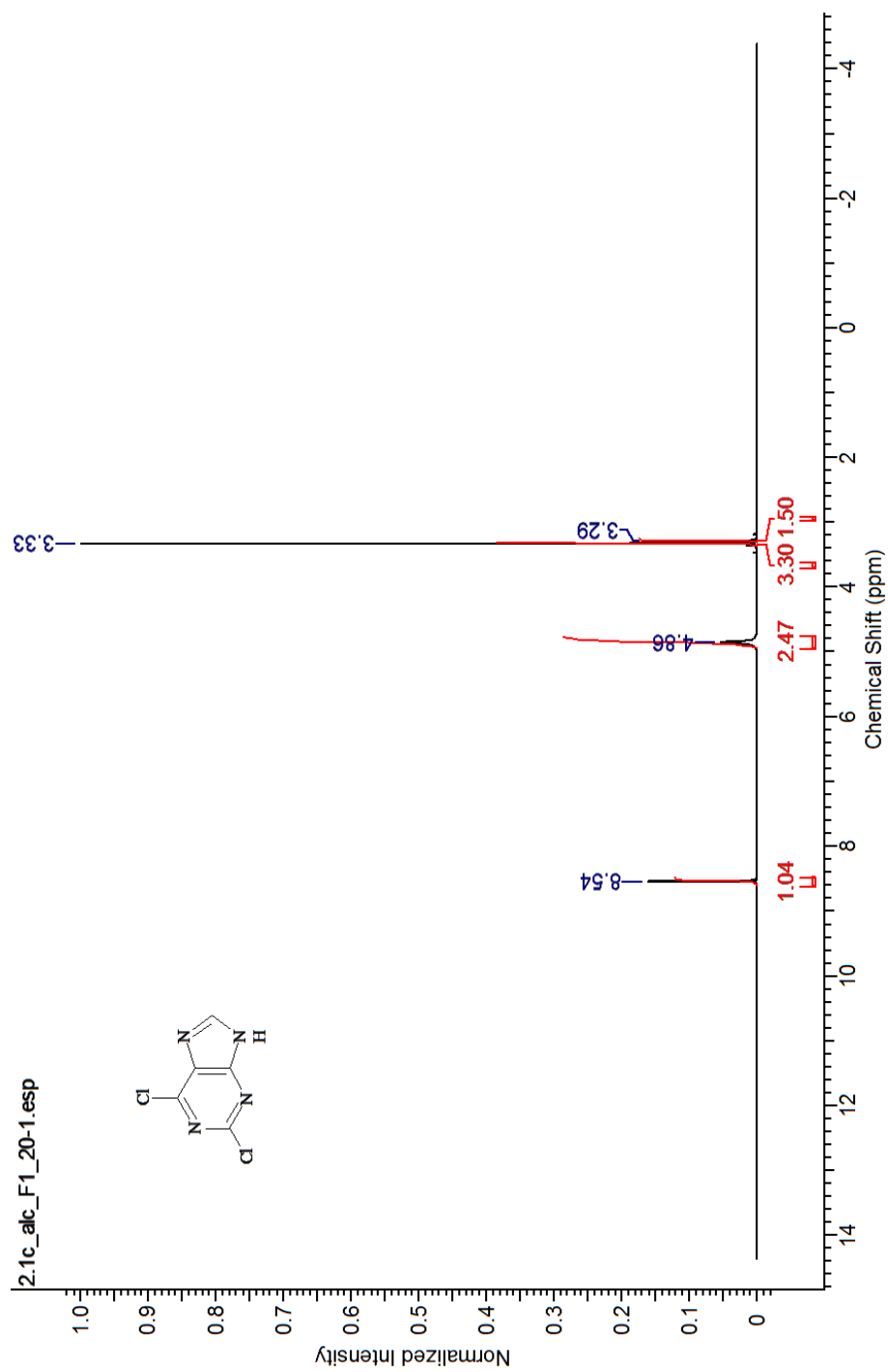
Appendix A
List of Abbreviations

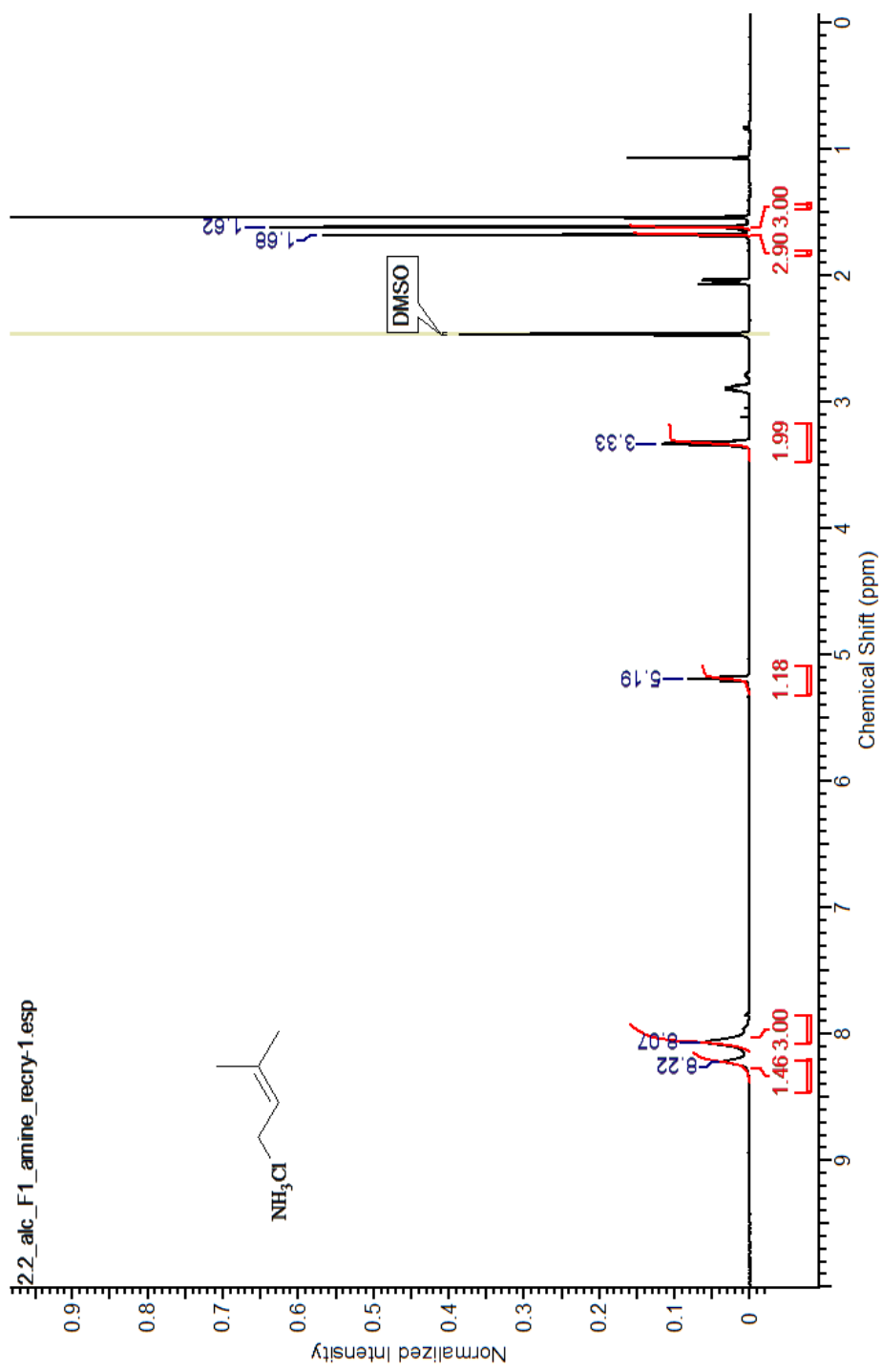
MiaE, 2-methylthio- N^6 -isopentenyl adenosine(37)-tRNA (ms^2i^6A -tRNA)
monooxygenase; tRNA, transfer ribonucleic acid; MiaA, Δ^2 -isopentenylpyrophosphate tRNA-
adenosine transferase; MiaB, 2-methylthio- N^6 -isopentenyl-adenosine synthase; DMAPP,
dimethylallyl pyrophosphate; SAM, S-adenosylmethionine; $ms^2i^6A_{37}$, 2-methylthio- N^6 -
isopentenyl-adenosine; i^6A_{37} , N^6 -isopentenyl-adenosine; $Cl^2i^6A_{37}$, 2-chloro- N^6 -isopentenyl-
adenosine; $mo^2i^6A_{37}$, 2-methoxy- N^6 -isopentenyl-adenosine; $ms^2io^6A_{37}$, 2-methylthio- N^6 -(4-
hydroxyisopentenyl)-adenosine; io^6A_{37} , N^6 -(4-hydroxyisopentenyl)-adenosine; $Cl^2io^6A_{37}$, 2-chloro-
 N^6 -(4-hydroxyisopentenyl)-adenosine; ACSL, anticodon stem loop; TLC, thin layer
chromatography; HPLC, high-performance liquid chromatography; TEV, tobacco etch virus
protease; IPTG, isopropyl β -D-1-thiogalactopyranoside; EPR, Electron Paramagnetic
Resonance; ETC, electron transport chain; Fd, ferredoxin; FdR, ferredoxin reductase; NADPH,
nicotinamide adenine dinucleotide phosphate; NADH, nicotinamide adenine dinucleotide; MMO,
methane monooxygenase.

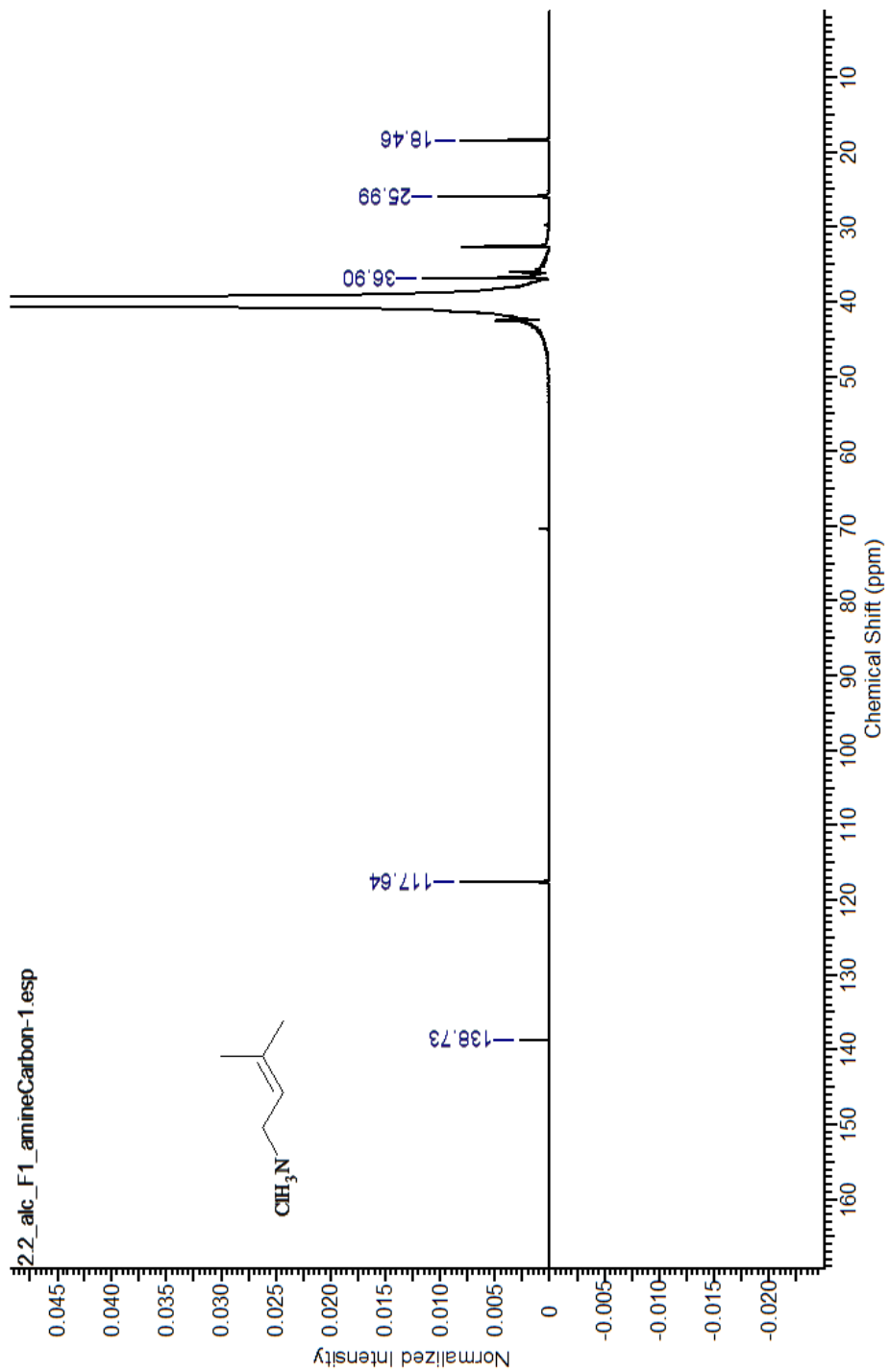
Appendix B
NMR Spectra

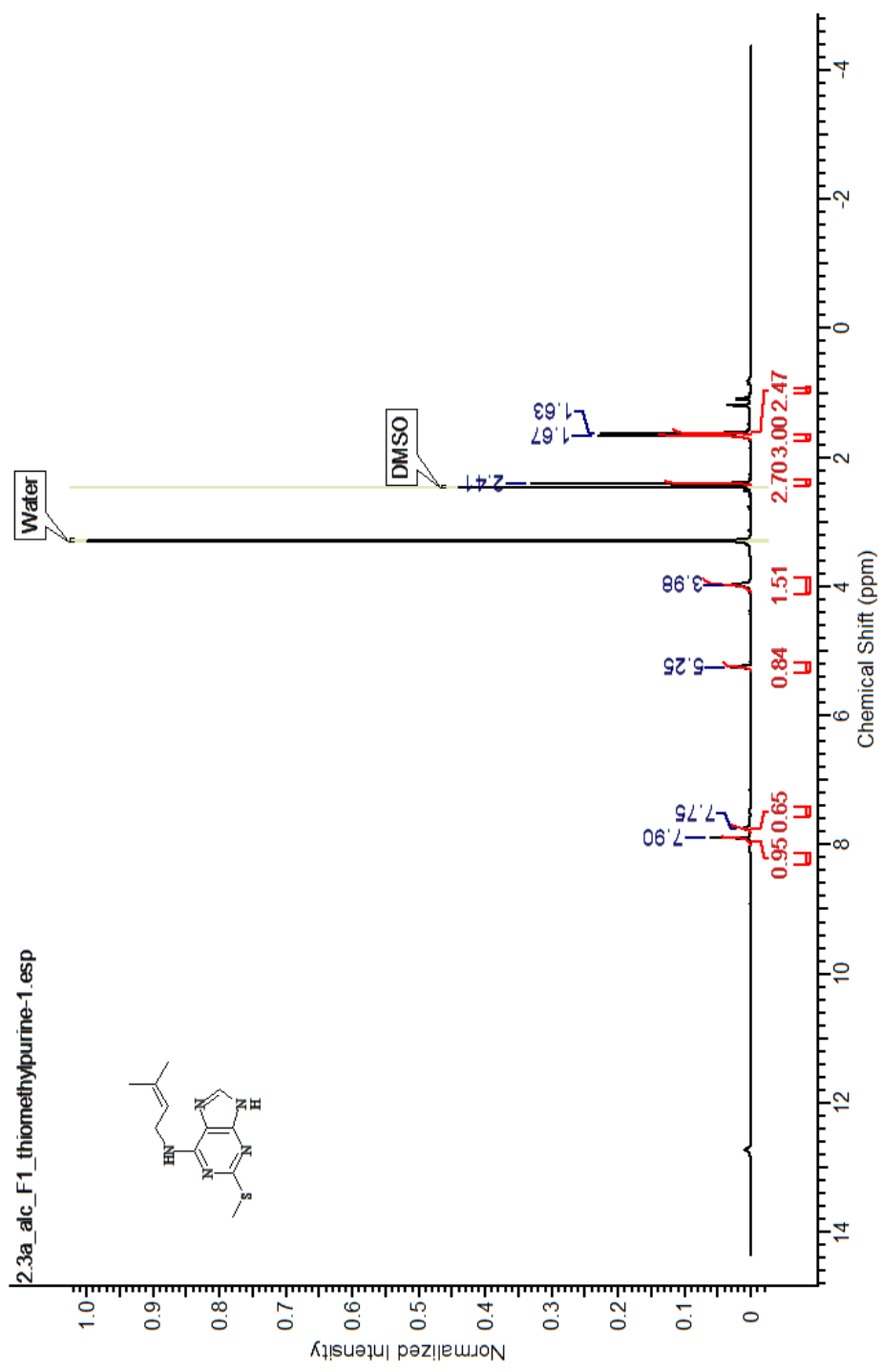
Appendix B: Chapter 2 NMR Spectra

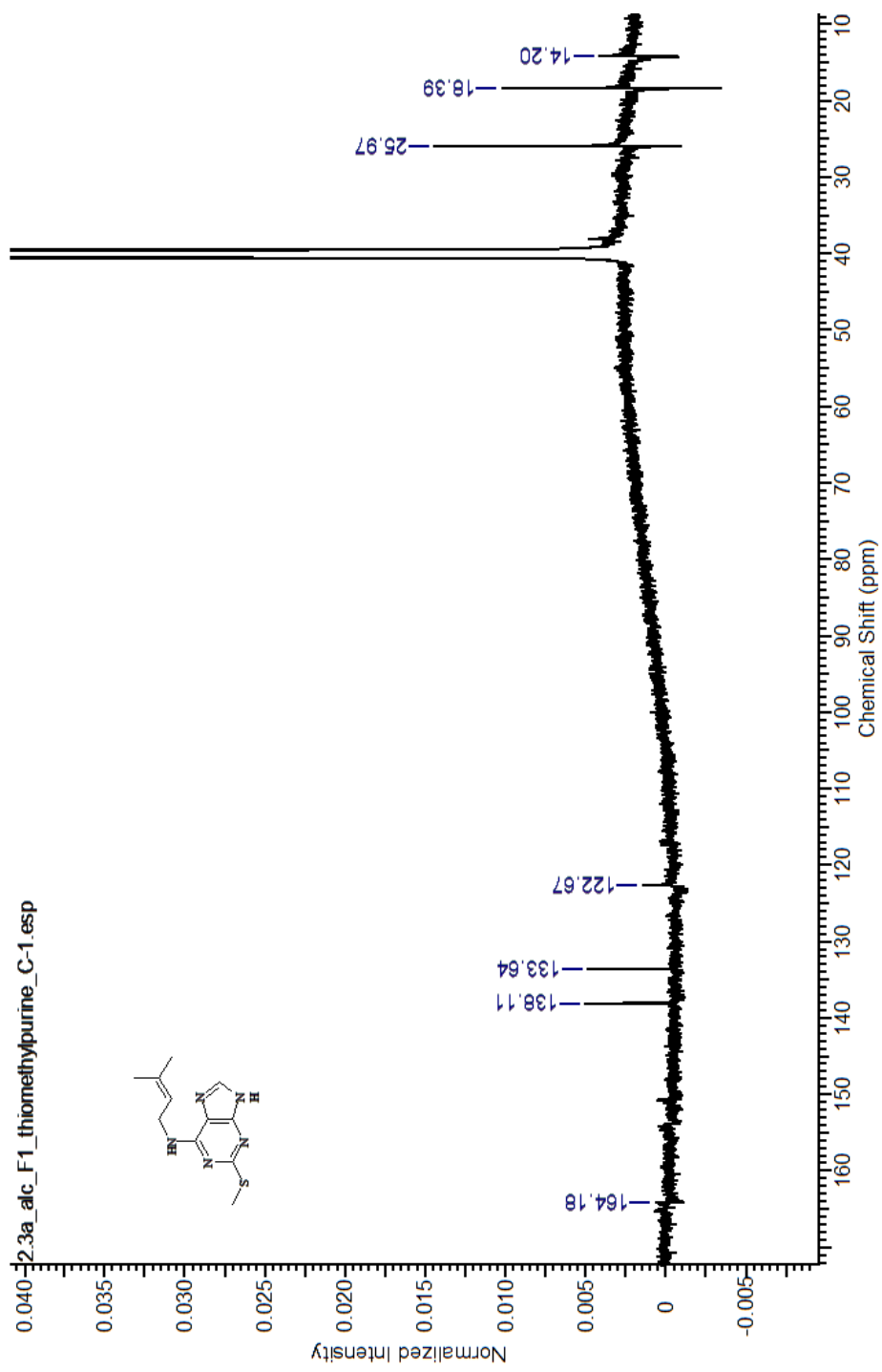


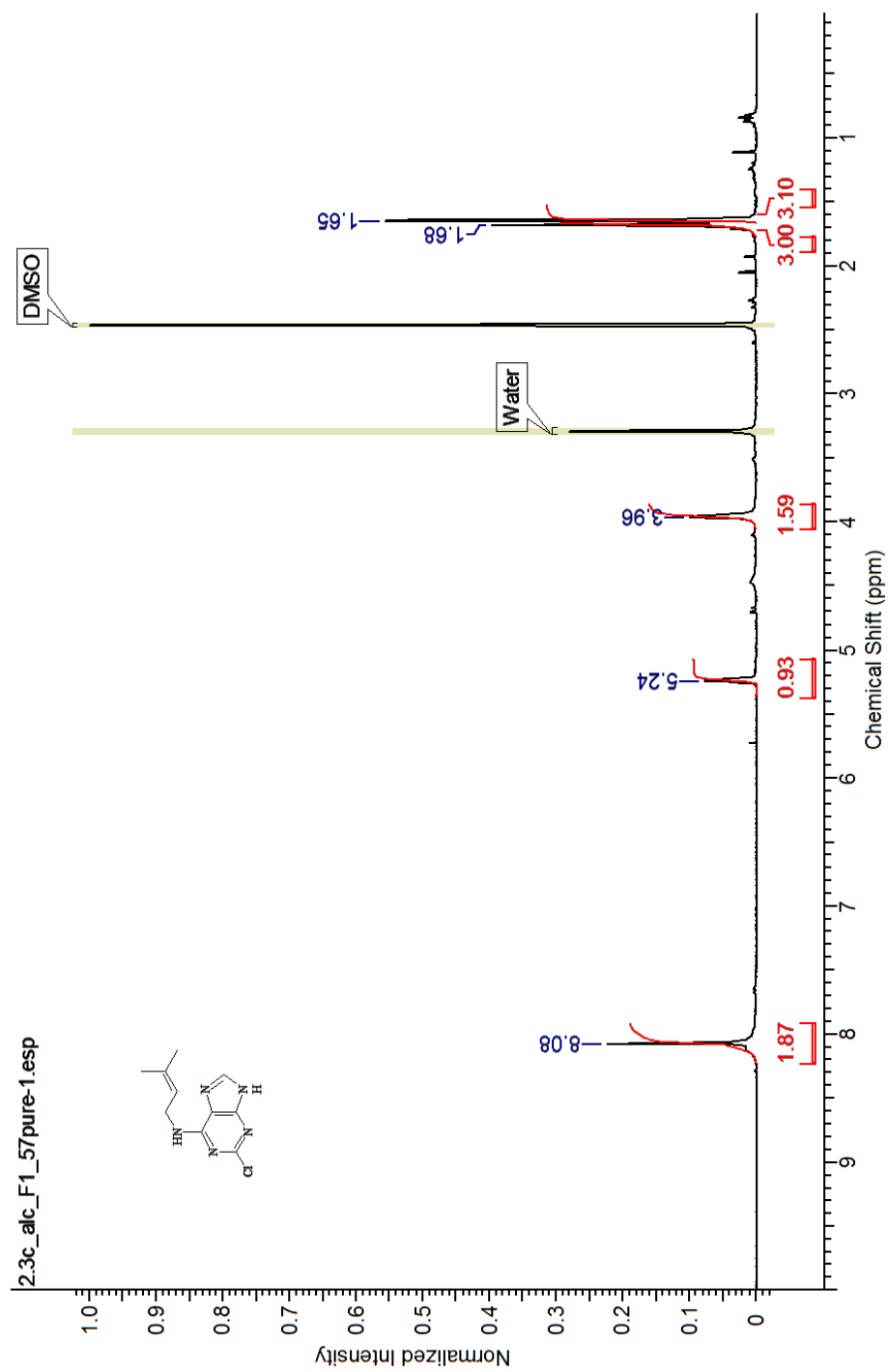


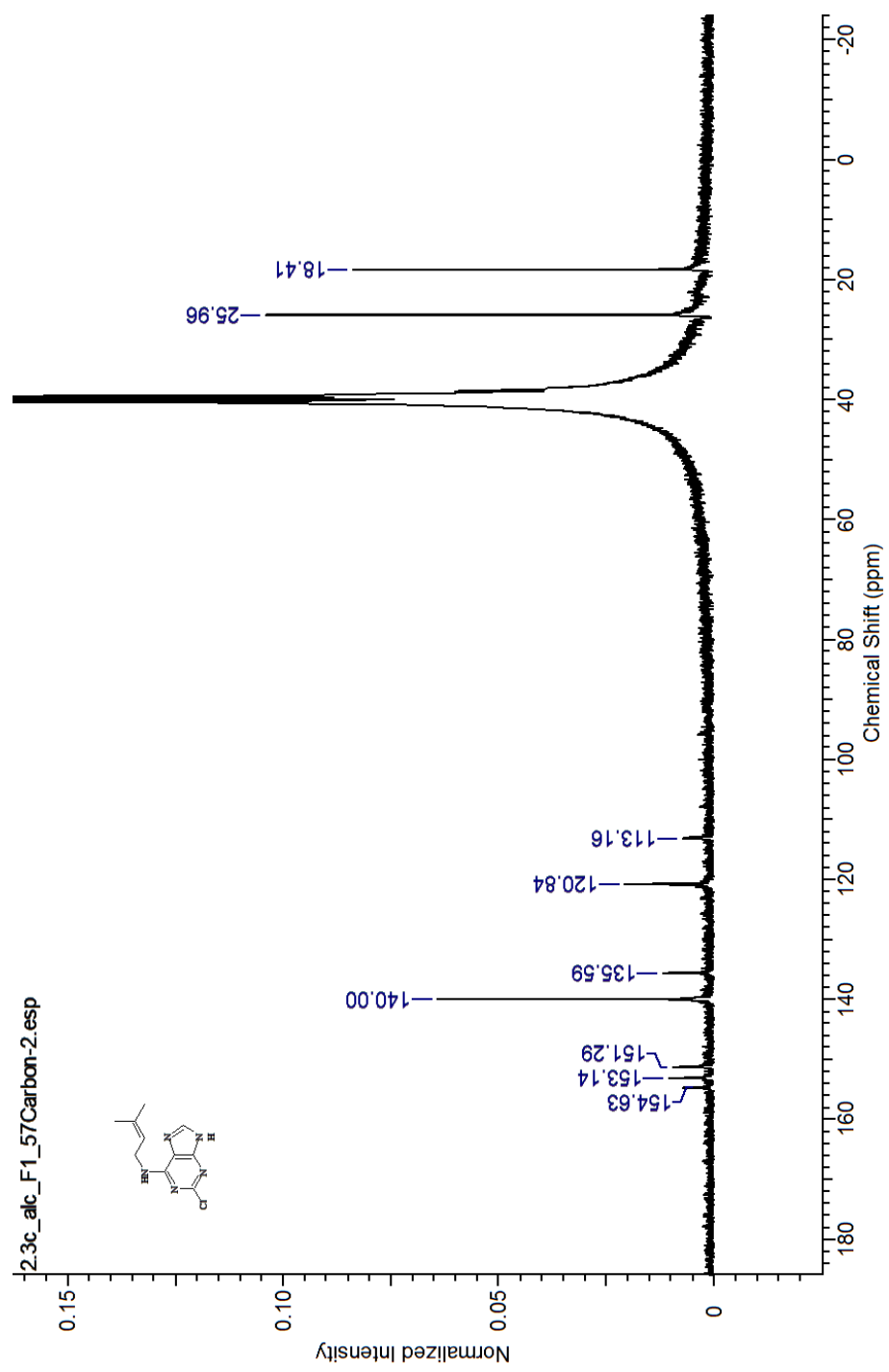


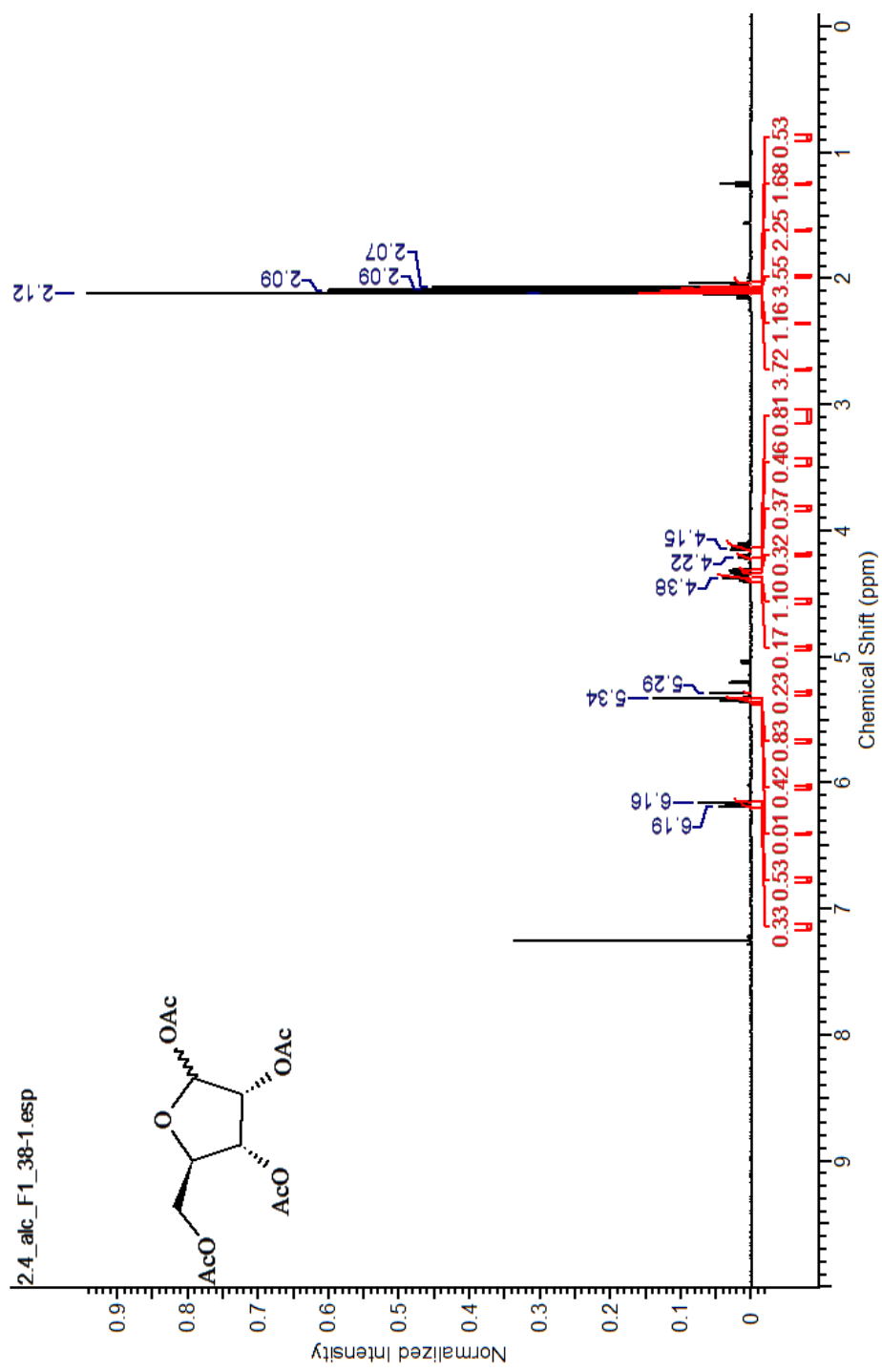


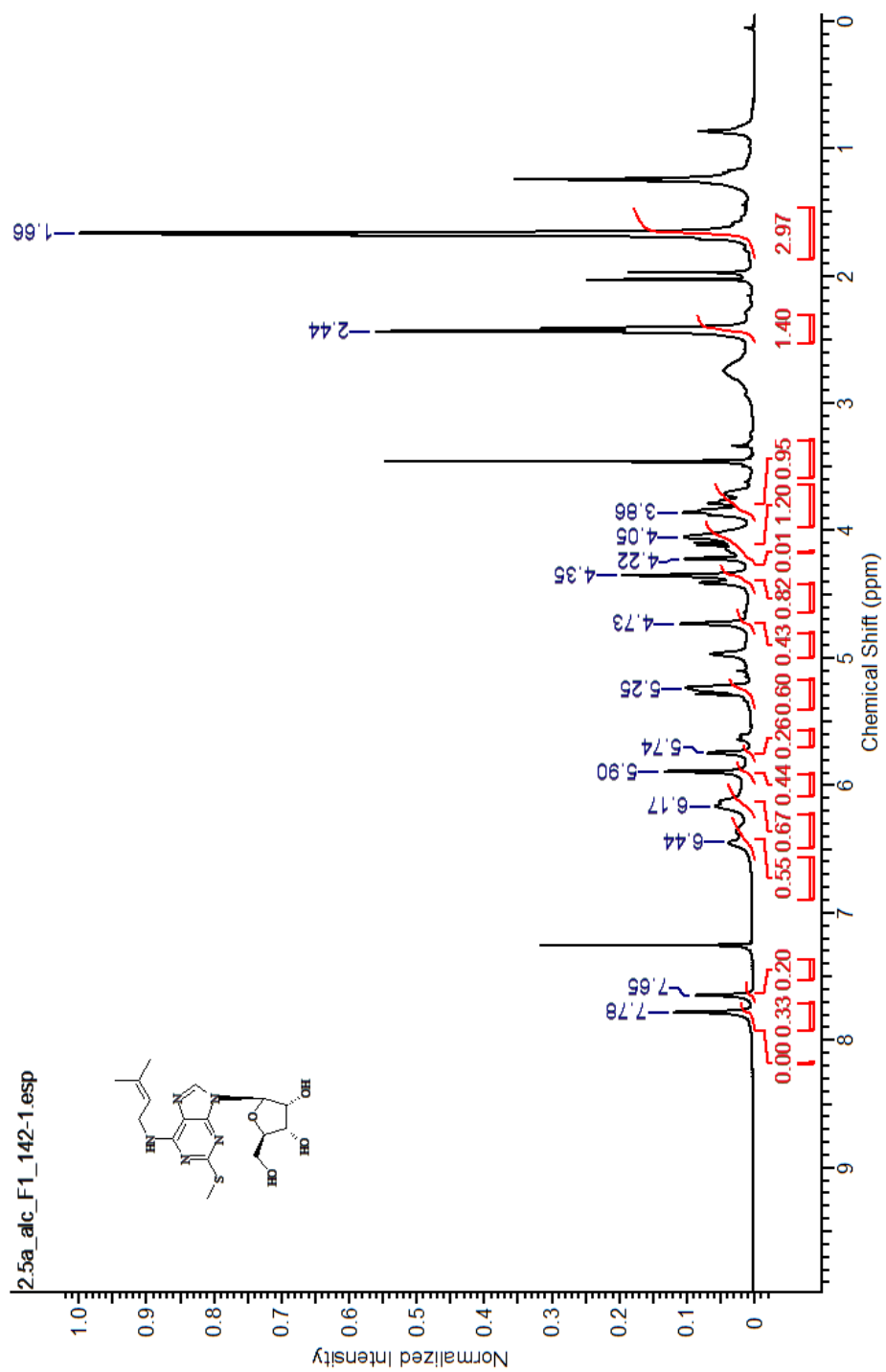


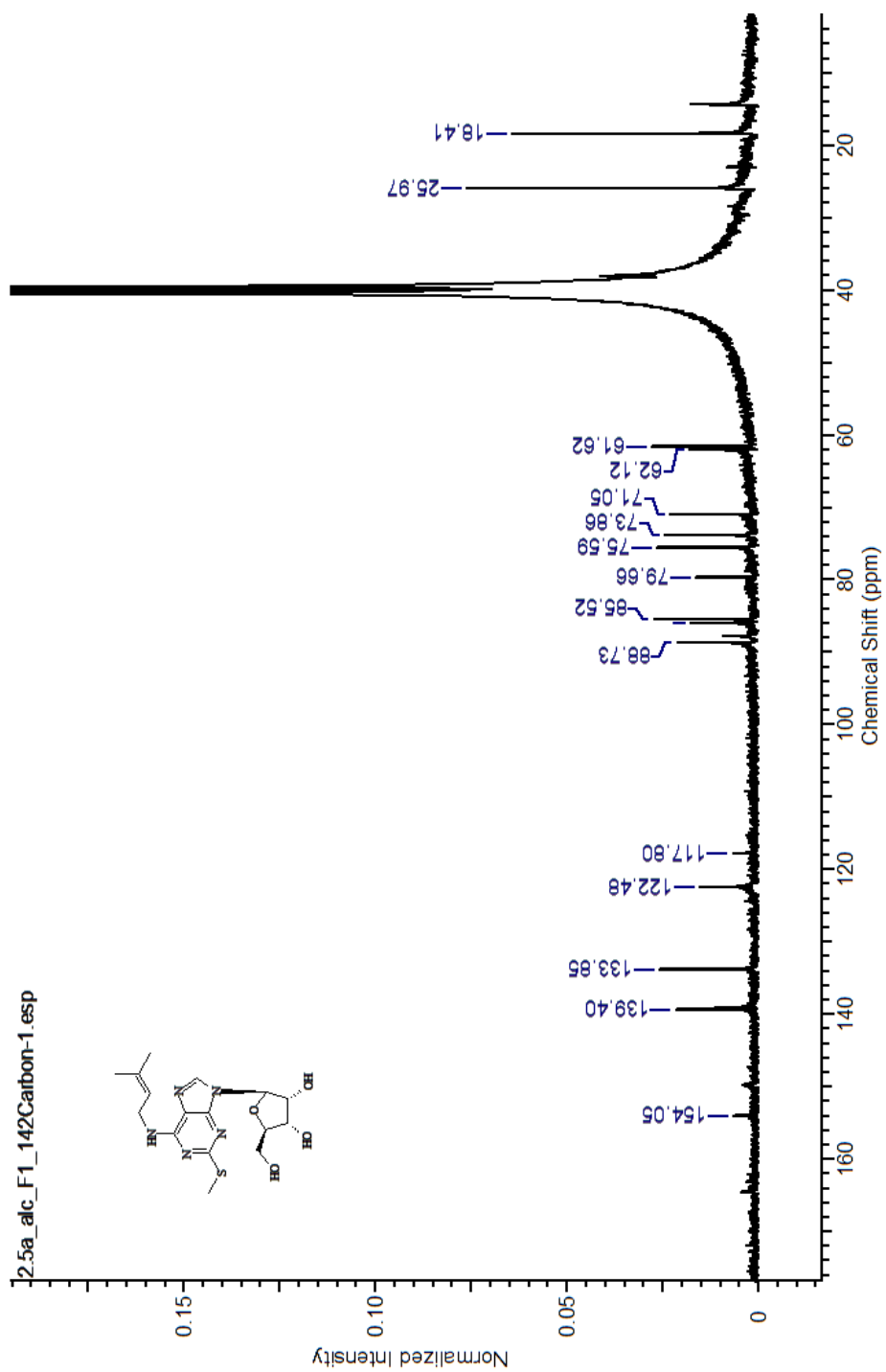


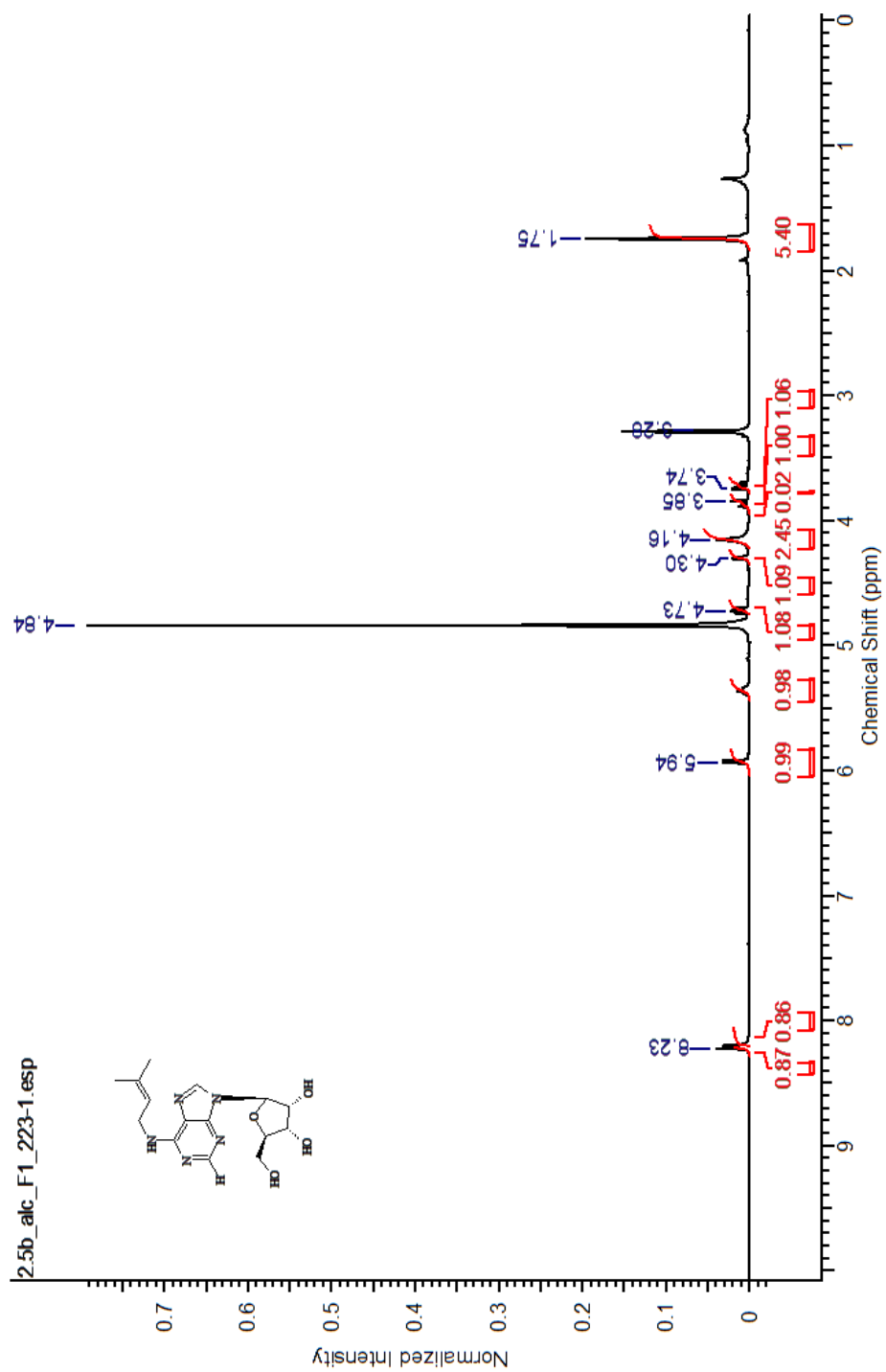


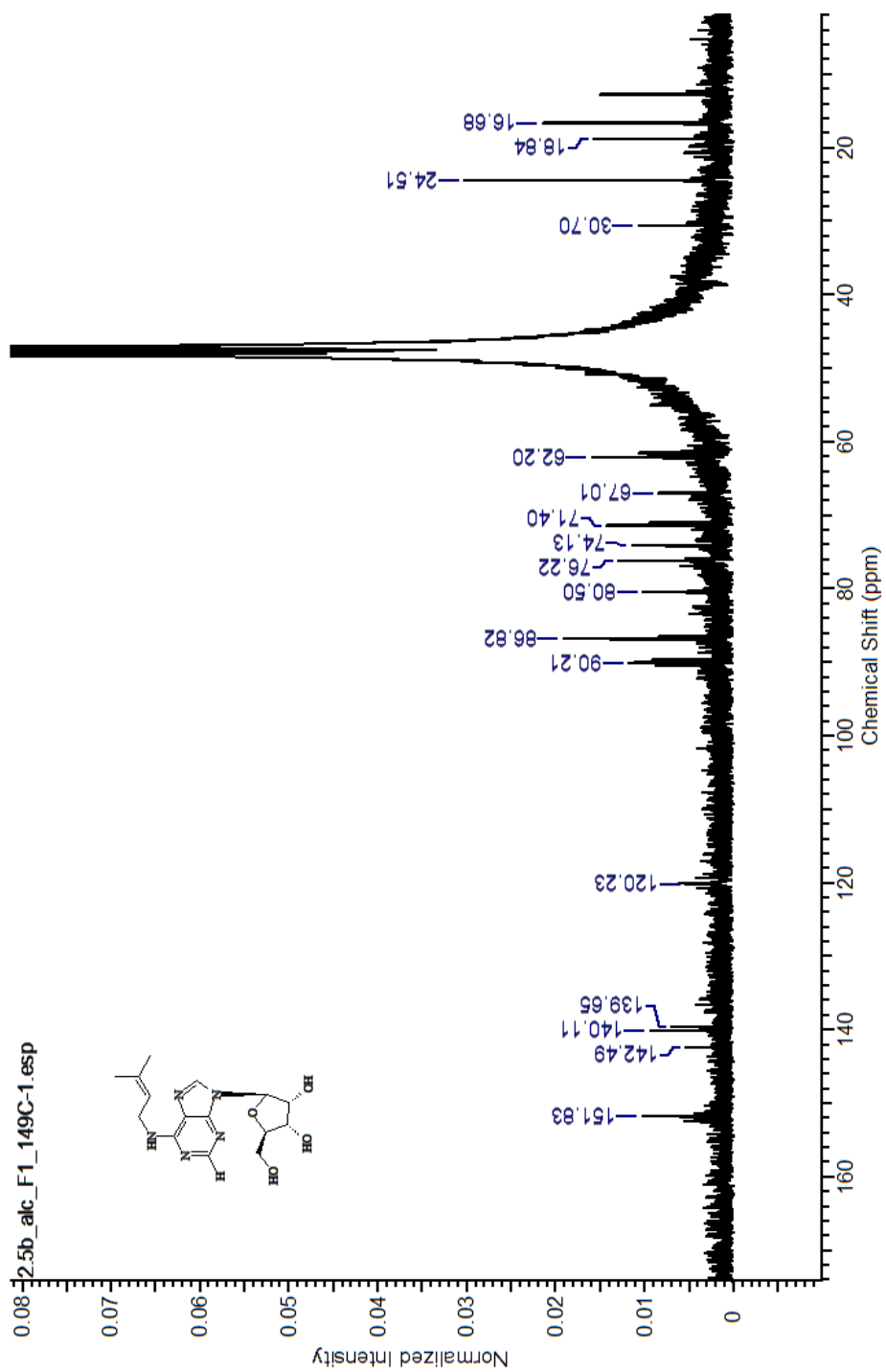


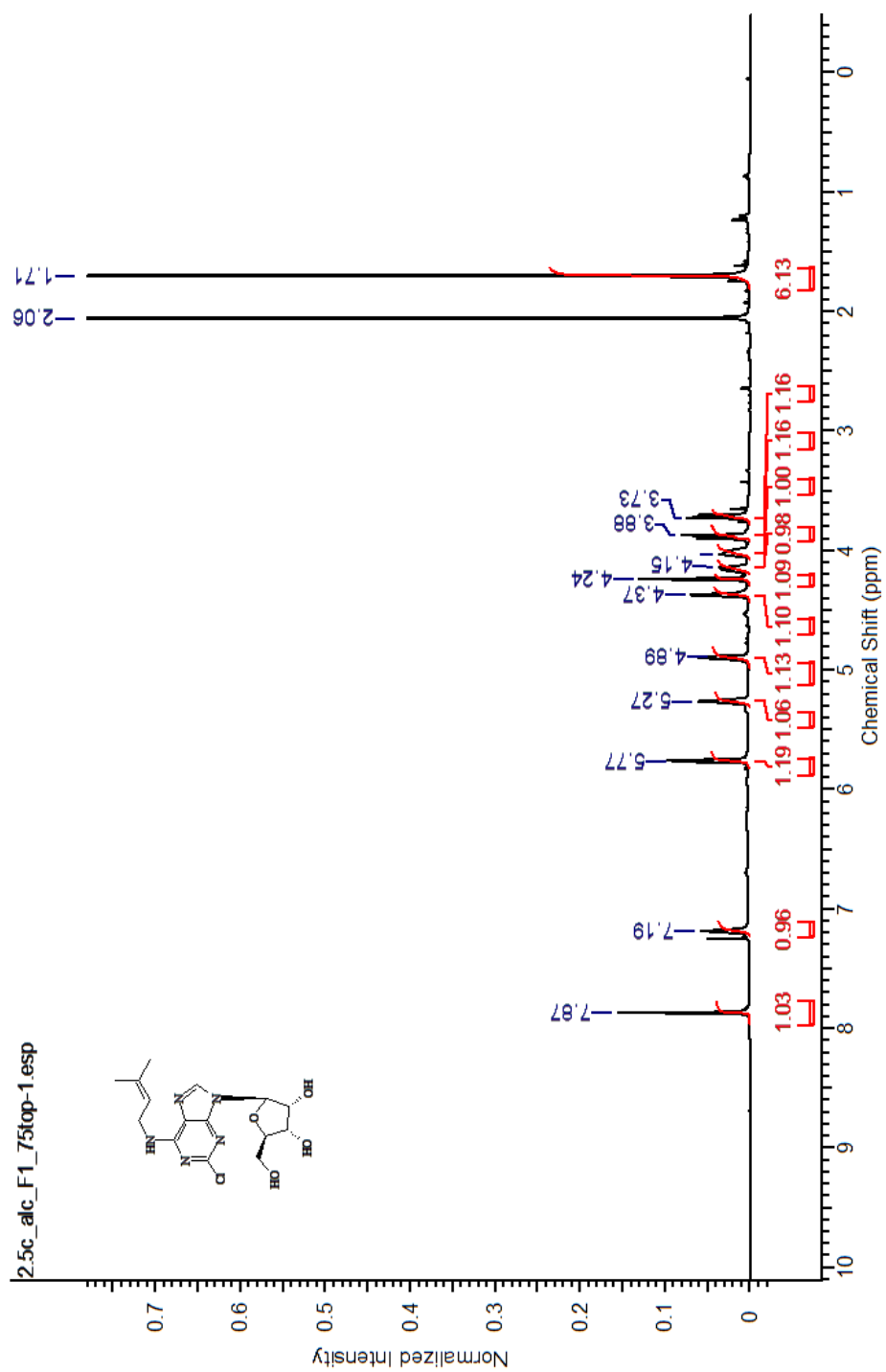


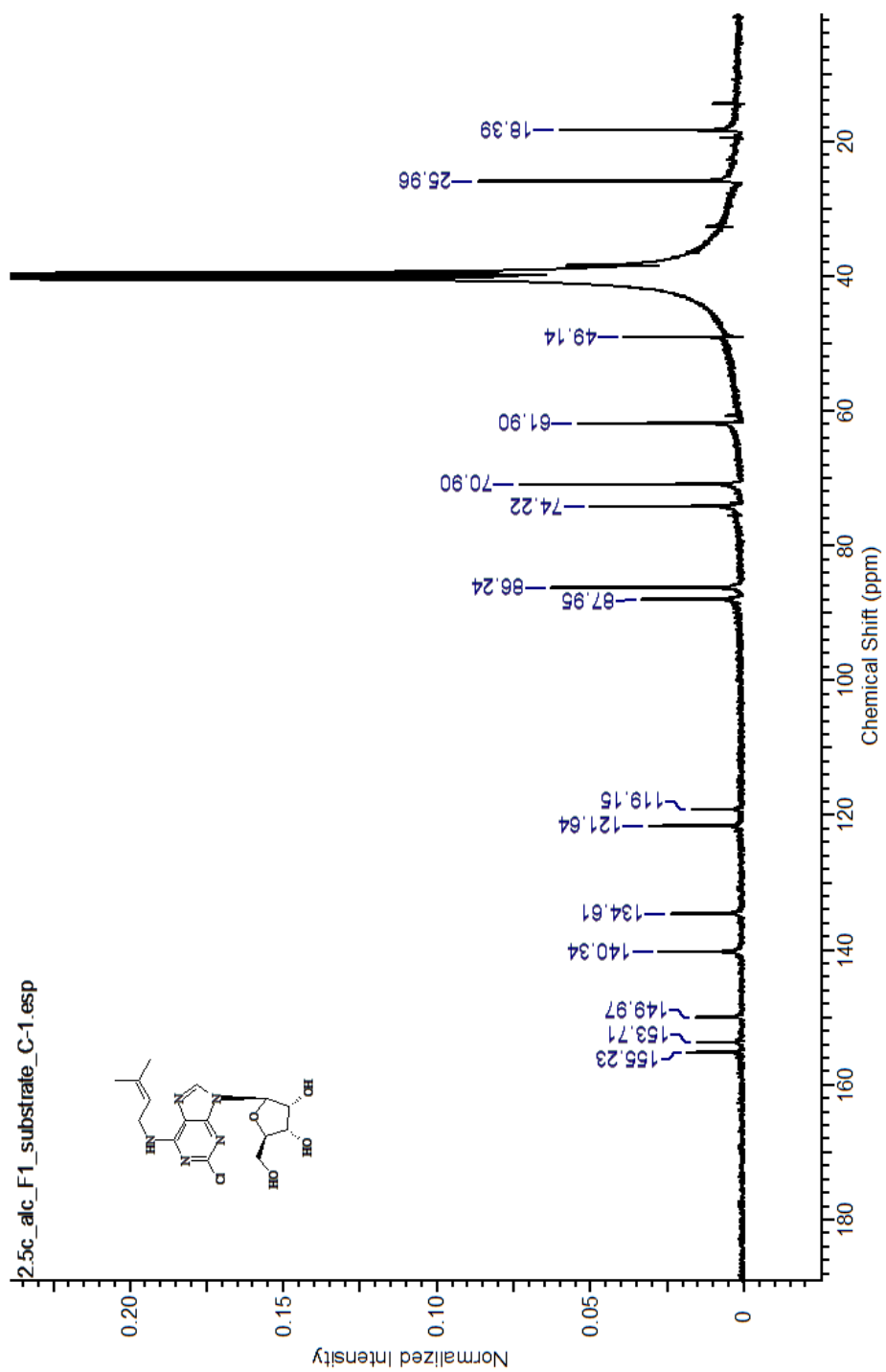


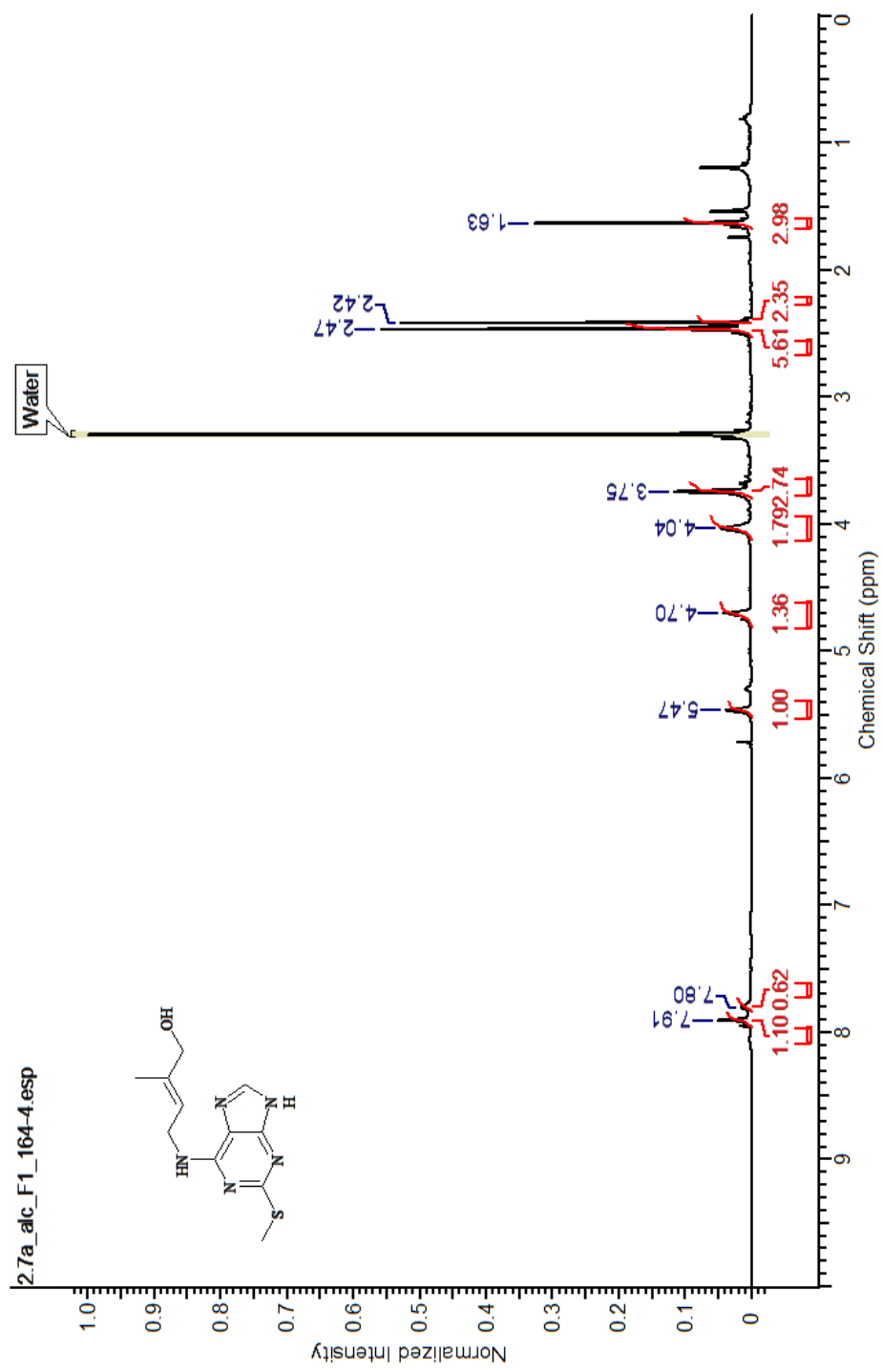


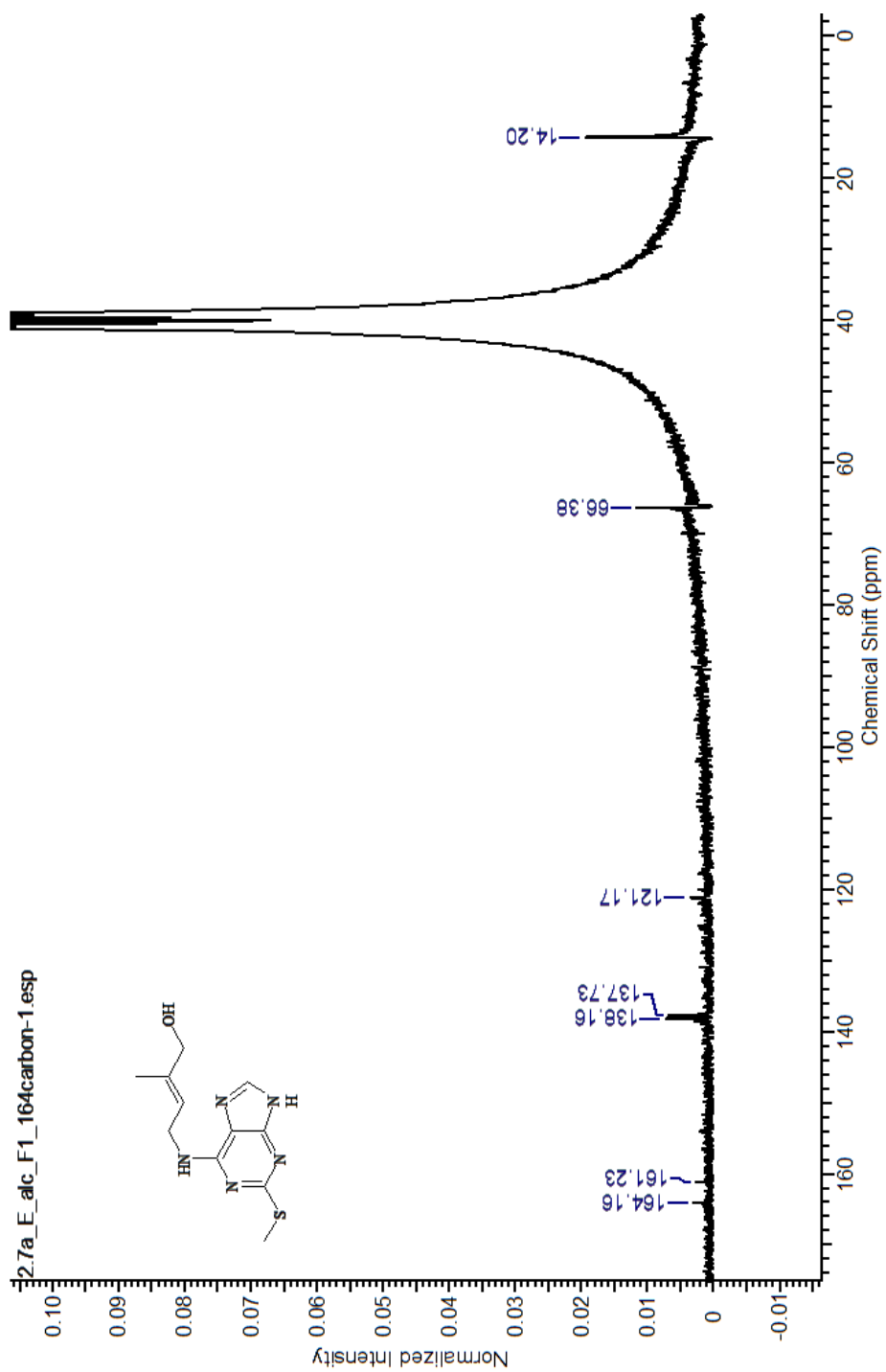


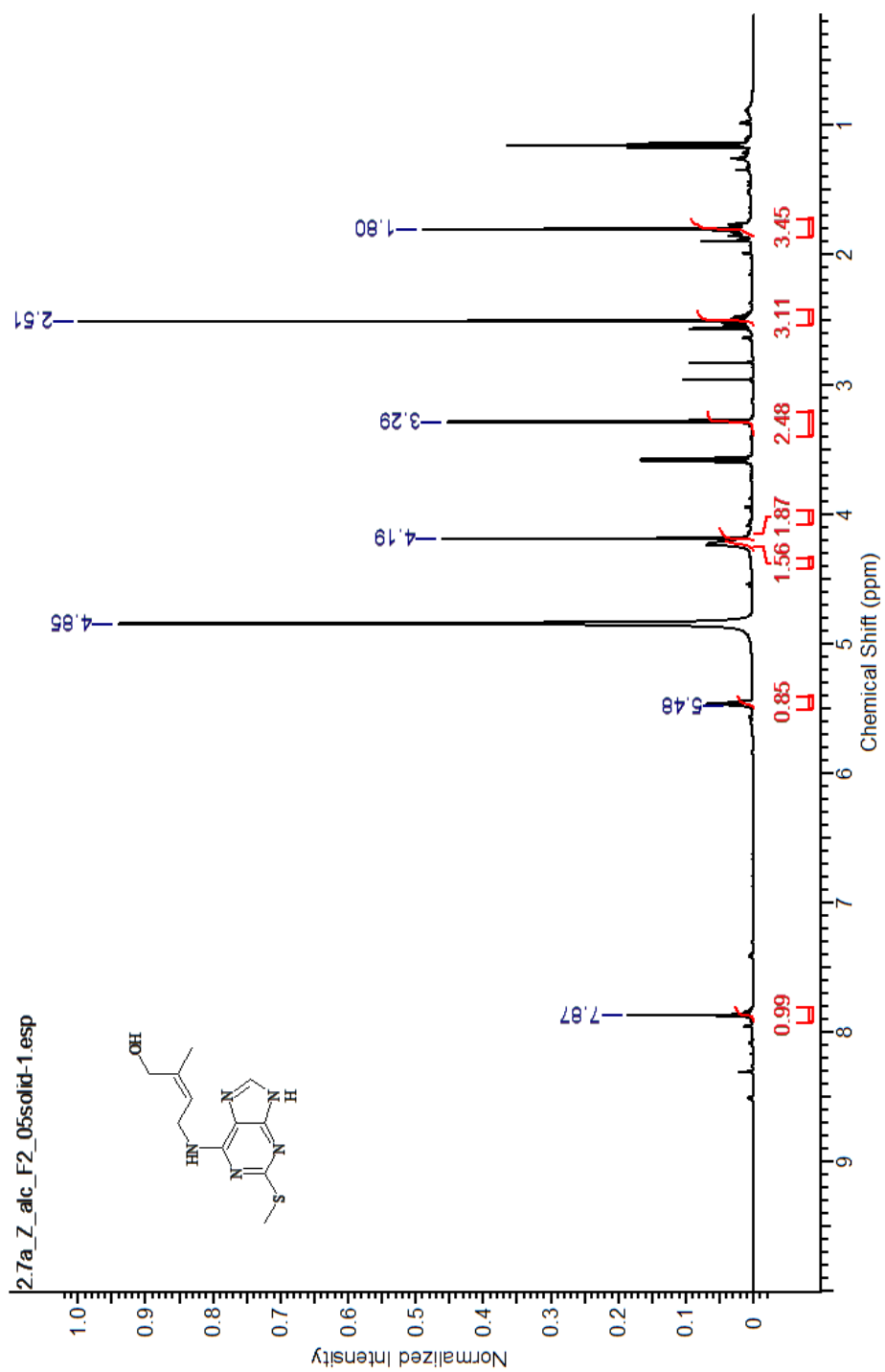


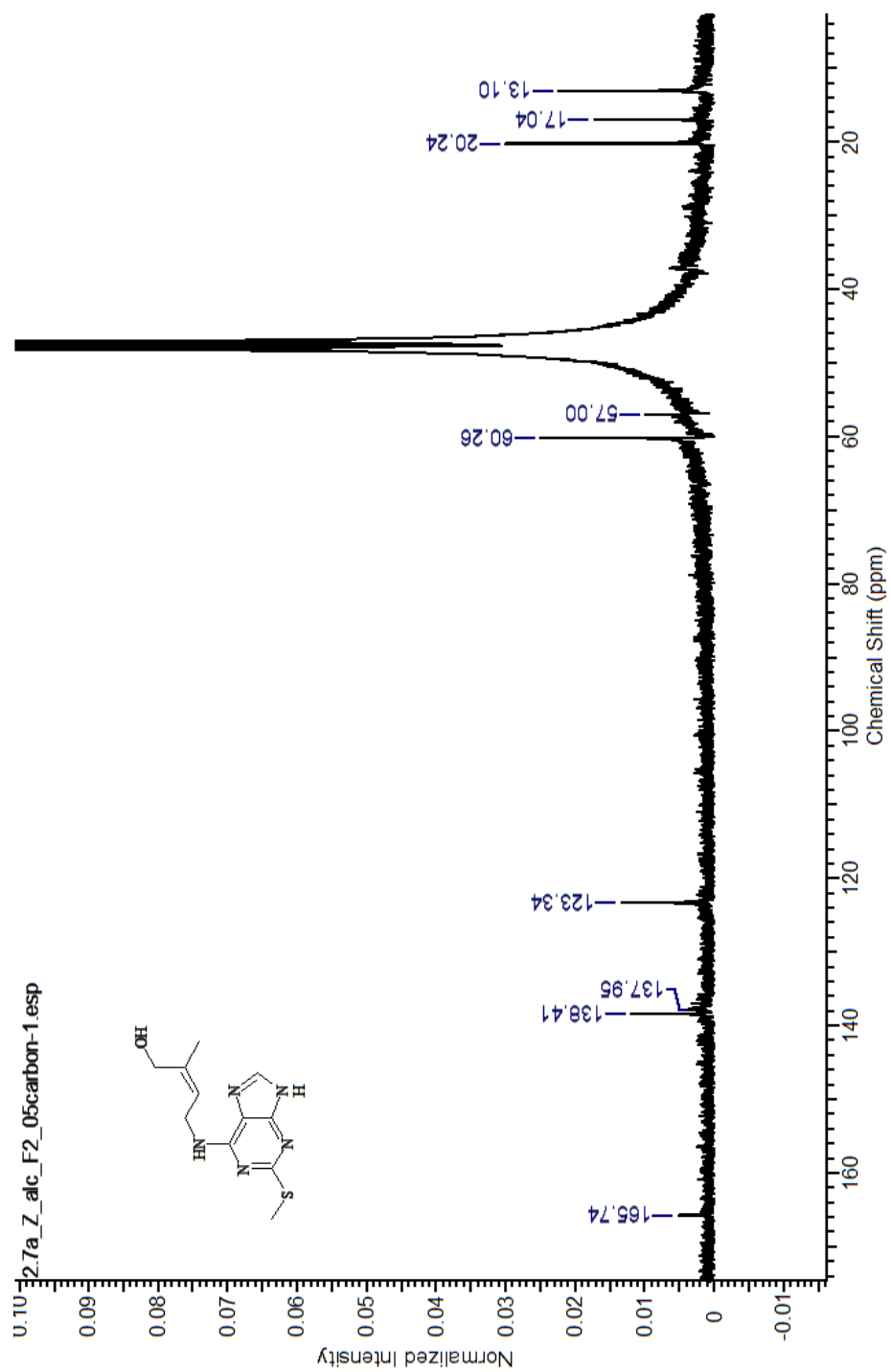


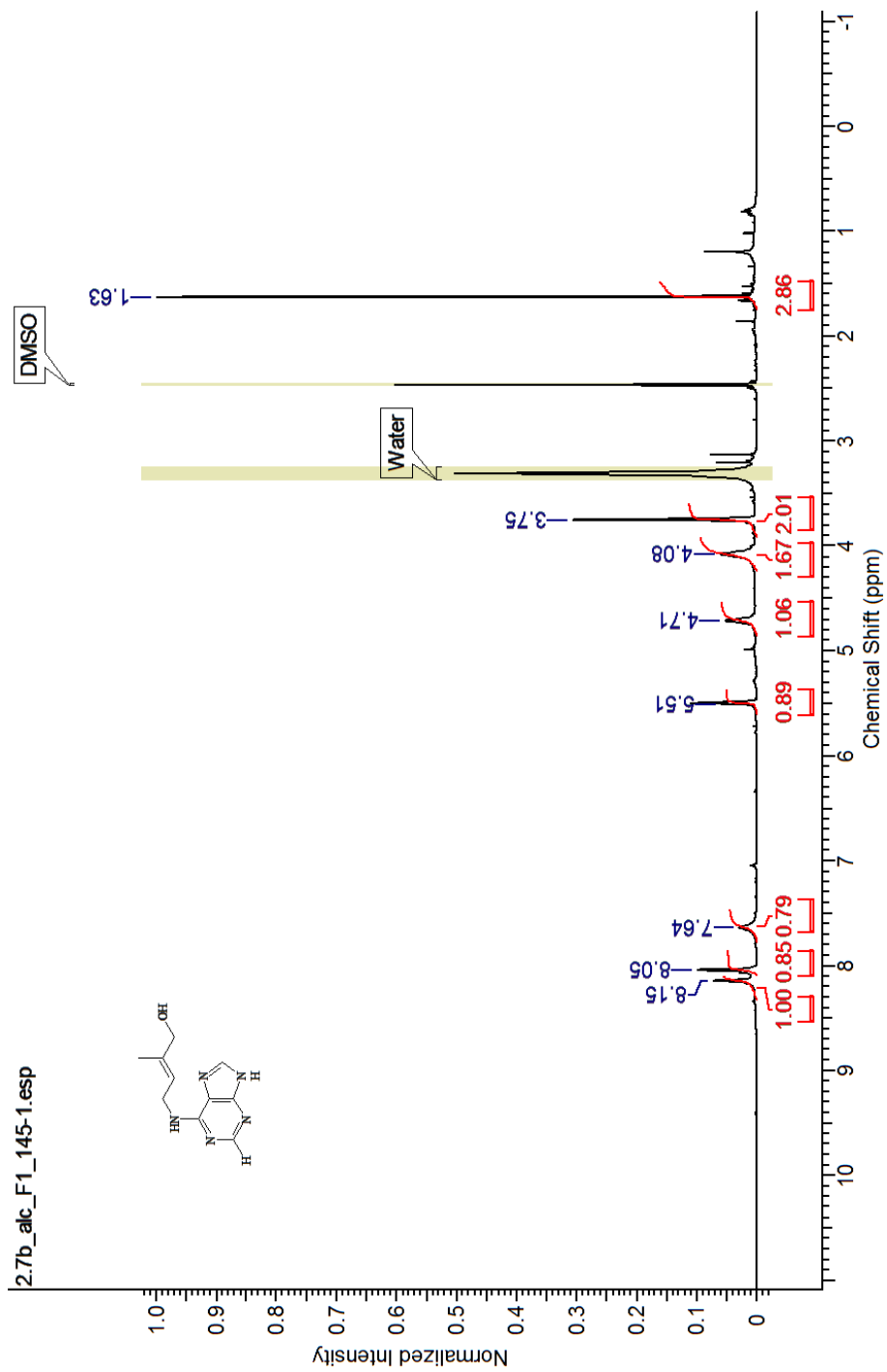


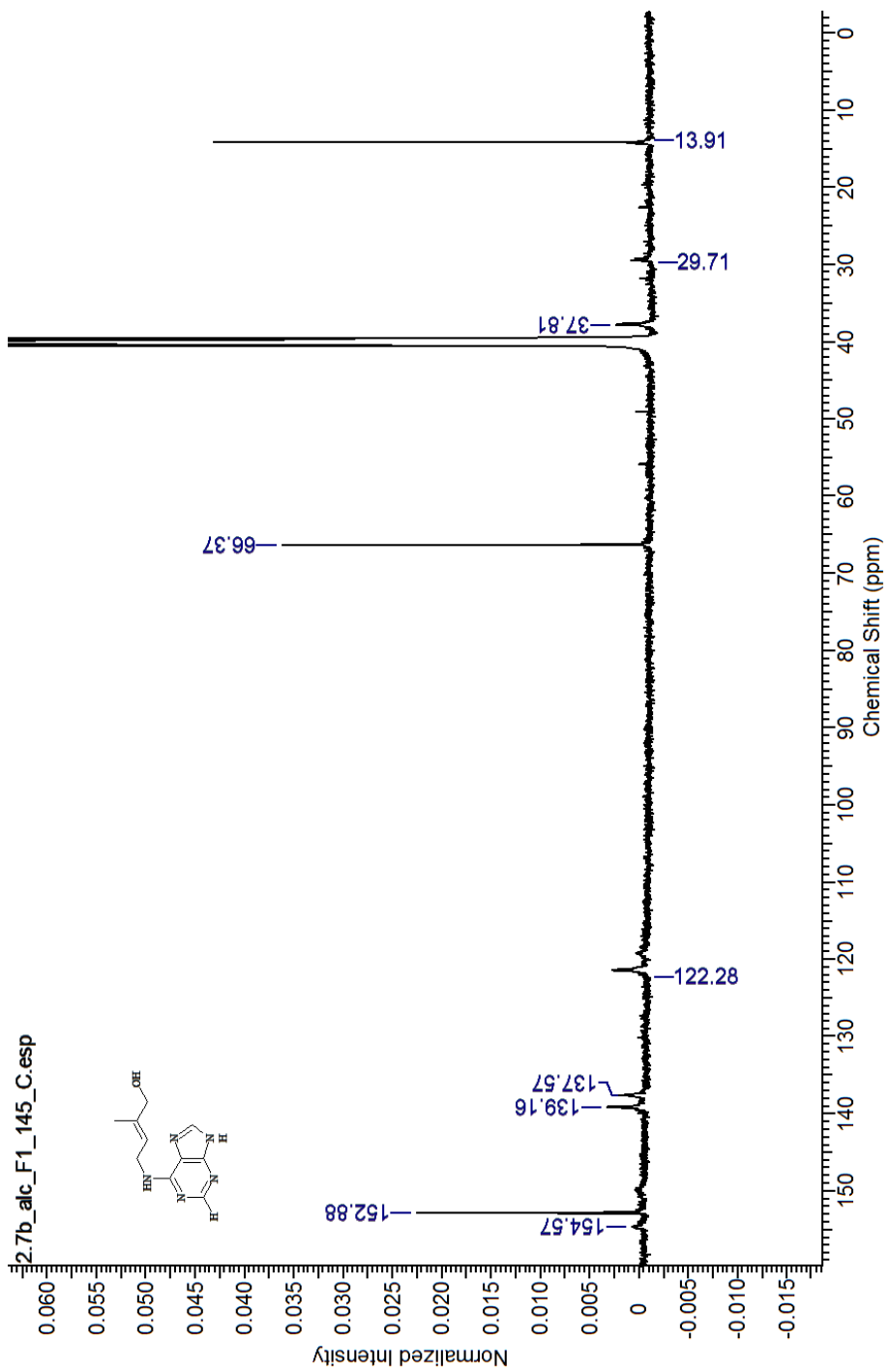


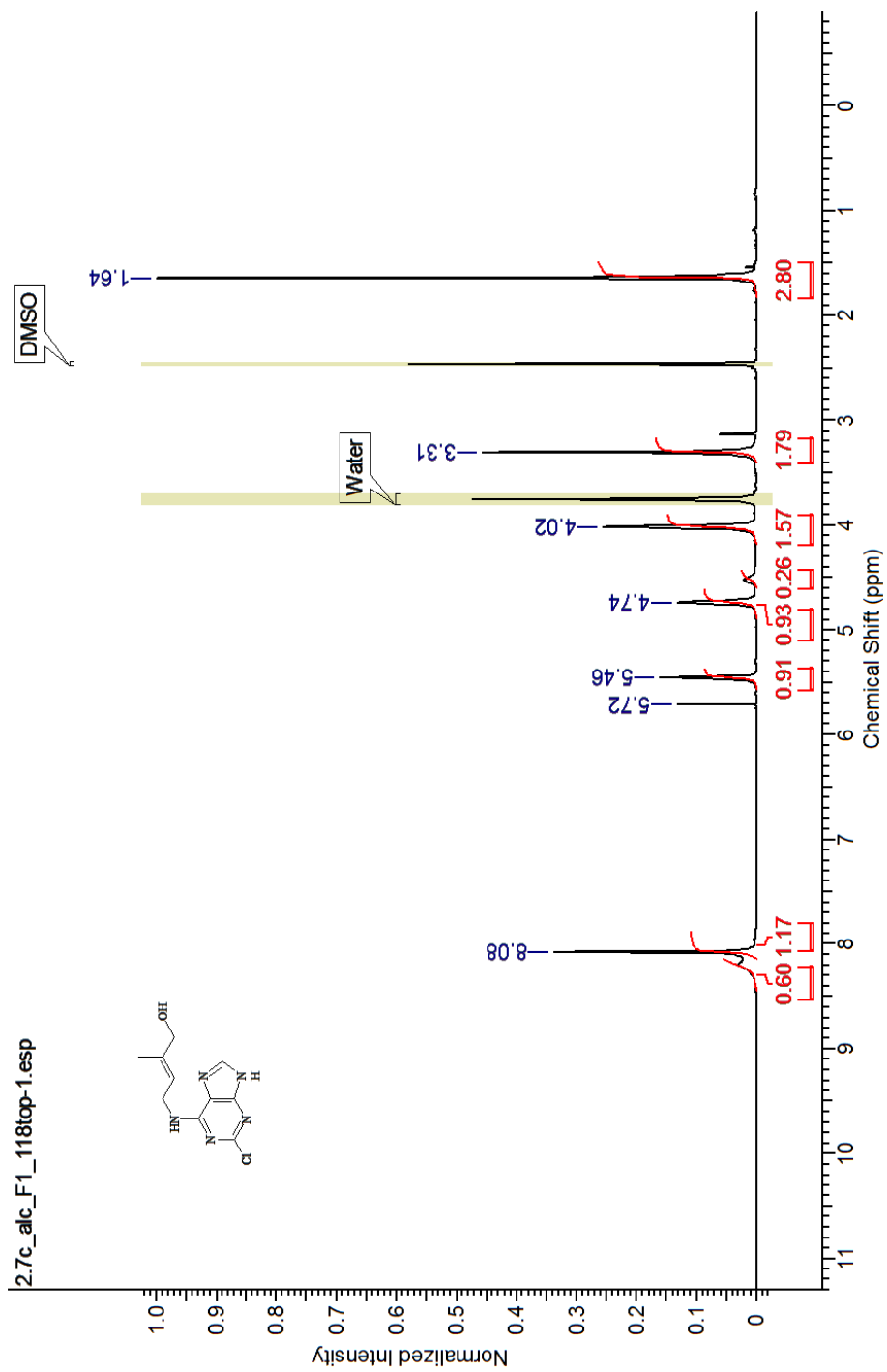


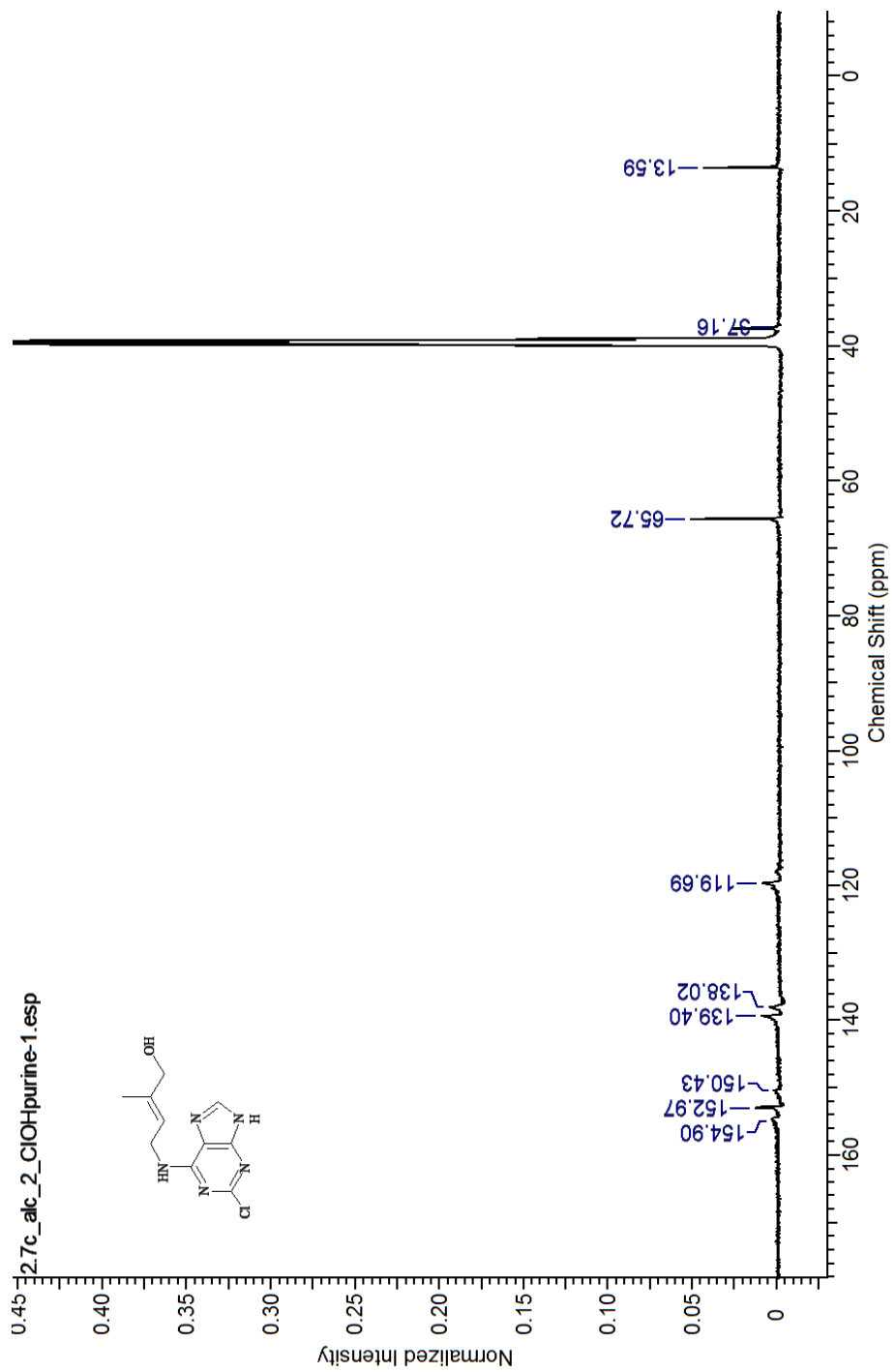


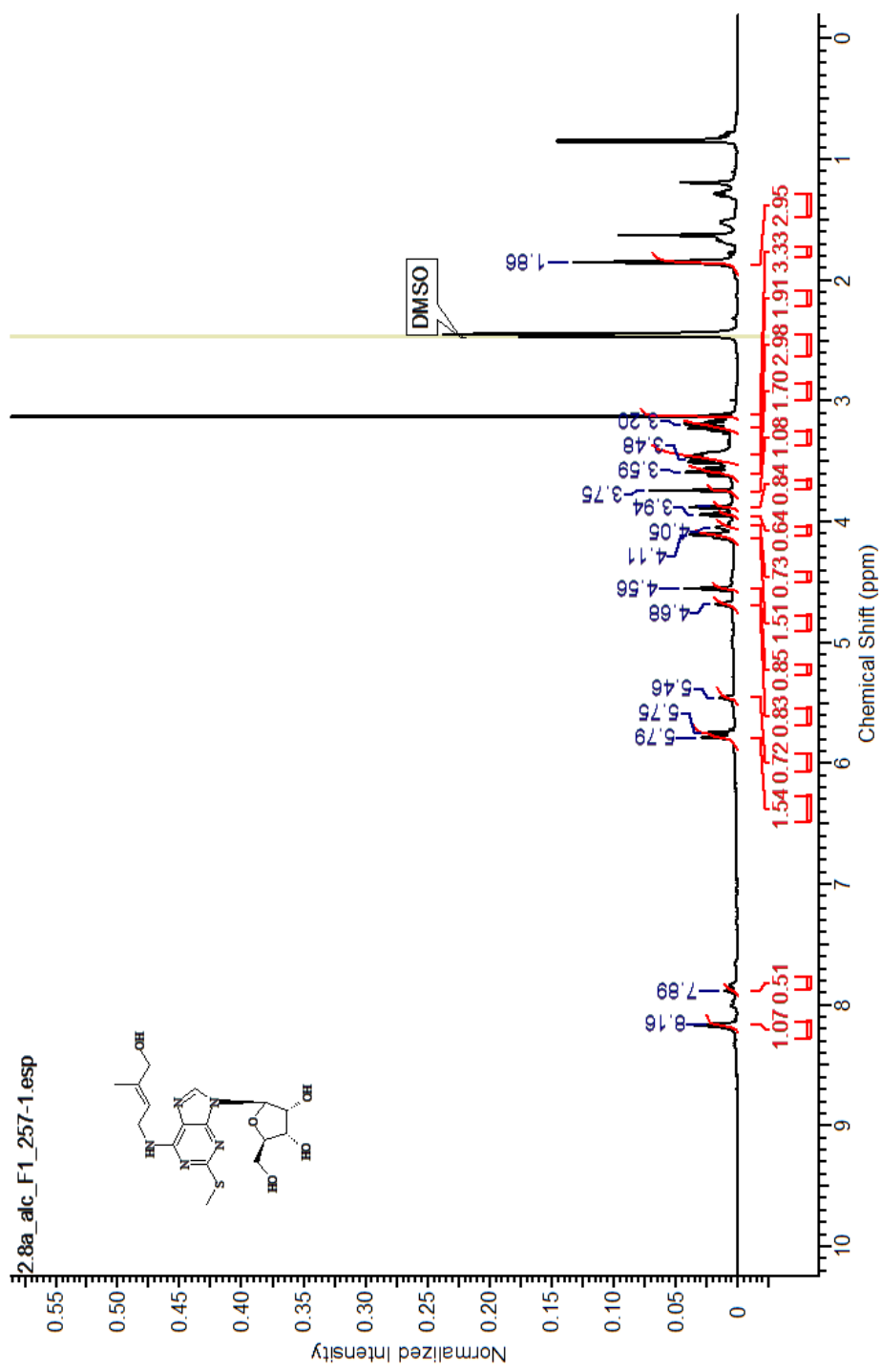


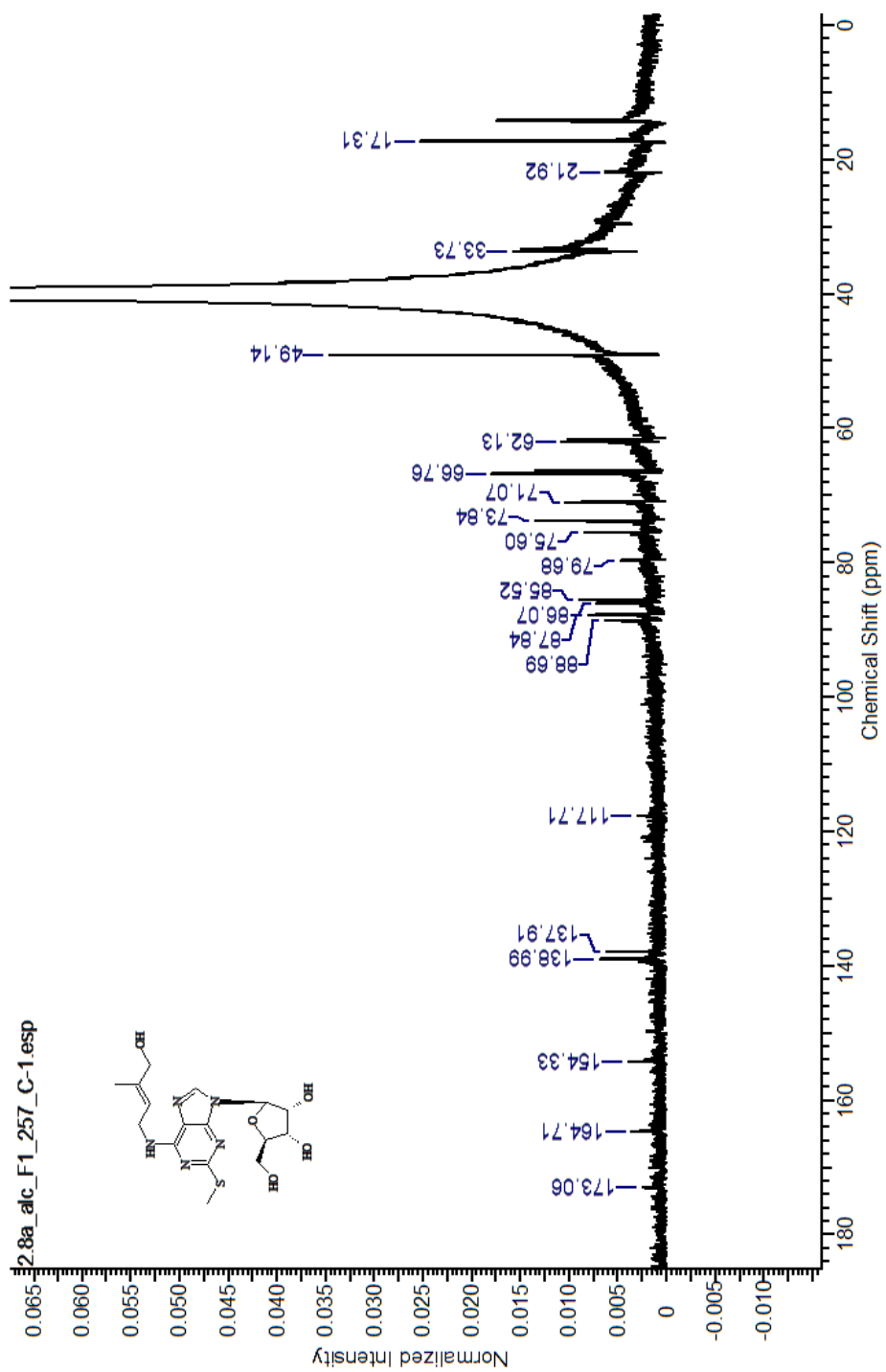


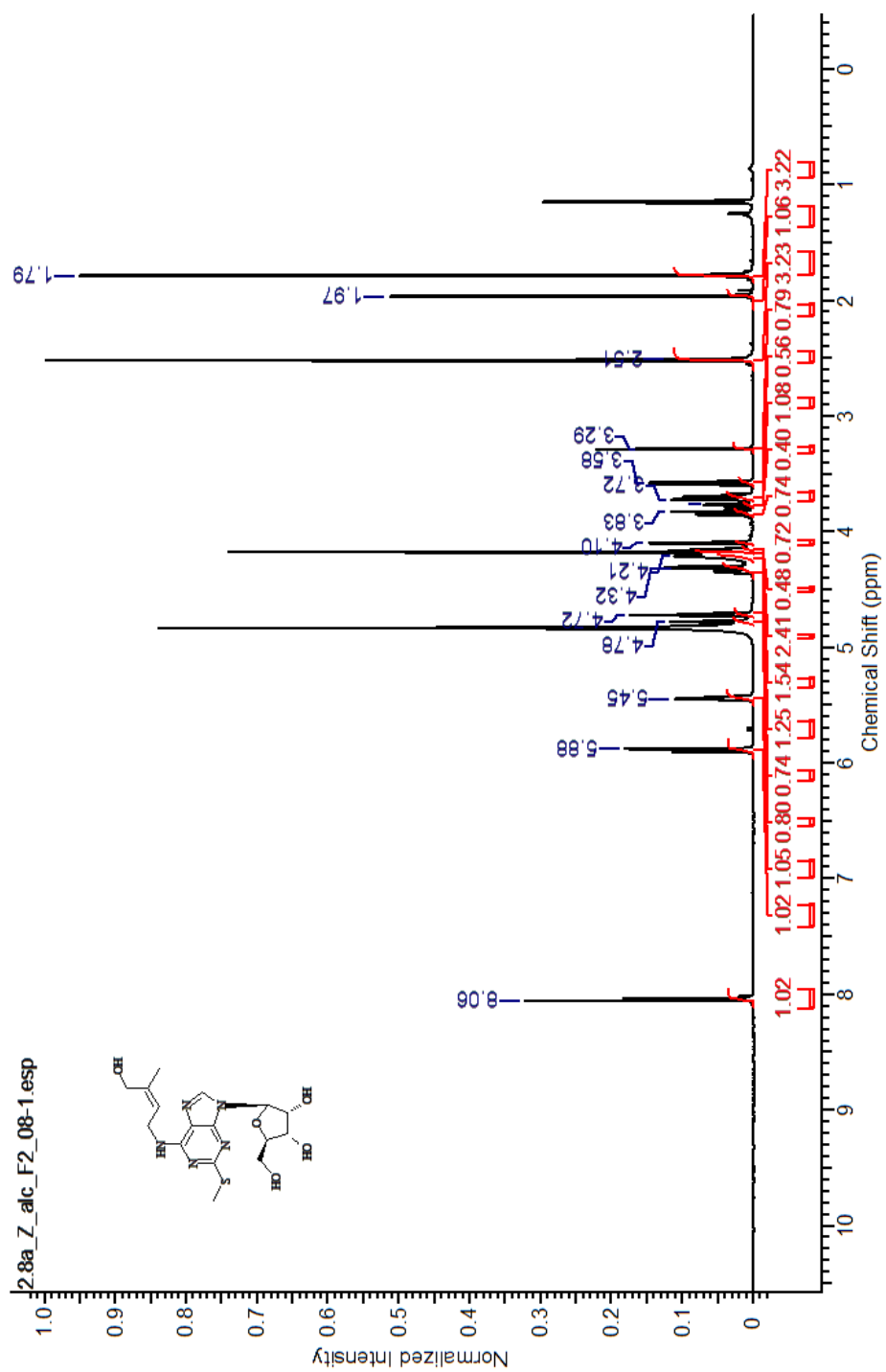


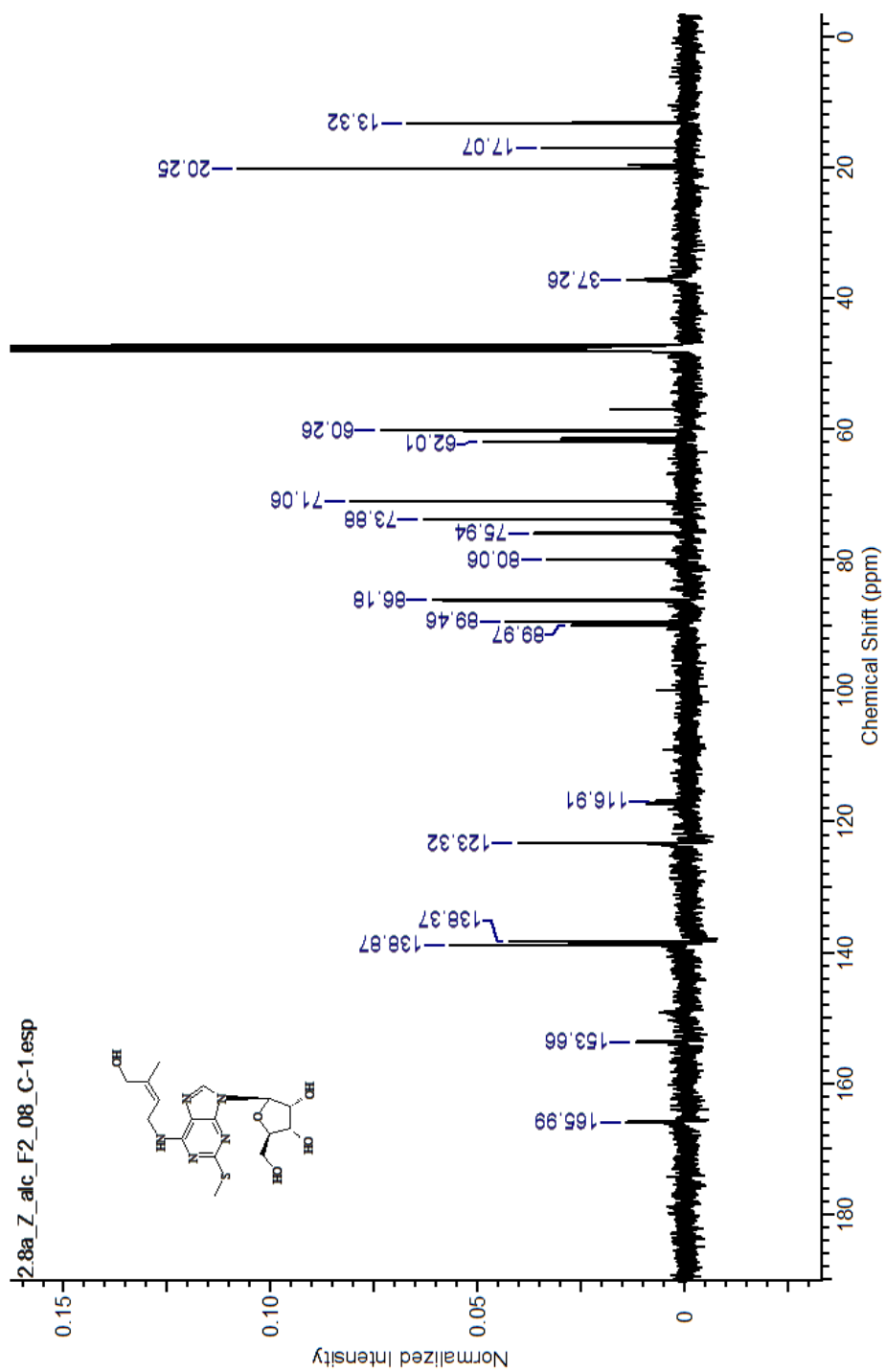


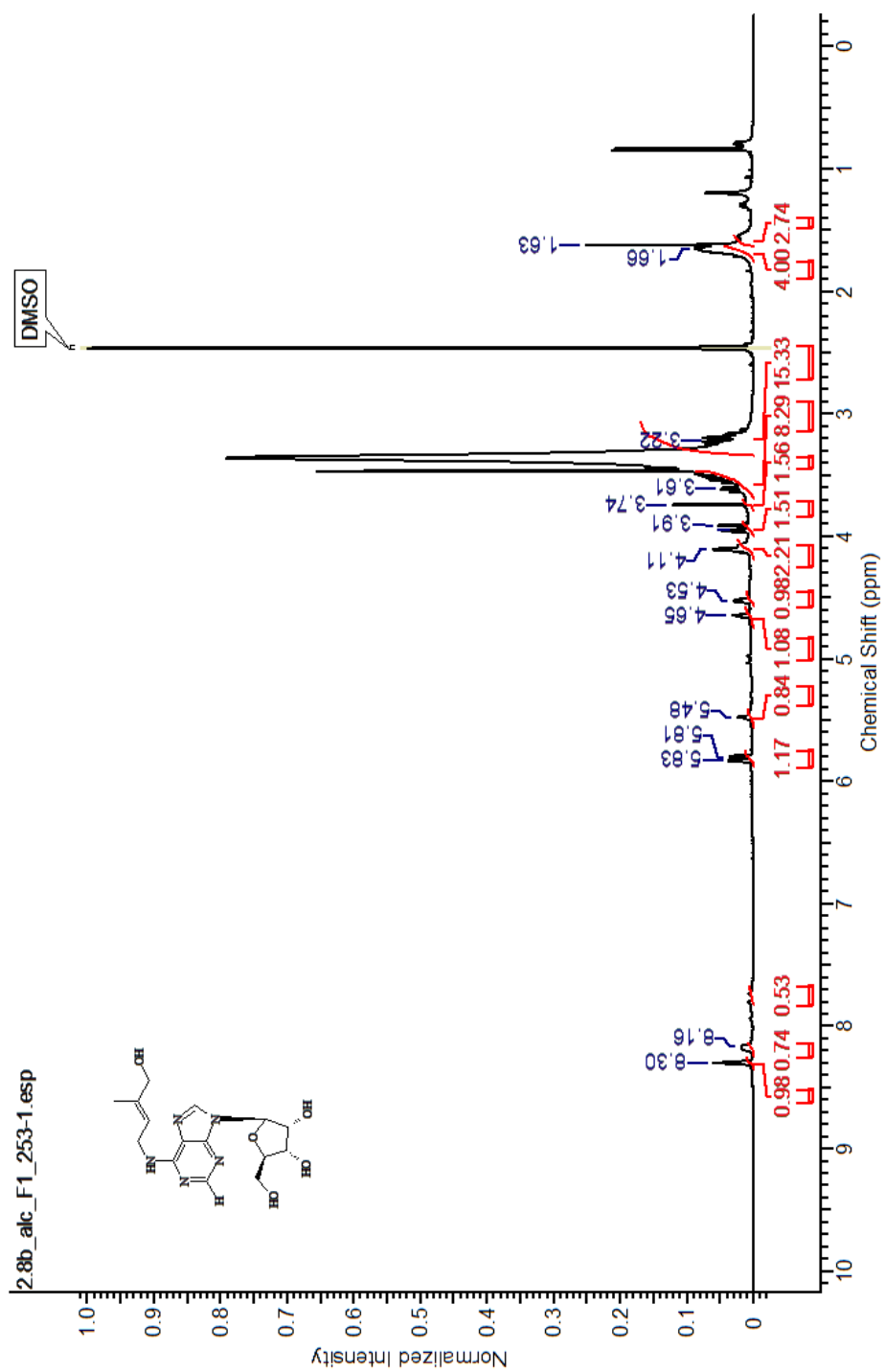


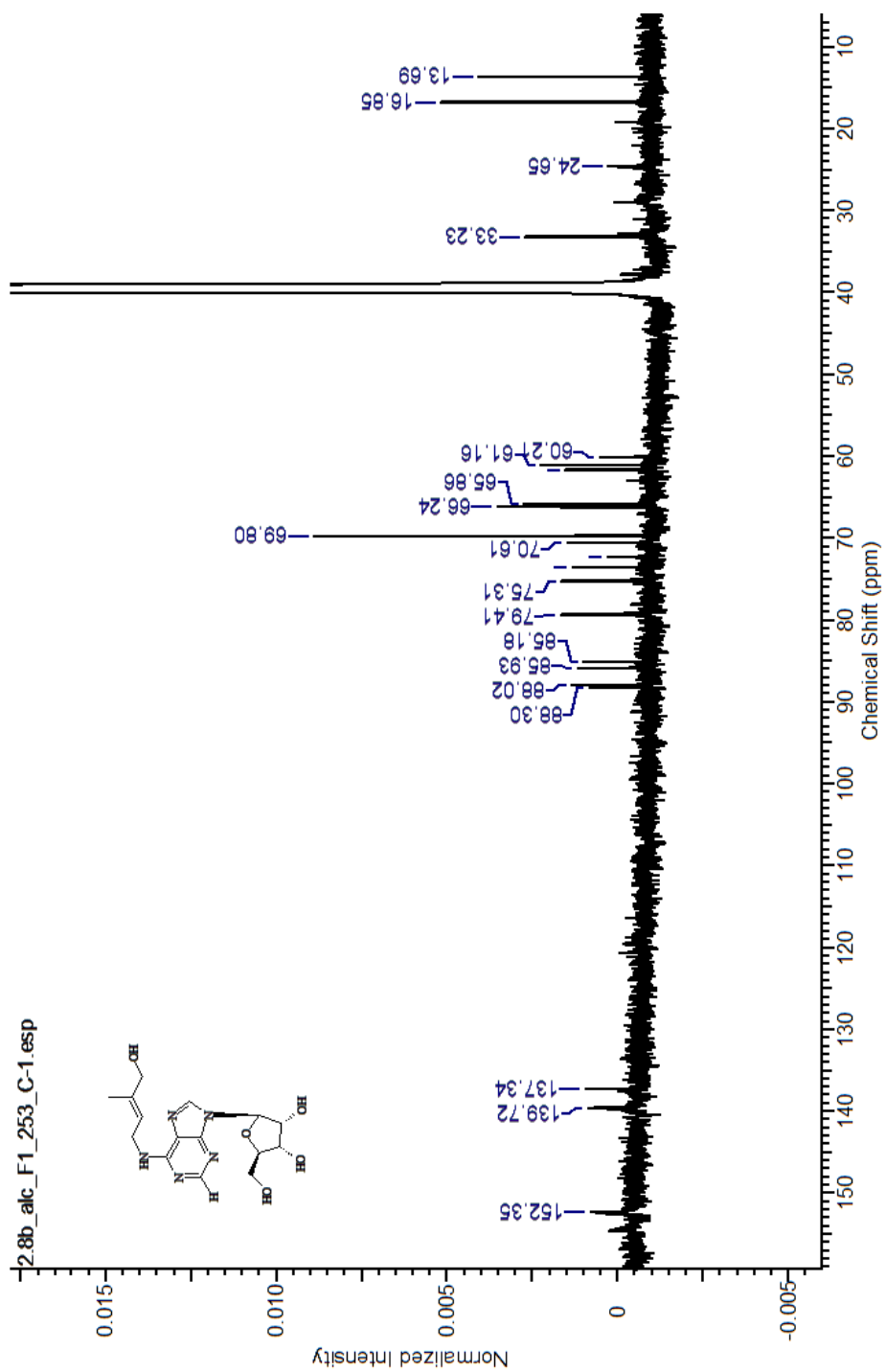


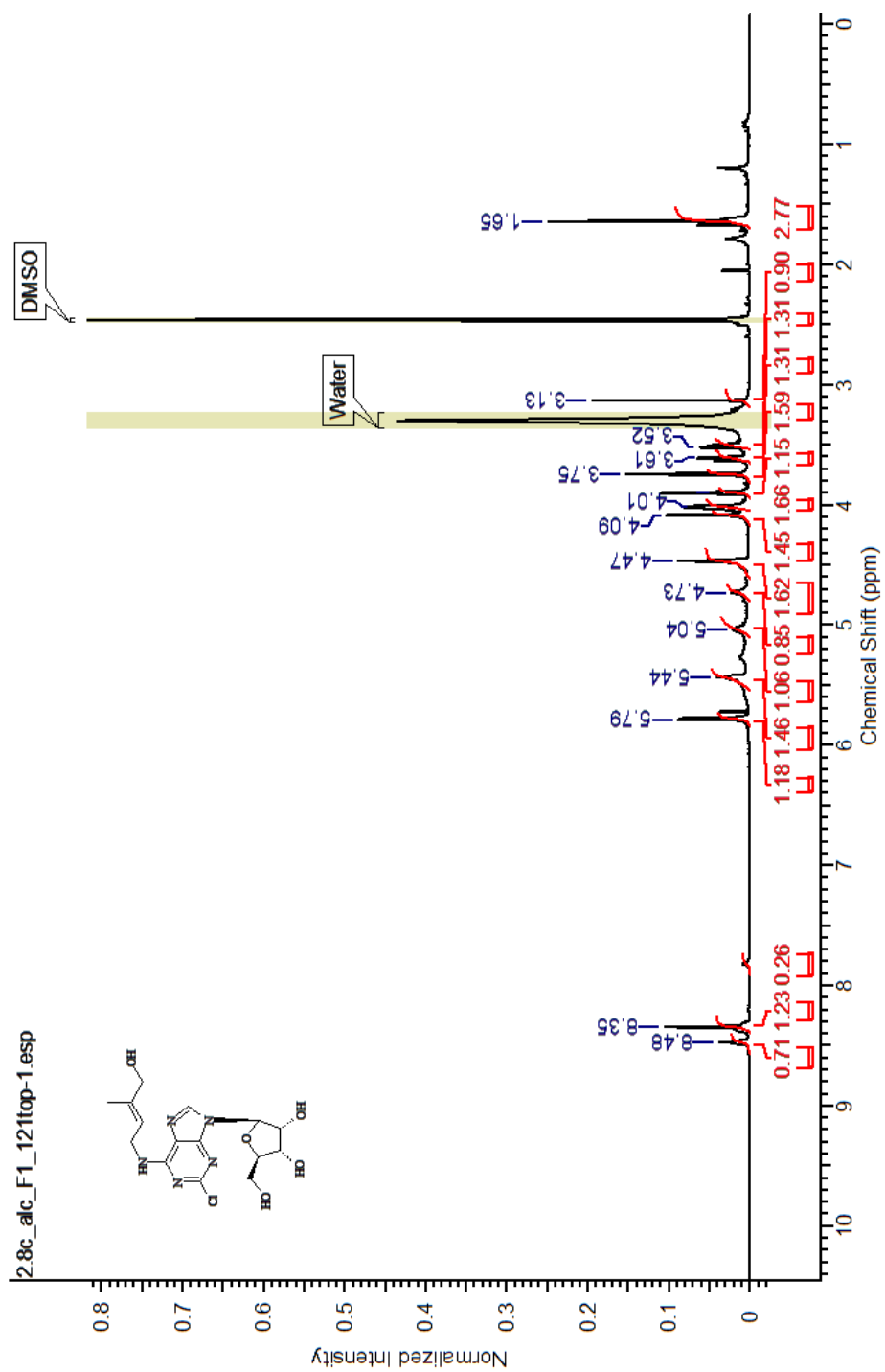


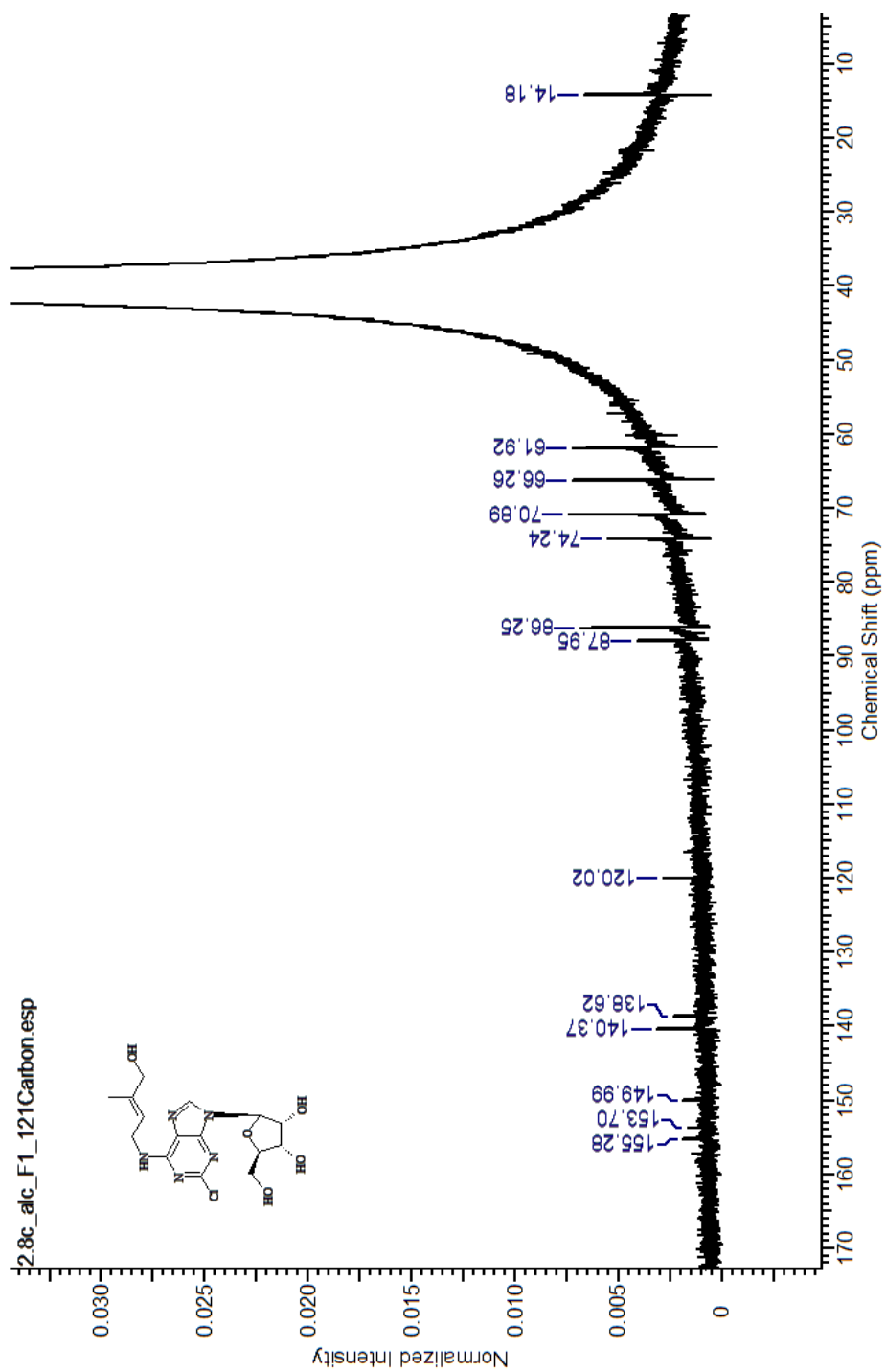


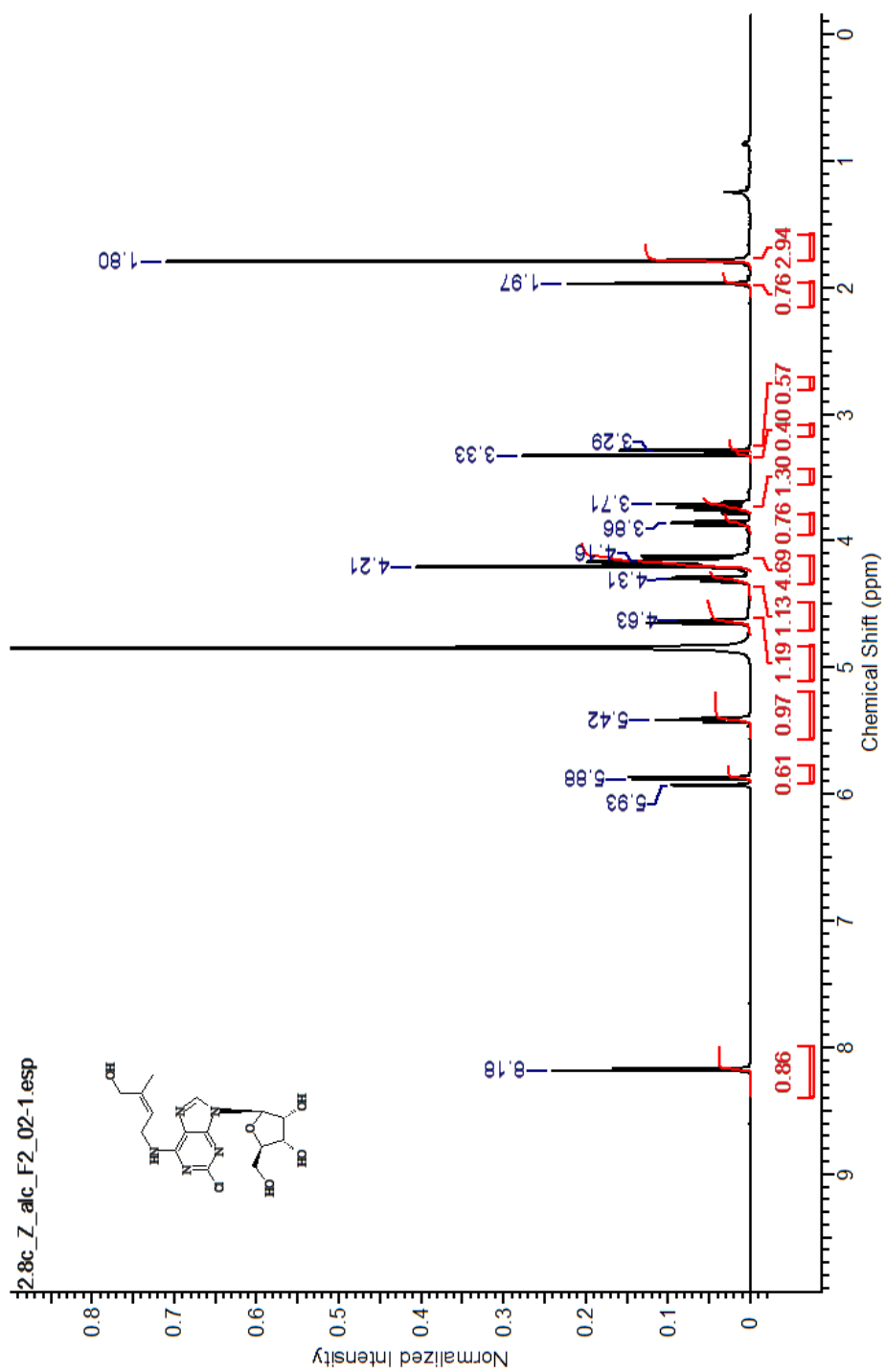


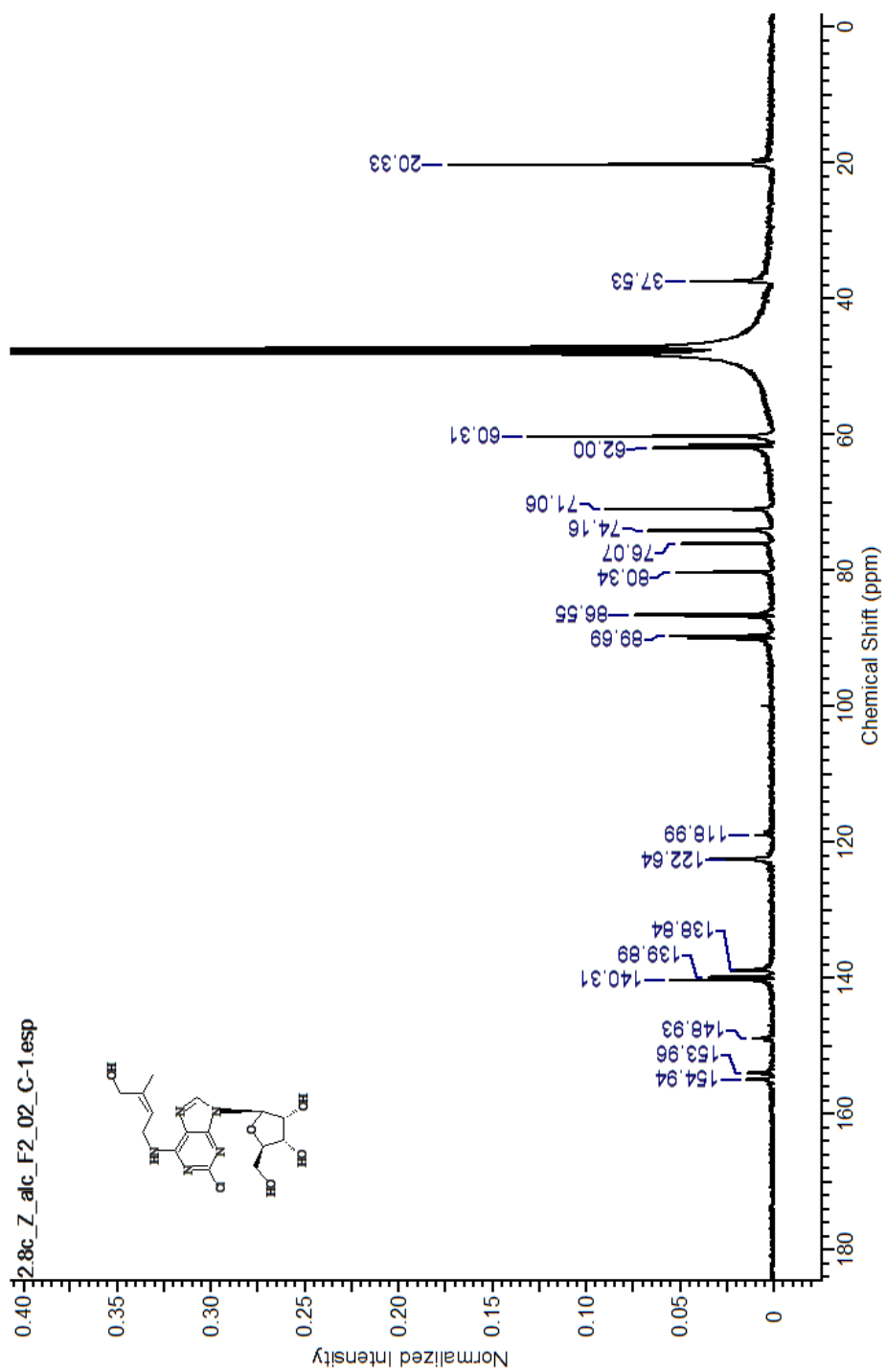


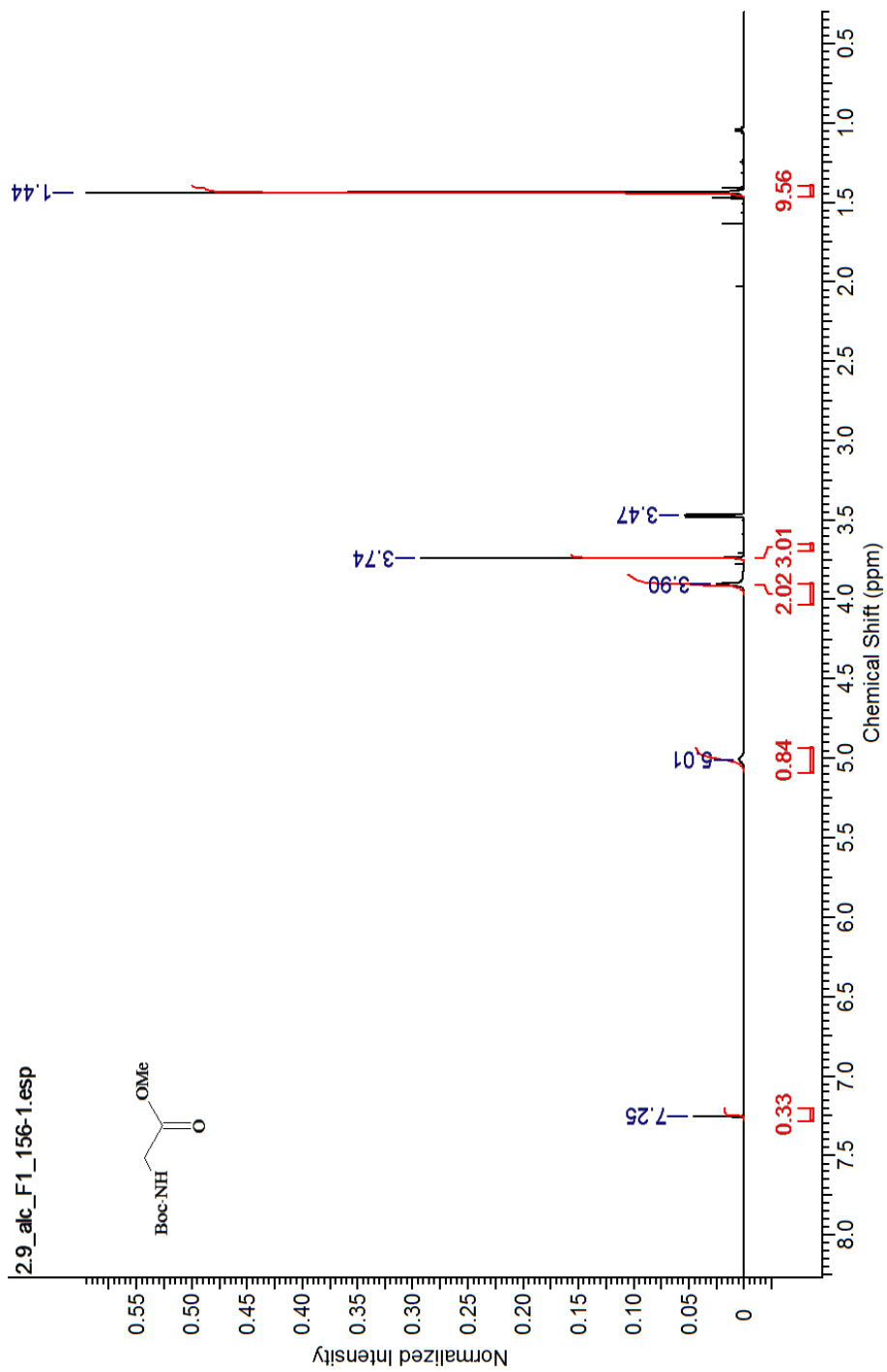


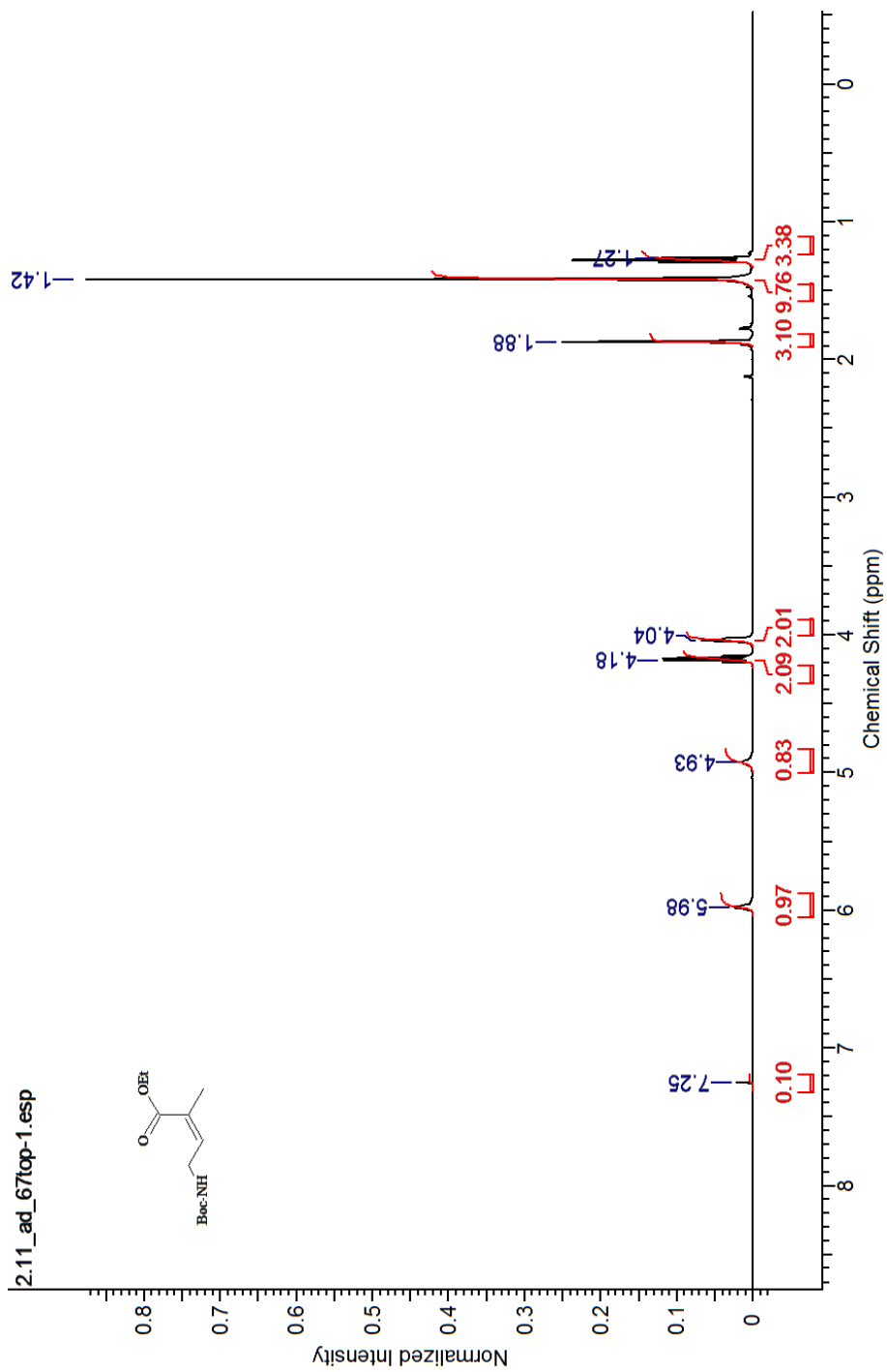


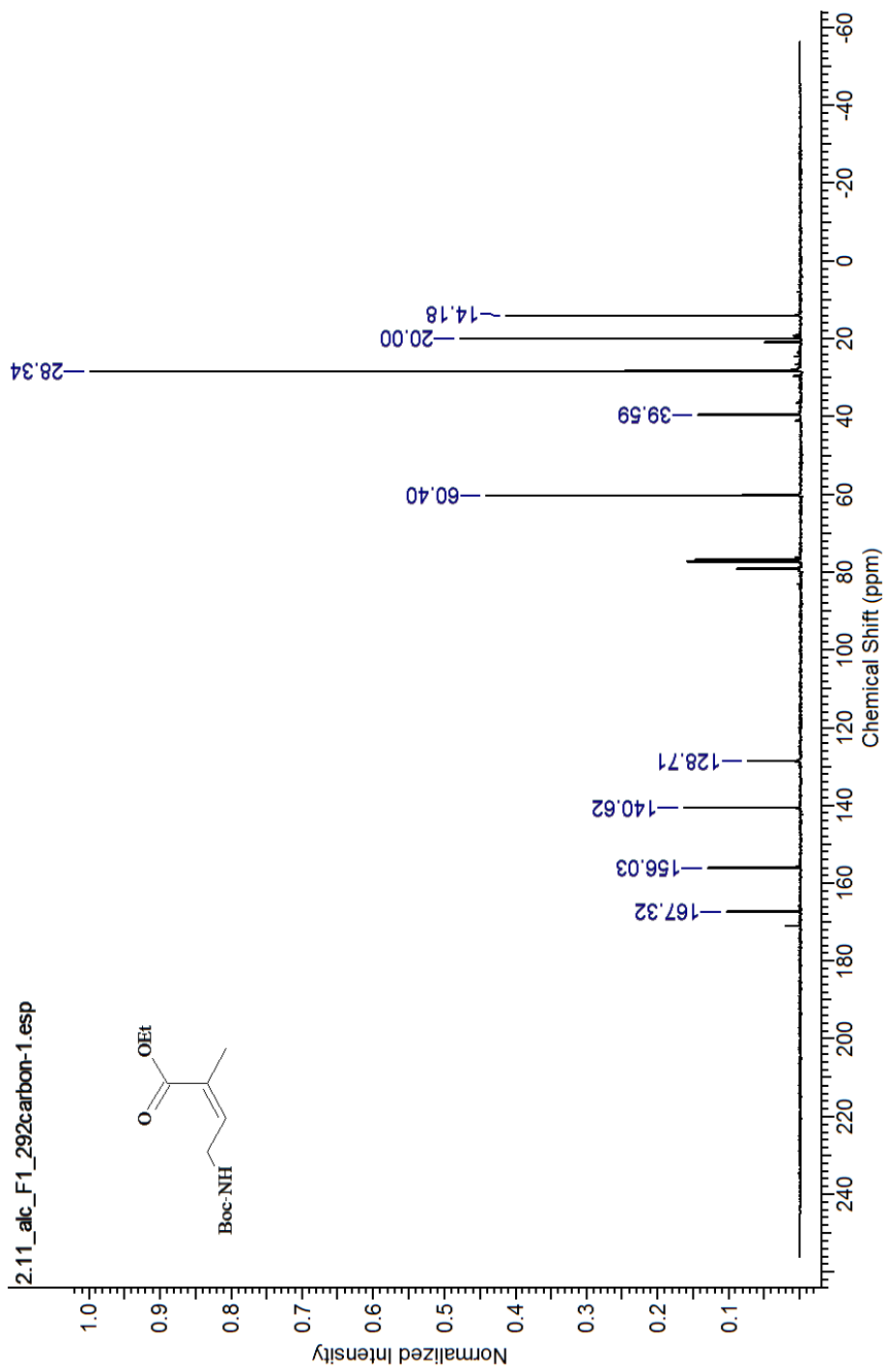


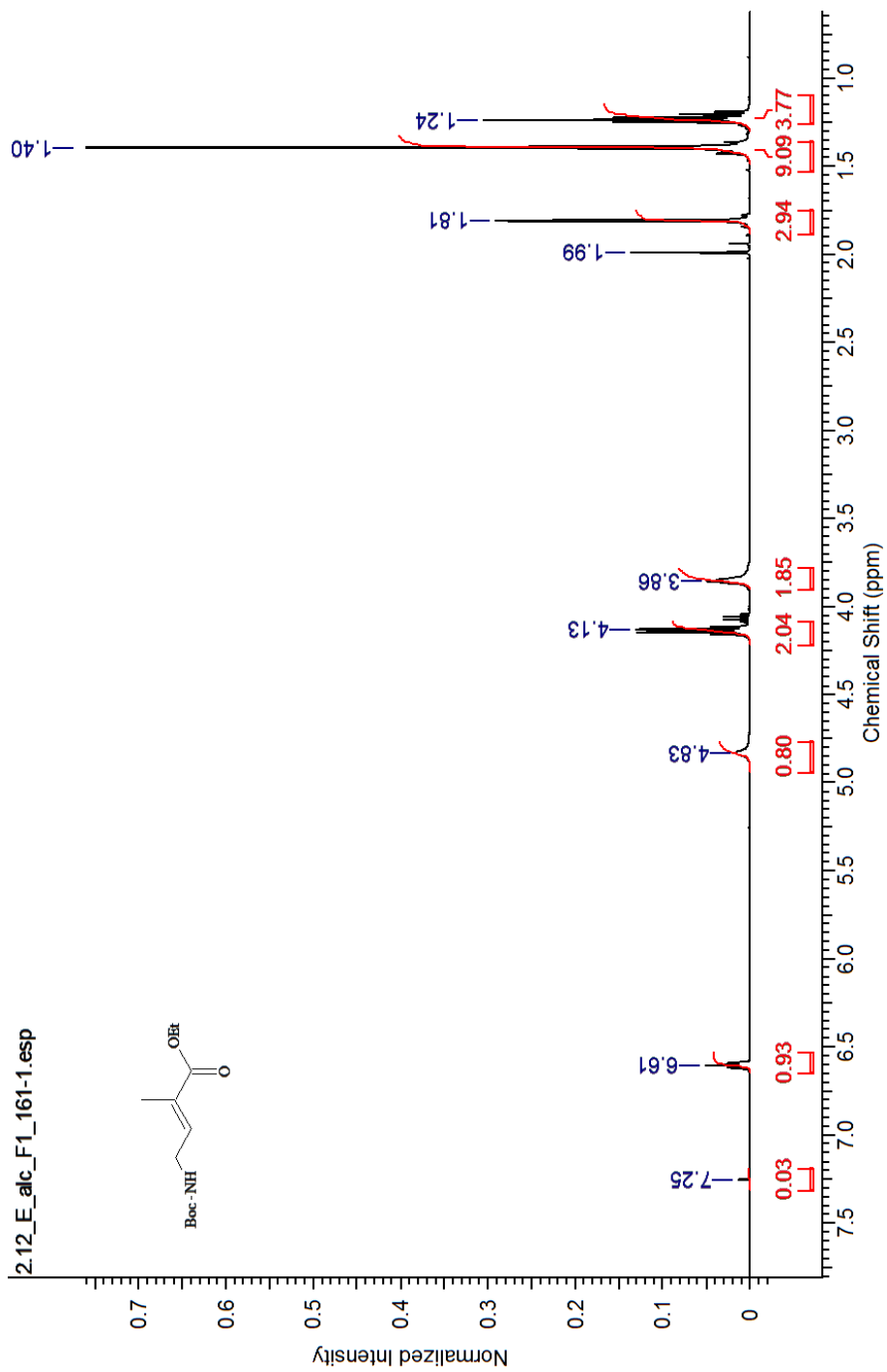


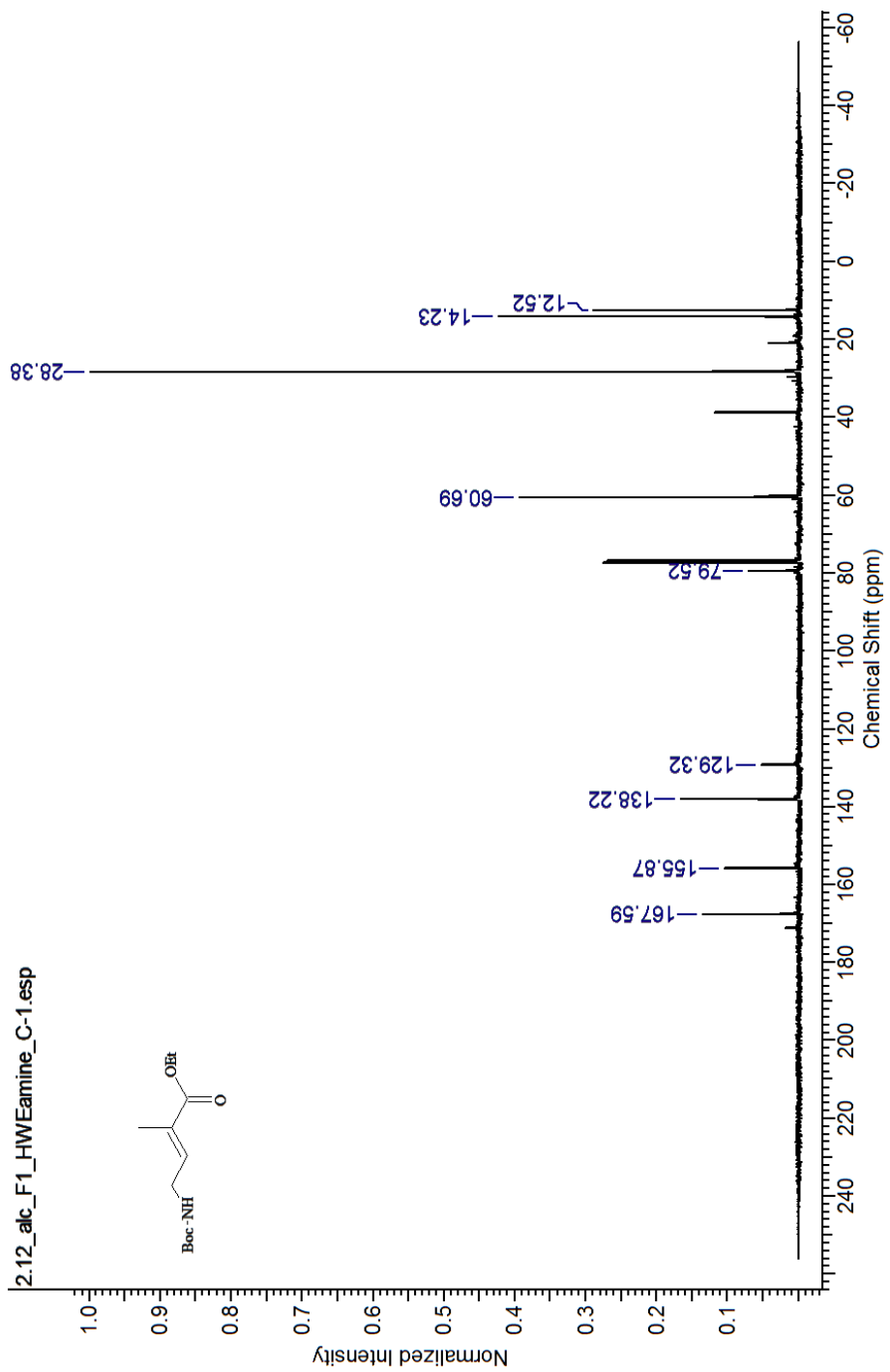


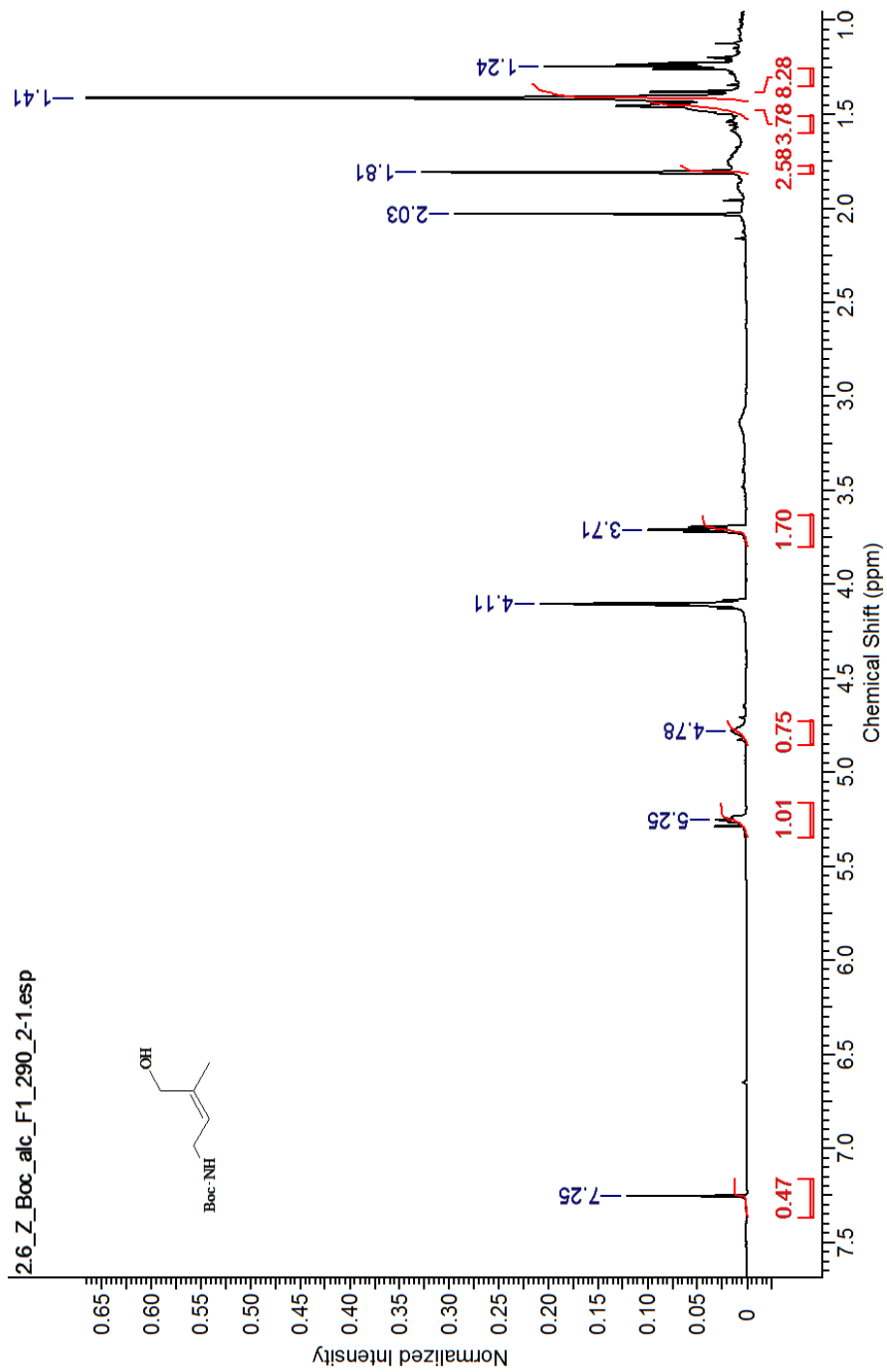


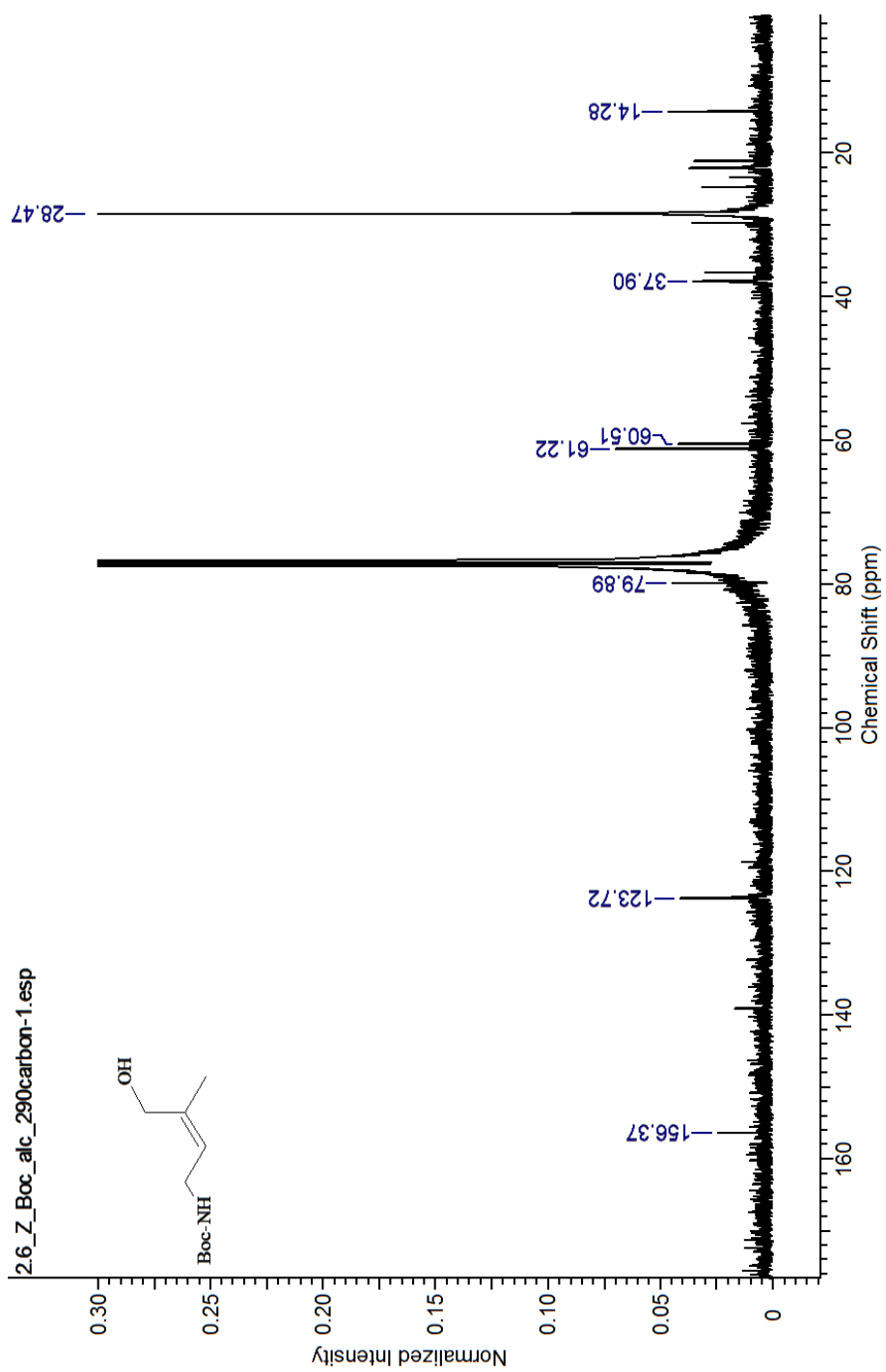


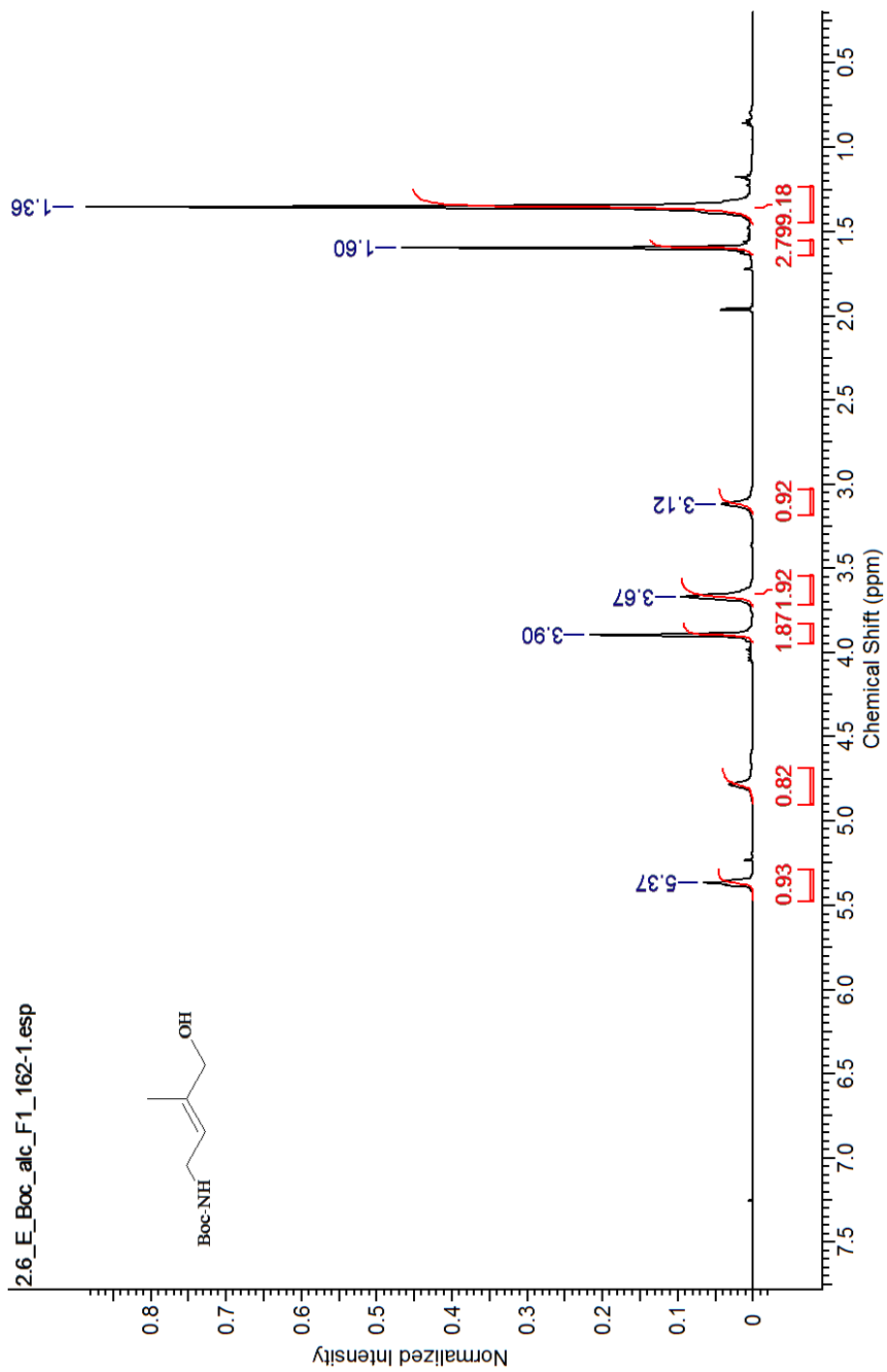


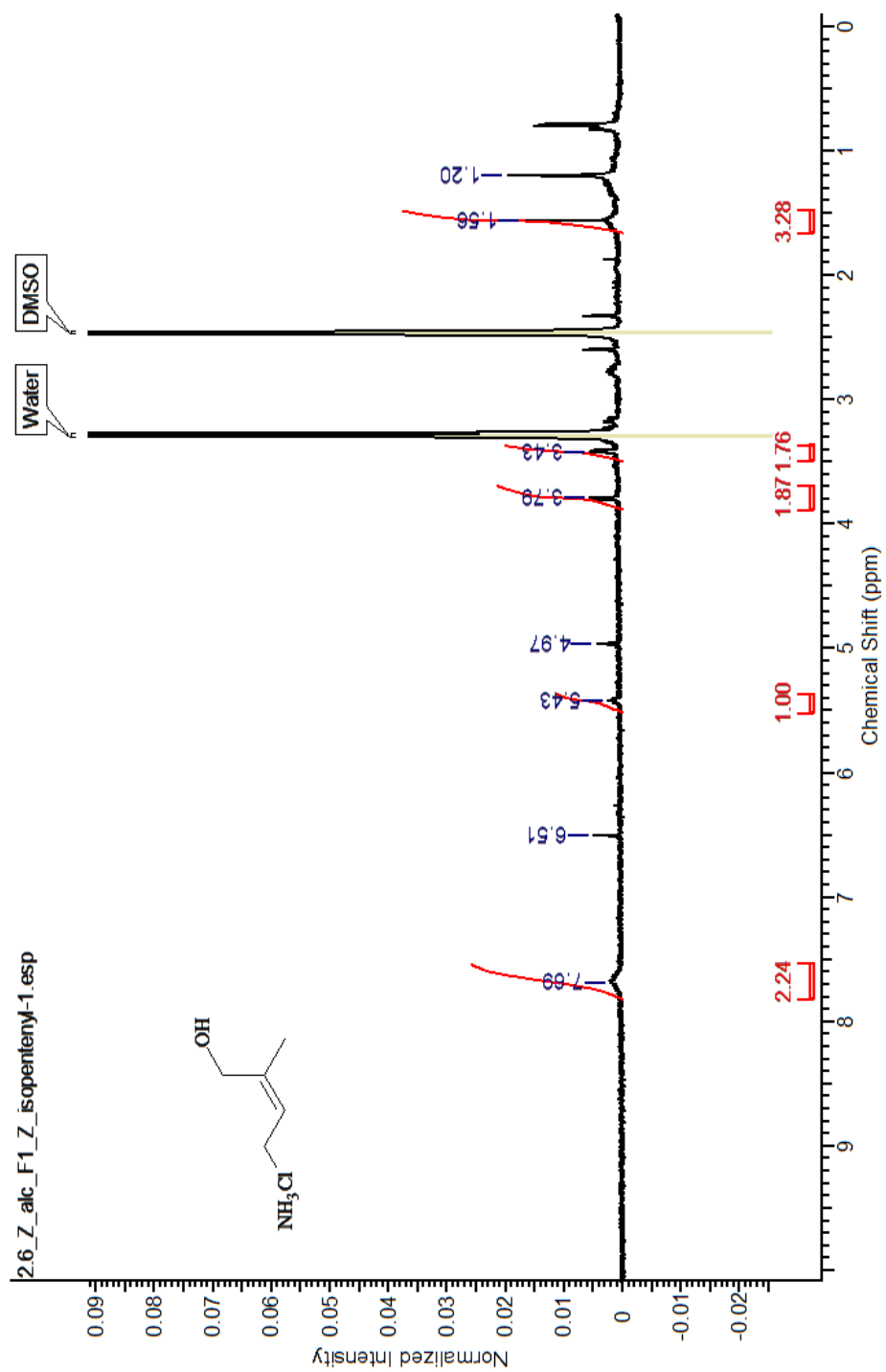


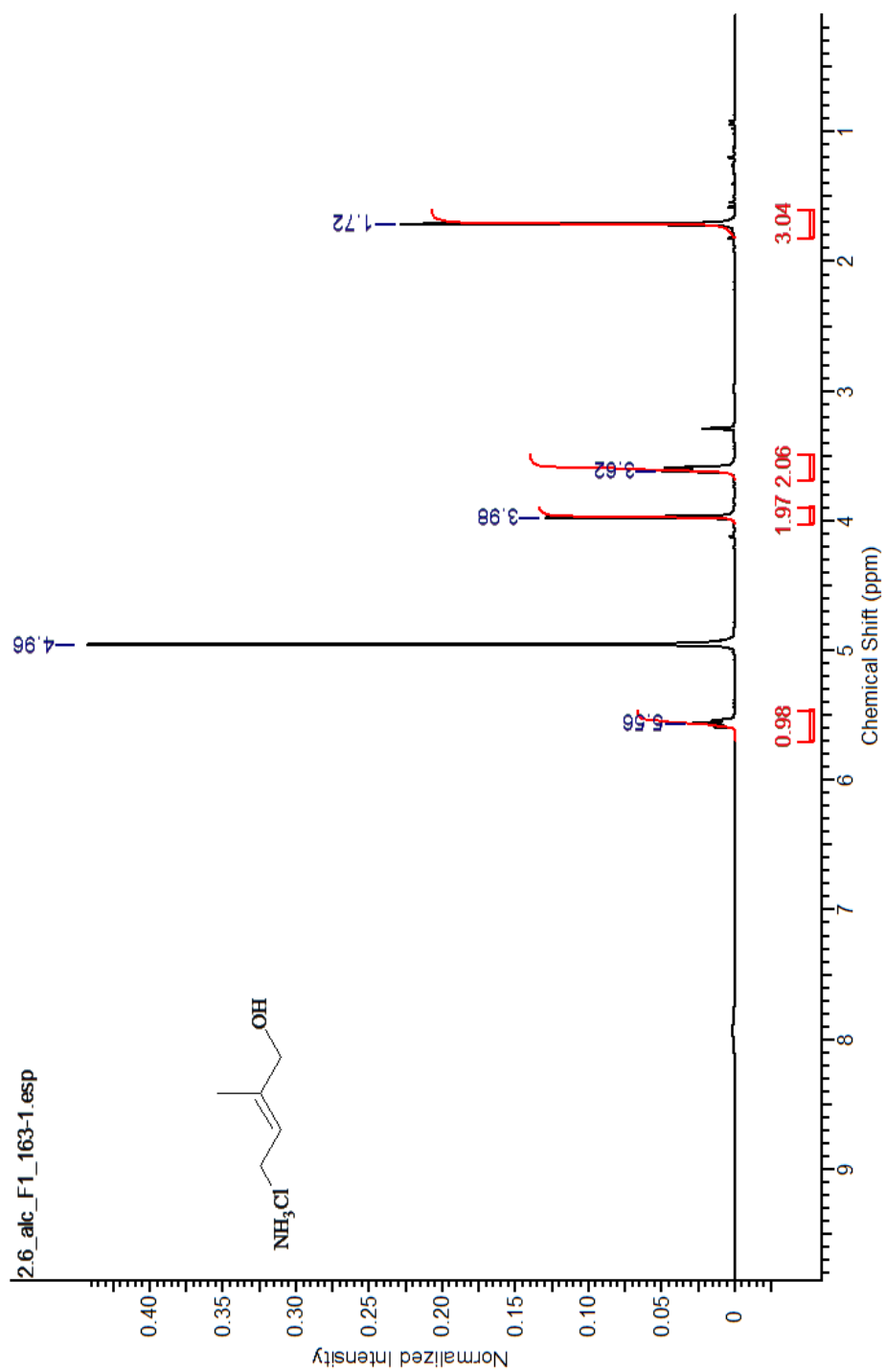


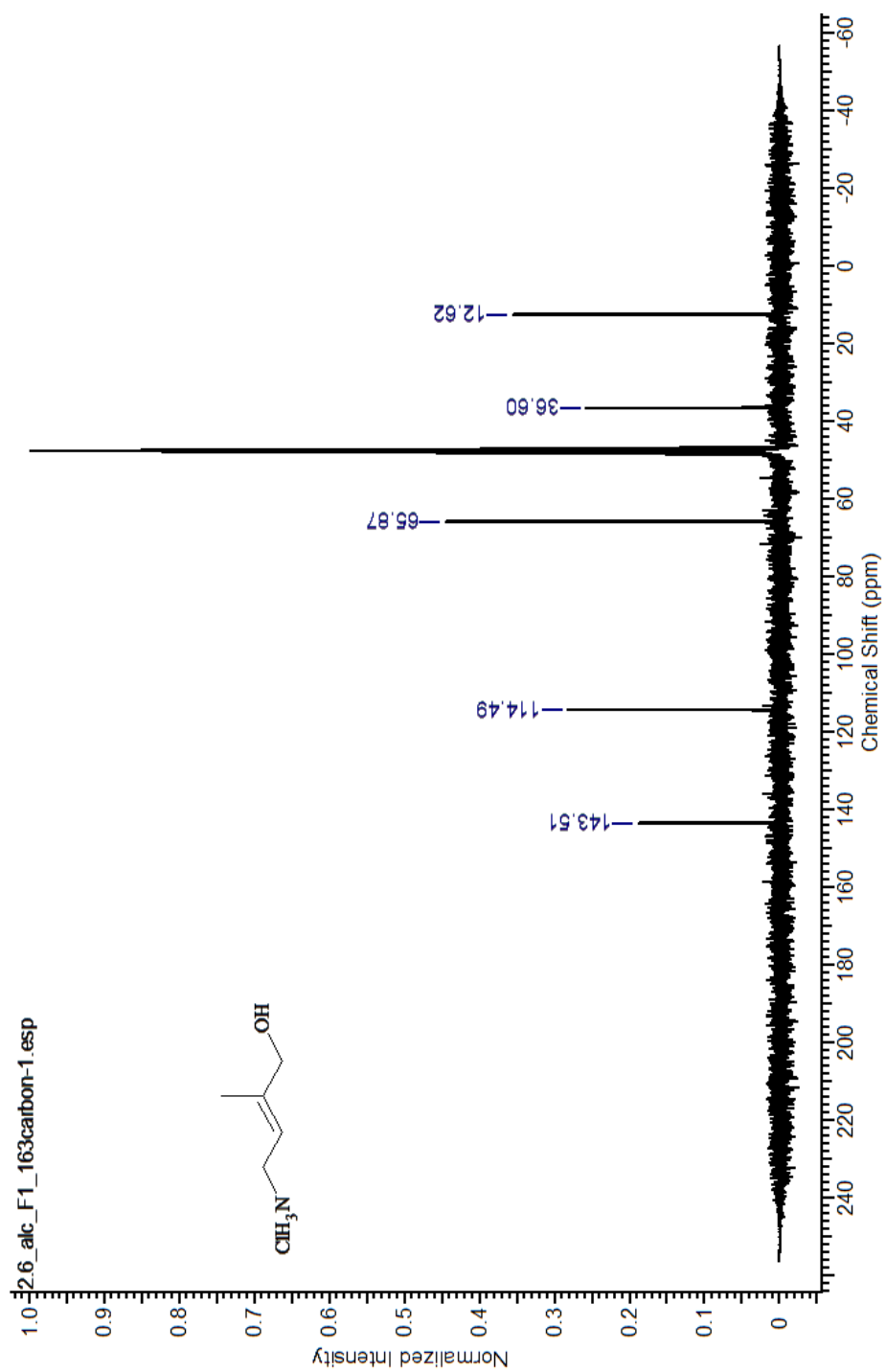




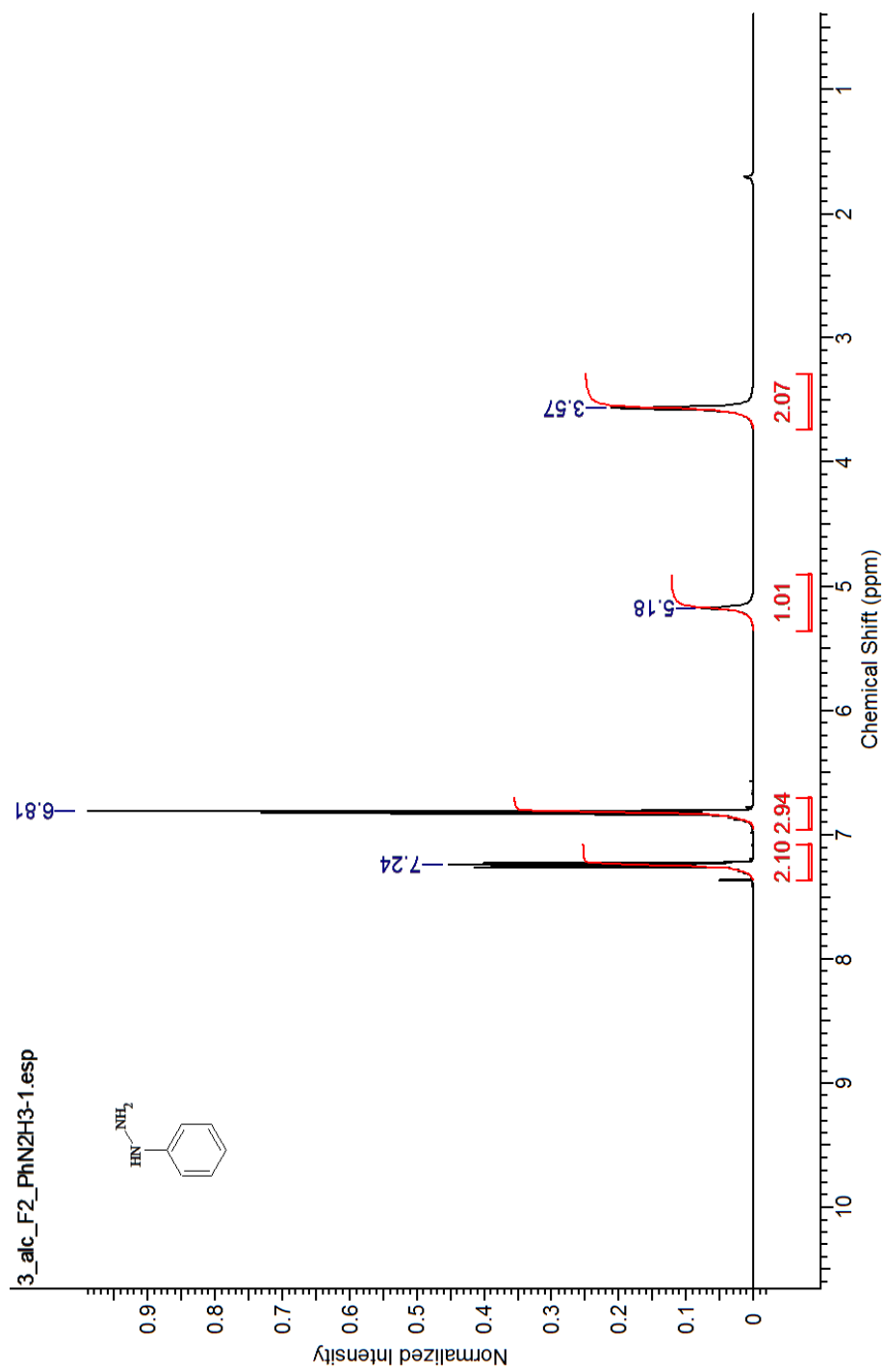


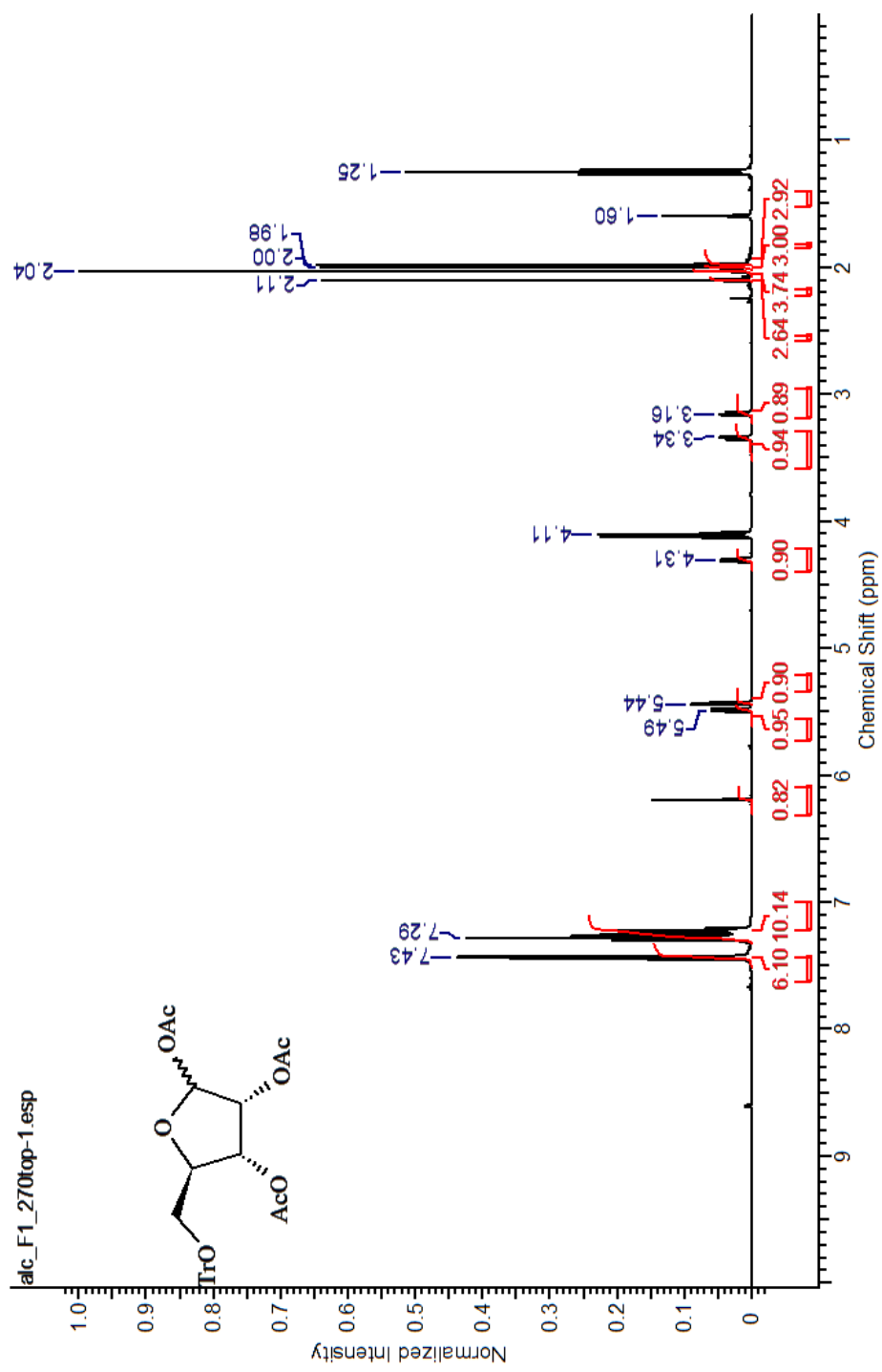


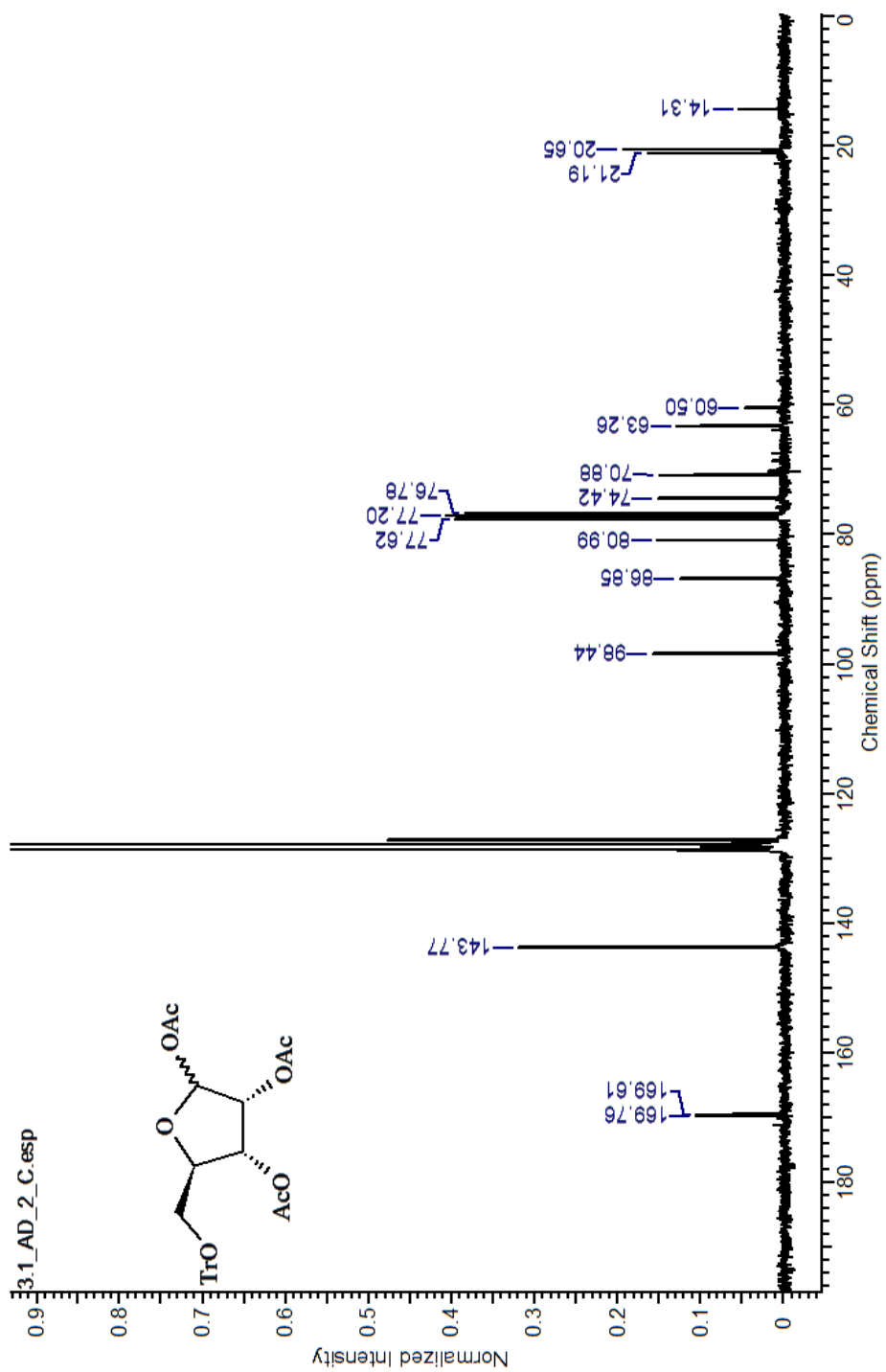


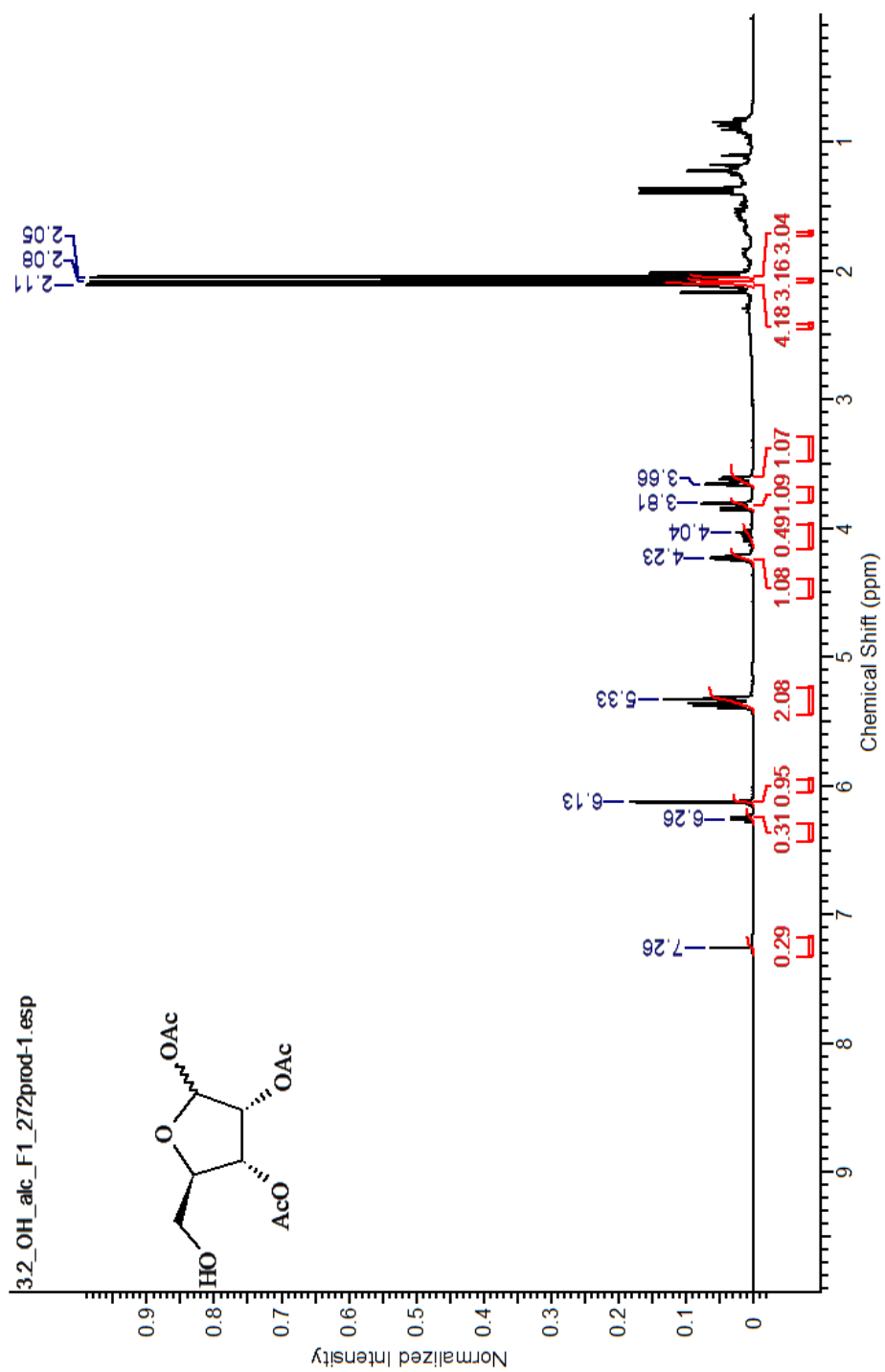


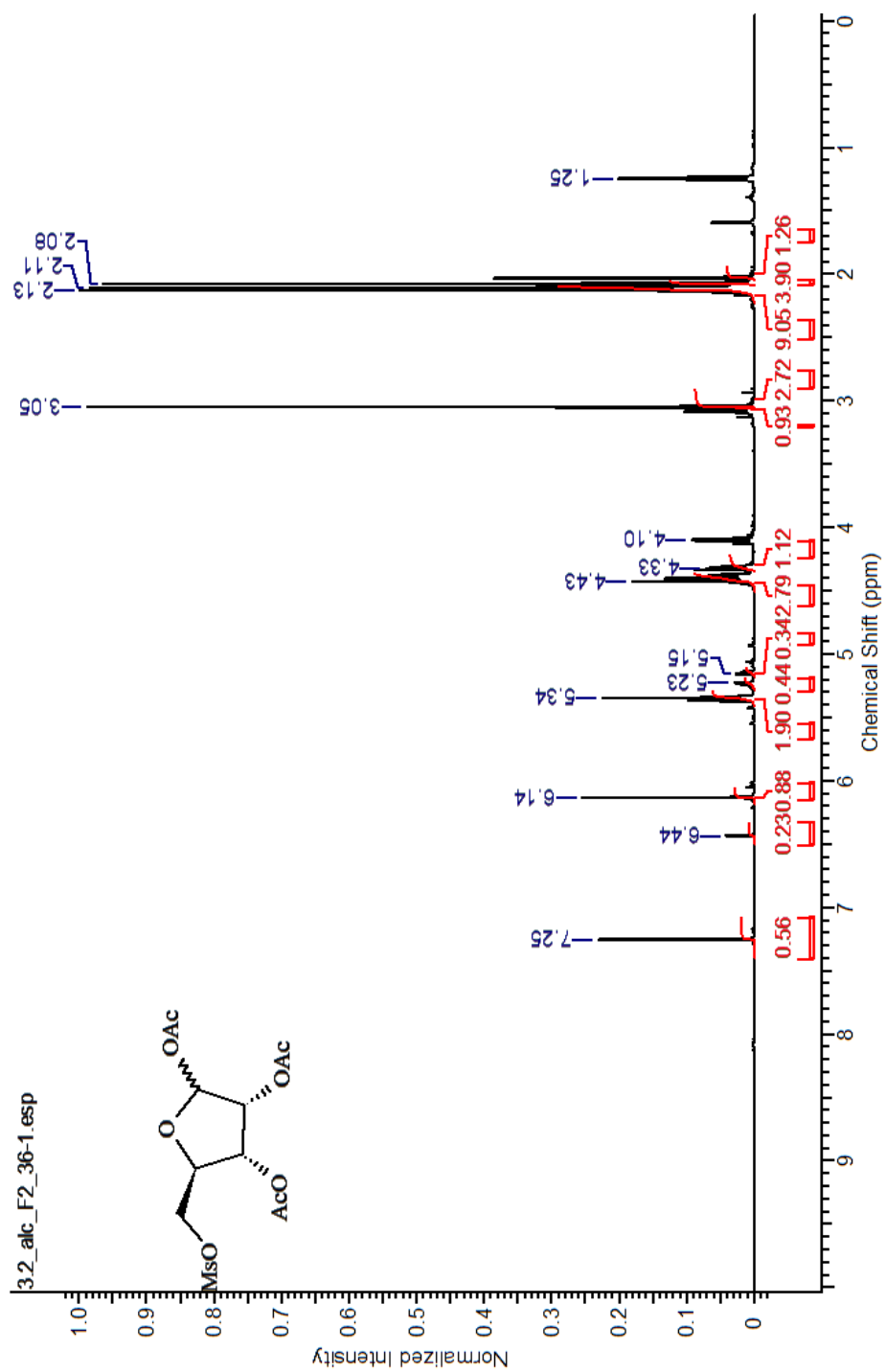
Appendix B: Chapter 3 NMR Spectra

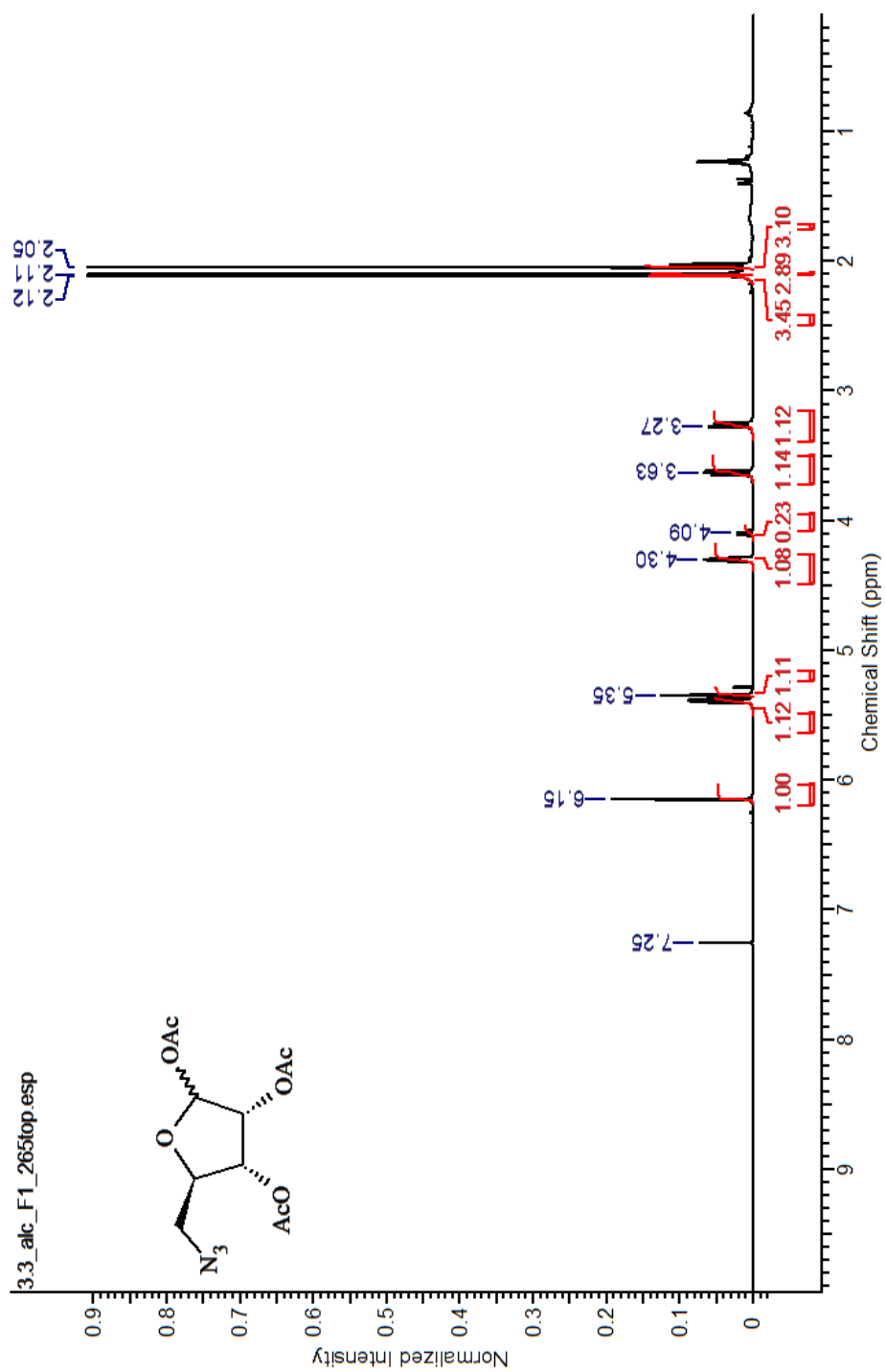


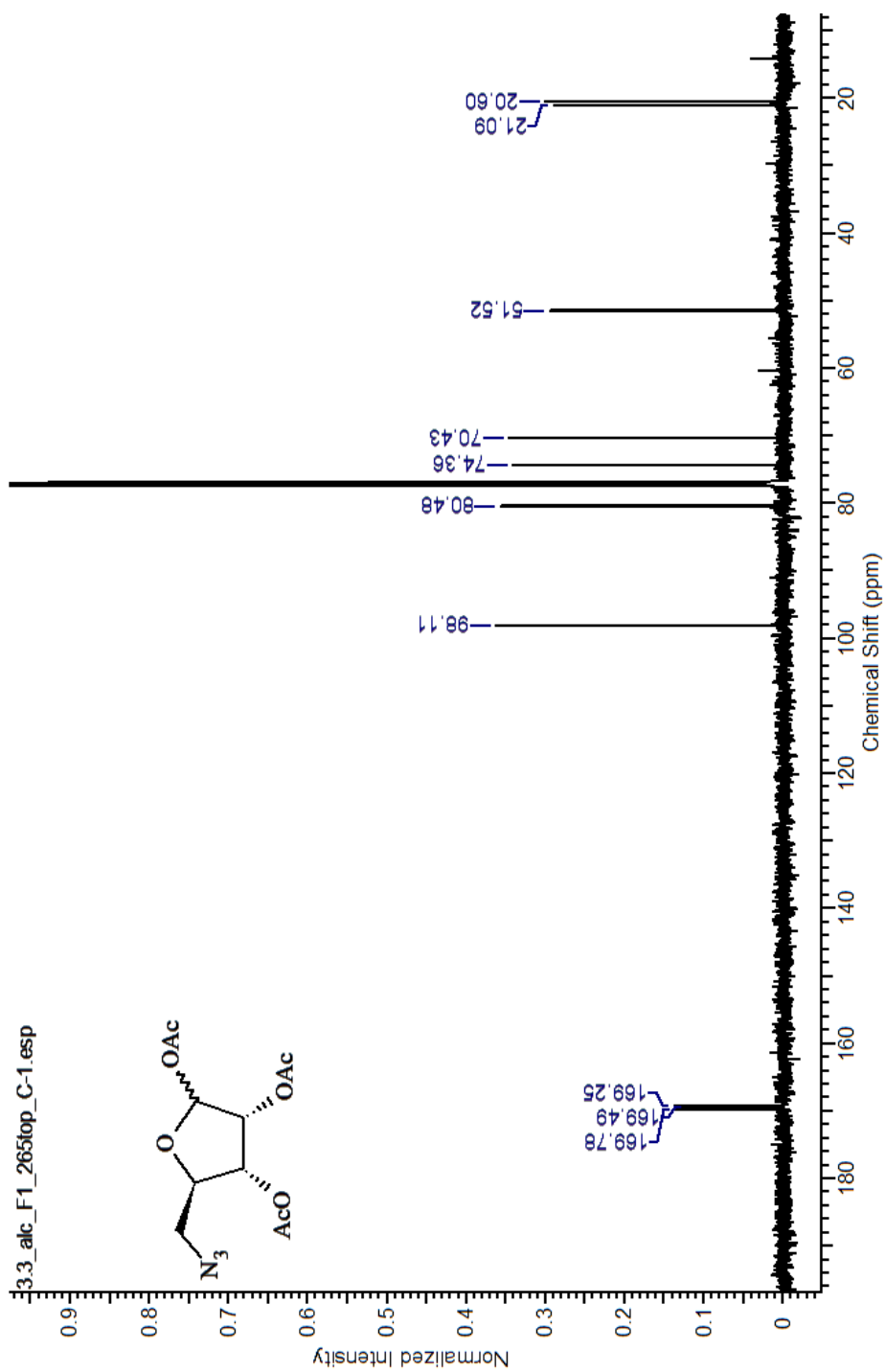


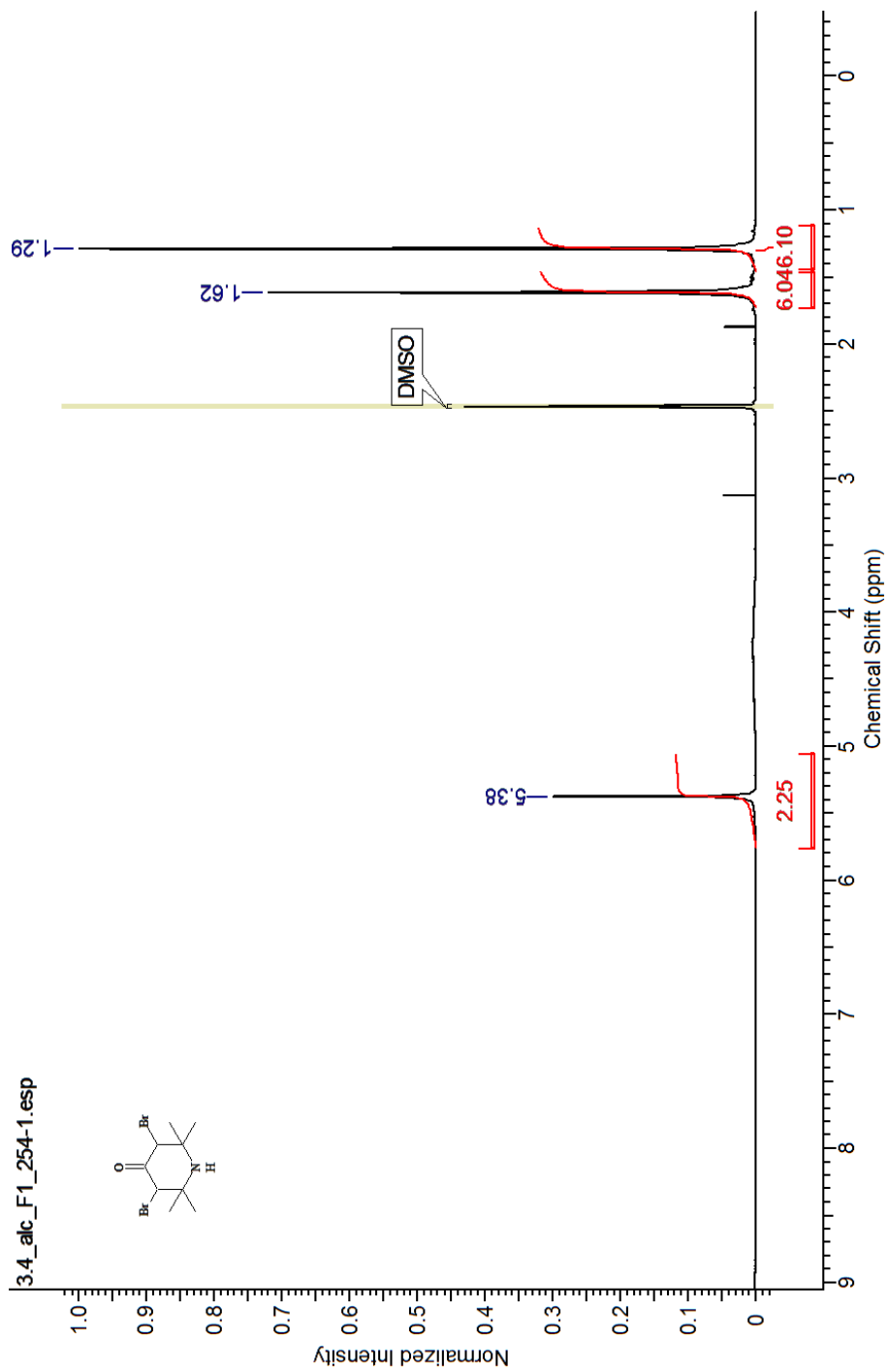


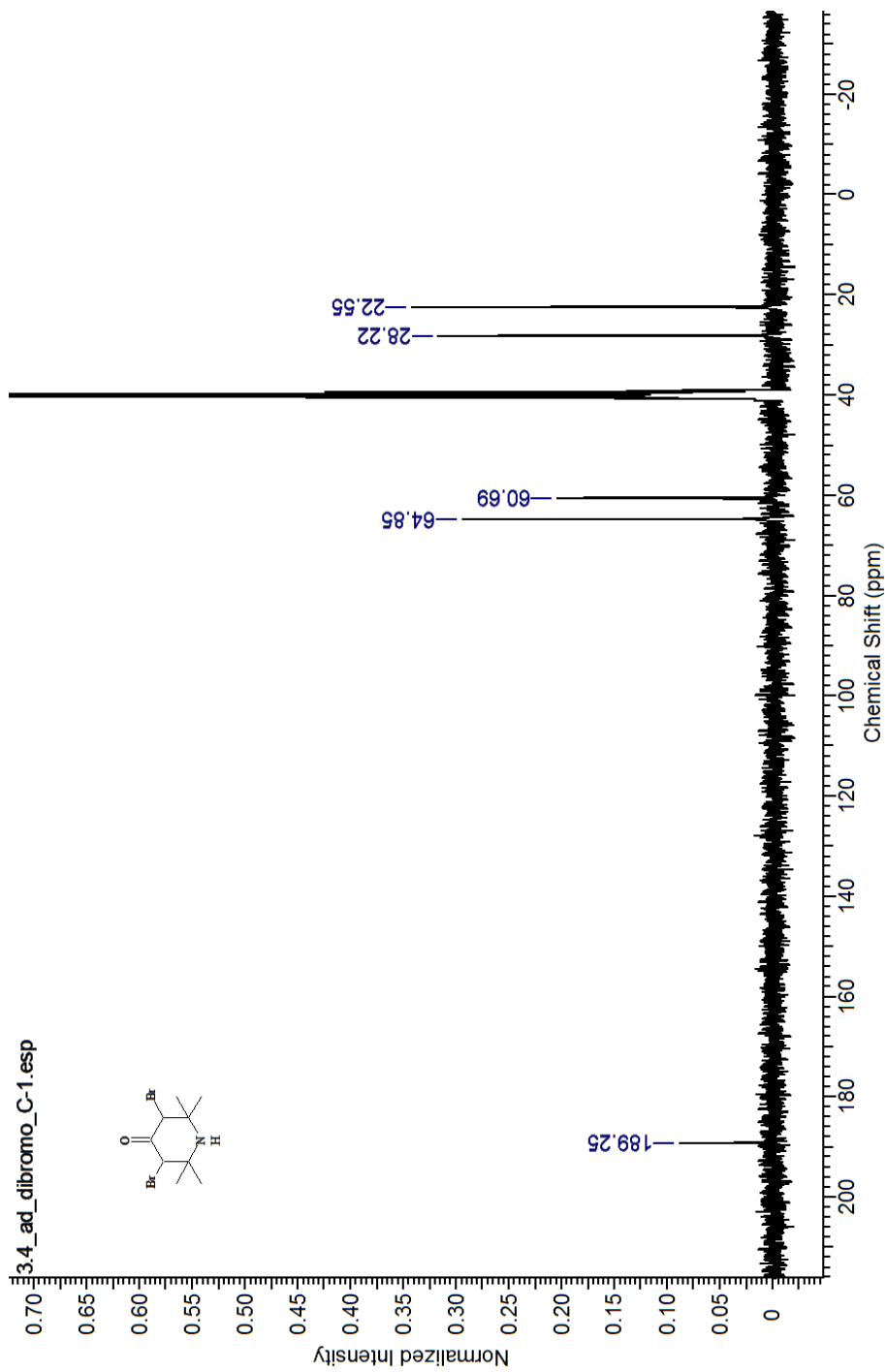


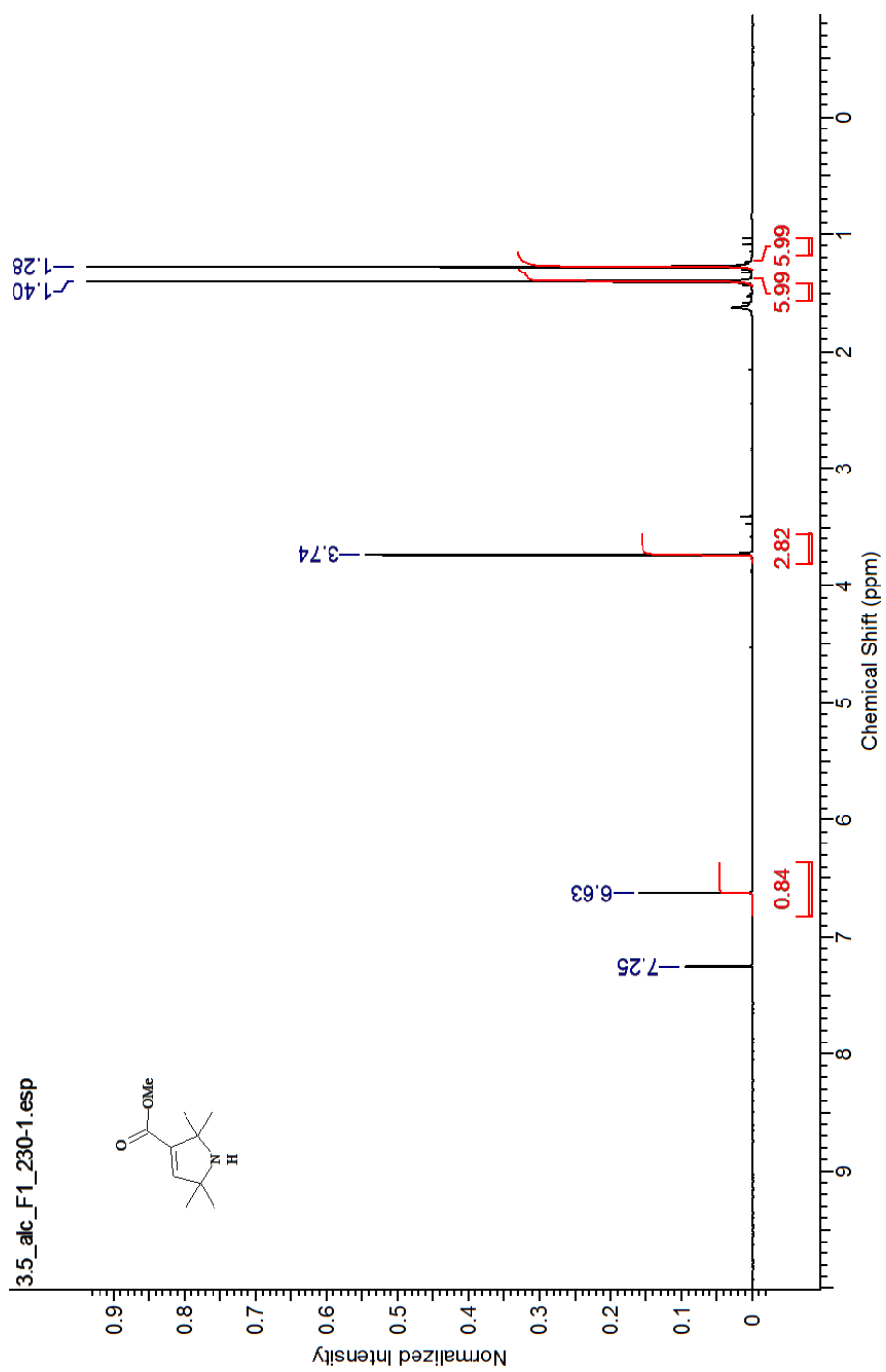


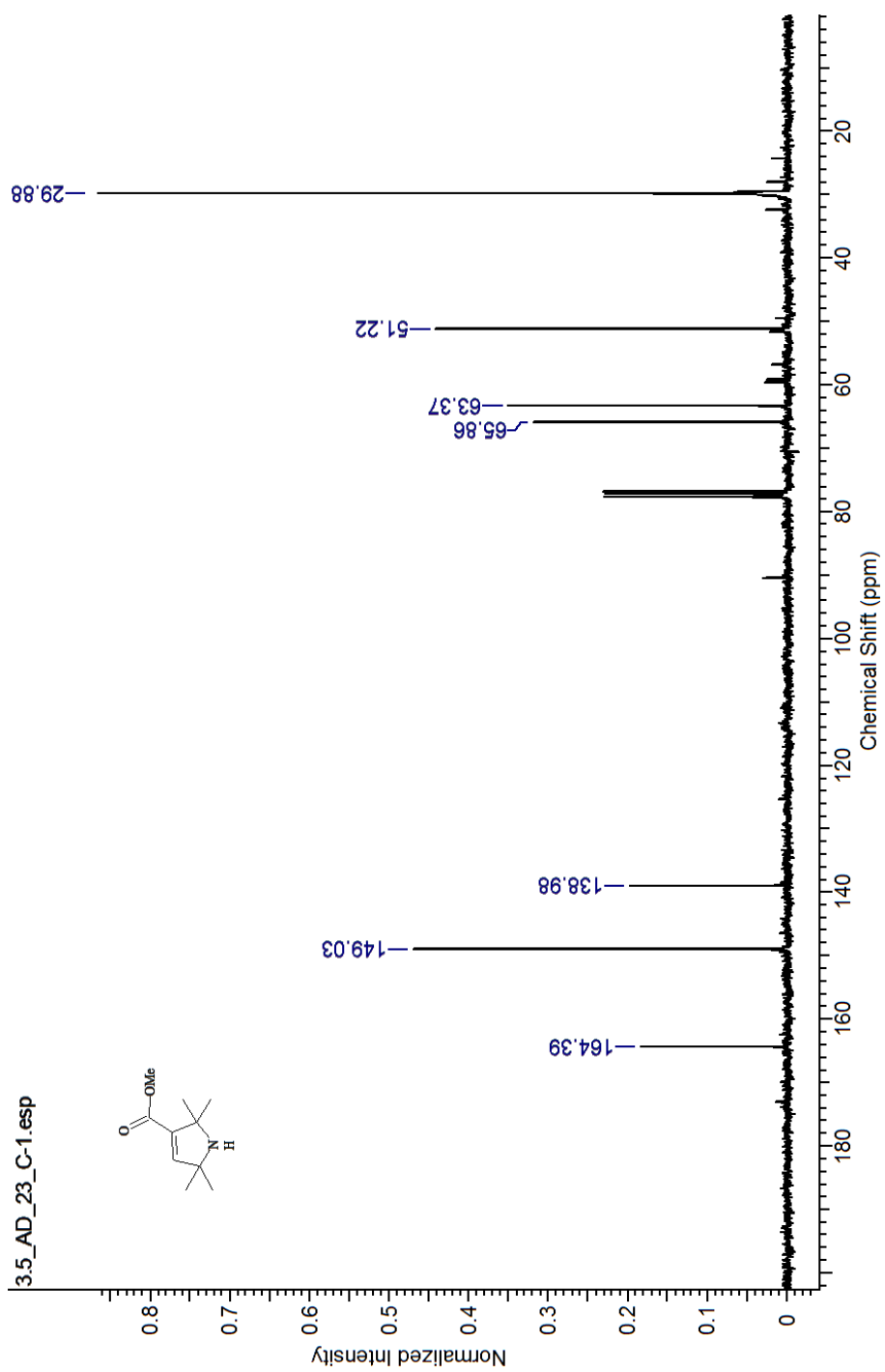


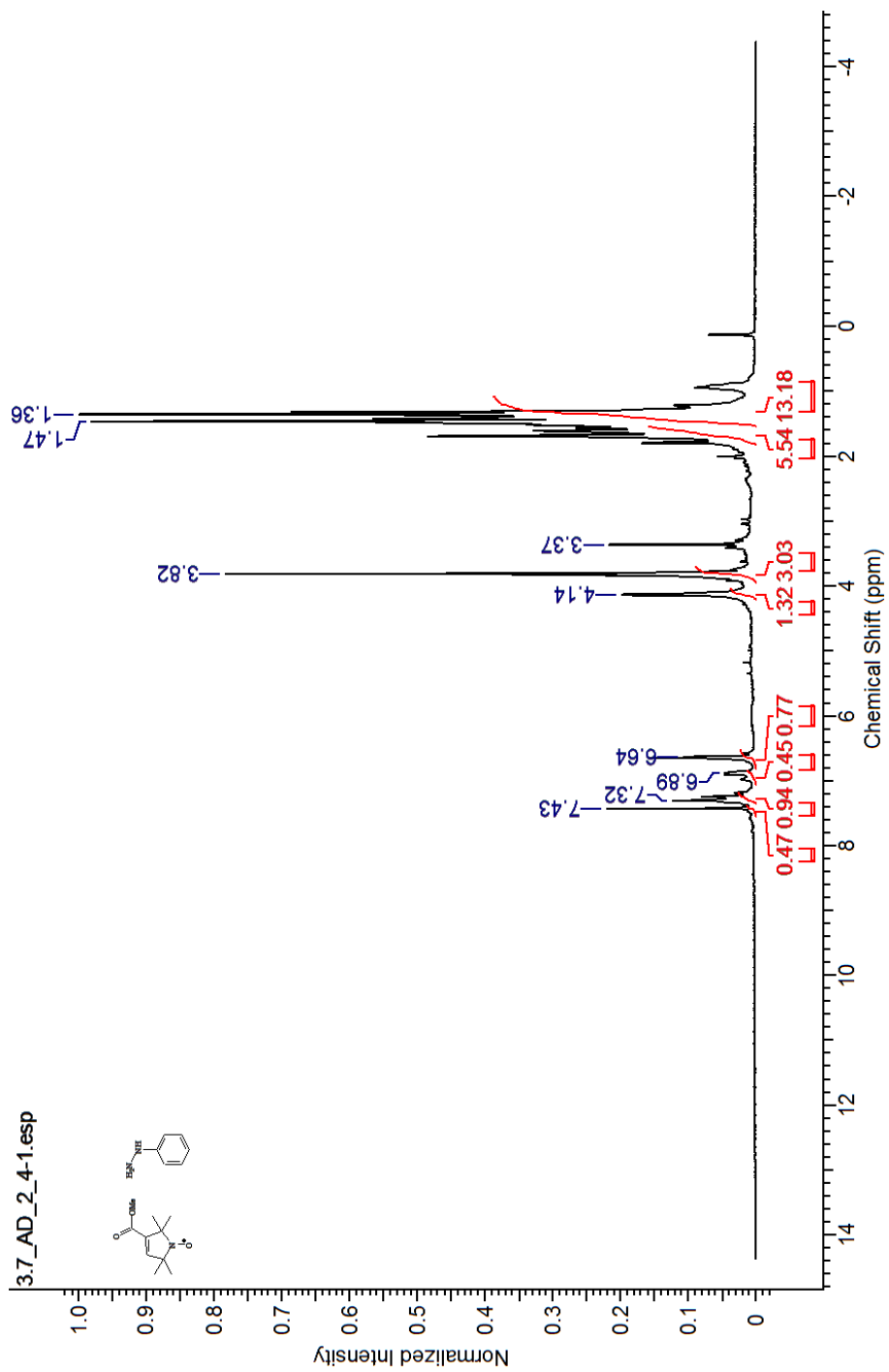


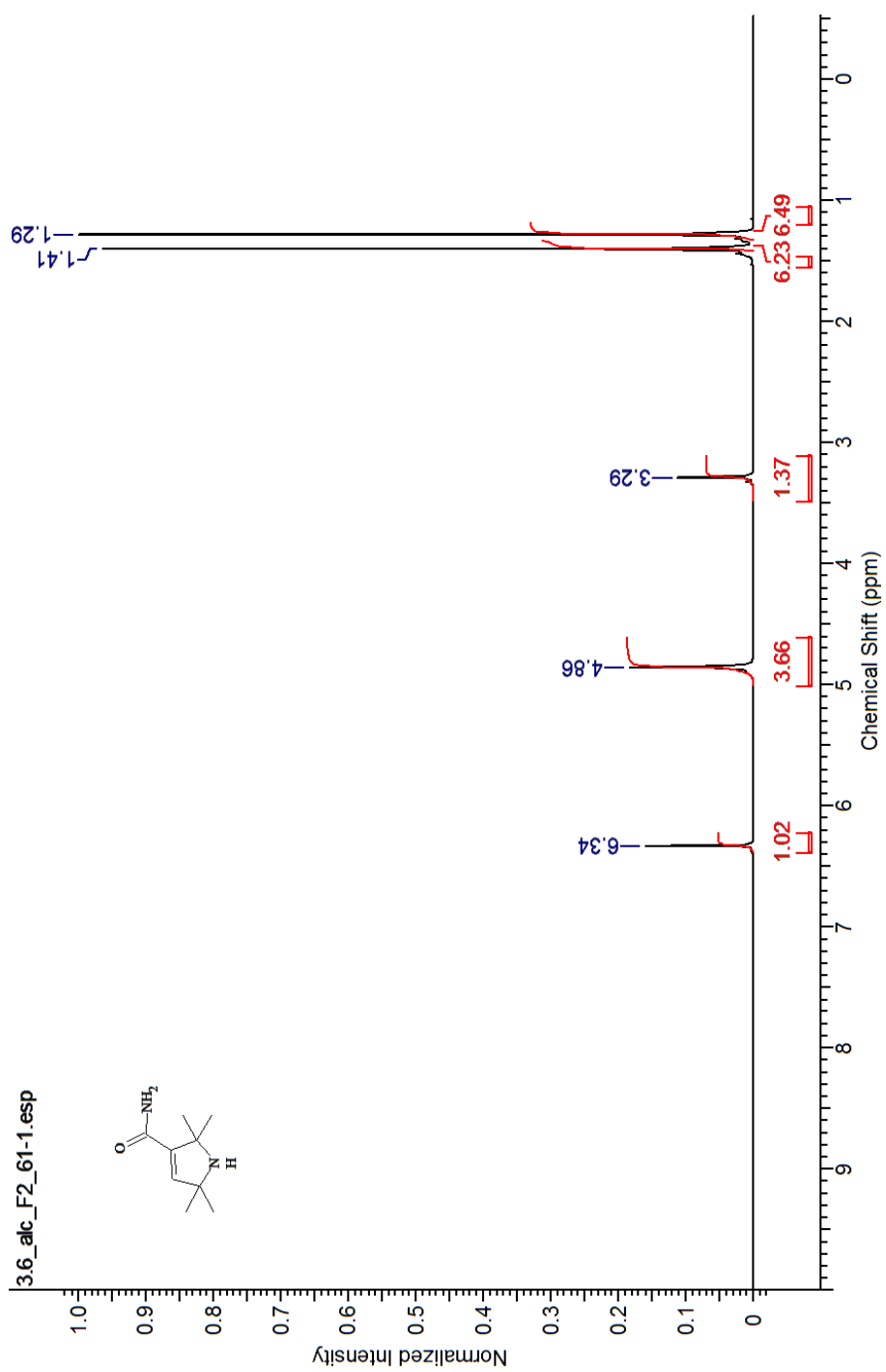


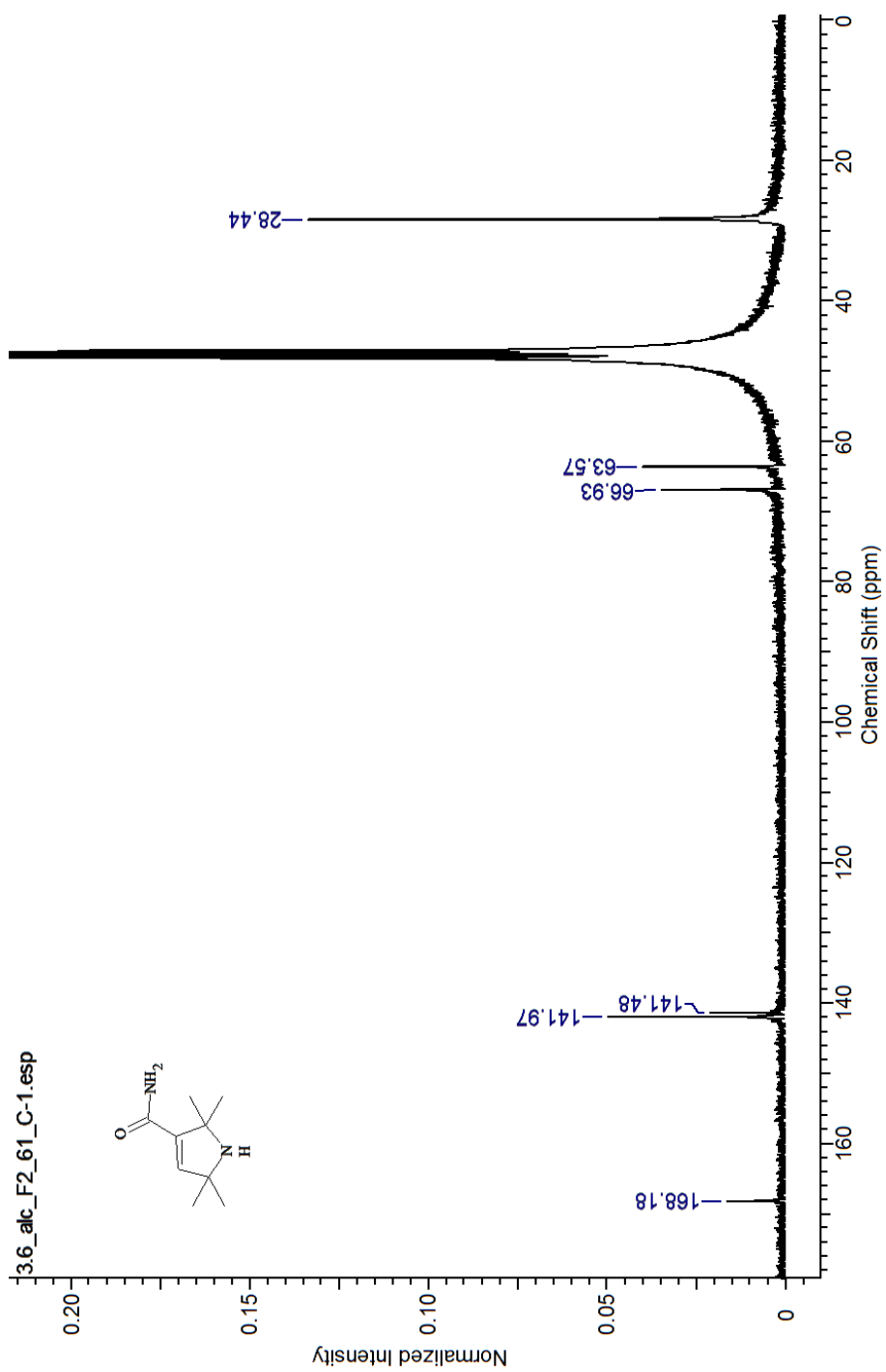


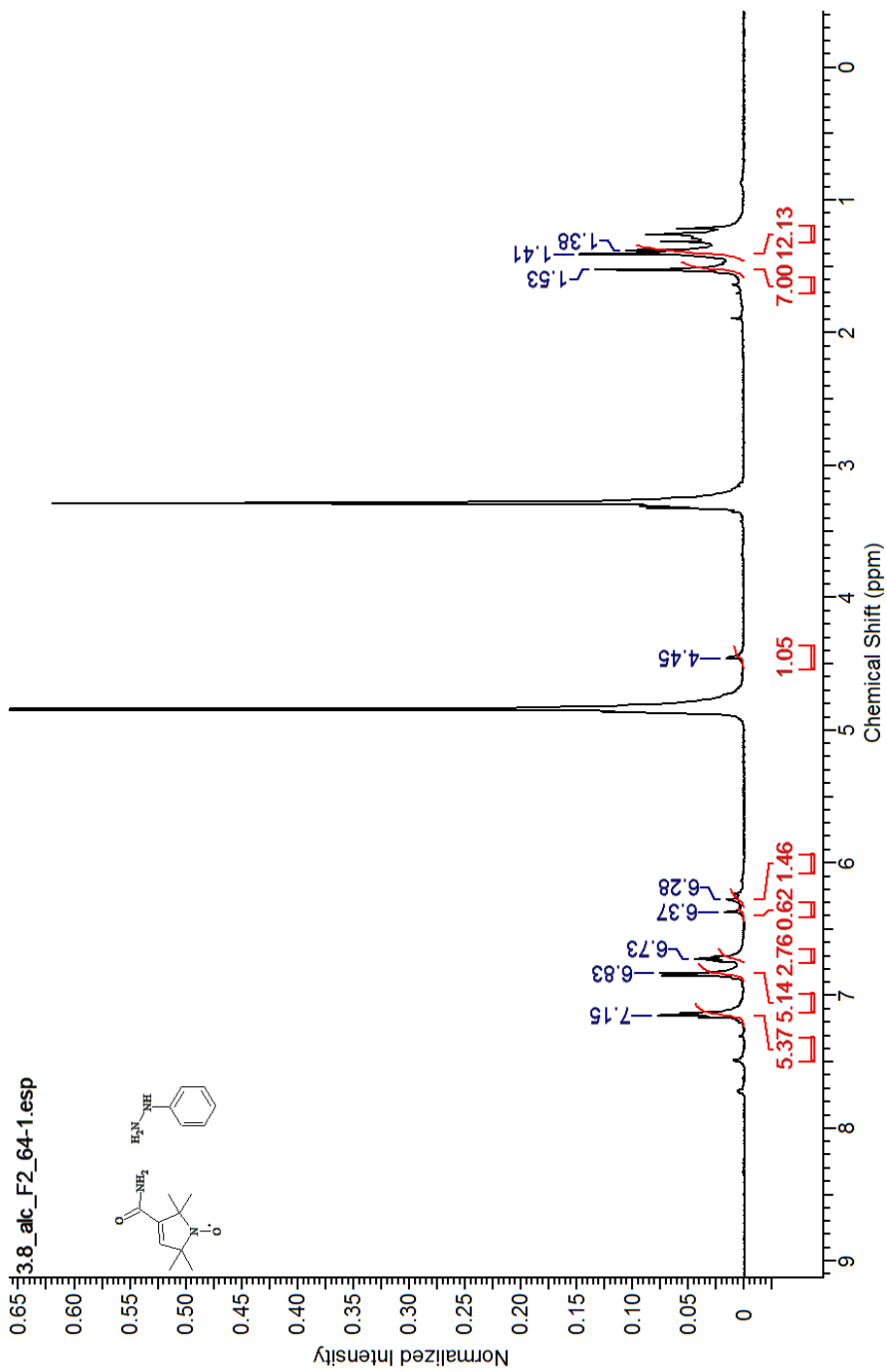


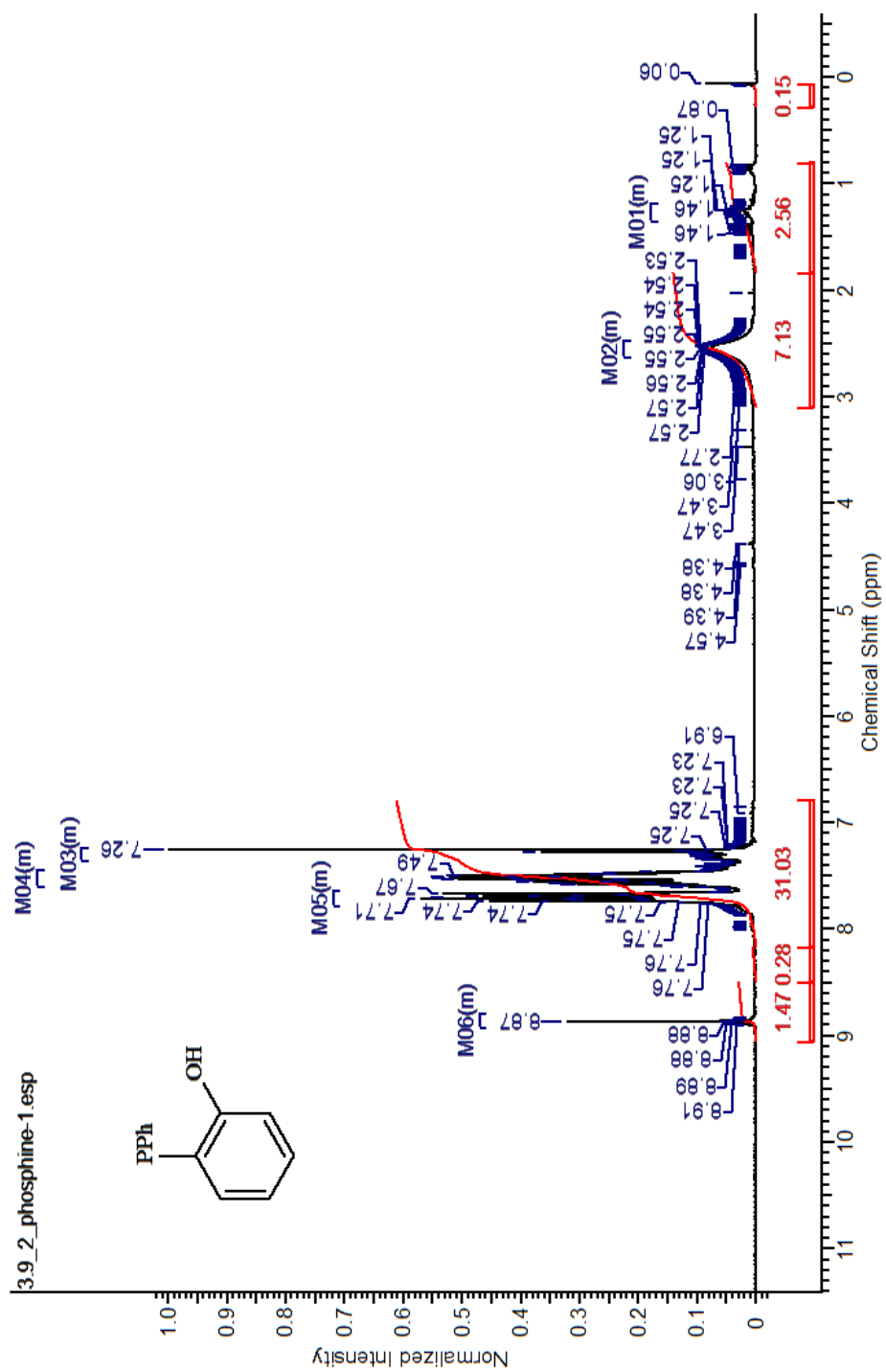


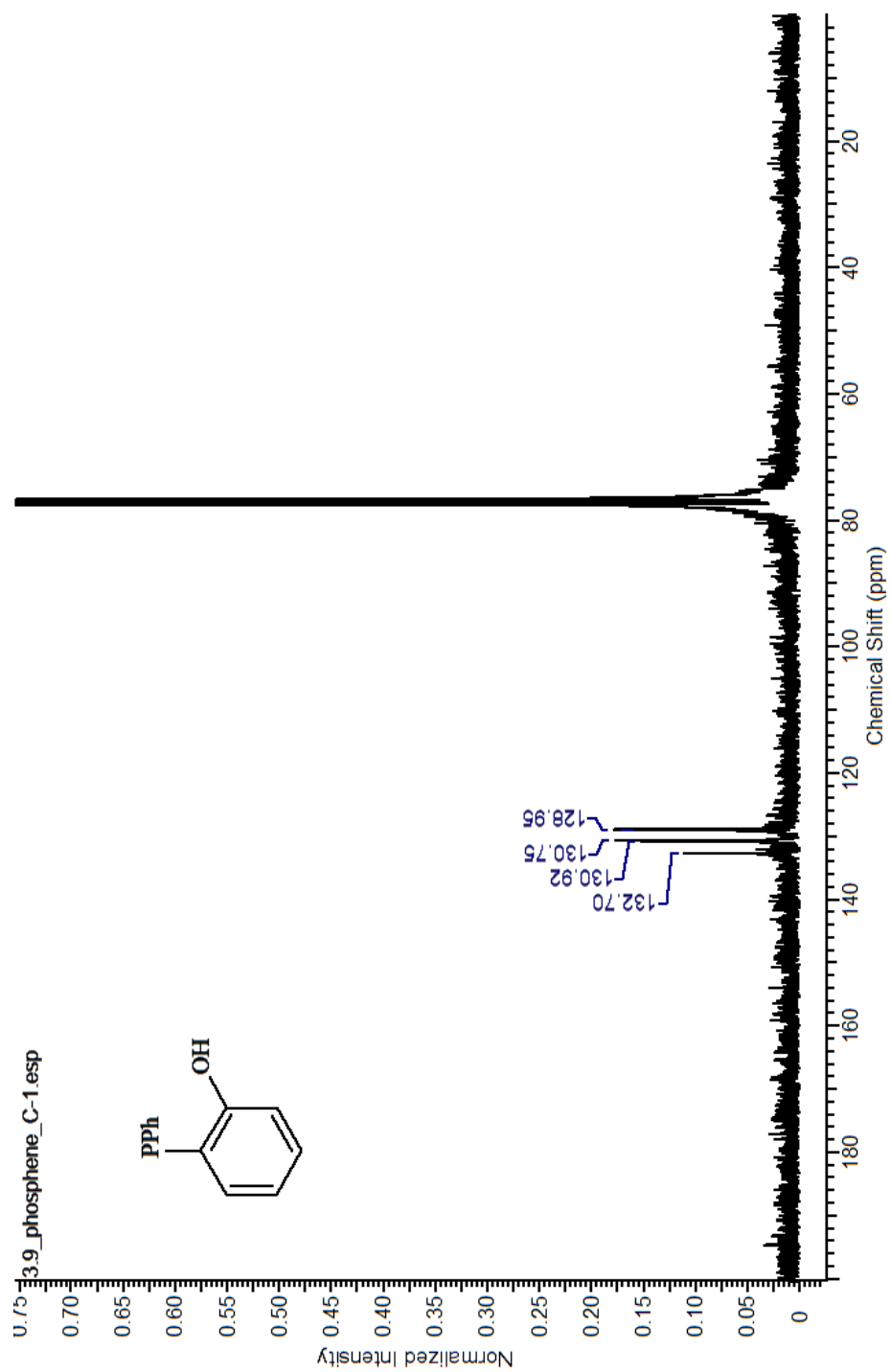


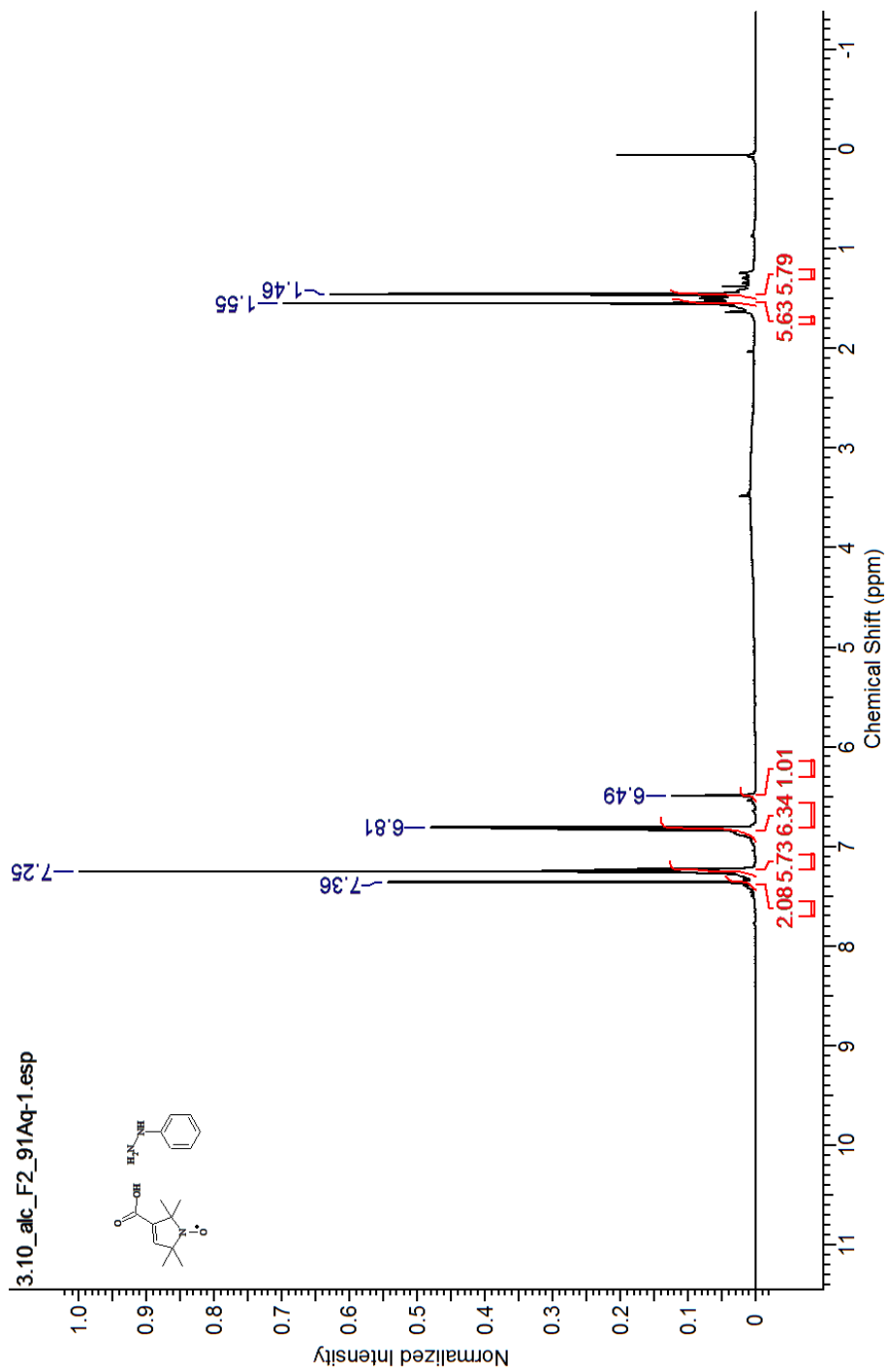


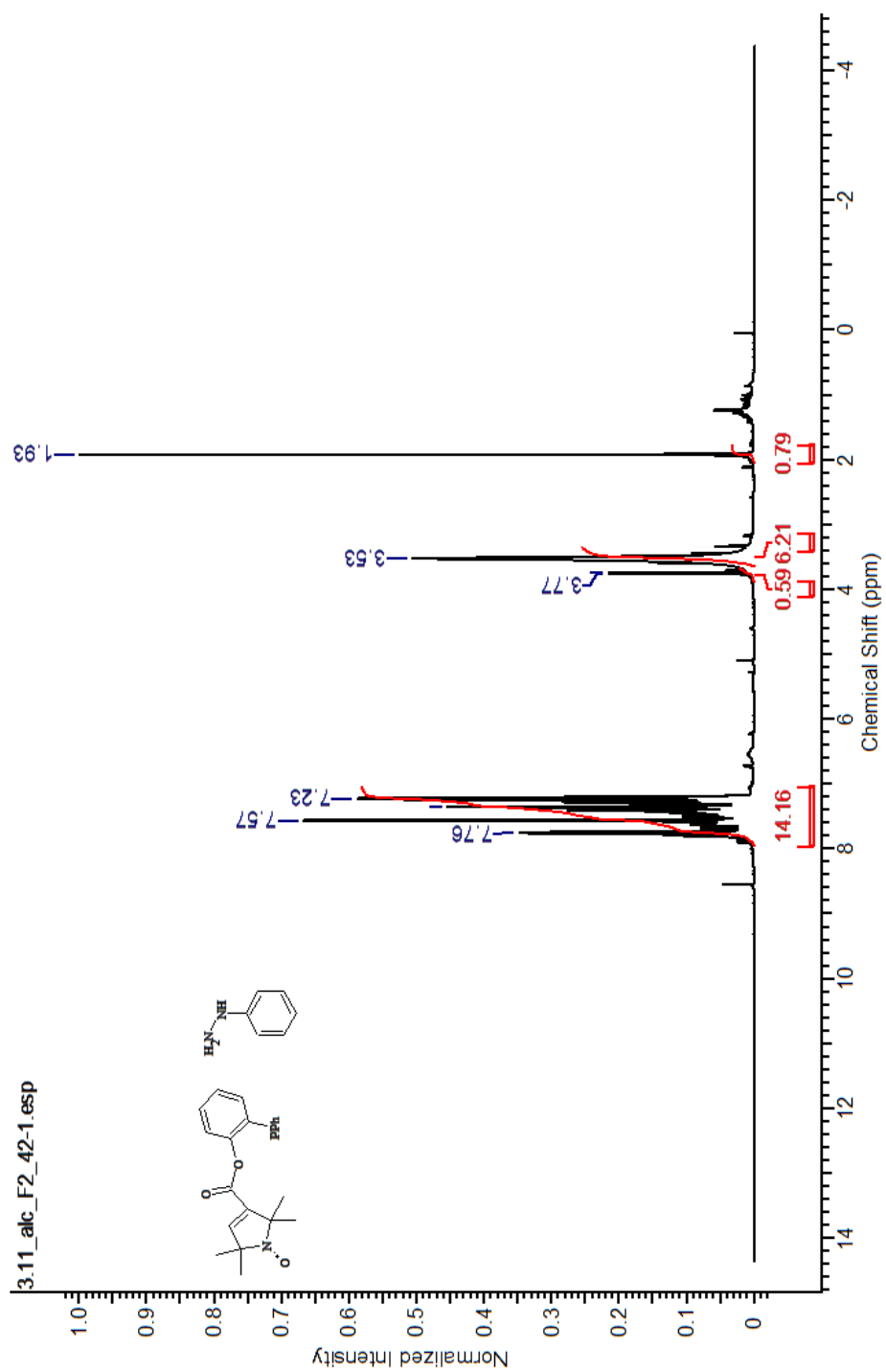


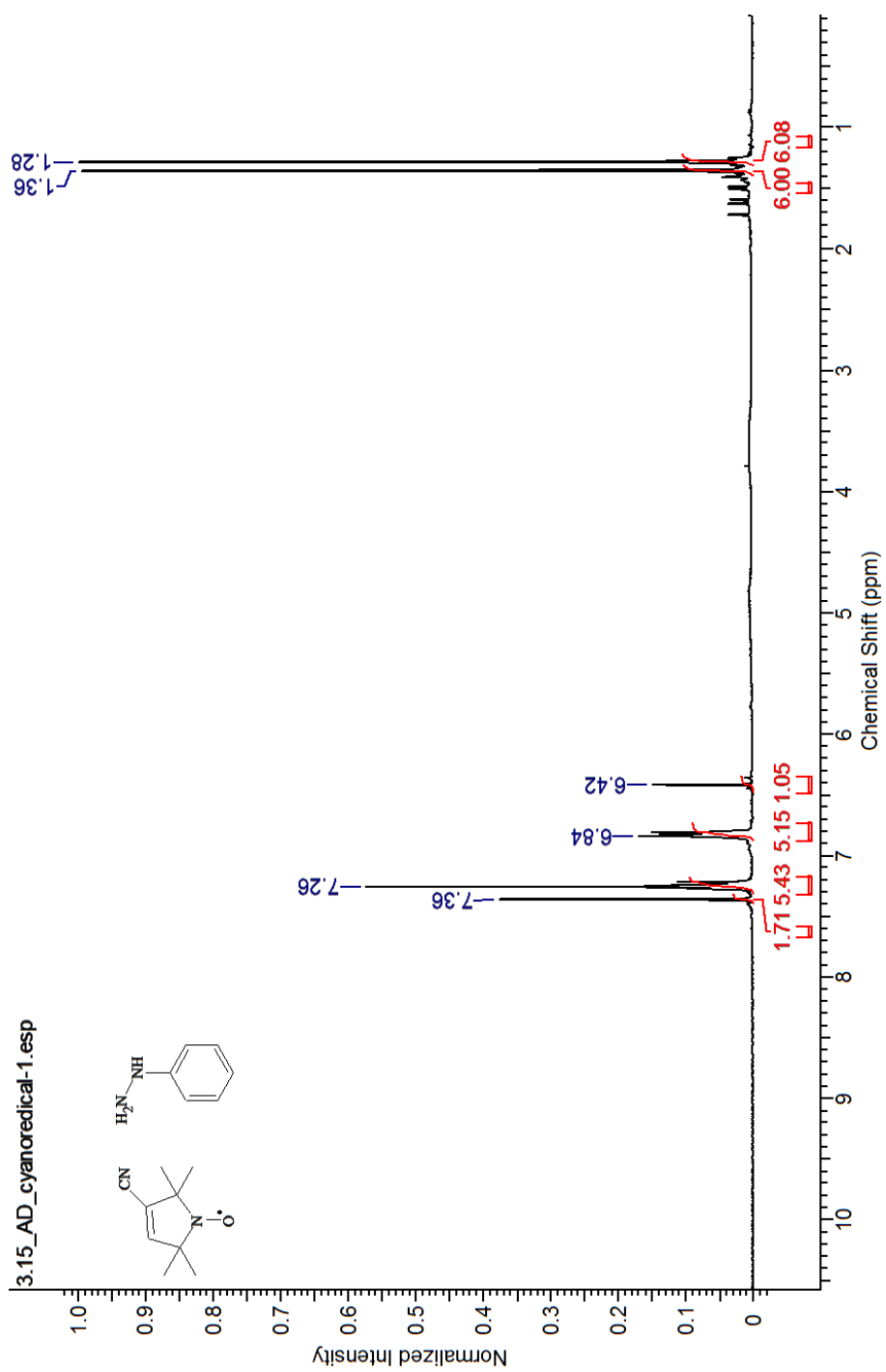


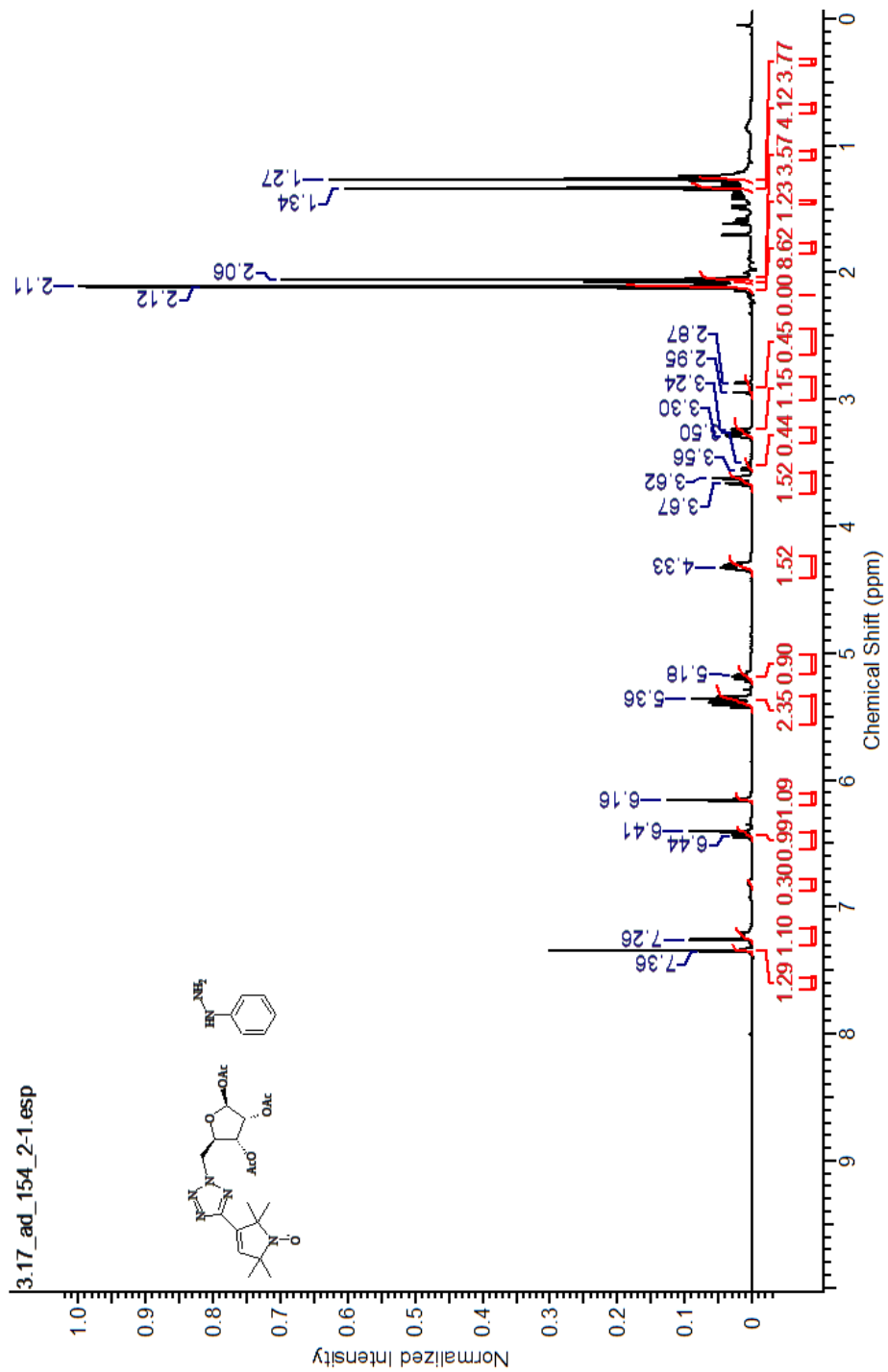


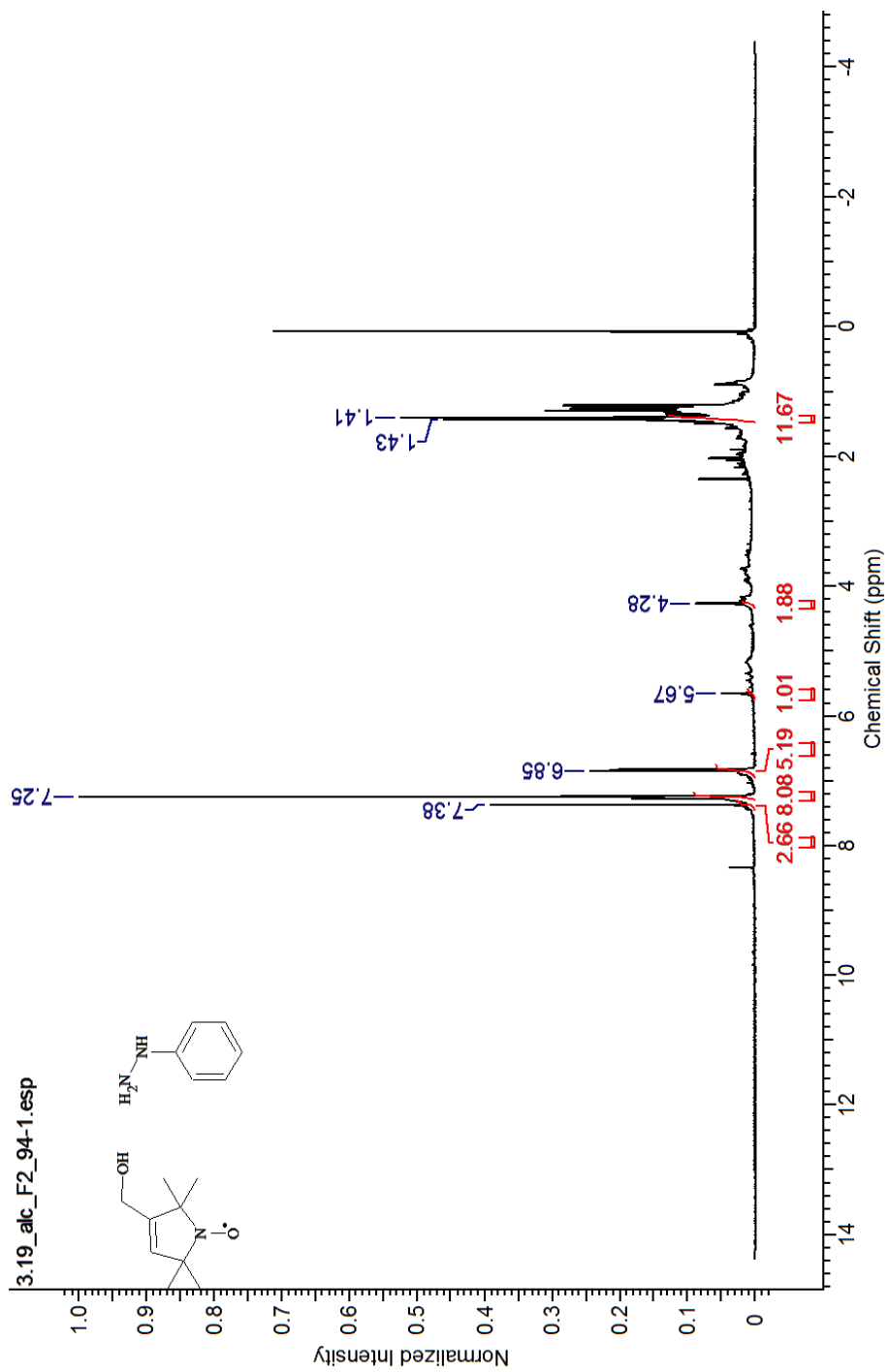


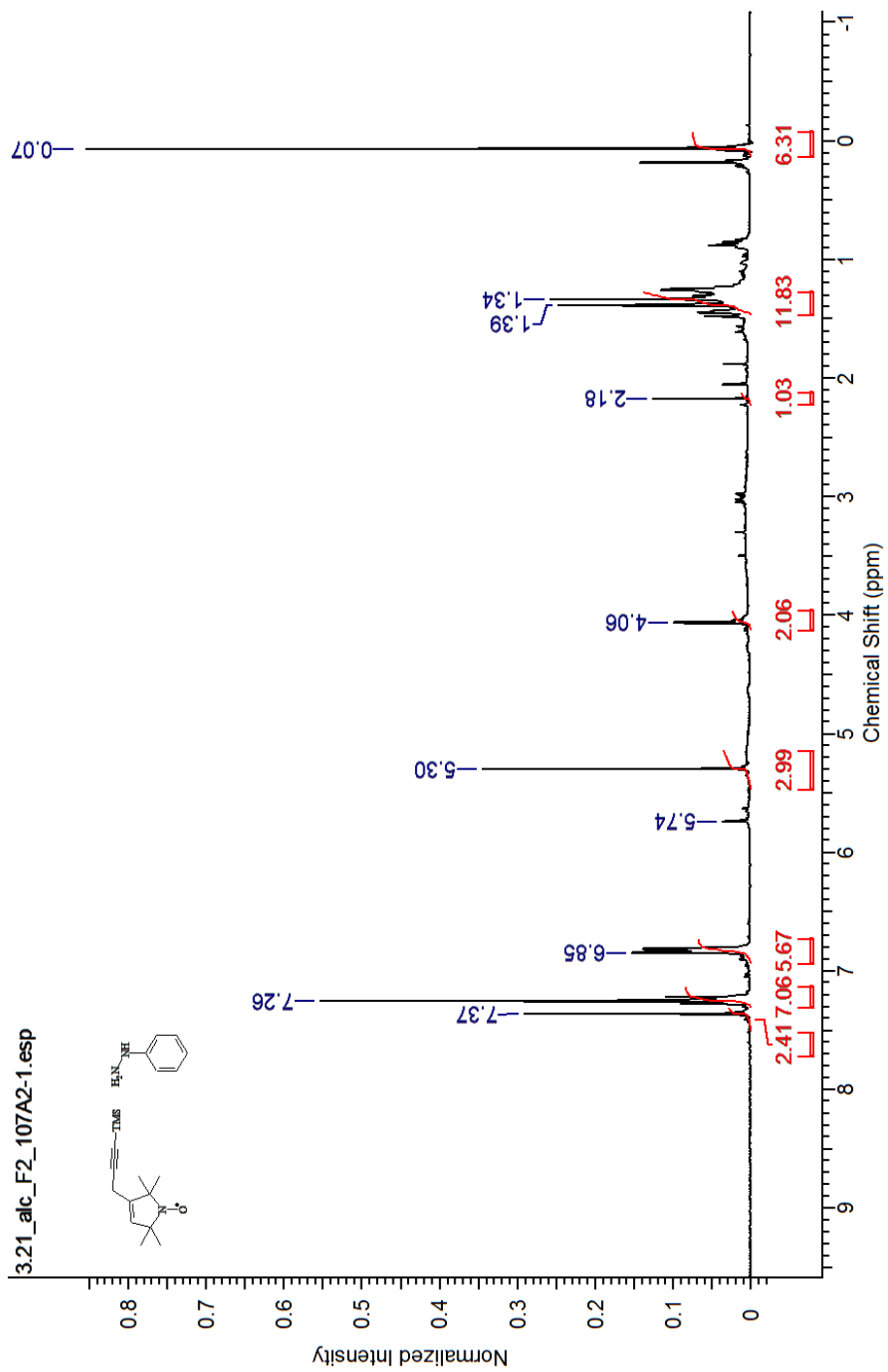


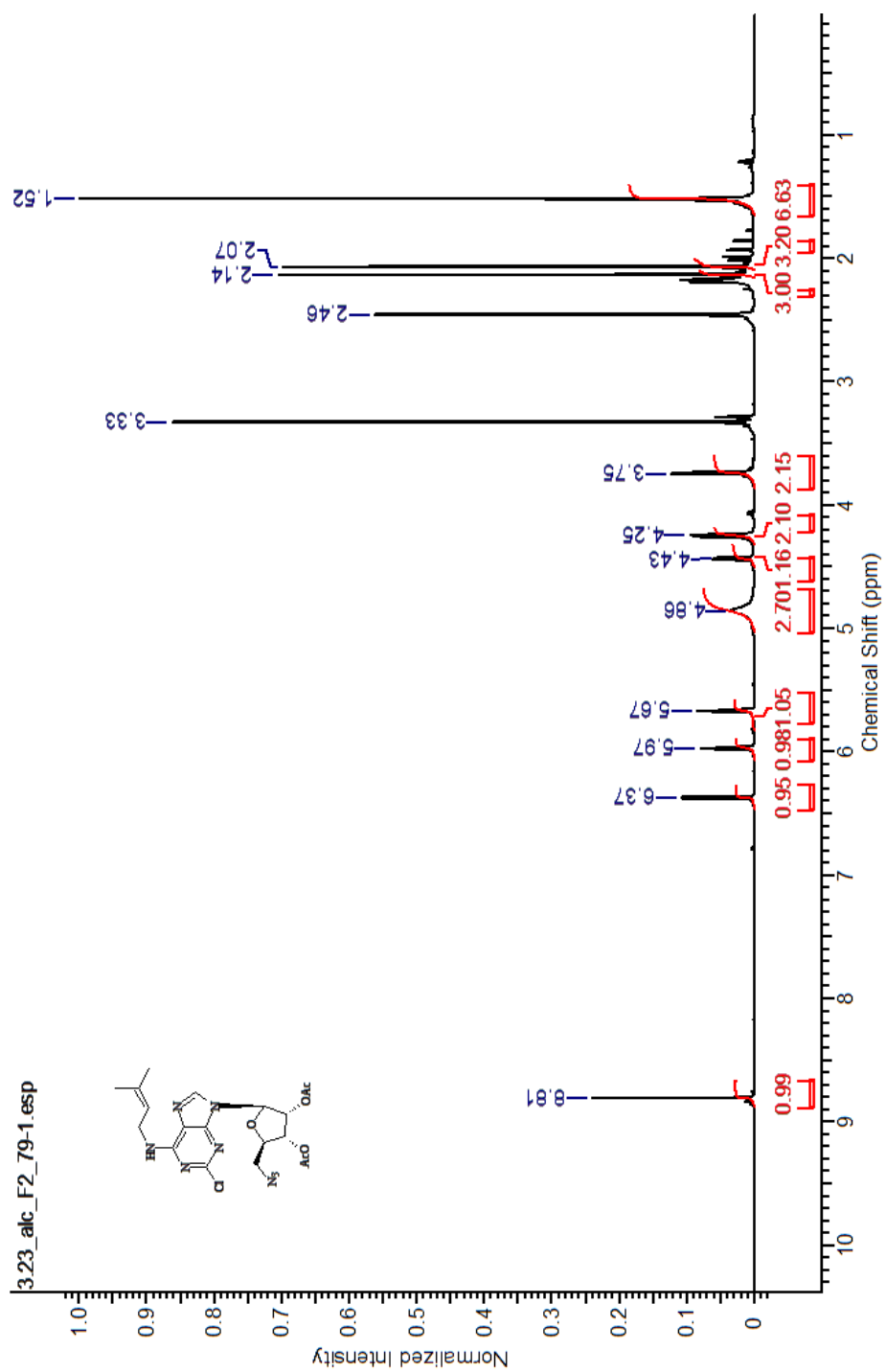


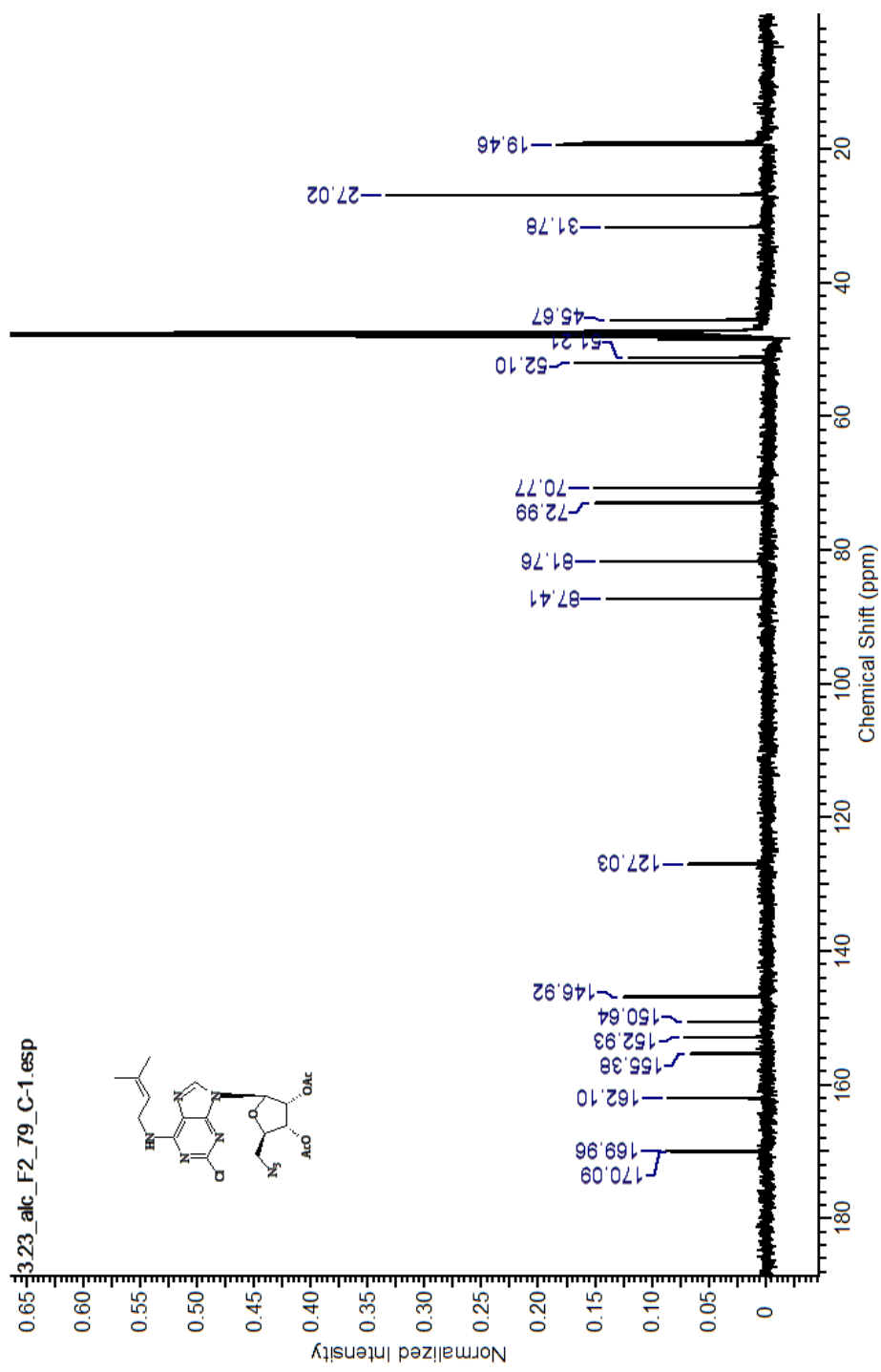


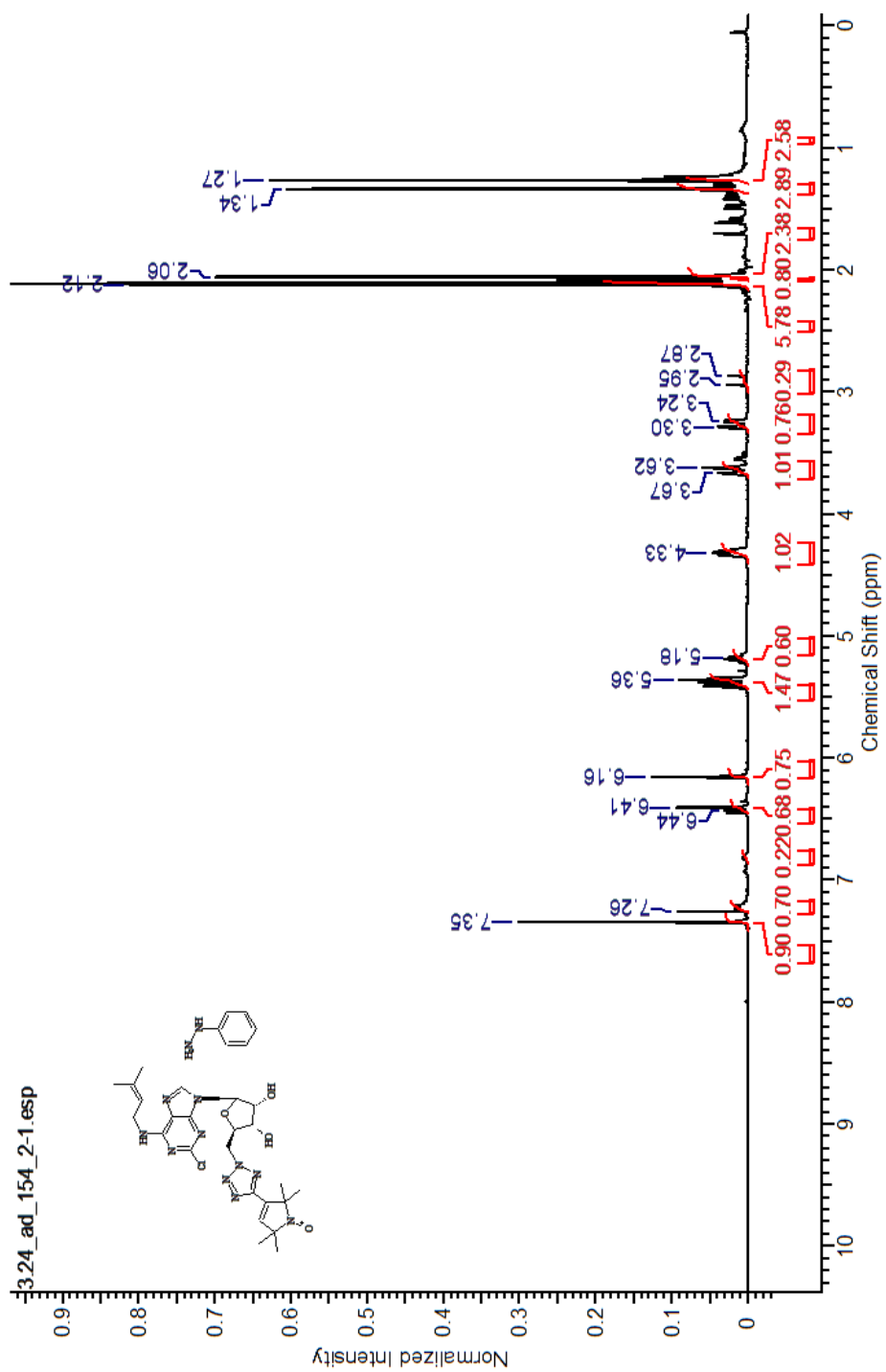












References

- (1) Bjork, G. R.; Durand, J. M.; Hagervall, T. G.; Leipuviene, R.; Lundgren, H. K.; Nilsson, K.; Chen, P.; Qian, Q.; Urbonavicius, J. *FEBS Lett.* **1999**, *452*, 47.
- (2) Gustilo, E. M.; Vendeix, F. A. P.; Agris, P. F. *Curr. Opin. Microbiol.* **2008**, *11*, 134.
- (3) Björk, G. R.; Ericson, J. U.; Gustafsson, C. E. D.; Hagervall, T. G.; Jonsson, Y. H.; Wikstrom, P. M. *Annu. Rev. Biochem.* **1987**, *56*, 263.
- (4) Persson, B. C. *Mol. Microbiol.* **1993**, *8*, 1011.
- (5) Petersson, L.; Graslund, A.; Ehrenberg, A.; Sjöberg, B. M.; Reichard, P. *J. Biol. Chem.* **1980**, *255*, 6706.
- (6) Persson, B. C.; Bjork, G. R. *J. Bacteriol.* **1993**, *175*, 7776.
- (7) Bjork, G.; Huang, B.; Persson, O. P. *RNA* **2007**, *13*, 1245.
- (8) Sakaguchi, R.; Giessing, A.; Dai, Q.; Lahound, G.; Liutkeviciute, Z.; Klimasauskas, S.; Piccirilli, J.; Kirpekar, F.; Hou, Y. *RNA* **2012**, *18*, 1687.
- (9) Bjork, G.; Wikstrom, P. M.; Bystrom, A. S. *Science* **1989**, *244*, 986.
- (10) Durand, J. M.; Bjork, G. R.; Kuwae, A.; Yoshikawa, M.; Sasakawa, C. *J. Bacteriol.* **1997**, *179*, 5777.
- (11) Moore, J. A.; Poulter, C. D. *Biochemistry* **1997**, *36*, 604.
- (12) Robins, M. J.; Hall, R. H.; Thedford, R. *Biochemistry* **1967**, *6*, 1837.
- (13) Soderberg, T.; Poulter, C. D. *Biochemistry* **2001**, *40*, 1734.
- (14) Motorin, Y.; Bec, G.; Tewari, R.; Grosjean, H. *RNA* **1997**, *3*, 721.
- (15) Soderberg, T.; Poulter, C. D. *Biochemistry* **2000**, *39*, 6546.
- (16) Anton, B. P.; Russell, S. P.; Vertrees, J.; Kasif, S.; Raleigh, E. A.; Limbach, P. A.; Roberts, R. J. *Nucleic. Acids. Res.* **2010**, *38*, 6195.
- (17) Atta, M.; Mulliez, E.; Arragain, S.; Forouhar, F.; Hunt, J.; Fontecave, M. *Curr. Opin. Struct. Biol.* **2010**, *20*.

- (18) Frey, P. A.; Hegeman, A. D.; Ruzicka, F. J. *Crit. Rev. Biochem. Mol. Biol.* **2008**, *43*.
- (19) Forouhar, F.; Arragain, S.; Atta, M.; Gambarelli, S.; Mouesca, J.; Hussain, M.; Xiao, R.; Kieffer-Jaquinod, S.; Seetharaman, J.; Acton, T.; Montelione, G.; Mulliez, E.; Hunt, J.; Fontecave, M. *Nat. Chem. Biol.* **2013**, *9*.
- (20) Pierrel, F.; Douki, T.; Fontecave, M.; Atta, M. *J. Biol. Chem.* **2004**, *279*, 47555.
- (21) Booker, S. J.; Cicchillo, R. M.; Grove, T. L. *Curr. Opin. Chem. Biol.* **2007**, *11*.
- (22) Landgraf, B. J.; Arcinas, A. J.; Lee, K.-H.; Booker, S. J. *J. Am. Chem. Soc.* **2013**, *135*, 15404.
- (23) Mathevon, C.; Pierrel, F.; Oddou, J.-L.; Garcia-Serres, R.; Blondin, G.; Latour, J.-M.; Menage, S.; Gambarelli, S.; Fontecave, M.; Atta, M. *Proc. Natl. Acad. Sci.* **2007**, *104*, 13295.
- (24) Esberg, B.; Leung, H.-C. E.; Tsui, H.-C. T.; Björk, G. R.; Winkler, M. E. *J. Bacteriol.* **1999**, *181*, 7256.
- (25) Buck, M.; Ames, B. N. *Cell* **1984**, *36*, 523.
- (26) Esberg, B.; Björk, G. R. *J. Bacteriol.* **1995**, *177*, 1967.
- (27) Persson, B.; Olafsson, O.; Lundgren, H.; Hederstedt, L.; Björk, G. *J. Bacteriol.* **1998**, *180*, 3144.
- (28) Ajitkumar, P.; Cherayil, J. D. *J. Bacteriol.* **1985**, *162*, 752.
- (29) Kaminska, K. H.; Baraniak, U.; Boniecki, M.; Nowaczyk, K.; Czerwoniec, A.; Bujnicki, J. M. *Proteins* **2008**, *70*, 1.
- (30) Merkx, M.; Kopp, D. A.; Sazinsky, M. H.; Blazyk, J. L.; Müller, J.; Lippard, S. J. *Angew. Chem. Int. Ed. Engl.* **2001**, *40*, 2782.
- (31) Cherayil, J. D.; Lipsett, M. N. *J. Bacteriol.* **1977**, *131*, 741.

- (32) Subedi, B. P.; Corder, A. L.; Zhang, S.; Foss, F. W.; Pierce, B. S.; University of Texas at Arlington: 2014.
- (33) Feig, A. L.; Lippard, S. *Chem. Rev.* **1993**, *94*, 759.
- (34) Wallar, B. J.; Lipscomb, J. D. *Chem. Rev.* **1996**, *96*, 2625.
- (35) Solomon, E. I.; Decker, A.; Lehnert, N. *Proc. Natl. Acad. Sci.* **2003**, *100*, 3589.
- (36) Murray, L. J.; Lippard, S. J. *Acc. Chem. Res.* **2007**, *40*, 466.
- (37) Kopp, D. A.; Gassner, G. T.; Blazyk, J. L.; Lippard, S. J. *Biochemistry* **2001**, *40*, 14932.
- (38) Lee, D.; Lippard, S. J. *Inorg. Chem.* **2002**, *41*, 827.
- (39) Baik, M. H.; Newcomb, M.; Friesner, R. A.; Lippard, S. J. *Chem. Rev.* **2003**, *103*, 2385.
- (40) Lipscomb, J. D. *Annu. Rev. Microbiol.* **1994**, *48*, 371.
- (41) Froland, W. A.; Andersson, K. K.; Lee, S.-K.; Liu, Y.; Lipscomb, J. D. *J. Biol. Chem.* **1992**, *267*, 17588.
- (42) Bailey, L. J.; Fox, B. G. *Biochemistry* **2009**, *48*, 8932.
- (43) Prusoff, W. *Biochim. Biophys. Acta.* **1959**, *32*, 295.
- (44) Isono, K. *Pharmacol. Ther.* **1991**, *52*, 269.
- (45) Corder, A. L.; Subedi, B. P.; Zhang, S.; Dark, A. M.; Foss, F. W.; Pierce, B. S. *Biochemistry* **2013**, *52*, 6182.
- (46) Hollenstein, M. *Molecules* **2012**, *17*, 13569.
- (47) Lippard, S. J.; Tshuva, E. Y. *Chem. Rev.* **2004**, *104*, 987.
- (48) Kopp, D.; Lippard, S. J. *Curr. Opin. Chem. Biol.* **2002**, *6*, 568.
- (49) Lei, Q. P.; Cui, X.; Kurtz, D. M.; Amster, I. J.; Chernushevich, I. V.; Standing, K. G. *Anal. Chem.* **1998**, *70*, 1838.

- (50) Notomista, E.; Lahm, A.; Di Donato, A.; Tramontano, A. *J. Mol. Evol.* **2003**, *56*, 435.
- (51) Kuo, H. H.; Mauk, A. G. *Proc. Natl. Acad. Sci.* **2012**, *109*, 13966.
- (52) Brookes, E. H.; Demeler, B. In *Proceedings of the 9th annual conference on Genetic and evolutionary computation 2007*, p 361.
- (53) Demeler, B.; Brookes, E. *Colloid Polym. Sci.* **2008**, *286*, 129.
- (54) Newman, L.; Wackett, L. *Biochemistry* **1995**, *34*.
- (55) Gehrke, C. W.; Kuo, K. C. *J Chromatogr* **1989**, *471*, 3.
- (56) Zhang, S., University of Texas at Arlington, 2013.
- (57) Chomczynski, P.; Sacchi, N. *Anal. Biochem.* **1987**, *162*, 156.
- (58) Connolly, D. M.; Winkler, M. E. *J. Bacteriol.* **1989**, *171*, 3233.
- (59) Yost, R. A.; Fetterolf, D. D. *Mass Spectrom Rev.* **1983**, *2*, 1.
- (60) Spichal, L. 2009; Vol. 2,009,003,428.
- (61) Katritzky, A.; Baykut, G.; Rachwal, S.; Miroslaw, S.; Caster, K.; Eyler, J. *J. Chem. Soc., Perkin Trans. 2* **1989**, 1499.
- (62) Maguire, M.; Nobbs, D.; Einstein, R.; Middleton, J. *J. Med. Chem.* **1971**, *14*, 415.
- (63) Kim, H.; Ohno, M.; Xu, B.; Kim, H.; Choi, Y.; Ji, X.; Maddileti, S.; Marquez, V.; Harden, T.; Jacobson, K. *J. Med. Chem.* **2003**, *46*, 4974.
- (64) Ragnarsson, U.; Grehn, L. *Acc. Chem. Res.* **1991**, *24*, 285.
- (65) Dumas, D. J. *J. Org. Chem.* **1988**, *53*, 4650.
- (66) Mahmud, H., The University of Texas at Arlington, 2000.
- (67) Montgomery, J. A.; Holum, L. B. *J. Am. Chem. Soc.* **1957**, *79*, 2185.
- (68) Oumata, N.; Ferandin, Y.; Meijer, L.; Galons, H. *Org. Process Res. Dev.* **2009**, *13*, 641.
- (69) Liu, H.; Pinto, B. M. *J. Org. Chem.* **2004**, *70*, 753.

- (70) Ginisty, M.; Gravier-Pelletier, C.; Le Merrer, Y. *Tetrahedron-Asymmetry* **2006**, *17*, 142.
- (71) Vorbruggen, H.; Ruh-Pohlenz, C. *Handbook of nucleoside synthesis*; John Wiley & Sons, Inc., 2001.
- (72) Sun, Z.; Wang, H.; Wen, K.; Li, Y.; Fan, E. *J. Org. Chem.* **2011**, *76*, 4149.
- (73) Piguel, S.; Legraverend, M. *J Org Chem.* **2007**, *72*, 7026.
- (74) Hara, R.; Sato, K.; Sun, W.; Takahashi, T. *Chem. Commun.* **1999**, 845.
- (75) Powell, D. A.; Batey, R. A. *Organic letters* **2002**, *4*, 2913.
- (76) Evidente, A.; Piccialli, G.; Sisto, A.; Ohba, M.; Honda, K.; Fujii, T. *Chem. Pharm. Bull.* **1992**, *40*, 1937.
- (77) Hemström, P.; Irgum, K. *J. Sep. Sci.* **2006**, *29*, 1784.
- (78) Haas, J. A.; Fox, B. G. *Biochemistry* **1999**, *38*, 12833.
- (79) Broadwater, J. A.; Ai, J.; Loehr, T. M.; Sanders-Loehr, J.; Fox, B. G. *Biochemistry* **1998**, *37*, 14664.
- (80) Vreman, H. J.; Schmitz, R. Y.; Skoog, F. *Phytochemistry* **1974**, *13*, 31.
- (81) Lichtenthaler, F. W.; Voss, P.; Heerd, A. *Tetrahedron Lett.* **1974**, *15*, 2141.
- (82) Ottria, R.; Casati, S.; Manzocchi, A.; Baldoli, E.; Mariotti, M.; Maier, J. A. M.; Ciuffreda, P. *Bioorg. Med. Chem.* **2010**, *18*, 4249.
- (83) Kao, W. C.; Wang, V. C.; Huang, Y. C.; Yu, S. S.; Chang, T. C.; Chan, S. I. *J. Inorg. Biochem.* **2008**, *102*, 1607.
- (84) Xiong, J.; Kurtz, D. M., Jr.; Ai, J.; Sanders-Loehr, J. *Biochemistry* **2000**, *39*, 5117.
- (85) Xiong, J.; Phillips, R. S.; Kurtz, D. M., Jr.; Jin, S.; Ai, J.; Sanders-Loehr, J. *Biochemistry* **2000**, *39*, 8526.
- (86) Sjöberg, B. M.; Karlsson, M.; Jornvall, H. *J. Biol. Chem.* **1987**, *262*, 9736.

- (87) Ge, J.; Perlstein, D. L.; Nguyen, H. H.; Bar, G.; Griffin, R. G.; Stubbe, J. *Proc. Natl. Acad. Sci.* **2001**, *98*, 10067.
- (88) Sommerhalter, M.; Voegtli, W. C.; Perlstein, D. L.; Ge, J.; Stubbe, J.; Rosenzweig, A. C. *Biochemistry* **2004**, *43*, 7736.
- (89) Cadieux, E.; Vrajmasu, V.; Achim, C.; Powlowski, J.; Münck, E. *Biochemistry* **2002**, *41*, 10680.
- (90) Sabina, R.; Paul, A.; Ferl, R.; Laber, B.; Lindell, S. *Plant Physiol.* **2007**, *143*, 1752.
- (91) Knapp, S. *Chem. Rev.* **1995**, *95*, 1859.
- (92) Merino, P.; Franco, S.; Merchan, F.; Tejero, T. *J. Org. Chem.* **2000**, *65*, 5575.
- (93) Braun, P.; B., N.; Wittman, V.; Drescher, M. *Angew. Chem. Int. Ed.* **2011**, *50*, 8428.
- (94) Macosko, J.; Pio, M.; Tinoco, I.; Y, S. *RNA* **1995**, *5*, 1158.
- (95) Barhate, N.; Cekan, P.; Massey, A. P.; Sigurdsson, S. T. *Angew. Chem. Int. Ed.* **2007**, *46*, 2655.
- (96) Riedl, J.; Pohl, R.; Ernsting, N. P.; Orsag, P.; Fojta, M.; Hocek, M. *Chemical Science* **2012**, *3*, 2797.
- (97) Fauster, K.; Hartl, M.; Santner, T.; Aigner, M.; Kreutz, C.; Bister, K.; Ennifar, E.; Micura, R. *ACS Chem. Biol.* **2012**, *7*, 581.
- (98) Smellie, I. A.; Bhakta, S.; Sim, E.; Fairbanks, A. J. *Org. Biol. Chem.* **2007**, *5*, 2257.
- (99) Bessodes, M.; Komiotis, D.; Antonakis, K. *Tetrahedron Lett.* **1986**, *27*, 579.
- (100) Angyal, S. J. *Angew. Chem. Int. Ed.* **1969**, *8*, 157.
- (101) Hatano, B.; Araya, H.; Yoshimura, Y.; Sato, H.; Ito, T.; Ogata, T.; Kijima, T. *Heterocycles* **2010**, *81*, 349.

- (102) Rozantzev, E. G.; Krinitzkaya, L. A. *Tetrahedron* **1965**, *21*, 491.
- (103) Saxon, E.; Armstrong, J. I.; Bertozzi, C. R. *Org. Lett.* **2000**, *2*, 2141.
- (104) Bianchi, A.; Bernardi, A. *J. Org. Chem.* **2006**, *71*, 4565.
- (105) Laemmerhold, K. M.; Breit, B. *Angew. Chem. Int. Ed.* **2010**, *49*, 2367.
- (106) Kirilyuk, I. A.; Polienko, Y. F.; Krumkacheva, O. A.; Strizhakov, R. K.; Gatilov, Y. V.; Grigor'ev, I. A.; Bagryanskaya, E. G. *J. Org. Chem.* **2012**, *77*, 8016.
- (107) Bosch, L.; Vilarrasa, J. *Angew. Chem. Int. Ed.* **2007**, *46*, 3926.
- (108) Kalai, T.; Hubbell, W.; Hideg, K. *Synthesis* **2009**, *8*, 1336.
- (109) Milligan, J.; Groebe, D.; Witherell, G.; Uhlenbeck, O. *Nucl. Acids Res.* **1987**, *15*, 8783.
- (110) Grodberg, J.; Dunn, J. J. *J. Bacteriol.* **1988**, *170*, 1245.
- (111) Davanloo, P.; Rosenberg, A.; Dunn, J.; Studier, F. W. *Proc. Natl. Acad. Sci.* **1984**, *81*, 2035.
- (112) Li, Y.; Wang, E.; Wang, Y. *Protein Expression Purif.* **1999**, *16*, 355.
- (113) Hobbs, J. B.; Eckstein, F. *J. Org. Chem.* **1977**, *42*, 714.
- (114) Leung, H.-C. E.; Chen, Y.; Winkler, M. E. *J. Biol. Chem.* **1997**, *272*, 13073.
- (115) Sambrook, J. F.; Russell, D. W. *Molecular Cloning: A Laboratory Manual*, 3rd ed.; Cold Spring Harbor Laboratory Press: Cold Spring Harbor, New York, 2001.
- (116) Chen, H.; Zhao, J.; Li, Y.; Shen, F.; Li, X.; Yin, Q.; Qin, Z.; Yan, X.; Wang, Y.; Zhang, P.; Zhang, J. *Bioorg. Med. Chem. Lett.* **2011**, *21*, 574.
- (117) Baksi, K.; Rogerson, D. L.; Rushizky, G. W. *Biochemistry* **1978**, *17*, 4136.
- (118) Ibach, J.; Dietrich, L.; Koopmans, K. R. M.; Nöbel, N.; Skoupi, M.; Brakmann, S. *J. Biotechnol.* **2013**, *167*, 287.
- (119) Ozer, A.; Bruick, R. K. *Nat. Chem. Biol.* **2007**, *3*, 144.
- (120) Kovaleva, E.; Lipscomb, J. D. *Nat. Chem. Biol.* **2008**, *4*, 186.

- (121) Schaeffer, H. J.; Thomas, H. J. *J. Am. Chem. Soc.* **1958**, *80*, 3738.
- (122) Piguel, S.; Legraverend, M. *J. Org. Chem.* **2007**, *72*, 7026.
- (123) Serebryany, V.; Beigelman, L. *Tetrahedron Lett.* **2002**, *43*, 1983.
- (124) Dellinger, D. J.; Timár, Z.; Myerson, J.; Sierzchala, A. B.; Turner, J.; Ferreira, F.; Kupihár, Z.; Dellinger, G.; Hill, K. W.; Powell, J. A.; Sampson, J. R.; Caruthers, M. H. *J. Am. Chem. Soc.* **2011**, *133*, 11540.
- (125) Wei, X. *Tetrahedron* **2013**, *69*, 3615.
- (126) Sazinsky, M. H.; Lippard, S. J. *Acc. Chem. Res.* **2006**, *39*, 558.
- (127) Mitchell, K. H.; Studts, J. M.; Fox, B. G. *Biochemistry* **2002**, *41*, 3176.
- (128) Bailey, L. J.; McCoy, J. G.; Phillips, G. N.; Fox, B. G. *Proc. Natl. Acad. Sci.* **2008**, *105*, 19194.
- (129) Chang, S.; Waller, B. J.; Lipscomb, J. D.; Mayo, K. H. *Biochemistry* **1999**, *38*, 5799.
- (130) Pierce, B. S.; Sobrado, P.; Elsen, N. L.; Charkrabarti, M.; Münck, E.; Fox, B. G. (*unpublished results*).
- (131) Vreman, H. J.; Schmitz, R. Y.; Skoog, F.; Playtis, A. J.; Frihart, C. R.; Leonard, N. *J. Phytochemistry* **1974**, *13*, 31.
- (132) Grison, C.; Genève, S.; Halbin, E.; Coutrot, P. *Tetrahedron* **2001**, *57*, 4903.
- (133) Coutrot, P.; Claudel, S.; Didierjean, C.; Grison, C. *Bioorg. Med. Chem. Lett.* **2006**, *16*, 417.
- (134) Tarkowski, P.; Václavíková, K.; Novák, O.; Pertry, I.; Hanuš, J.; Whenham, R.; Vereecke, D.; Šebela, M.; Strnad, M. *Anal. Chim. Acta.* **2010**, *680*, 86.
- (135) Young, H.; Letham, D. S.; Hocart, C. H.; Eichholzer, J. V. *Phytochemistry* **1990**, *29*, 385.
- (136) Sosnovsky, G.; Cai, Z.-w. *J. Org. Chem.* **1995**, *60*, 3414.

- (137) Murray, R.; Singh, M. *Tetrahedron Lett.* **1988**, 29, 4677.
- (138) Herd, O.; Heßler, A.; Hingst, M.; Machnitzki, P.; Tepper, M.; Stelzer, O. *Catal. Today* **1998**, 42, 413.
- (139) Hoffman, B. M.; Schofield, P.; Rich, A. *Proc. Natl. Acad. Sci.* **1969**, 62, 1195.
- (140) Sar, C.; Jeko, J.; Fajer, P.; Hideg, K. *Synthesis* **1999**, 6, 1039.
- (141) Wright, K.; Dutot, L.; Wakselman, M.; Mazaleyrat, J.-P.; Crisma, M.; Formaggio, F.; Toniolo, C. *Tetrahedron* **2008**, 64, 4416.
- (142) But, T.; Toy, P. *Chem. -- Asian J.* **2007**, 2, 1340.
- (143) Swamy, K.; Kumar, N.; Balaraman, E.; Kumar, K. *Chem. Rev.* **2009**, 109, 2551.
- (144) But, T.; Toy, P. *J. Am. Chem. Soc.* **2006**, 128, 9636.
- (145) O'Brien, C. J.; Tellez, J. L.; Nixon, Z. S.; Kang, L. J.; Carter, A. L.; Kunkel, S. R.; Przeworski, K. C.; Chass, G. A. *Angew. Chem. Int. Ed.* **2009**, 48, 6836.

Biographical Information

Andra Corder acquired her Bachelor of Science in Biology from the University of Texas at Arlington in 2009. She then began her graduate career in organic chemistry at UTA under the direction of Dr. Christopher O'Brien, investigating the Wittig and Mitsunobu reactions catalytic in phosphine. After her first year, Andra decided to incorporate more of her biological training from her undergraduate career, and joined the research efforts of Dr. Frank Foss and Dr. Brad Pierce. Her thesis project lies at the interface of biophysics and synthetic chemistry. Specifically, most of her work focused on the synthesis of viable nucleoside substrate analogues to characterize the enzymology of a novel carboxylate-bridged non-heme diiron enzyme (MiaE).